THE UNIVERSITY OF QUEENSLAND

AUSTRALIA

Influence of Muscovite Content on the Flotation of Pyrite and Arsenopyrite

Erica Cristina Avelar

B. E. Chemical Engineering

Master in Mineral Technology

A thesis submitted for the degree of Doctor of Philosophy at

The University of Queensland in 2019

Sustainable Minerals Institute

Julius Kruttschnitt Mineral Research Centre

Abstract

Muscovite is a hydrophilic, platy micaceous mineral, classified as a phyllosilicate. Previous research identified that micas and clays can have a deleterious effect on the flotation of sulfide minerals; for example, the presence of muscovite is associated with an increase in pulp viscosity, the formation of slime coatings and high recovery of muscovite through entrainment. The majority of previous studies relating to the effect of mica and clays on sulfide minerals were conducted using copper ores. Barrick Gold Corporation has a sub-economic refractory gold orebody with a high content of muscovite. The flotation circuit designed for this project has a high capital cost, due to the high throughput and the relatively long residence time required to recover the gold-bearing sulfide mineral. In addition, muscovite is readily recovered to the concentrate, which affects downstream processes.

The effect of the presence of muscovite on the flotation of pyritic gold-bearing minerals has not been reported in the literature. This work investigates the effect of muscovite on pyrite and arsenopyrite floatability at laboratory-scale using a synthetic ore consisting of pyrite, arsenopyrite, quartz (silica) and muscovite. The experimental program applied a Central Composite Rotatable Design (CCRD) to identify the potential causes for the detrimental effect of muscovite. The aim was to identify the most significant factors affecting to the floatability of pyrite and arsenopyrite in this synthetic system, with the factors investigated being frother dosage (ppm), the percentage of solids, the percentage of muscovite in the gangue, pH and muscovite size distribution (P_{80}).

In order to investigate the underlying mechanisms behind the effects observed in the CCRD, zeta potential measurements were done to investigate the formation of slime coatings, viscosity measurements of the pulp monitored any changes in viscosity, and Time-of-flight secondary ion mass spectrometry (ToF-SIMS) and X-ray photoelectron spectroscopy (XPS) were used to investigate changes in surface chemistry of the pyrite and arsenopyrite. The froth height of selected experiments was measured to detect changes on froth stability.

The results of the CCRD analysis indicated that the factors that significantly affected the kinetics of arsenopyrite and pyrite are the positive interaction of pH with frother and the interaction of %solids with muscovite size distribution which is a negative term. It can be speculated that positive effect of the term pH x frother dosage on the flotation rates of

arsenopyrite and pyrite is due to the combined effect of the frother and pH on the froth stability, as limited tests showed that the increase of pH increases the froth height.

The results showed that the proportion of muscovite in the gangue has no effect on the flotation rate of arsenopyrite. Furthermore, the effect of the proportion of muscovite in the flotation kinetics of pyrite is not deleterious and has low significance, according to the regression.

No direct correlation was found between the measured viscosity and the flotation rate of pyrite or arsenopyrite. In addition, the proportion of muscovite in the gangue does not affect significantly pulp viscosity. Therefore, the presence of muscovite may not affect the flotation kinetics through an increase in pulp viscosity.

No evidence of muscovite slime coatings on the pyritic minerals was found by the zeta potential measurements. The ToF-SIMS and XPS analyses indicated that the increase in the particle size distribution of muscovite was related to an increase of the levels of K and Al, which originate from the muscovite lattice, on the surface of pyrite. A corresponding decrease of the level of Cu and collector, in the presence of coarser muscovite, leads to a decrease of particle hydrophobicity of pyritic minerals. The leaching of K and Al from muscovite was found to be size-dependent, increasing with the increase in muscovite particle size, which explains the effect of muscovite P_{80} on the kinetics of arsenopyrite and pyrite. These results suggest that the reason for the deleterious effect of the interaction term %solids x muscovite P_{80} is due to the increase in K and Al ions on the pyritic minerals surfaces. As the percentage of solids increases, more muscovite is available for leaching and less solution is available to carry those ions; therefore, the concentration of K and Al ions increases significantly, leading to the slower flotation kinetics.

In conclusion, contrary to the expected, the deleterious effect of muscovite on the flotation rate is not caused by physical mechanisms, such as the increase of viscosity or the formation of slime coatings on the surface. The dominant deleterious effect of muscovite is due to the chemical modification of the surfaces of pyritic minerals by K and Al ions from its lattice.

Declaration by author

This thesis *is composed of my original work, and contains* no material previously published or written by another person except where due reference has been made in the text. I have clearly stated the contribution by others to jointly-authored works that I have included in my thesis.

I have clearly stated the contribution of others to my thesis as a whole, including statistical assistance, survey design, data analysis, significant technical procedures, professional editorial advice, financial support and any other original research work used or reported in my thesis. The content of my thesis is the result of work I have carried out since the commencement of my higher degree by research candidature and does not include a substantial part of work that has been submitted *to qualify for the award of any* other degree or diploma in any university or other tertiary institution. I have clearly stated which parts of my thesis, if any, have been submitted to qualify for another award.

I acknowledge that an electronic copy of my thesis must be lodged with the University Library and, subject to the policy and procedures of The University of Queensland, the thesis be made available for research and study in accordance with the Copyright Act 1968 unless a period of embargo has been approved by the Dean of the Graduate School.

I acknowledge that copyright of all material contained in my thesis resides with the copyright holder(s) of that material. Where appropriate I have obtained copyright permission from the copyright holder to reproduce material in this thesis and have sought permission from co-authors for any jointly authored works included in the thesis.

Publications included in this thesis

No publications included

Submitted manuscripts included in this thesis

No manuscripts submitted for publication.

Other publications during candidature

J.J. Frausto, **E.C. Avelar**, G. Figueroa, Y. Reja, D.K. Tungpalan, M.A. Corona-Arroyo, R. Alanis, S. Gómez, A.J. Lynch (2018, September). *Have you been to a mine site? The SMI-JKMRC student venture.* Paper presented at XXIX International Mineral Processing Congress.

Avelar, E. C.; Alvarenga, C. L. G; Resende, G. P. S.; Morais, C. A.; Mansur, M. B. (2017) Solvent extraction reaction of uranium (VI) sulfate with Alamine 336. *Brazilian Journal of Chemical Engineering*, 34-1, 355-362. 2017.

Avelar, E. C.; C. L. G; Resende, G. P. S.; Mansur, M. B.; (2014, September) *Solvent extraction reaction of uranium (VI) sulfate with Alamine 336*. ISEC2014 – International Solvent Extraction Conference.

Contributions by others to the thesis

My supervisors Dr Cathy Evans and Dr Kym Runge provided technical support on the project development, the design of the experimental program, data analysis, and critically reviewed the thesis.

Dr Barun Gorain provided the data of Barrick's project, which was the start point of this thesis, and valuable guidance on the development of the project with my supervisors Dr Emmy Manlapig and Dr Chris Fountain, who made significant contribution to set up the scope of the project.

Dr Elaine Wightman, Kellie White and Dr Cathy Evans provided assistance in the mineralogical characterisation using MLA of Barrick’s reference ore.

Dr Alex-Anthony Cavallaro performed ToF-SIMS and Dr Chris Bassell performed the XPS analysis of the flotation samples in the University of South Australia. Dr Susana Brito e Abreu provided assistance in the interpretation of the surface analysis data.

Professor Tim Napier-Munn provided assistance with the CCRD factorial experimental design and interpretation of the statistics of the regression analyses.

Barrick Gold Corporation provided funding for this research.

Dr Barun Gorain provided the data of Barrick's project, which was the start point of this thesis, and valuable guidance on the development of the project with Dr Emmy Manlapig and Dr Chris Fountain.

Professor N.W. Johnson and Dr Francois Vos were part of my milestone panels providing valuable advice and critical review.

Statement of parts of the thesis submitted to qualify for the award of another degree

No works submitted towards another degree have been included in this thesis.

Research Involving Human or Animal Subjects

No animal or human subjects were involved in this research.

Acknowledgements

I would like to formally express gratitude to my advisory team, Dr Cathy Evans, Dr Kym Runge Professor Emmy Manlapig and Dr Chris Fountain, for the fruitful discussions, assistance, comments and critical review during the development of my PhD research. A special mention to my principal advisor, Dr Cathy Evans, for the patience, encouragement and the incredible support she has provided me on the second half of my research and in the final writing stages of the thesis. I wish to acknowledge Dr Chris Fountain for his support and guidance at the beginning of my journey, and particularly for recruiting me with Professor Emmy Manlapig. I want to especially thank Dr Kym Runge for supporting my scholarship until the completion of the project.

I am grateful to Dr N. W. (Bill) Johnson for his invaluable advice comments and input on my six-monthly PhD reviews, and for keeping interested on in my progress despite not being part of my advisory team.

Special thanks go to Professor Tim Napier-Munn for his assistance with the experimental design and the statistical analysis, and to Dr Susana Brite e Abreu, for providing insightful comments and suggestions, many times delivered in Portuguese (my mother language).

My sincere appreciation to Dr Elaine Wightman, Tess Dobinson and Jacqueline Ross. My candidature would have been impossible without your aid and support.

I want to thank David Garcia and JKMRC pilot plant personnel for support during the development of the testwork program, and to Karen Holtham, for promptly helping me to navigate the library file cabinets.

I am profoundly grateful to Dr Barun Gorain for providing the basis for this project, the constructive feedback, and to Barrick Gold Corporation for funding this research.

To my fellow colleagues, thank you for your friendship, advice and support. I was very fortunate to meet many amazing people at JKMRC. In particular, I want to thank Bianca Foggiatto, Juan Jose, Nerrida Scott, Raphael Picorelli, Constanza Paredes, Pia Lois and Pricilla Esteves for the close friendship and support on this ride, and to Konuray Demir for keeping me caffeinated in the final stage of the writing

Last by not least, to my husband, who has to put up with the many disruptions of being married to someone doing a PhD, thank you for your love, care and support.

Financial support

This research was supported by Barrick Gold Corporation, through the AMIRA P9P project and the Julius Kruttschnitt Mineral Research Centre.

This research was also supported by an Australian Government Research Training Program Scholarship.

Keywords

Flotation, muscovite, flotation rate, pyrite, arsenopyrite, CCRD, viscosity, surface analysis

Australian and New Zealand Standard Research Classifications (ANZSRC)

ANZSRC code: 091404, Mineral Processing/Beneficiation, 100%

Fields of Research (FoR) Classification

FoR code: 0914, Resources Engineering and Extractive Metallurgy, 100%

Table of Contents

List of Figures

List of Tables

List of Abbreviations used in the thesis

AR	Analytical reagent
BET	Brunauer-Emmett-Teller
BSE	Back-Scattered Electron Detector
CCD	Counter-current decantation
CIL	Carbon in leach
c-matter	Carbonaceous matter or carbonaceous material
EDTA	Ethylenediaminetetraacetic acid
ICP	Inductively coupled plasma
JKMRC	The Julius Kruttschnitt Mineral Research Centre
MCF2	Mill-Chemistry-Float-Mill-Chemistry-Float
MLA	Mineral Liberation Analysis
NSG	Non-sulfide gangue
NPV	Net present value
PAX	Potassium amyl xanthate
QXRD	Quantitative X-ray Diffraction Analysis
POX	Pressure oxidation
SIMS	Secondary-ion mass spectrometry
ToF-LIMS	Time-of-flight laser- ionisation mass spectrometry
ToF-RIMS	Time-of-flight resonance-ionisation mass spectrometry
XBSE	Extended BSE Analysis
XRD	X-ray diffraction
XPS	X-ray Photoelectron Spectroscopy

Chapter 1 Introduction

1 Thesis Introduction

1.1 Overview

Hundreds of millions of dollars are typically spent to design and build processing plants to extract valuable minerals from ore. The flowsheet selection at the conceptual level of a greenfield project is based on diagnosing the process behaviour of a broad range of ore types to select the most viable. The variability of the deposit is tested using a range of samples based on a selected flow sheet. Prediction of the plant performance is based on bench-scale tests performed using the major ore types that will be treated, according to the mining plan. (Lane et al., 2012).

Barrick Gold Corporation ('Barrick') is the world's largest gold producer, with mines, advanced exploration and development projects on five continents (Barrick, 2014). Barrick has a significant data set for its operations and greenfield projects, based on metallurgical test programs conducted by various vendors, using different methods to design and optimise process facilities (B. Gorain, personal communication, April 14, 2014).

Barrick has requested the JKMRC to review the project design data of a currently unfeasible greenfield project to determine whether they could unlock new flow sheet options that would allow Barrick to reduce the capital cost. The project is commercially sensitive, so its identity is masked by using a code name: 'White Mountain'.

The White Mountain project consists of a Carlin-type gold refractory deposit with arsenopyrite and pyrite as the main gold carriers. It is currently not feasible due to its high capital and operating cost. The flowsheet includes a pre-concentration of the arsenopyrite and pyrite via flotation, followed by pressure oxidation and carbon in leach process. The flotation plant has a large footprint due to the high throughput, of 2,397 t/h, and residence time of 105 minutes for the primary and secondary rougher banks. The engineering studies showed that the flotation circuit alone consists of seventy-two 160 m^3 cells, arranged in four rows in the rougher banks, eight 160 m^3

cells in the cleaner bank and six 160 m^3 cells the cleaner–scavenger circuit (B. Gorain, personal communication, December 24, 2014; AMTEL, 2007).

The feasibility of the White Mountain could be improved by the reduction of the footprint of the flotation circuit. The identification of alternatives to reduce the residence time of the flotation circuit could be the key to unlocking an alternative economic outcome for the project.

The assessment of the White Mountain feasibility study reports showed that the elevated percentage of muscovite has deleterious effects on the flotation and pressure oxidation circuits. The QEMSCAN analysis of the flotation streams of the pilot plant shows that liberated muscovite is reporting to the flotation concentrate and, as it is the main carrier of chlorine and fluorine, it is affecting the pressure oxidation process by necessitating an elevated operating temperature in the autoclave to minimise the chloride effect (B. Gorain, personal communication, April 14, 2014; AMEC, 2011; AMTEL, 2007).

The engineering studies acknowledged the issues of having the micas and clays but did not model alternative scenarios with a low content of phyllosilicates, to evaluate if the residence time of the flotation circuit could be reduced by effectively removing the micas from the flotation feed. It also did not consider alternative processing routes to remove micas.

Muscovite is a hydrophilic, platy phyllosilicate, classified as part of the mica group. The recovery of muscovite to the concentrate can occur through a range of mechanisms such as natural floatability (‘true flotation’), entrainment, the formation of slime coatings on sulfide minerals or entrapment. According to Silvester et al. (2013), muscovite does not have inherent natural floatability, although significant amounts report to the concentrate. Li et al. (2014) describe the mechanism of recovery of muscovite as entrainment. There are a number of potential ways which muscovite could adversely affect the flotation of pyrite. He et al. (2009) observed a hetero-aggregation (slime coating) between muscovite and chalcopyrite. Forbes et al. (2014) observed that the presence of slime coatings reduced the flotation rate of the chalcopyrite.

Pulp rheology has been identified as a factor that affects flotation rates of sulfide minerals and gangue entrainment (Wang et al.; 2015). The increase of muscovite concentration in the slurry can result in a rise in pulp viscosity (Ndlovu, 2013). He et al. (2009) inferred that the increase of viscosity in the pulp could be a result of the formation of slime coatings and or change of surface charge of minerals.

Forbes et al. (2014) observed the presence of kaolinite, a clay phyllosilicate, reduces the flotation rate of chalcopyrite. In their study, an increase of pulp viscosity and formation of slime coating was identified. Moreover, the increase of pulp viscosity and formation of slime coatings have a detrimental effect on the flotation rate of sulfide minerals.

Based on the literature, it is expected that the presence of muscovite in the flotation could cause an increase of pulp viscosity, the formation of slime coating on the surface of pyrite and consequently a reduction of the flotation rate of the sulfide minerals. Therefore, the removal of muscovite in the early stages of the process could improve the White Mountain flow sheet by reducing the deleterious effect of muscovite in the flotation circuit, consequently reducing the capital cost of the project.

Studies mainly considered copper minerals when reporting the behaviour of muscovite and its effects on sulfide minerals. No studies were found to correlate the behaviour of muscovite with the flotation rate of pyrite and arsenopyrite, which is one of the main carriers of gold in Carlin-type ores.

This thesis focuses on an investigation of flotation behaviour of pyrite and arsenopyrite in the presence of muscovite.

1.2 Research Questions

1. Does the presence of a high proportion of muscovite in an ore adversely affect the flotation rate of arsenopyrite and pyrite?
2. What is the mechanism by which muscovite effects arsenopyrite and pyrite flotation?

1.3 Hypotheses

This study has three principal hypotheses. These are:

Hypothesis 1:

The presence of high concentrations of muscovite has a detrimental effect on the flotation rate of pyrite and arsenopyrite.

Hypothesis 2:

The presence of muscovite affects pyrite and arsenopyrite floatability by changing pulp viscosity.

Hypothesis 3:

The detrimental effect on muscovite in the flotation rate of pyrite and arsenopyrite is due to modification of pyrite and arsenopyrite mineral surfaces.

1.4 Objectives

The central objective of this research is to understand how muscovite affects the flotation rate of pyrite and arsenopyrite to understand the conditions that would minimise the effect of muscovite on the flotation rates of the pyritic minerals. From the literature, the presence of muscovite is associated with increases in pulp viscosity (Ndlovu, 2013), the formation of slime coatings (He et al., 2009) and high recovery of muscovite through entrainment (Li et al. 2014; Silvester et al., 2013). The increase in viscosity can reduce flotation performance, and the presence of slime coatings can adversely affect the flotation rate of sulfide minerals (Forbes et al., 2014). The understanding of the factors that drives the behaviour of gangue is useful since its behaviour can have a deleterious effect on the flotation rate of sulfide minerals

The objectives of this research are to:

- Determine whether the amount of muscovite in an ore affects the flotation rate of arsenopyrite and pyrite
- Identify the main factors that have a deleterious effect on the flotation performance of arsenopyrite and pyrite in a system containing muscovite

- Determine whether an increase of pulp viscosity caused by the presence of muscovite has a detrimental effect on the flotation rate of pyrite and arsenopyrite
- Determine whether the presence of muscovite is associated with the formation of slime coating on arsenopyrite and/or pyrite surfaces
- Determine whether the effect of the poor flotation rate of pyrite and arsenopyrite is due to surface chemistry modification.

1.5 Scope of Work

The study of the flotation performance was done at laboratory scale, using a synthetic mineral mixture consisting of pyrite, arsenopyrite, quartz (silica) and muscovite. The use of a synthetic mineral mixture allows the identification of specific effects of the mineral of interest without the interference of the complex mineralogy of the ore. In addition, the composition of the synthetic mineral mixture can be easily modified to explore the effect of changes in composition, in contrast to real ores.

To test the hypotheses of this thesis, a large number of batch laboratory flotation tests were performed using a synthetic ore according to a Central Composite Rotatable Design (CCRD) factorial design. Factors varied included the percentage of muscovite in the gangue, the percentage of solids in the flotation feed and the size distribution of the muscovite. The aim was to understand whether the amount and type of muscovite in the gangue affects the flotation rates of pyrite and arsenopyrite. Other variables tested in the CCRD included frother dosage and pH.

The results from the CCRD were analysed using regression analysis and the key variables affecting flotation rate were identified. Measurements of viscosity, ToF-SIMS and XPS surface analysis, muscovite leachability and froth stability were conducted and analysed to help interpret the experimental results.

According to Klimpel (1984), flotation performance is affected by machine, chemistry and operational factors that includes ore characteristics. This research focuses on specific flotation chemistry and operational factors that influence the effect of muscovite on the flotation rate of arsenopyrite and pyrite. Figure 1-1 highlights the

flotation parameters investigate in this research and indicates which parameters are not investigated in the scope of this work.

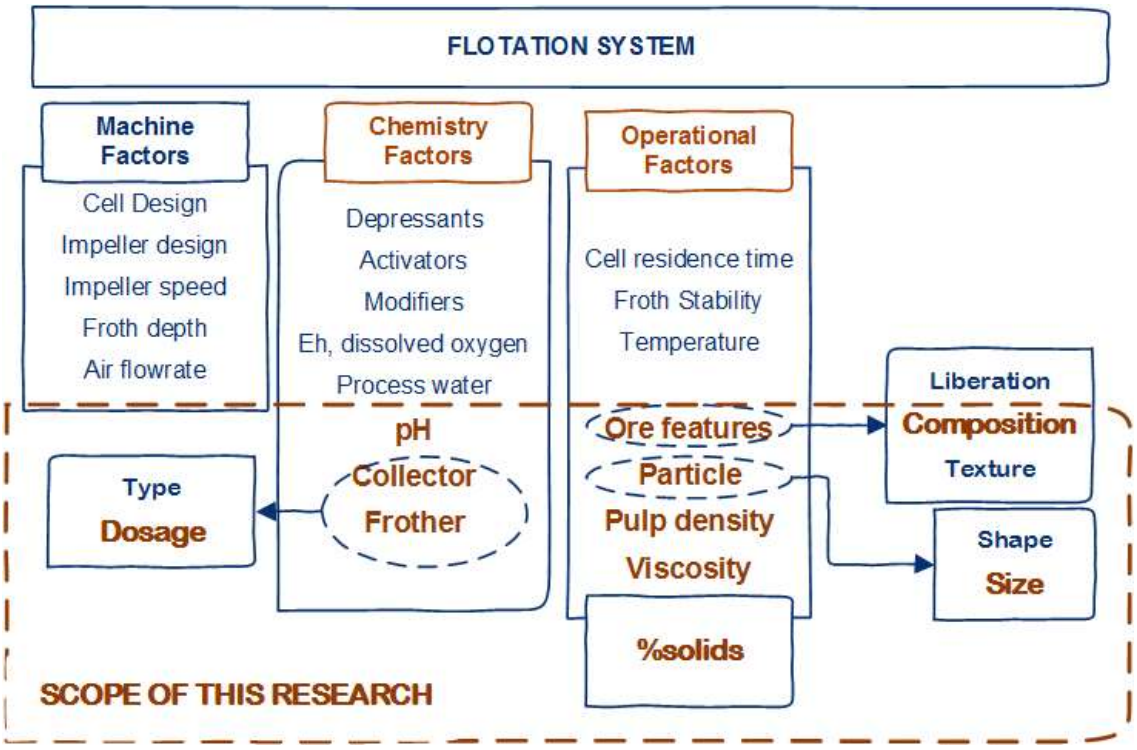

Figure 1-1 – Research scope diagram

1.6 Thesis Outline

The thesis outline is as follow:

Chapter 2: presents a literature review of the key factors that affect flotation and the behaviour of phyllosilicates in flotation with emphasis on the characteristics of muscovite and its behaviour in flotation.

Chapter 3: presents the research methodology to test the hypothesis and details the materials and experimental procedure used to perform the CCRD flotation testwork program

Chapter 4: describes the preliminary analyses of the samples used in the flotation tests. It involves determining what size and composition of minerals should be used in the synthetic ore to provide similar characteristics to those of the Barrick White

Mountain ore. It also involves an assessment of the purity of the minerals used to create the synthetic ore.

Chapter 5: presents the key findings from the flotation tests. It describes the significant variables affecting the flotation rate constants of arsenopyrite and pyrite determined using the CCRD method.

Chapter 6: investigates the effect of pulp viscosity in the flotation system studied.

Chapter 7: investigates the effect of surface modification on the flotation rate of pyrite and arsenopyrite

Chapter 8: *presents the* thesis conclusions, contributions to knowledge and suggestions for future work.

Chapter 2

Literature Review

2 Literature Review

2.1 Introduction

The focus of the thesis is to understand how muscovite affects the flotation performance of pyrite and arsenopyrite in the context of Barrick's White Mountain project.

This literature review presents relevant information about Barrick's White Mountain project to understand the flotation plant design challenges and the behaviour of non-sulfide gangue in the ore.

A brief review of flotation fundamental and the factors that affect the flotation of arsenopyrite and pyrite is provided to contextualise the factors that affect the flotation performance of the pyritic minerals studied. In addition, the mechanisms by which the presence of non-sulfide gangue minerals affect the flotation performance of sulfide minerals are outlined.

A summary of the behaviour of non-sulfide gangue, classified as phyllosilicate minerals, in flotation is presented, focussing on how muscovite is possibly affecting the arsenopyrite and pyrite.

This section closes with a summary of the literature and the gaps found.

2.2 White Mountain Project

The White Mountain Gold Project is a joint venture to build a gold mining project in North America. Currently, Barrick is continuing to monitor the long-term viability of its investment in White Mountain Gold. Although the White Mountain project contains large, mineral resources, with significant leverage to the price of gold, there is the uncertainty about it meeting Barrick's investment criteria, given the required large initial capital investment (Barrick, 2014).

The White Mountain flowsheet design is based on a life of plant of 20 years, with a throughput of over 50,000 t/d and production of approximately 4,000 ounces of gold

per day. The overall plant availability is 93%, with a nominal throughput of 2,397 t/h. The safety design factor applied is 1.35 to provide a maximum capacity of 4,630 t/h (AMEC, 2011).

White Mountain is a refractory gold deposit. Pyrite is the dominant sulfide mineral, followed by arsenopyrite (the carrier of arsenic). The main host mineral of the gold is arsenopyrite, which carries 80% to 90% of the gold as a solid solution. Pyrite hosts 10% to 20% of the gold, also in solid solution form. Less than 1% of the contained gold is free gold. The liberated particles are less than 20 µm in diameter (SGS, 2007b). The gold grade of the deposit is 2.58 g/t (AMEC, 2007a).

The gold in White Mountain ores is exclusively in a submicron ('sub-µ') disseminated form in the crystal structure of arsenopyrite and pyrite. Arsenopyrite is the principal gold carrier, strongly enriched over pyrite, at a ratio of approximately 20. However, pyrite must be recovered to maximise gold recovery (SGS, 2007a).

The flowsheet of White Mountain Project includes the following unit operations (AMEC, 2007b):

- Primary crushing.
- Pebble crushing.
- Integrated grinding and flotation circuit.
- Concentrate washing to remove soluble chorine.
- Pre-acidification of flotation concentrate.
- Pressure oxidation (POX).
- Acid recovery via a CCD (counter-current decantation) circuit on POX discharge.
- Carbon-in-leach (CIL) circuit for oxidised concentrate.
- Neutralisation of acid liquor using flotation tailings.
- CIL tailings detoxification.

The integrated grinding and flotation circuit is based on a Mill-Chemistry-Float-Mill-Chemistry-Float circuit ('MCF2'). MCF2 is the name given to a circuit that takes the primary rougher concentrate directly to leaching and regrinds the primary rougher

tailings ahead of the secondary rougher flotation cells. A generic MCF2 flow sheet is shown in Figure 2-1. The primary grinding consists of a SAG mill. The target is a P_{80} of 121 µm. The primary grinding product feeds the flotation rougher circuit. The rougher flotation tailings report to the secondary grinding, which consists of a ball mill, to be reduced to a product with a P_{80} of 50 µm. The secondary mill discharge feeds the secondary rougher flotation cells (AMEC, 2007b).

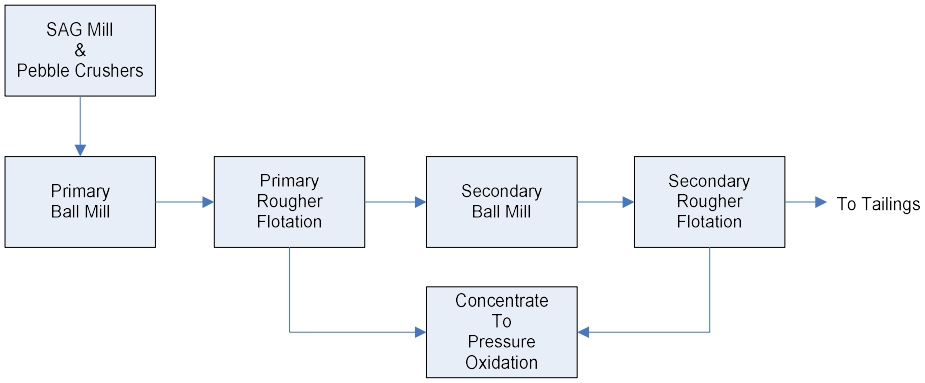

Figure 2-1 - Illustration of MCF2 generic flow sheet (AMEC, 2007)

The objective of the flotation circuits is to concentrate the gold-carrying minerals, which are pyrite and arsenopyrite. The flotation concentrate must have a sulfide-sulfur grade of about 7% for reducing the heat requirement of the autoclave. The composition of the flotation feed in shown in Figure 2-2.

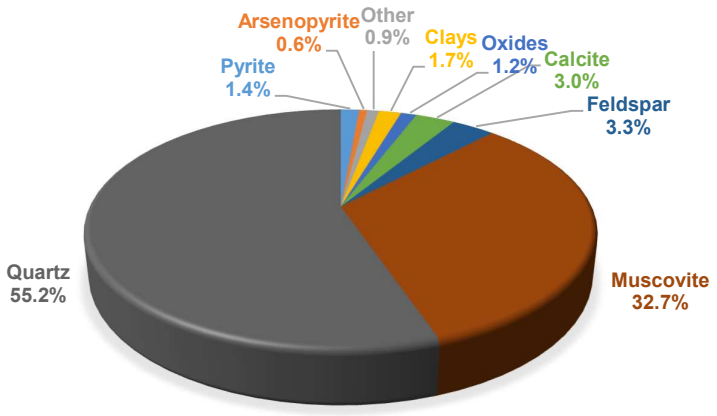

Figure 2-2 – Composition of White Mountain Flotation Feed (SGS, 2007b)

Figure 2-2 shows that pyrite is the most abundant sulfide in the flotation feed, representing 1.4% of the mineral content, followed by arsenopyrite. The most abundant gangue mineral is quartz, representing 55.2% of the total, followed by muscovite, accounting for 32.7%. Feldspar and calcite are the third most prevalent gangues. Kaolinite, chlorites and amphibole account for the clays, representing 1.7% of the feed.

The sulfide mineral content increases significantly in the rougher concentrate. Muscovite is distributed in the concentrate and tailings streams, accounting 20% of the rougher concentrate, 37.1% of the scavenger concentrate, 38.8% of the cleaner concentrate and tailings, and 28.9% in the final tails (SGS, 2007b). According to SGS (2007b), muscovite has a preferential response in flotation in comparison with quartz, as indicated in the primary rougher concentrate stream. Therefore, it can be inferred that the mica species have either been activated or entrained in the flotation process.

The flotation bench-scale testwork campaign indicated that a long retention time, of approximately 110 minutes, was found to be necessary to achieve maximum recovery of arsenopyrite. Pyrite and coarser arsenopyrite have higher kinetic flotation rates, but much of the gold is associated with the very fine and slower floating arsenopyrite (AMEC, 2007b).

The testwork showed that a high mass pull of approximatively 20% plus was required for achieving high recovery. It indicated that the mass pull from the rougher and scavenger circuits were dictated by entrainment of clays during the long residence time (AMEC, 2007b).

The equipment selection of the flotation circuit was based on the simulation work developed by JKTech (2007) and economic trade-offs. The 160 m^3 flotation cells were selected over the 300 m^3 flotation cells based on lip-loading data. The total residence time selected for the primary and secondary rougher banks was 105 minutes. To deliver the demanded throughput of 45,000 t/d at the selected residence time, seventy-two 160 m^3 cells, arranged in four rows, are required for the rougher banks. The cleaner circuit consists of eight 160 m^3 and the cleaner–scavenger circuit six

160 m^3 cells. The flotation reagents used were potassium amyl xanthate ('PAX'), frother, dispersant and copper sulfate.

2.2.1 White Mountain Project Summary

The White Mountain project is currently sub-economic. The project consists of refractory gold ore, with arsenopyrite and pyrite as the gold-bearing minerals. Pyrite is more abundant than pyrite. Gold is found as sub-microscopic, locked in the arsenopyrite and pyrite matrix.

The main gangue minerals in order of abundance in the flotation feed are quartz and muscovite. Quartz accounts for 55.2%, while muscovite, 32.7%. Muscovite is a major contaminant of the concentrate, comprising 20% of the rougher concentrate, 37.1% of the scavenger concentrate and 38.8% of the cleaner concentrate.

The flotation plant has a large footprint due to the high throughput, of 2,397 t/h, and residence time of 105 minutes for the primary and secondary rougher banks. The engineering studies acknowledged the issues of having the micas and clays. However, it did not evaluate if the residence time of the flotation circuit could be reduced by effectively removing the micas from the flotation feed, because one possible reason for the required long flotation residence tile is the high content of muscovite in the ore.

The summarised flotation conditions and reagent dosage in grams per tonne of ore (g/t) are as follow (AMEC, 2007a):

- pH: 5 to 7, adjusted using H_2SO_4.
- Frothers: Methyl Isobutyl Carbinol (MIBC) at 95 g/t and F549 at 5 g/t.
- Collector: Potassium Amy Xanthate (PAX) at 200 g/t.
- Activator: $CuSO_4$ at 100 g/t.
- Depressant: Cytec E40, at 50 g/t.
- Soda Ash: 50 g/t.

2.3 The Carlin Type Ore

As the White Mountain is a Carlin-type deposit, this section summarises the definition of Carlin type-ores.

The definition of a Carlin-type gold deposit is a sediment-hosted disseminated gold deposit in which invisible gold is disseminated in pyrite and arsenopyrite (Tabatabaei, 2011). Those ores containing gold encapsulated in the solid solution of the mineral matrix, generally sulphides, are classified as refractory (Thella, 2018; Fraser et al., 1991). Carlin-type ores are considered refractory ores, because of the presence of sulfides, tellurides, cyanides and carbonaceous matter. When the Carlin ore presents sulfides and carbonaceous matter, it can be classified as double-refractory gold ore (Tabatabaei, 2011).

These deposits were named Carlin after the first large deposit found with this composition in the Carlin Unconformity, Nevada, USA. These deposits can be found in western North America and south-west China (Tabatabaei, 2011; Chryssoulis & McMullen, 2005). The unique characteristics of Carlin-type gold deposits can be summarised as (Michaud, 2015):

- Hosted in ‘dirty carbonate’ rocks.
- Gold occurs in disseminated microscopic form, embedded in pyrite and arsenopyrite.
- The absence of silver and base metals.
- Large size (100s to 1000s of tonnes of Au) (Cline et al., 2005).

The composition of Carlin-type pyrite contains 1 to less than 10 wt.% As and several hundred to several thousand parts per million of Au, Sb, Tl and Hg. The gold to silver ratios generally exceeds 10 and base metal contents are typically low (Meffre, et al., 2016).

The mineralogy of the deposits consists of associations of Au with As, Sb, Tl, and Hg in preference to base metals and Ag. Gold is mainly deposited in gold-bearing arsenian-pyrite and marcasite, quartz, kaolinite, dickite, and illite. These minerals are fine-grained and typically volumetrically minor to insignificant in comparison to the

host-rock minerals that include quartz, micas, and clay minerals, dolomite, calcite, pyrite, and various forms of carbon (Cline et al., 2005). The typical mineral groups in this type of ore are shown in Table 2-1.

Because of the nature of gold in refractory ores, the recovery via cyanidation is not satisfactory, accounting for less than 80%, according to Fraser et al. (1991).

Table 2-1 - Mineral grouping of the double-refractory gold ore (Tabatabaei, 2011)

Mineral grouping of the double-refractory gold ore					
Pyrite	Pyrite	Arsenopyrite	Arsenian Pyrite		
Carbonaceous matter					
Carbonates	Calcite	Dolomite			
Quartz	Quartz				
Clays	Kaolinite	Illite	Mica	Chlorite	
Others	Apatite	Barite	Goethite	Rutile	Illmenite
	Pyrrhotite	Realgar	Chalcopyrite		

The processing routes to treat refractory ores, especially the Carlin-type is often complex and involves high capital and operating costs because of the high costs associated with the processes required to break the refractory matrix to liberate the gold.

2.4 Pyrite and Arsenopyrite in Gold-Bearing Ores

Pyrite is the sulfide mineral most commonly associated with gold, while arsenopyrite is the second (Marsden & Iain House, 2006). A list of pyrite and arsenopyrite physical and chemical properties is provided in Table 2-2.

Table 2-2 – Properties of pyrite (Hudson Institute of Mineralogy, 2018)

Property	Pyrite	Arsenopyrite
Formula	FeS_2	FeAsS
Impurities	Ni,Co,As,Cu,Zn,Ag,Au,Tl,Se,V	Ag,Au,Co,Sn,Ni,Sb,Bi,Cu,Pb
Transparency	Opaque	Opaque
Colour	Greenish-black, brassy yellow	Silver-white to steel-gray
Lustre	Metallic	Metallic, Sub-Metallic
Hardness	6 - 6½ on Mohs scale	5½ - 6 on the Mohs scale
Tenacity	Brittle	Brittle
Fracture	Irregular/Uneven	Irregular/Uneven
Density	4.8 - 5 g/cm^3	6.07 g/cm^3
Cleavage	cubic	Distinct/Good

Pyrite and arsenopyrite have the capacity of bearing significant amounts of gold in the solid structure. The capacity for bearing gold in arsenopyrite is higher than pyrite because of the atomic spacing in arsenopyrite structure. It has been found that the gold content in the arsenopyrite can vary from less than 0.2 to 15,200 g/t, while in pyrite Au has only been observed up to 132 g/t. This characteristic makes pyrite and arsenopyrite the main carrier of gold in some ores (Chryssoulis & McMullen, 2005).

The beneficiation of refractory gold ores, in which gold is locked in arsenopyrite and pyrite, usually includes pre-concentration by flotation and a stage to break the sulfide matrix prior cyanidation. The process stage to break the sulfide matrix usually consists of the oxidation of the sulfide mineral to liberate gold. The oxidation can be done either via bacterial oxidation (BIOX process), pressure oxidation (POX) or roasting. Due to the high cost of the oxidation processes, a pre-concentration of the sulfide minerals prior to oxidation is usually required (Adams, 2016; Fraser et al., 1991).

2.5 Fundamental Principles of Flotation of Pyrite and Arsenopyrite

Flotation is commonly used to pre-concentrate pyrite and arsenopyrite in refractory gold-bearing ores. The flotation properties of arsenopyrite and pyrite are very similar (Adams, 2005).

Flotation, according to Wills & Finch (2012), is defined as:

'A separation process that exploits natural and induced differences in surface properties of the minerals, whether the surface is readily wetted by water, that is, hydrophilic, or repels water, that is, hydrophobic. If hydrophobic the mineral particle can attach to air bubbles and be floated.'

Flotation is a physicochemical-based separation process involving three phases: solid, liquid and gas (Crozier, 1992). The process usually takes place in a tank, where the pulp consisting of valuable and gangue minerals and reagents is agitated and aerated. The hydrophobic particles attach to bubbles and are collected in the froth phase as a concentrate. Hydrophilic minerals are discharged as tailings (Crozier, 1992; Wills, 1988; Sutherland & Wark, 1955). This principle is illustrated in Figure 2-3.

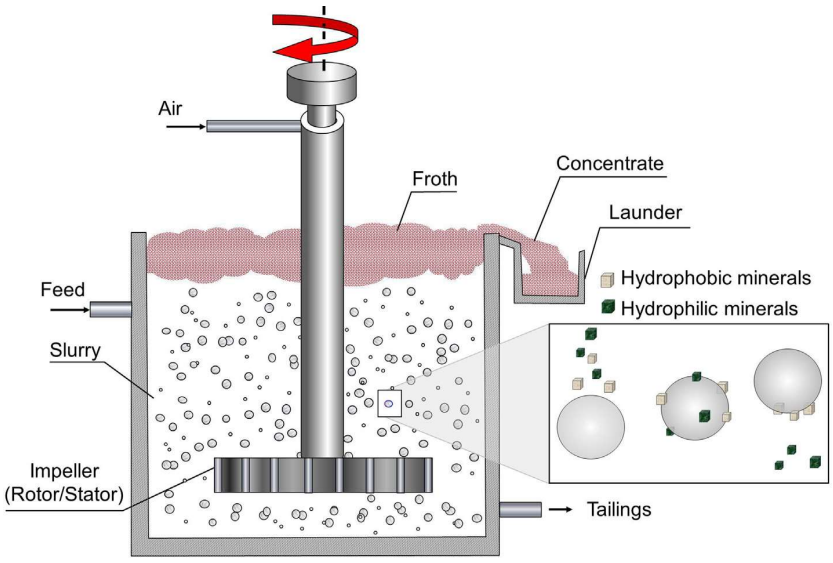

Figure 2-3 – Principles of flotation (Wills & Finch, 2016)

The efficiency of the process depends on the valuable minerals selectively attaching to the bubbles, so that the particle-bubble aggregate can rise to the froth phase, while the gangue particles, which contain no-valuable minerals, are collected in the tailings (Vianna, 2004, Woods, 2003; Sutherland & Wark, 1955).

The selective attachment of a particle to a bubble depends on the particle hydrophobicity. Figure 2-4 (a) illustrates the forces that hold the particle-bubble aggregate together. The terms $\gamma_{s/a}$, $\gamma_{s/w}$ and $\gamma_{w/a}$ are the surface tensions between solid,

air and water (Ralston et al., 2001). Figure 2-4 (b) shows a representation of the contact angle θ.

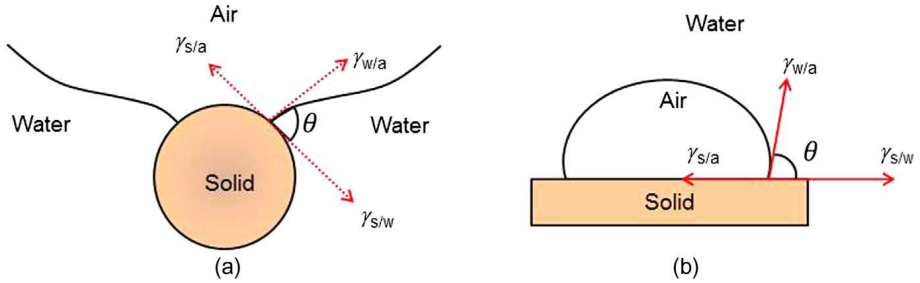

Figure 2-4 – (a) Particle attached to the bubble and, a classic representation of contact angle and surface tension forces (Wills & Finch, 2016).

The contact angle can be used as a 'proxy' for particle hydrophobicity as it increases with the mineral hydrophobicity (Wills & Finch, 2016). Highly naturally hydrophobic minerals such as graphite, sulfur, molybdite, diamond, coal, and talc present a contact angle between 60° and 90° and therefore can be directly floated (Wills & Finch, 2016; Vianna, 2004; Woods, 2003). The hydrophobicity of a mineral particle is a surface property that is either defined by the natural composition of the mineral or created by surface modification by the use of reagents (Wills & Finch, 2016).

The particles from the pulp can be recovered to the froth in flotation due to three mechanisms (Sutherland & Wark, 1955; Rickard & Ralston, 1917):

1. Selective attachment to air bubbles, or 'true flotation.'

2. Entrainment in the water, which passes through the froth.

3. Physical entrapment between particles in the froth attached to air bubbles.

King (2012) proposed that the floatability of minerals is characterised by a series of flotation sub-processes in order to a particle being successfully collected to the froth phase:

1. *'The particle must achieve a level of hydrophobicity that will permit it to attach to a rising bubble.'*
2. *'The particle must be suspended in the pulp phase of the cell.'*
3. *'The particle must collide with a rising bubble.'*

4. *'The particle must adhere to the bubble.'*
5. *'The particle must not detach from the bubble during passage through the pulp phase.'*
6. *'The particle must not detach from the bubble as the bubble leaves the pulp phase and enters the froth phase.'*

These basic sub-processes governs the rate of recovery of the valuable minerals and can be represented by collection efficiency (E_{coll}), which is a function of the efficiency of particle-bubble collision (E_c), attachment (E_a) and stability (E_s) (Derjaguin & Dukhi, 1961):

$$E_{coll} = E_c \, x \, E_a \, x \, E_s \qquad \text{(Equation 2-1)}$$

According to Duan et al. (2003): 'Collision is dominated by bulk hydrodynamics inside the flotation cell (e.g., bubble velocity and turbulence), while attachment is dominated by the interfacial behaviour between the particle and bubble (e.g., particle hydrophobicity influences thin film drainage). As for stability, its efficiency depends on both hydrodynamics and interfacial events'.

Flotation can be described by a pseudo-first-order kinetic model, by analogy with chemical reactions, in which the reactants are bubbles and particles and the product is the bubble-particle aggregate (Amelunxen & Runge, 2014; Sandoval-Sambrano, 2013; Vianna, 2004; Beloglazov, 1939). Flotation recovery is calculated as per equation 2-2, where R is recovery, k is the flotation rate constant and t is time.

$$R = 1 - e^{-kt} \qquad \text{(Equation 2-2)}$$

The collection efficiency, or flotation rate constant, is a function of particle size and contact angle, bubble size and velocity (Duan et al., 2003).

2.6 Factors that Affect Flotation Performance

Klimpel (1984) was the first to propose a diagram to summarise the factors that affect flotation performance. Figure 2-5 presents the Klimpel (1984) diagram modified by

Vianna (2004). Vianna (2004) describes the ore characteristics from the Klimpel (1984) diagram as mineralogy, texture and liberation.

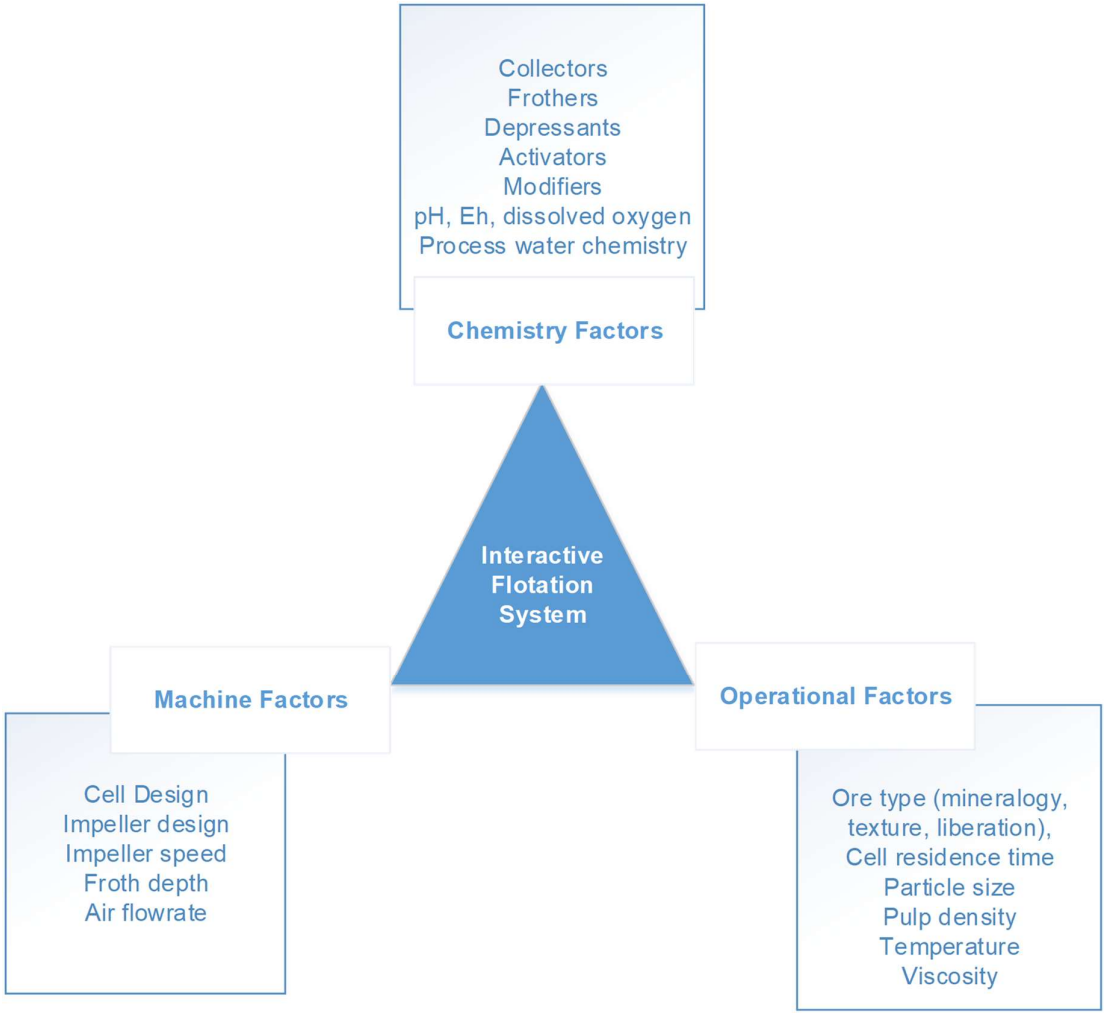

Figure 2-5 – Factors affecting flotation, modified from Klimpel (1984) and Vianna (2004)

This section of the literature review discusses the factors presented by Klimpel (1984) and how they potentially affect flotation performance and the flotation rate constant (k) of arsenopyrite and pyrite, through their influence on particle-bubble collision, attachment and detachment.

2.6.1 Role of Reagents in the Flotation of Arsenopyrite and Pyrite

Reagents are used in flotation to enhance the selectivity of the valuable minerals from gangue. A summary of the reagent types and functions in flotation is shown in

Table 2-3 (Fuerstenau et al., 2007; Crozier, 1992; Fuerstenau and Herrera-Urbina, 1989; Fuerstenau et al., 1985).

Table 2-3 – Role of reagents in flotation

Reagent type	Function
Activators	Modify mineral surface to enhance floatability and collector adsorption
Collectors	Enhance hydrophobicity of minerals
Frother	Promote froth formation and preservation of bubbles
Modifiers	Changes the action of the collectors
Depressants	Increase the selectivity by preventing the flotation of gangue
Dispersants	Acts on aggregates to improve selectivity

The role of the typical reagents used in the flotation of arsenopyrite and pyrite are summarised in this section. It focusses at presenting the mechanism of the action of the common reagents used for arsenopyrite and pyrite flotation.

2.6.1.1 Activators

Activators generally consist of inorganic salts that react with the mineral surface, resulting in a product that is more reactive with the collector, therefore enhancing the collector coverage of the particle. The selection of the appropriate activator depends on the mineral to be floated, and the collector selected (Fuerstenau et al., 2007).

Copper sulfate is a widely used activator in pyrite flotation because copper acts as an activator for pyrite. The hydrophobicity of pyrite is enhanced significantly when activated by copper, in a range of pulp potentials from -505 to +595 mV, and in the range of pH from 4.7 to 11 (Moslemi & Gharabaghi, 2017).

The proposed mechanism of activation is that Cu^{2+} adsorbs on the sulfide sites at slightly acidic pH and is reduced to Cu^{+} as the disulfide is oxidised (Moslemi & Gharabaghi, 2017; Fuerstenau et al.; 2007). The formation of $Cu(OH)_2$ is observed at pH values greater than 6 (Fuerstenau et al.; 2007). In alkaline pH conditions, the activation of pyrite by copper occurs by the adsorption of Cu^{2+} as $Cu(OH)_2$, followed by formation of Cu(I)S through the oxidation of sulfide S_2^{1-} or polysulfide S_n^{2-} (Moslemi & Gharabaghi, 2017).

The adsorption of cupric ions decreases with the increase of pulp potential because of the increase of pyrite surface oxidation, reducing the sites available for copper adsorption (Moslemi & Gharabaghi, 2017).

As well as pyrite, copper ions activate arsenopyrite. The activation occurs due to the formation of copper arsenosulfide (CuAsS) at low pH and copper arsenate ($Cu_3(AsO_4)_2$) or arsenite ($Cu_3(AsO_3)_2$) at high pH (Valdivieso et al., 2006; Wang et al.; 1989).

2.6.1.2 Collectors

The hydrophobicity of minerals can be enhanced by collectors, which facilitates the attachment of the mineral particle to the bubbles. Collectors are organic compounds with polar and non-polar components (Fuerstenau et al., 2007; Fuerstenau and Herrera-Urbina, 1989). The polar component adsorbs to the mineral, and the non-polar fraction facilitates the adsorption to air bubbles. A diagram of collector adsorption on the mineral surface is shown in Figure 2-6.

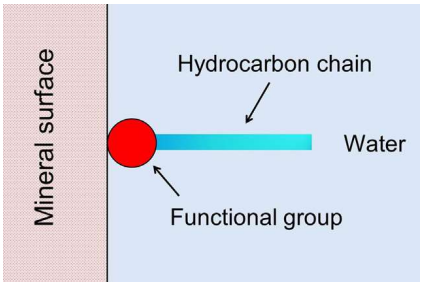

Figure 2-6 - Adsorption of the collector on the mineral surface showing the hydrocarbon chain oriented toward the water and making the site hydrophobic (Wills & Finch, 2016)

Collectors such as xanthates, dithiophosphates, dithiocarbamates, fatty acids, and amines are widely used in the flotation of sulphide minerals. The xanthates are the most commonly used collector for arsenopyrite and pyrite. Potassium amyl xanthate (PAX) is the collector selected for the flotation of arsenopyrite and pyrite in the White Mountain project. The formula of PAX is $C_6H_{11}KOS_2$, and its structure is shown in Figure 2-7.

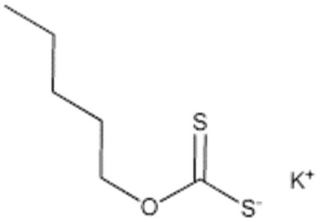

Figure 2-7 - Potassium Amyl Xanthate structure (Harrison, 2018)

The mechanisms by which xanthates adsorb on the pyrite surface is dependent on the pulp potential, surface oxidation and degree of activation of pyrite. In non-activated pyrite, the xanthate adsorption process happens in four steps, as described by Wang (1995):

1- Surface oxidation of pyrite.
2- Xanthate ion adsorption on pyrite surfaces and formation of ferric xanthates.
3- Xanthate ion oxidation and dixanthogen formation.
4- Dixanthogen adsorption on pyrite through ferric xanthates.

A schematic of the oxidation of pyrite and dixanthogen formation in non-activated pyrite in the presence of xanthate is shown in Figure 2-8.

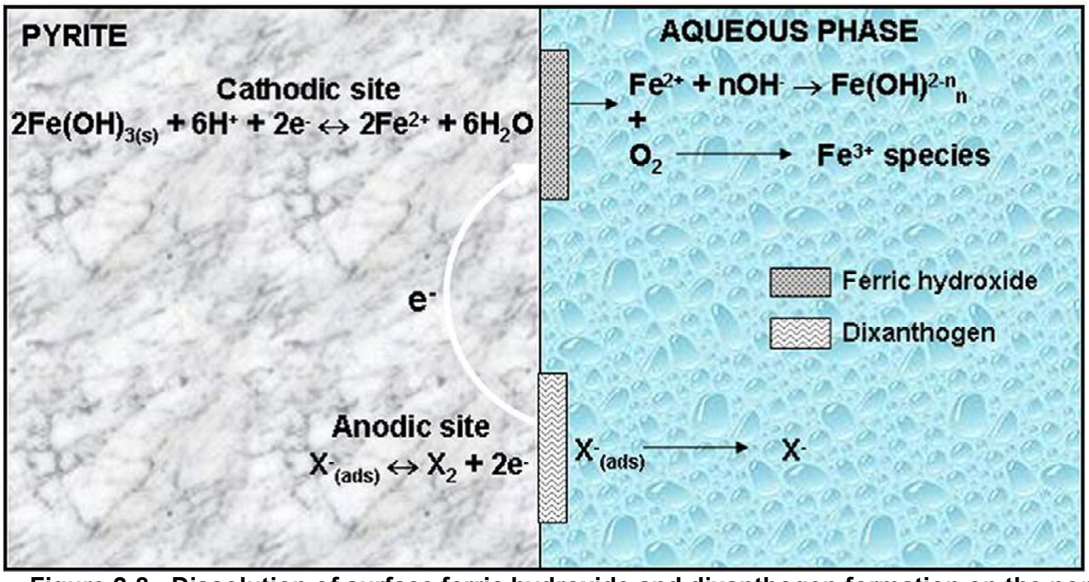

Figure 2-8 - Dissolution of surface ferric hydroxide and dixanthogen formation on the non-activated pyrite surface with xanthate addition (Original picture from Valdivieso et al., 2005, redrawn by Moslemi & Gharabaghi, 2017)

The mechanism of adsorption of xanthate on arsenopyrite surfaces is associated with the oxidation of xanthate ions (X^-) to dixanthogen (X_2). The formation of dixanthogen on arsenopyrite is favourable at lower pH values. As reported by Gaudin (1957) and Sirkeci (2000), the highest flotation recovery of arsenopyrite when using xanthates occurs at pH 4 to 5 (Valdivieso et al., 2006).

The mechanism of adsorption of xanthates when pyrite is activated by copper occurs by the formation of a monolayer of cuprous xanthate, which is a hydrophobic product of the reaction of xanthate with the copper-activated surface (Moslemi & Gharabaghi, 2017; Chandra & Gerson, 2009; He, Fornasiero, & Skinner, 2005).

In addition, Valdivieso et al. (1994) observed that the activation by copper ions reduces the xanthate dosage required for arsenopyrite flotation.

The review presented in this section indicated that in the presence of Cu ions, the preferential mechanism of collection of pyrite and arsenopyrite is via the formation of cuprous xanthate instead of the adsorption of dixanthogen (Moslemi & Gharabaghi, 2017). Consequently, as pointed by Valdivieso et al. (1994), it can be advantageous using Cu ions as an activator for pyrite and arsenopyrite as it can reduce the consumption of xanthate.

2.6.1.3 Frother

According to Klimpel and Isherwood (1991), the key functions of frothers in flotation are:

- Aid formation and preservation of small bubbles.
- Reduce the bubble rise velocity.
- Aid formation of froth.

Frothers promote the formation of a stable froth so that valuable minerals are collected concentrate, and the return of these minerals to the pulp via drainage is minimised. The frother type and frother dosage also affect the bubble size in the pulp. Increase in frother concentration can result in an increase in the number of bubbles, which increases the total surface area of bubbles, leading to an increase of the collision

probability between particles and bubbles, thus increasing flotation kinetics (Zhang et al., 2012; Cho & Laskowski, 2002)

Examples of the structures of three frothers widely used in flotation are shown in Figure 2-9. The White Mountain project is designed to use a mixture of Methyl Isobutyl Carbinol (MIBC) and F549.

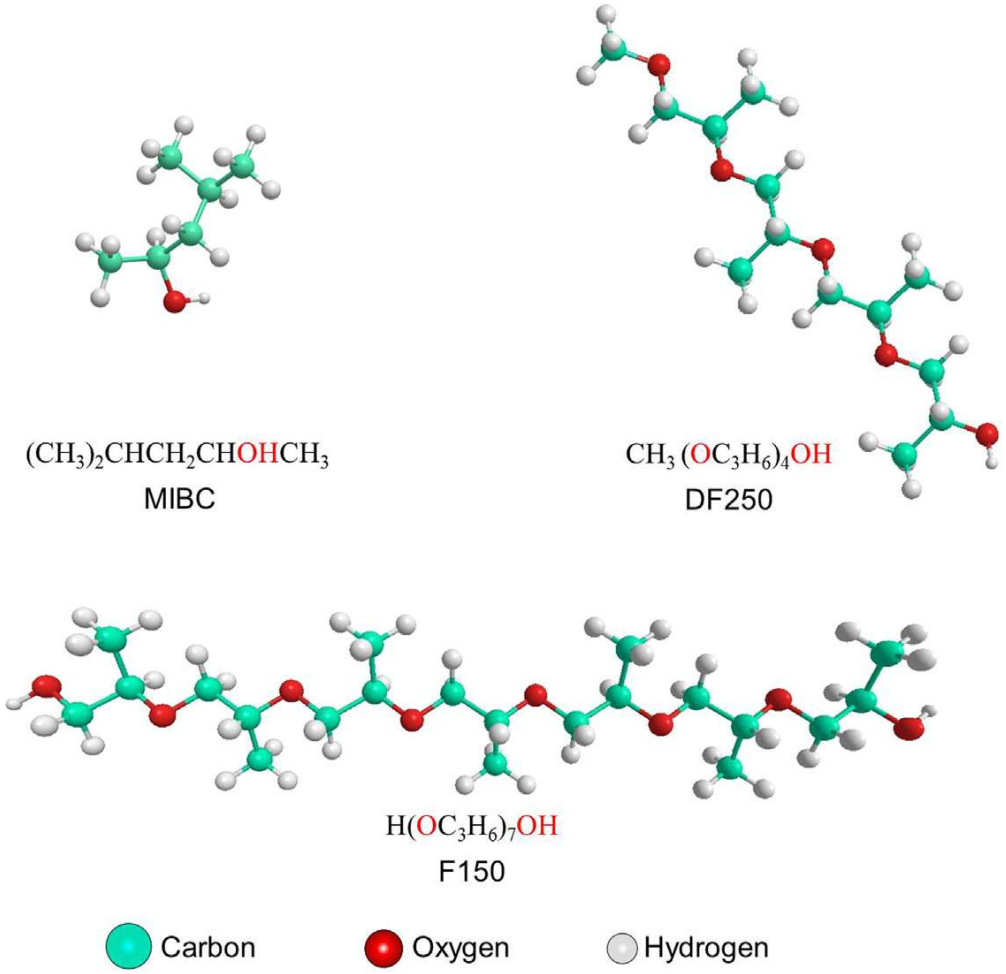

Figure 2-9 - Example structures of three frothers: MIBC, DF250, and F150 (Wills & Finch, 2016)

The increase of frother concentration in a flotation system leads to the reduction of the bubble Sauter mean diameter (D_{32}). An illustration of the reduction of bubble Sauter diameter (D_{32}) with an increase of frother concentration is shown in Figure 2-10.

The frother critical coalescence concentration (CCC) is the minimal concentration of frother, where the minimum (D_{32}) is reached (Cho & Laskowski, 2002). Any increase in frother dosage above the CCC has no effect on the pulp bubble size.

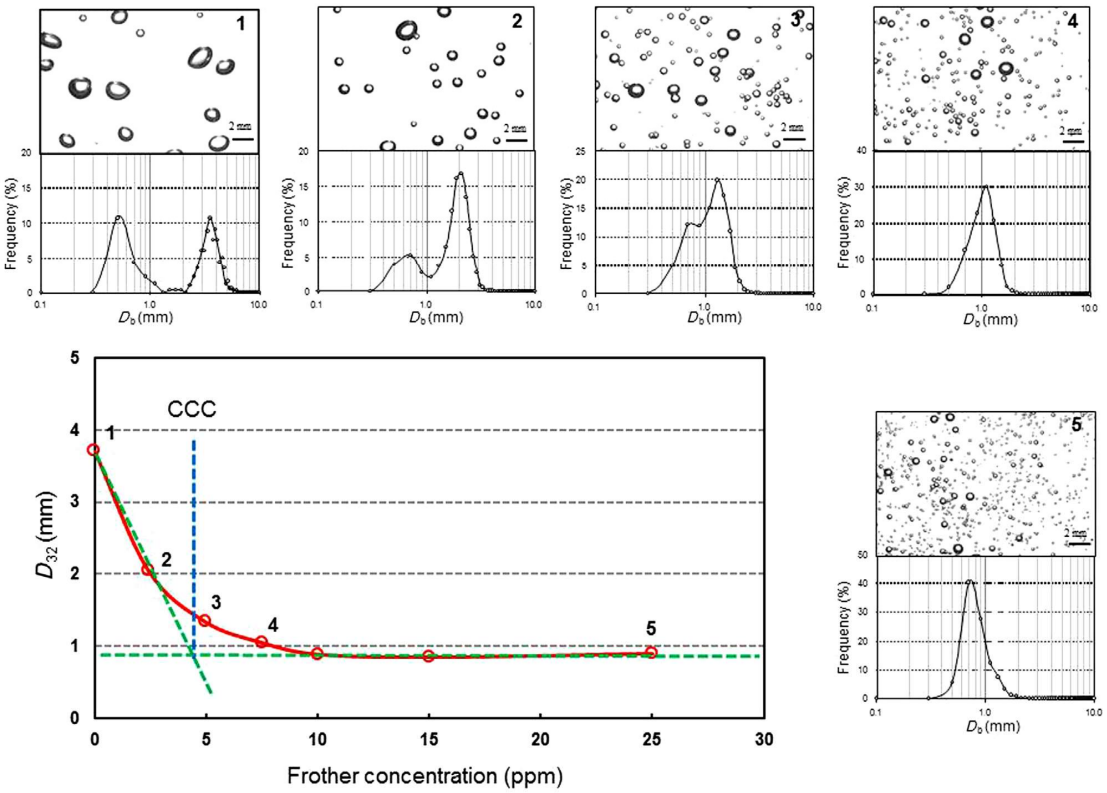

Figure 2-10 - Reduction in bubble size (Sauter mean diameter) as a function of frother concentration illustrated with images and number frequency distribution. (Wills & Finch, 2016; adapted from Nesset and Finch, 2013).

Jiang and Holtham (1986) studied the particle-bubble collision efficiency. The study concluded that the collision efficiency is inversely proportional to the bubble size and directly proportional to particle size. Thus, the reduction of bubble size increases the collision probability, for the same feed size distribution. Later, this relationship was found to be true for fine particles (<75 μm) by Igusti-Ngurah (1989).

Tan et al., (2013); Gupta et al. (2007) and Harvey et al. (2005) observe that by increasing the frother dosage, the bubble size decreased and the air holdup and foamability increased, as shown in Figure 2-11.

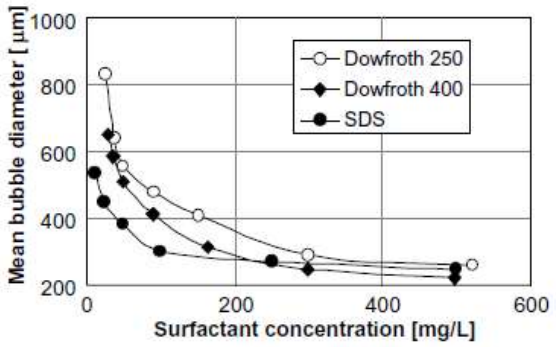

(a)

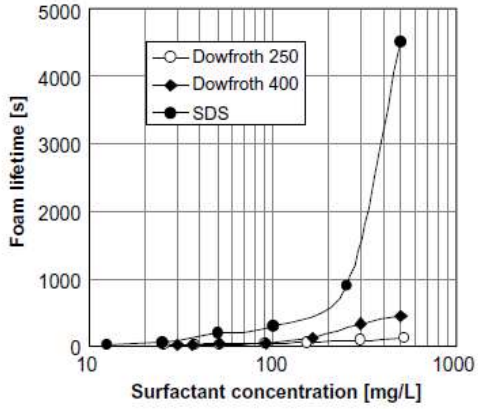

(b)

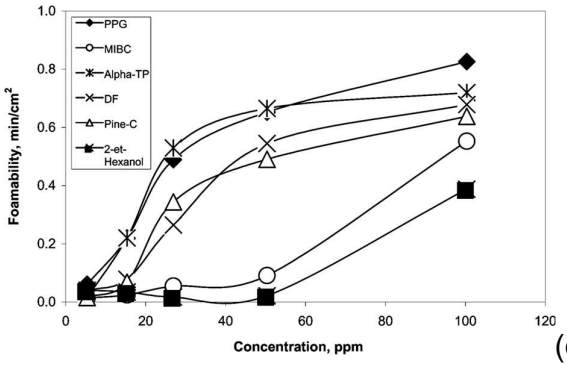

(c)

Figure 2-11 – (a) Mean bubble diameter versus surfactant concentration (Gupta et al. 2007); (b) Foam lifetime versus surfactant concentration measured at 4.4 cm/s superficial airflow rate (Harvey et al. 2005); (c) Foamability as a function of frother concentration (Gupta et al. 2007)

2.6.1.4 Modifiers

A broad range of reagents can be classified as modifiers according to the mechanism by which it changes the action of the collector. There is no consensus of a single classification of modifiers with it including pH modifiers, froth modifiers, depressants, dispersants activators, deactivators, promoters, viscosity modifiers and slime-blinding

modifiers (Fuerstenau et al.; 2007). According to Nagaraj (2005), the modifiers consist of the third apex of the reagents triangle, as per Figure 2-12.

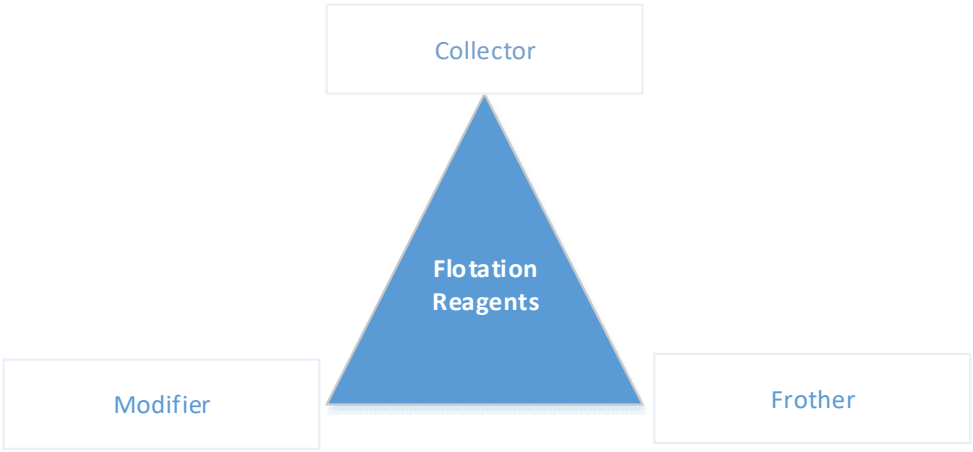

Figure 2-12 – Flotation reagent triangle

The modifiers used in the White Mountain flotation design consisted of pH modifiers and dispersant. The pH is the most important modifier in the flotation of pyrite and arsenopyrite because it affects pulp potential, the mechanism of activation by copper ions and the mechanism of adsorption of xanthate, the dispersion of the pulp and the degree of oxidation of the sulfide minerals (Kawatra and Eisele, 2001).

2.6.1.5 Depressants

Depressants are used in flotation to improve the selectivity of flotation to the mineral of interest and inhibit the collection of undesirable minerals to the froth. There are several mechanisms by which depressants can inhibit the flotation of a given mineral, such a deactivation by removing the activating species and inhibition of the collector from the mineral surfaces (Fuerstenau et al., 2007).

The pH can act as an activator or depressant, as it controls the collector adsorption reactions at the mineral surface. The optimum flotation pH for pyrite is in the range from pH 4 to 8 due to the presence of dixanthogen on the surface of pyrite. Depression is observed below pH 2 and above pH 12. The depression at an acidic pH is due to decomposition of xanthate, while at an alkaline pH it is because of the thermodynamic instability of the dixanthogen at high concentrations of OH^- (Fuerstenau et al., 2007).

The depression of pyrite is associated with the increase of hydrophilic ferric hydroxide coverage on the surfaces of pyrite. This can occur in the range from pH 5 to 9 at low concentrations of xanthate. The increase of xanthate concentration leads to the dissolution of surface-ferric hydroxide phase, increasing the floatability of pyrite (Deng et al., 2013; Valdivieso et al.,2005).

Cyanide is used to depress pyrite because it reacts with the pyrite surface, forming ferric ferrocyanide complex, a more stable species than ferric xanthate, which is hydrophilic and capable to dissolving metal xanthates from sulfide surfaces, blocking the collector adsorption sites. (Fuerstenau et al., 2007).

Arsenopyrite is depressed at high pH and under oxidising conditions. Reagents such as hydrogen peroxide (H_2O_2), potassium permanganate ($KMnO_4$), manganese dioxide (MnO_2) and hypochlorous acid (HClO), ammonium–magnesium salts, strontium and barium ions promote the depression of arsenopyrite and inhibit activation by copper ions (Valdivieso et al., 2006).

2.6.1.6 Dispersants

Dispersants act on the surface of the particles by modifying the surface charge, which makes the particles less prone to aggregation. Dispersants can also be used in conjunction with depressants. Some examples of reagents used as dispersants include sodium silicate, sodium hydrosulfide and sodium sulfide (Fuerstenau et al., 2007).

2.6.2 Pulp density and Viscosity

Shi and Napier-Munn (1995) affirms that the viscosity of the pulp is a function of particle size, solids concentration, temperature and pH. The composition of the slurry, not studied by the former, is also a factor that affects viscosity, as suggested by the studies of Cruz et al. (2013) that observed an increase in viscosity when the proportion of clays increased in the mineral system.

According to Ralston et al. (2007), the slurry viscosity affects both the energy dissipation profile through the cell and bubble rise velocity. Hence, it will directly affect the bubble-particle collision frequency, consequently the flotation kinetics.

Shabalala et al. (2011) found an increase in solids concentration led to a decrease in the gas holdup, accompanied by a decrease in bubble size. The decrease of bubble size was attributed to the effect of solids concentration on slurry viscosity. The increase in viscosity results in the formation of a 'cavern' of slurry around the impeller. This phenomenon resulted in poor dispersion of bubbles throughout the cell, resulting in low gas hold-ups (Shabalala et al., 2011).

2.6.3 Ore Characteristics

2.6.3.1 Particle size

Flotation performance is strongly related to ore properties such as particle size, liberation and surface properties. These relationships are interconnected; therefore, the discussion about the effect of particle size assumes that the particles are fully liberated.

Flotation performance is strongly related to ore properties with particle size, liberation and surface properties all play a role. These relationships are interconnected; therefore, the discussion about the effect of particle size assumes that the particles are fully liberated.

The effect of particle size in flotation has been known since the work of Gaudin et al. (1931), who studied the optimum particle size for the recoveries of lead, zinc and copper. Trahar (1981) proposed a size-by-size floatability relationship (cited by Vianna, 2004).

According to Trahar (1981), as shown in Figure 2-13, the intermediate sizes presented higher recoveries. The low recovery of the fine sizes was attributed to insufficient collision rates due to the low inertia of the particles. Figure 2-14 illustrates this reduction in the kinetics of fine particles by converting the recoveries of Figure 2-13 to flotation rate constants (Wills & Finch 2016).

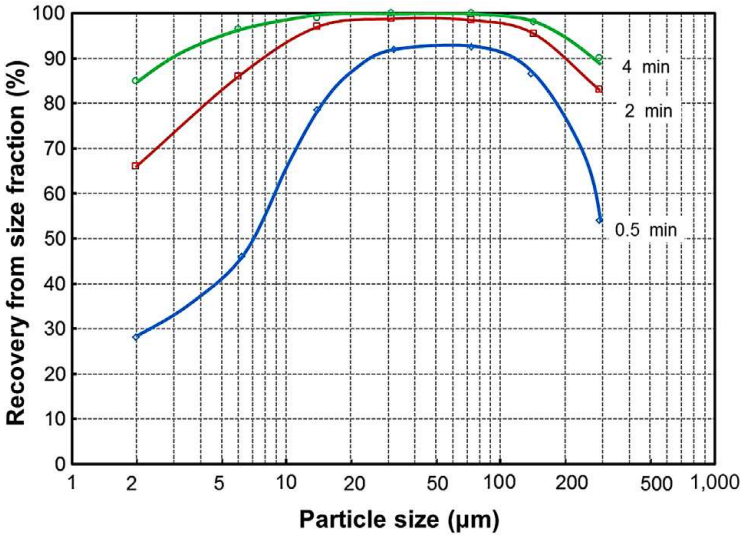

Figure 2-13 - Typical recovery trend as a function of particle size and time (Wills & Finch, 2016; adapted from Trahar, 1981).

As per Figure 2-13 and Figure 2-14, the coarse particles also present poor flotation kinetics. This is associated with a decrease of stability of attachment, which increases the detachment probability (Wills & Finch 2016; Cheng & Holtham, 1995).

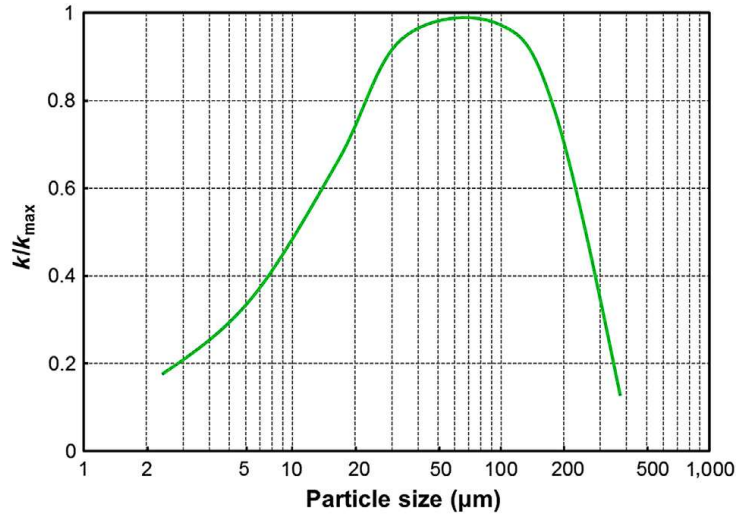

Figure 2-14 - Trend in Figure 2-13 converted to the relative rate constant (relative to the maximum rate constant, k/kmax) as a function of particle size (Wills & Finch, 2016).

2.6.3.2 Mineralogy and Particle Composition

The hydrophobicity of a particle depends on its composition. The flotation separability of a composite particle, expressed as flotation rate constant, as proposed by Evans (2010), is a proportional sum of the flotation rate of the mineral components on the particle surface. An example of this approach for a three-component particle is shown in Figure 2-15. The calculation is shown in equation 2-3 (Wightman & Sandoval, 2011).

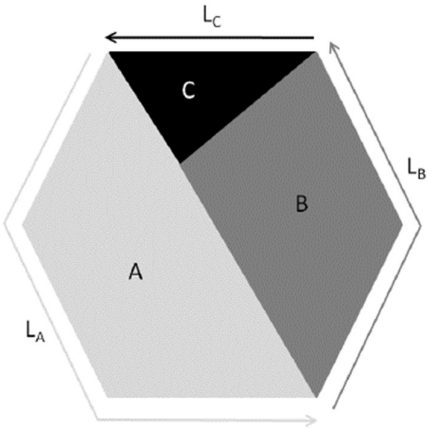

Figure 2-15 - Schematic representation of a composite particle containing three minerals (A, B and C) and their corresponding exposed perimeters LA, LB and LC (Evans, 2010)

$$k_{particle} = \frac{k_A L_A + k_B L_B + k_C L_c}{L_A + L_B + L_C} \quad \text{(Equation 2-3)}$$

2.6.3.3 Liberation

Liberation and composition are interconnected particle properties. The term liberation represents the extent to which a particle is composed of one mineral component and increases with size reduction. A liberated particle contains one mineral (Evans & Morrison, 2016).

An increase in liberation is usually associated with an increase in mineral surface exposure. An increase in the proportion of the floatable mineral on the particle surfaces, according to equation 2-3, increases the particle flotation rate.

The flotation rate constant has been shown to be a strong function of liberation is shown in Figure 2-16, based on the recovery-by-size-by liberation, data reproduced by Welby et al. (2010). Figure 2-16 shows that as liberation increases, the flotation rate increases.

Liberation is usually poorer for the coarser particles than the fines, and this is another reason for the observed decrease in the flotation rate of coarser particles.

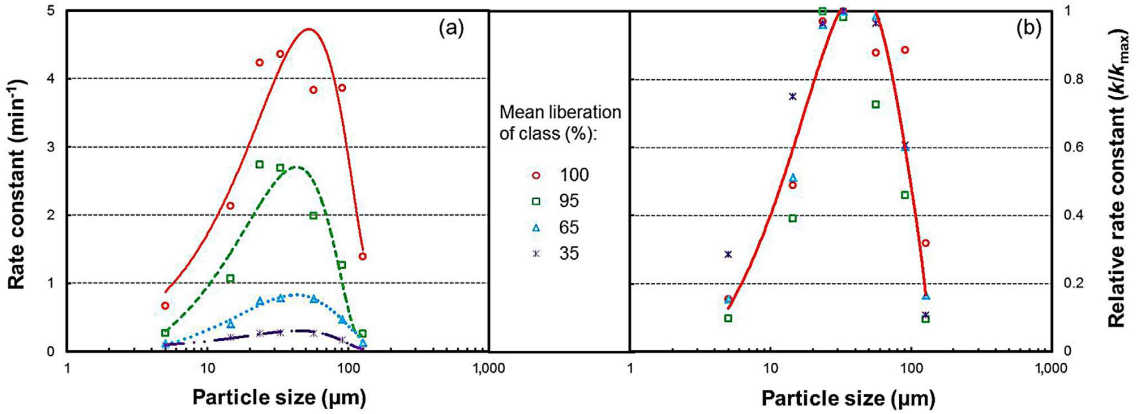

Figure 2-16 - (a) Rate constant-by-size-by-liberation, and (b) same data but as rate constant relative to the maximum rate constant showing a common trend among size classes (Data from Welsby et al.,2010 cited by Wills & Finch, 2016).

2.6.3.4 Particle shape

Vizcarra (2010) found that particles of chalcopyrite with angular shape have faster flotation kinetics compared with rounded shaped chalcopyrite particles. The angular shaped particles of chalcopyrite had higher coverage of hydrophobic polysulfide species, which could be enhancing the particle attachment to the bubbles.

2.6.3.5 Surface chemistry

As discussed in the previous sections of this literature review, the particle hydrophobicity has a fundamental role in flotation efficiency and kinetics. Collectors, activators and depressants are agents that modify the surface chemistry of particles to enhance (or inhibit) the particle hydrophobicity. Ions in solution originated from the dissolution of gangue minerals can also modify the surface chemistry of the interest minerals, therefore, affecting the flotation performance and kinetics.

Brito e Abreu (2010) studied the correlation between the chemistry of chalcopyrite surfaces, surface hydrophobicity and chalcopyrite recovery. The hydrophobicity property measure was the contact angle. The surface chemistry properties were obtained via Time-of-Flight Secondary Ion Mass Spectrometry (ToF-SIMS).

The work of Brito e Abreu et al. (2010) classified the species found on the surface of chalcopyrite into hydrophobic or hydrophilic categories, according to the effect of the presence and concentration of those species on the contact angle of chalcopyrite particles. The higher the contact angle, the higher the flotation recovery. Table 2-4 summarises the species found in the hydrophobic and hydrophilic categories.

Table 2-4 – Hydrophobicity classification of the chemical species found on the surface of chalcopyrite based on Brito e Abreu et al. (2010)

Hydrophobic	Hydrophilic
Cu, S, SO_2/S_2, CuO, and collector fragment C_7H_7O	F, Na, Ca, O, Si, Mg, and K Fe, FeO, FeOH, FeOOH, and SO_3

The hydrophilic species F, Na, Ca, O, Si, Mg, and K originated from oxidation and gangue minerals, such as clays, while the species Fe, FeO, FeOH, FeOOH, and SO_3 originated from the oxidation of the chalcopyrite surface (Brito e Abreu et al., 2010).

Basnayaka et al. (2017) studied the effect of the concentration of Ca^{2+} ions on the flotation kinetics of gold-bearing pyrite ore. It was observed that the flotation rate of pyrite decreases with the increase of Ca^{2+} ions in solution. The origin of the Ca^{2+} ions in the flotation feed was the leaching of Ca from kaolin and bentonite. The results of Basnayaka et al. (2017) align with the Brito e Abreu et al. (2010) proposition that Ca ions are hydrophilic species that can reduce the hydrophobicity of sulphide minerals.

2.6.4 Equipment Factors

The equipment factors listed by Klimpel (1984), which affects flotation kinetics include:

- Airflow rate.
- Bubble size.
- Impeller speed.

The airflow rate and bubble size affect the flotation rate constant because they affect the bubble surface area flux (S_b). The bubble surface area flux (S_b) is given by equation 2-4 (Finch & Dobby, 1990; Jamerson & Allum, 1984, cited by Gorain, 1998).

$$S_b = \frac{6J_g}{D_{32}} \qquad \text{(Equation 2-4)}$$

Where J_g is the superficial gas (air) velocity, airflow rate divided by the cell cross-section area, and D_{32} is the bubble Sauter mean diameter.

The bubble surface area flux has been found to be directly proportional to the flotation rate constant, as shown in Figure 2-17 (Alexander et al., 2000).

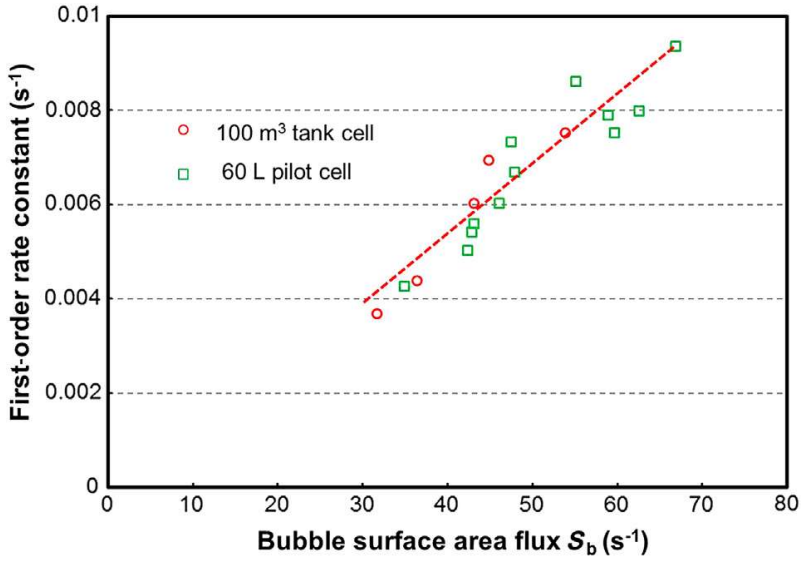

Figure 2-17 - First-order rate constant and S_b relationship in a 60 L pilot cell and a 100 m³ cell (Wills & Finch, 2016, adapted from Alexander et al., 2000).

Therefore, increases in airflow and/or reduction in bubble size increases the flotation rate constant.

Increased impeller speed promotes suspension of the particles in the cell and dispersion of the gas in the pulp, therefore, promoting particle collision and attachment to bubbles. It is believed to increase the degree of turbulence in the cell, which promotes bubble-particle attachment. The detachment probability increases with an increase in particle size and the degree of turbulence in the flotation cell. The impeller

speed can increase the recovery of fines but decrease recovery of the coarse particles, which are more susceptible to detachment (Xu et al., 2011; Cheng & Holtham, 1995; Sutherland, 1948; cited by Gorain, 1998).

2.6.5 Froth Phase and Stability

In the froth phase, only a fraction of particles that attach to bubbles are effectively transported to the concentrate launder are hydrophobic.

The structure and stability of the froth affect the concentrate mineral grade and recovery to the concentrate. Moreover, the factors that affect the froth structure and stability affects the flotation performance (Farrokhpay, 2011).

The froth recovery (R_f) is given by Savassi et al. (1997) in equation 2-5:

$$R_f = \frac{Mass\ rate\ of\ particles\ reporting\ to\ the\ concentrate\ via\ true\ flotation}{Mass\ rate\ of\ attached\ particles\ at\ the\ pulp - froth\ interface}$$

(Equation 2-5)

The froth stability can be quantified by using the dynamic stability factor, Σ, calculated by equation 2-6.

$$\Sigma = \frac{V_f}{Q} = \frac{H_{max}A}{Q} \qquad \text{(Equation 2-6)}$$

Where V_f is the froth volume, Q is the gas volumetric flow rate, H_{max} is the maximum equilibrium height achieved, and A is the cross-sectional area of the column (Sheni et al., 2018; Bikerman, 1973).

The residence time of the bubbles in the froth phase is a function of the superficial gas velocity, froth depth and cell characteristics (Zanin et al., 2009). Furthermore, gas flow rate and cell geometry are key parameters affecting the froth recovery.

Hadler et al. (2012) in the study of the relationship of gas flow rate and flotation performance suggested that the highest cumulative grade and recovery was obtained when the flotation circuit was operating at an intermediate gas flow rate.

The frother type and concentration play an important role of bubble coalescence and froth stability. According to Subrahmanyam & Forssberg (1988), cited by Aktas et al. (2008), frothers reduce the surface tension of the air-liquid interface to produce stable bubbles.

The froth stability is also a function of the nature, size and hydrophobicity of particles. The froth height in a froth stability column increases with the increase of the proportion of fine particles in a froth (Zanin et al., 2009; Aktas et al., 2008). The froth can be destabilised and destroyed by a particle of all sizes when they are extremely hydrophobic (Dippenaar, 1982; Harris, 1982; cited by Farrokhpay, 2011). According to Ata et al. (2003), the maximum froth stability is achieved when the froth phase is loaded with moderately hydrophobic particles (Zanin et al., 2009).

Sheni et al. (2018) observed the effect of pulp potential (Eh), pH, dissolved oxygen (DO) and ionic strength (IS) in the froth stability of PGM bearing ores from South Africa via stability column and batch flotation tests. The study concluded that the increase of IS, pH and Eh, and the decrease of DO, improved the froth stability and changes in the bubble size in the froth, with the exception of changes in DO resulting in no perceived effect on bubble size.

Farrokhpay and Zanin (2012) have shown that the concentration of ions such as Al and Ca in the slurry changes froth stability as the froth height increases with the increase of ions in the slurry.

2.7 The Role of Non-Sulfide Gangue in Flotation

2.7.1 Definition of gangue

'As generally used, gangue minerals have no commercial importance in a particular period of time, possibly becoming ore minerals at a later date. They are commonly silicates, carbonates, or fluorides, more rarely sulfides.' (Fairbanks, 1981)

2.7.2 Mechanisms of recovery

Gangue minerals can report to the concentrate via the following mechanisms (Duarte & Grano, 2007):

- 'True flotation' (attached to bubbles due to hydrophobicity).
- Entrainment.
- Entrapment.
- Slime coating of valuable mineral.

2.7.2.1 True flotation

Gangue can be recovered to the concentrate by natural flotation when in composite with a floatable mineral, and/or due to its natural or induced hydrophobicity (Johnson et al., 1974). Talc, pyrophyllite and carbonaceous minerals are examples of gangue minerals recovered in flotation due to hydrophobicity and attachment to bubbles (Wills & Finch, 2016; Chesworth, 2008; Vianna, 2004).

2.7.2.2 Entrainment

Entrainment is the most common mechanism of recovery of non-sulphide gangue smaller than 50 μm in particle size. The recovery by entrainment is due to suspended gangue minerals being carried to the froth phase by water (Wang, 2016; Johnson, 2005; Savassi, 1998).

According to Wang (2016), valuable and gangue minerals experience entrainment. The mass transfer throughout a flotation cell is shown in Figure 2-18 follows as:

1. *'Transfer of valuable mineral particles to the froth from the pulp by true flotation.'*
2. *'Transfer of valuable mineral particles to the concentrate from the froth by true flotation.'*
3. *'Transfer of mineral particles to the froth from the pulp by entrainment.'*
4. *'Transfer of entrained mineral particles to the concentrate from the froth by entrainment.'*
5. *'Transfer of mineral particles from the froth to the pulp due to the drainage of detached particles and entrained particles.'*

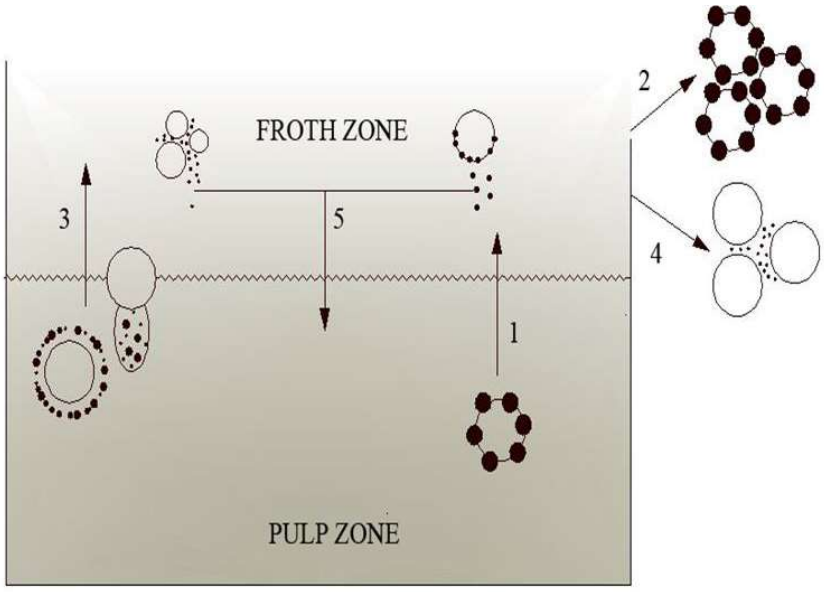

Figure 2-18 - Mechanisms of transfer of fully liberated mineral particles in a flotation cell (Wang, 2016)

Wang (2016) presented in his work an in-depth review of entrainment modelling. Therefore, this thesis comments on the fundamental factors that affect entrainment instead of giving a detailed discussion on this subject.

According to the work of Johnson et al. (1974), the degree of entrainment of gangue tends to 1 for the -10 μm size-fraction, decreases sharply with the increase of gangue particle size, and increases with a rise in pulp density.

Wang, Runge, & Peng (2015), as well as Johnson et al. (1974) and Johnson (2005), observed that particle size affects the degree of entrainment. The work of Wang, Runge, & Peng (2015) noted that entrainment was not only a function of particle size, but it also remarked that particle density, frother type and concentration, feed grade, and the interaction between gas rate and froth height affects the degree of entrainment. Those factors were not listed in the research of Johnson et al. (1974) and Johnson (2005).

Entrainment is also a function of particle shape and pulp viscosity, parameters not investigated by Wang, Runge, & Peng (2015). Wiese at al. (2015) investigated the relationship between entrainment and shape using a range of hydrophilic minerals, including ballotini, mica, talc (coated with a hydrophilic resin), vermiculite and

wollastonite. These materials represented groups of particles with different aspect ratios as per Figure 2-19 and Table 2-5.

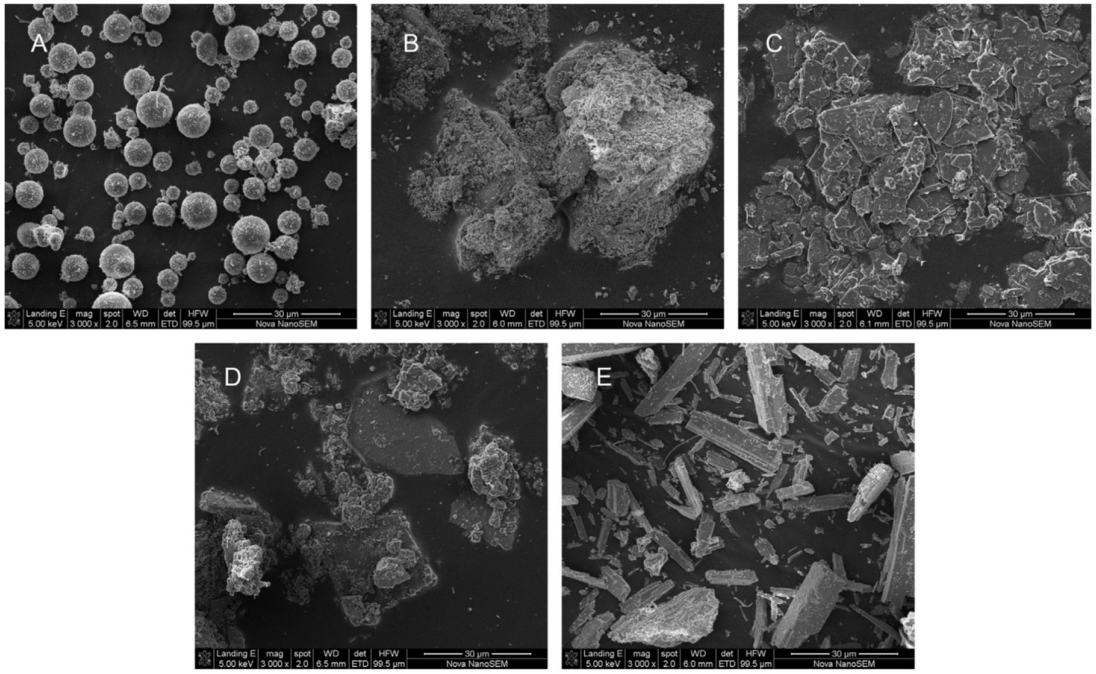

Figure 2-19 - SEM images (3000x magnification) of the minerals used: (A) – ballotini, (B) – mica, (C) – talc, (D) – vermiculite, (E) – wollastonite, (Wiese et al., 2015).

Table 2-5 – Aspect ratio for the different minerals used in Wiese et al. (2015) study (particle size 40 µm)

Sample	Ballotini	Talc	Vermiculite	Mica	Wollastonite
Aspect Ratio (short/long axis)	0.83	0.59	0.53	0.50	0.32

The study of Wiese et al. (2015) demonstrated that particles with different shapes in the same size class have different entrainment rates, as shown in Figure 2-20.

Note that the degree of entrainment can be inferred by the slope of the relationship between and mass recovery.

According to Figure 2-20 shape types more prone to entrainment are the acicular and platy, represented by Wollastonite in Figure 2-19 and, Wollastonite and Wollastonite/Ballot in Figure 2-20. This shape type has the lowest aspect ratio, according to Table 2-5. The effect of shape on entrainment was sustained even at different pH conditions, as shown in Figure 2-21.

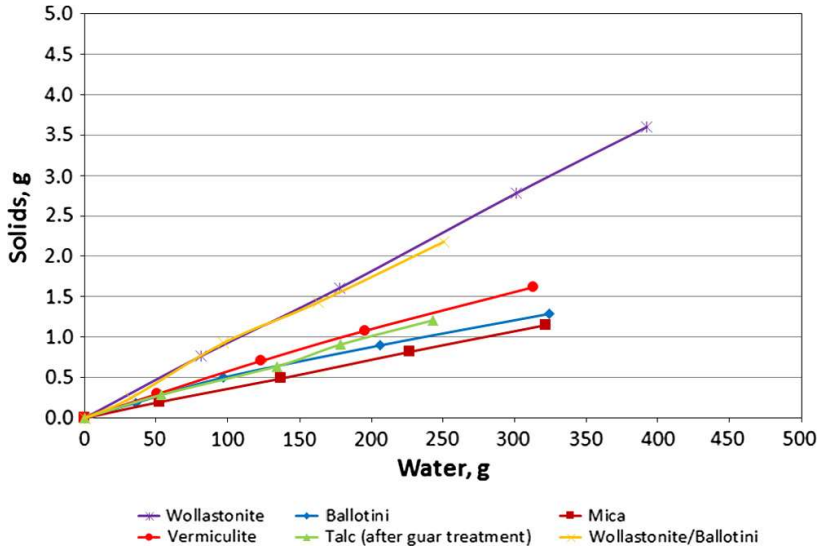

Figure 2-20 - Mass of solids recovered as a function of the mass of water recovered for the minerals used in this study at pH 8 (Wiese et al., 2015).

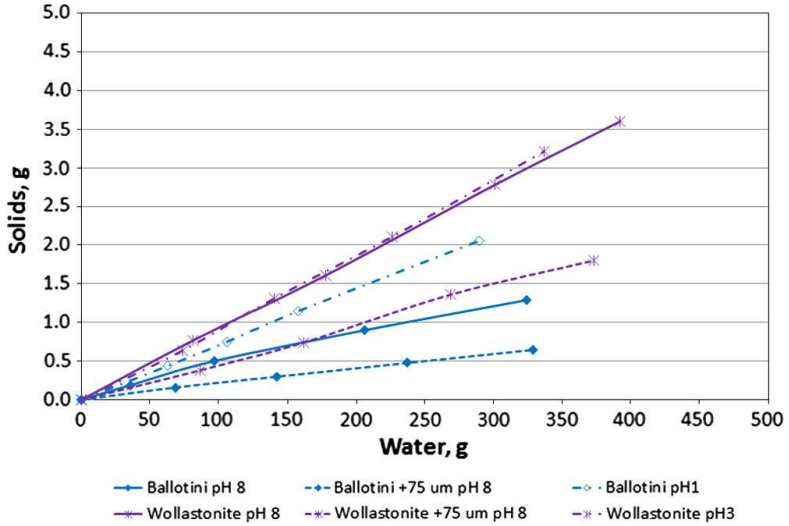

Figure 2-21 - Mass of solids recovered as a function of the mass of water recovered for ballotini and wollastonite at different pH and d_{80} values (Wiese et al., 2015).

2.7.2.3 Entrapment

Entrapment is an additional mechanism associated with entrainment in which gangue is entrapped in the plateau borders at highly mineralised froths, not able to drain back to the pulp phase. The diagram presented in Figure 2-22 illustrates the mechanism of gangue entrapment (Johnson, 2005; Vianna, 2004).

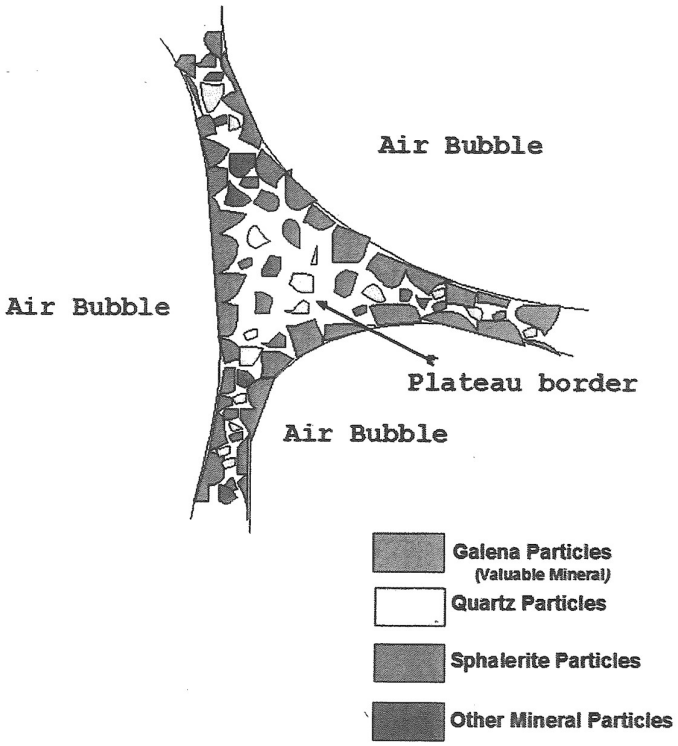

Figure 2-22 – Diagram illustrating the entrapment, Vianna (2004).

The mechanism of gangue recovery by entrapment can be detected by high values of entrainment (ENTi), greater than 1 unit, and recovery of coarse liberated gangue in the size range between 50 and 200 μm (Johnson, 2005).

2.7.2.4 Slime coating of valuable mineral

Fine gangue can attach to valuable minerals surface due to electrostatic attraction forces, forming an agglomerate. Slime coatings can affect the flotation rate constant and final recovery of the valuable minerals (Forbes et al. 2014; Ndlovu, 2013, He et al., 2009).

2.8 The Effect of Phyllosilicates in Flotation

This section is focussed on reviewing the behaviour of phyllosilicates in flotation. It defines phyllosilicate minerals, the problems associated with phyllosilicate minerals in the flotation of sulphide ores, the classification of muscovite in the phyllosilicate

mineral group, the behaviour of muscovite in flotation and a potential explanation of its recovery mechanisms.

2.8.1 Definition of Phyllosilicate Minerals

Phyllosilicate minerals consist of a group of silicate minerals built of tetrahedral 'T' and octahedral 'O' layers. Figure 2-23 shows the classification of several groups of phyllosilicate minerals (Ndlovu et al., 2014; Farrokhpay & Bradshaw, 2012; Vaughan & Pattrick, 1995).

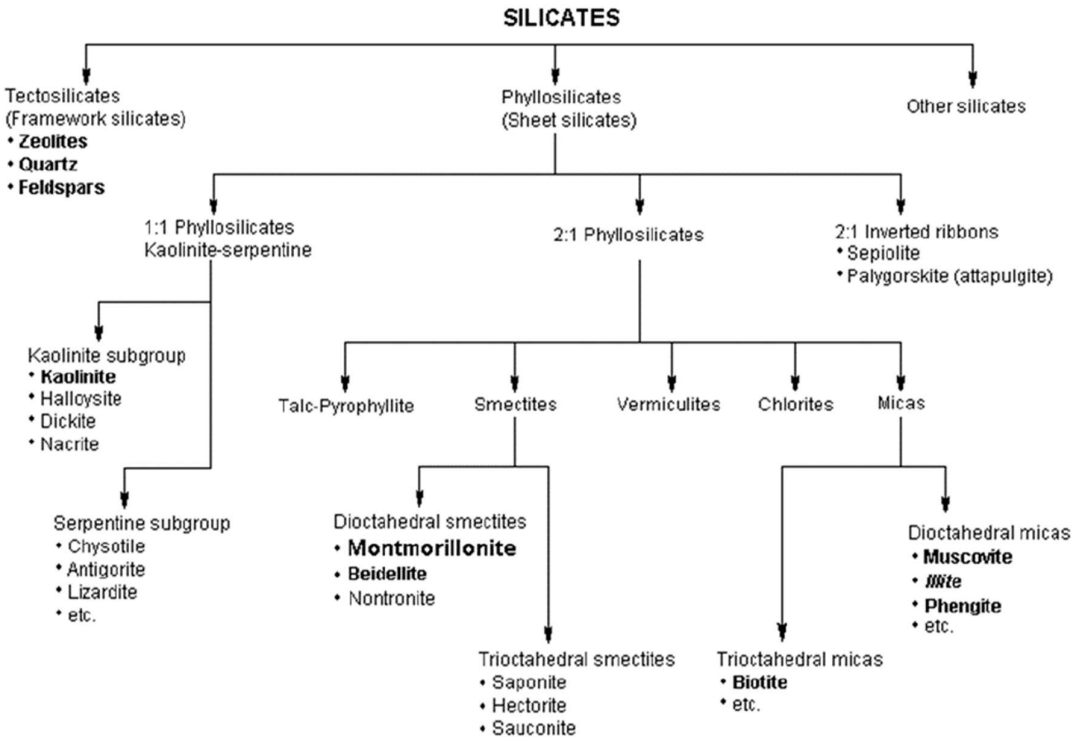

Figure 2-23 – Classification of clay minerals (Brindley, 1951; Farrokhpay & Bradshaw, 2012)

The groups of phyllosilicates are classified according to the proportion of tetrahedral and octahedral layers, and the connectors between the successive layers. The 'T' and 'O' layer configuration for several clay and mica minerals is shown in Figure 2-24.

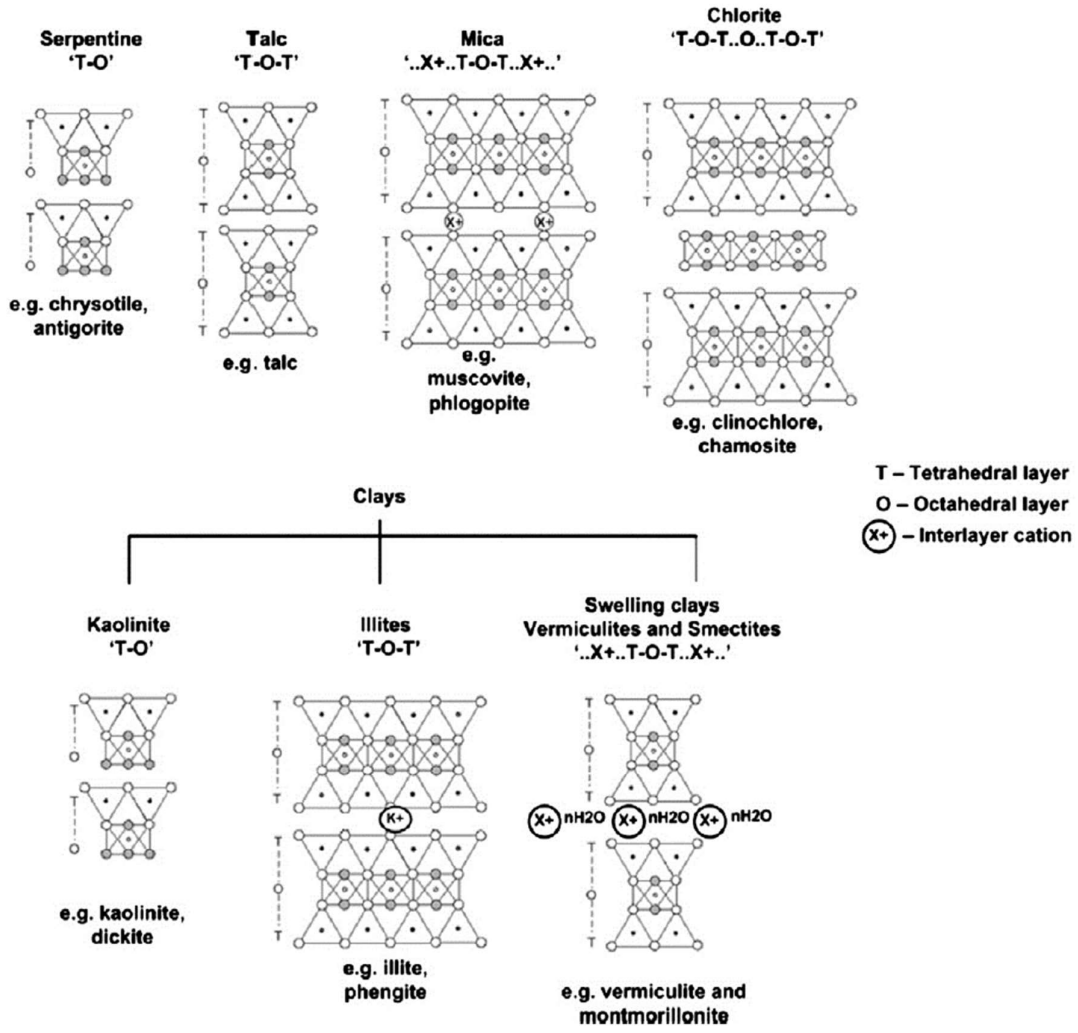

Figure 2-24 – Tetrahedral layer structure of phyllosilicate minerals (Ndlovu et al., 2014)

According to Grafe et al. (2017), *'clays have been variously described as particles of any composition below a certain size and/or as the phyllosilicate mineral group or part thereof and/or as materials that display certain physical properties such as plasticity when wet or hardening upon drying.'* Therefore, the chosen definition of clays is '*naturally occurring fine-grained phyllosilicate minerals plastic when wet harden on drying or firing'*.

Clay minerals can also be classified as swelling and non-swelling clay minerals. The swelling behaviour is associated with the capacity of the clay mineral to absorb a large amount of water, increasing in volume. Vermiculite and smectite present this property and are consequently classified as swelling clays, while kaolinite and illite are classified as non-swelling (Ndlovu et al., 2014; Ndlovu et al., 2011).

Mica minerals present perfect cleavage and have a flaky shape, formed by numerous stacked sheets, easily separated to as thin as 20 μm by delamination (Schoeman, 1989). The layer structure of micas presents the form 'X^+..T-O-T. X^+' as shown in Figure 2-24. Muscovite is a typical mica mineral classified as a genuine dioctahedral mica, and it is considered a non-swelling clay. The octahedral inter-layer sites of muscovites are occupied by Al^{3+} and Si^{4+} in a ratio close to 1:3. Illite is an interlayer-deficient mica with a layer structure very similar to muscovite, differing by the inter-layer species H_3O^+ replacing K^+. Micas can be transformed into swelling clays by weathering. Muscovite can be converted to illite, later transformed into vermiculite and smectite, resulting in a swelling behaviour, as shown in Figure 2-25 (Brigattia, et al., 2013; Bergaya & Lagaly, 2013; Ndlovu et al., 2011).

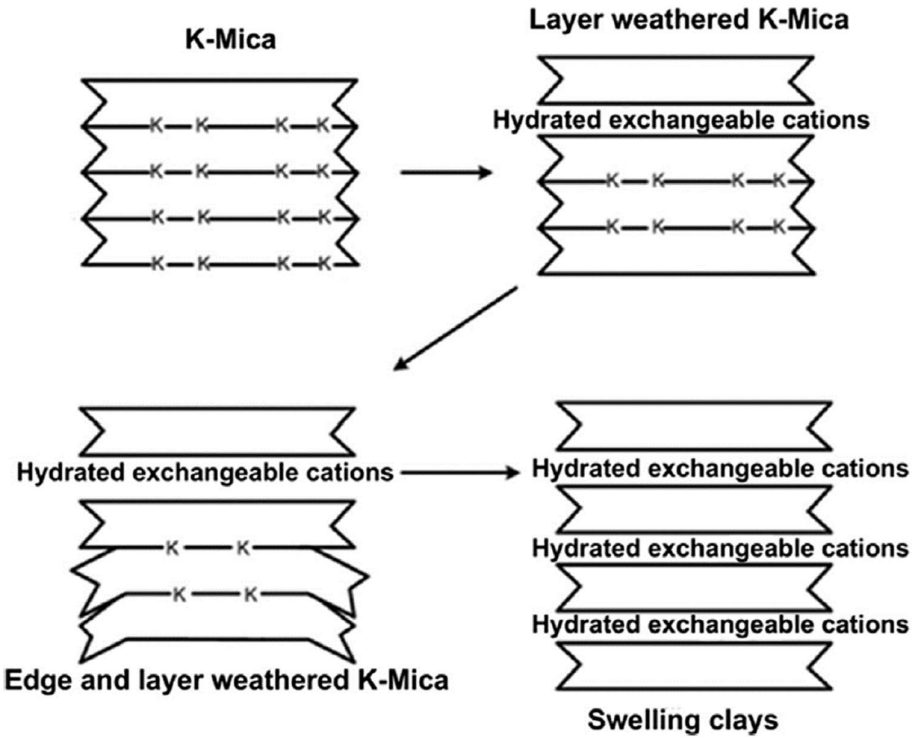

Figure 2-25 – Schematic illustrating the transformation of muscovite to vermiculite (Ndlovu et al., 2011)

Because of the platy nature of phyllosilicates, the mineral particles have distinct basal faces and edges, which presents different surface charge, becoming charge anisotropic. The basal plane charge is not solely negative. Its charge is pH-dependent. The edges faces are dominated by negative charges over most of the pH range

(Forbes and Chryss, 2017). The aluminol (-AlOH) and silanol (−SiOH) groups exposed on the edges of the particle may protonate or deprotonate, by H^+ and OH^- ions, depending upon pH (Forbes and Chryss, 2017; Nosrati et al., 2012). The illustration of the influence of pH on the surface charge of the faces and edges of kaolinite particles, expressed as zeta potential, is shown in Figure 2-26.

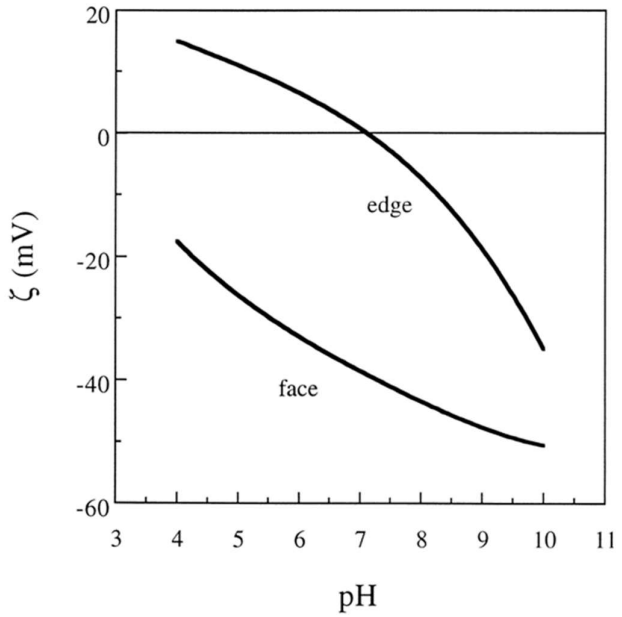

Figure 2-26 - The zeta potential properties of the edge and face surfaces of kaolinite in the presence of 0.01M NaCl background (Ndlovu, 2013)

Estimation of the surface charge of anisotropic minerals is not trivial. The use of zeta potential measurements to determine the surface charge of anisotropic minerals is not the most appropriate method because it represents an apparent value, which is the average zeta potential of the particle planes. Potentiometric titrations are the most accepted and widely used method to estimate the net surface charge density of anisotropic minerals, as it accounts for the H^+ and OH^- on the mineral surface (Forbes and Chryss, 2017).

The particle-particle association of phyllosilicate minerals depends on the surface charge of particle facets and the pH. The possible orientation of particle-particle association is shown in Figure 2-27.

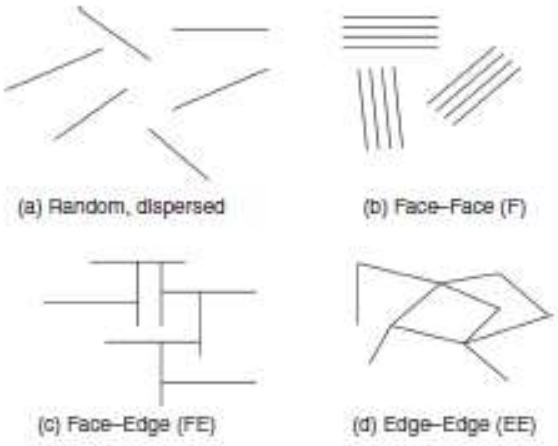

Figure 2-27 - Possible orientation of clay particles (van Olphen, 1951; cited by Forbes and Chryss, 2017)

The orientation of the particle associations, as shown in Figure 2-27, is pH-dependent and influence the rheological behaviour of the system, as shown in Figure 2-28.

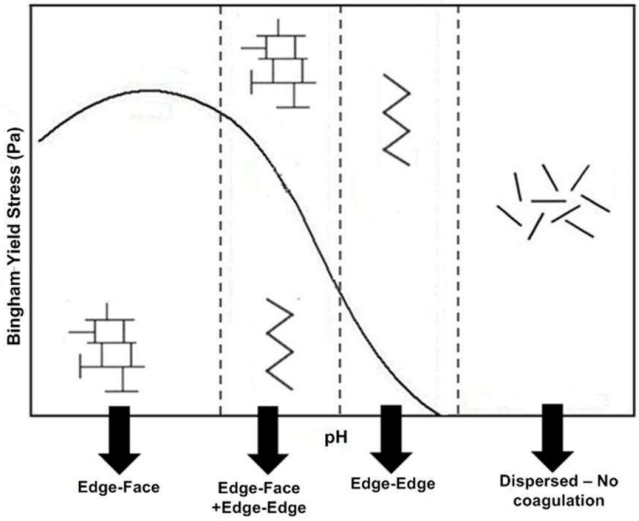

Figure 2-28 - Schematic representation of the modes of particle interaction inhomogeneous mineral suspensions as a function of pH and Bingham yield stress (Rand and Melton (1977) cited by Ndlovu, 2013).

2.8.2 The Detrimental Effect of Phyllosilicate Minerals in Mineral Processing

Clays and phyllosilicate minerals are typical gangue minerals associated with many valuable minerals, such as copper, nickel, iron, gold and uranium. Many processing problems in slurry transportation, beneficiation, dewatering and disposal are

associated with phyllosilicate-bearing ores because they are ‘sticky’ and viscous (Ndlovu et al., 2013; Ndlovu et al., 2014; Connelly, 2011).

The presence of phyllosilicate minerals in slurry transportation processes reduces the pumping capacity because of the increase in slurry viscosity. In comminution circuits, the presence of phyllosilicate minerals can be detrimental, by blinding screens, and reducing the sharpness of cyclone separation. Because phyllosilicate minerals cause an increase in pulp viscosity, the grinding process should be operated at a lower density to flush the clays from the mill. (Connelly, 2011).

In tailings dams, the presence of clays reduces the water recovery, geotechnical stability and slows the drying process. High clay content in tailings leads to an increased dam footprint and selection of complex tailing treatment circuits due to the increased pulp viscosity and amount of fines (Ndlovu et al., 2013; Connelly, 2011).

Due to the high surface area, phyllosilicates are very reactive, being detrimental to the flotation performance through (Ndlovu et al., 2013; Farrokhpay et al., 2013):

- Slime coating on the mineral surfaces and air bubbles.
- Increasing reagent consumption, reduction of selectivity and impeded flotation kinetics.
- Entrainment of gangue to concentrate.
- Increasing pulp viscosity.
- Increasing or decreasing froth stability.

Farrokhpay et al. (2014) studied the deleterious effect of the different phyllosilicates in chalcopyrite flotation. The study investigated the effect of selected phyllosilicate minerals on the froth stability, copper grade in the concentre and copper recovery. It concluded that the presence of phyllosilicates affects froth stability. The effect of the different phyllosilicate minerals can be ranked in the following order: talc >> montmorillonite > muscovite > kaolinite > illite. The study observed a significant decrease in the copper concentrate grade, from 32% to 1–4%, in the presence of the phyllosilicates. The copper grade is affected by phyllosilicate minerals in the following order: talc > montmorillonite > kaolinite> illite and muscovite, at a P_{80} of 90 µm.

The study of Farrokhpay et al. (2014), at the addition of the maximum amount of illite, kaolinite and muscovite tested (30%) the Cu recovery decreased from 90% to about 88%. The Cu recovery decreased to about 80% when 10% talc or 15% montmorillonite was added. Talc and montmorillonite have shown the most significant effect of the phyllosilicate minerals on the flotation recovery and grade, as well as froth stability. Montmorillonite also causes rheology issues. The increase of the content of talc, montmorillonite and muscovite in the ore leads to an increase of maximum froth height and froth half lifetime. Kaolinite is also shown to affect the froth height at increased levels.

Phyllosilicate minerals also affect the zeta potential of chalcopyrite particles. The effect varies with the type of phyllosilicate mineral and concentration. According to Farrokhpay & Ndlovu (2013), at 30% montmorillonite and kaolinite concentration, there was a very minimal effect, while the addition of 30% muscovite to the chalcopyrite slurry resulted in the zeta potential values being closer to that of pure muscovite. It suggested that muscovite coated the full surface of chalcopyrite particles.

Farrokhpay et al. (2013) investigated the effect of clays on the rheology and flotation of a Carlin Trend ore. The dominant clay minerals identified in the samples used for the study were illite, muscovite and kaolinite. The study compared the viscosity values of the ore slurry as a function of pulp density for three different P_{80} values, 53, 106 and 125 µm. The grade–recovery relationship was measured at different flotation pulp densities for gold, sulfur, arsenic and iron. The study found a significant increase of apparent viscosity with solids concentration, with a critical solids' concentration of 25% (w/w). The viscosity increased with the P_{80} following the order 125 µm < 106 µm < 53 µm.

These results obtained by Farrokhpay et al. (2013) agrees with the observations of Shi & Napier-Munn (1995), in which the viscosity rises with the increase of fines and percentage of solids. It was found that the recoveries of Au, As S and Fe were higher at higher pulp densities. The study reported that the recoveries of Au, As S and Fe, increases with the increase of pulp densities in the following order: 18% ≈ 25% <32% <38% solids (Farrokhpay et al., 2013).

The research of Forbes et al. (2014) showed that when the concentration of kaolinite exceeds 30% of the gangue phase, the floatability of chalcopyrite reduces. The flotation rate of the slow floating chalcopyrite significantly decreases. The negative effect of kaolinite is exacerbated in acidic pH regions (below pH 6). Figure 2-29 shows the decrease in copper recovery as the ratio of kaolinite increases in the gangue.

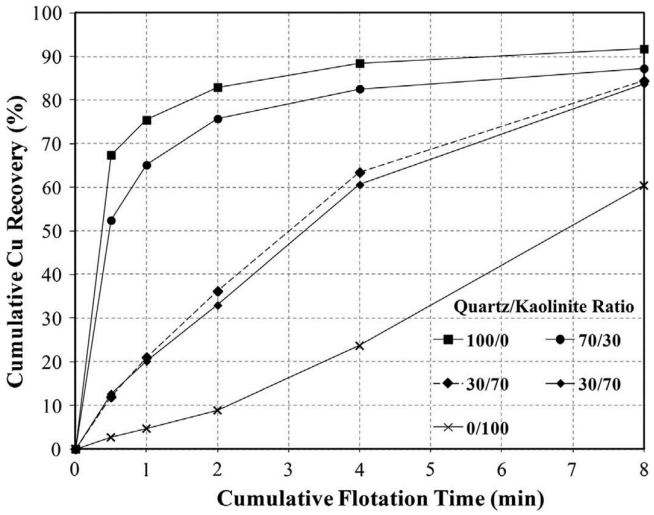

Figure 2-29 – Recovery of Cu for various ratios of quartz/kaolinite in the gangue fraction (Forbes et al., 2014).

Forbes et al. (2014) and Farrokhpay et al. (2014) found an equivalent decline in chalcopyrite recovery when the concentration of kaolinite in the pulp was 30%. However, the work of Farrokhpay et al. (2014) did not observe a further decline in recoveries, nor in flotation rates, because as demonstrated by Forbes et al. (2014), it required higher concentration kaolinite to observe a significant difference.

The presence of kaolinite increases the viscosity of the pulp because there is an increase in the effective volume of solids due to the plate-like geometry of kaolinite. The rheology effect reduced the probability of particle-bubble collision through turbulence dampening, which was used to explain the reduced flotation rate of chalcopyrite (Forbes et al., 2014).

It was not possible to isolate the effect of pulp rheology and slime coating as the two are inherently related. The two effects appear to have approximately equivalent

magnitudes, although the measured magnitude of the slime coatings effect is combined with the rheological effect (Forbes et al., 2014).

2.8.3 The Effect of Muscovite in Flotation

2.8.3.1 Muscovite

Muscovite is occasionally referred to as sericite in the literature. Sericite is defined as white fine-grained potassium mica, commonly muscovite or another mineral similar in composition to muscovite, including paragonite and illite (Hudson Institute of Mineralogy, 2016; American Geological Institute, 1997). It also includes a variety of phyllosilicates (sheet silicates) with the formula $K_2Al_4[Si_3AlO_{10}]_2(OH)_2$ formed from the alteration of feldspar by either hydrothermal alteration or later-stage weathering (Allaby, 2015). Mica is defined as the name for a group of complex sheet-layered phyllosilicate minerals, such as muscovite, biotite, phlogopite, zinnwaldite, lepidolite, roscoelite, paragonite, illite and sericite (Manutchehr-Danai, 2008).

Muscovite is a mica phyllosilicate. It is known to be an insulator. It has been used in biological research. Besides, because of its reactive surface and affinity for DNA, oligonucleotides, and lipids, muscovite become a possible template to investigate the origin of life (Leiro et al., 2017; de Poel et al., 2013; Franchi et al., 2003). The properties of muscovite are listed in Table 2-6.

Table 2-6 – Properties of muscovite (Hudson Institute of Mineralogy, 2018)

Property	**Muscovite**
Formula	$KAl_2(AlSi_3O_{10})(OH)_2$
Impurities	Cr,Li,Fe,V,Mn,Na,Cs,Rb,Ca,Mg,H_2O
Transparency	Transparent, Translucent
Colour	White, Gray, Silver white, Brownish white, Greenish white
Lustre	Vitreous, Silky, Pearly
Hardness	2½ on the Mohs scale
Tenacity	Elastic
Fracture	Micaceous
Density	2.77 - 2.88 g/cm^3
Cleavage	Perfect

Muscovite, as a dioctahedral phyllosilicate, has a 2:1 structure, consisting of an octahedral layer 'O', Al – O – M (where M is Al, or Fe, Mg), in between two tetrahedral 'T' layers, 'T-O-T', stabilised through electrostatic attraction of the interlayer cations such as K^+ or Na^+ (Nosrati et al., 2012; Ndlovu, 2013). As described by Ndlovu, (2013): '*The continuous stacking of successive T-O-T units results in the platy morphology of muscovite particles which typically exist as long, thin flaky sheets. Each plate has a distinct 'T' faces and 'TO-T' edges'*. The tetrahedral basal plane (face) is characterised by the K cations and the edge by Al.

The platy morphology of muscovite is shown in Figure 2-30 though SEM images obtained by Ndlovu (2013).

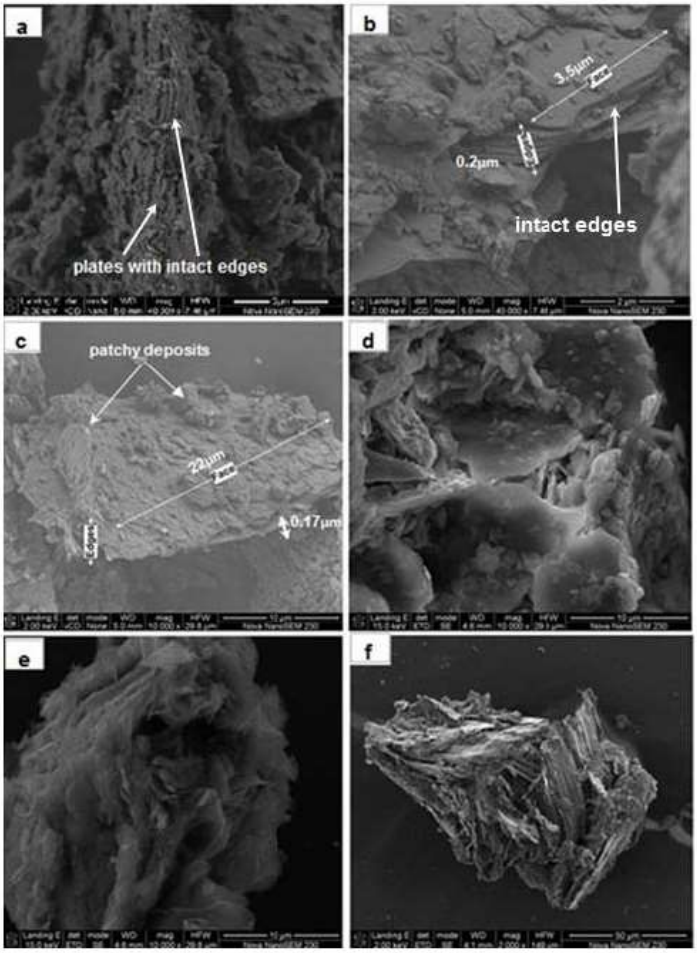

Figure 2-30 – SEM images demonstrating the platy morphology, high aspect ratio and smooth surface structure of muscovite (Ndlovu, 2013)

The atomic structure of muscovite is shown in Figure 2-31.

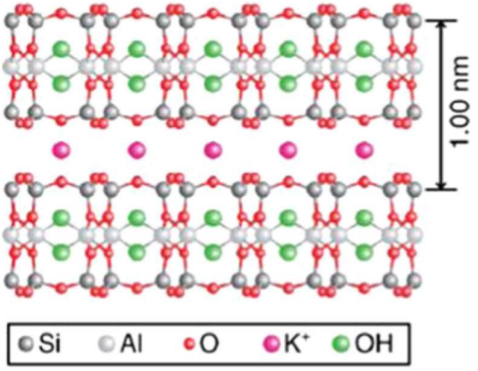

Figure 2-31 – Atomic structure of muscovite, Christenson and Thomson (2016)

Although muscovite is a phyllosilicate, it does not present 'clay-like' characteristics, according to the definition of Grafe et al. (2017), as '*naturally occurring fine-grained phyllosilicate minerals plastic when wet and harden on drying or firing'*, because it does not present swelling properties.

Figure 2-32 shows the surface charge of muscovite obtained via potentiometric titration by Ndlovu (2013). Ndlovu (2013) found an isoelectric point for muscovite at pH 4.6 $\pm$ 0.3, which is different from Scales et al. (1990) who found the zeta potential of muscovite to be negative over the pH range from 3 to 10.

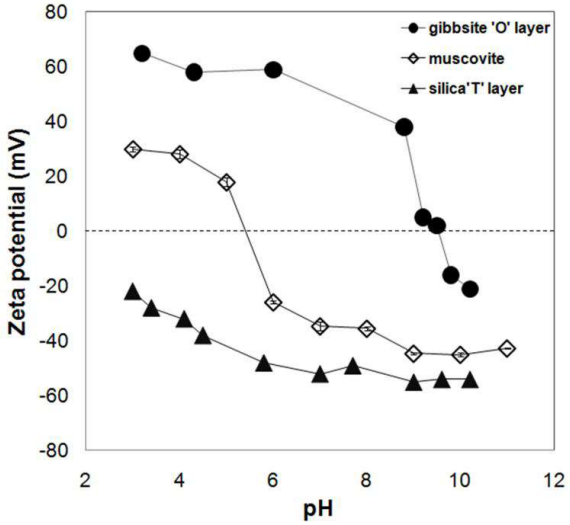

Figure 2-32 - The zeta potential of gibbsite and silica, compared to the electrokinetic zeta potential of muscovite (obtained in NaCl 0.001-0.1 M). The error bars represent 95% confidence interval of average values (Ndlovu, 2013)

The contribution of the edge faces of muscovite to the overall particle surface charge is approximately 5–10%, because the aspect ratio of muscovite is approximately 20, because of the high ratio of the surface area of basal to edge face (Maslova et al., 2004).

Muscovite can exchange the surface potassium ions for several ions in a solution including Ag, Ca, V, Mn, Fe, Ni, Cu, Zn, Co, Cs, Li, La and Cd. The occupancy of those ions on the surface of muscovite is proportional to the total ion concentration in solution (de Poel et al., 2017; Nosrati et al., 2012; Maslova et al., 2004; Scales et al.,1990).

Nosrati et al. (2009) studied the leaching of Al^{3+}, Si^{4+}, and K^{+} species from muscovite to the solution in the pH range from 9 to 2, at 8% and 57% solids by weight. The ion concentration in the solution is shown in Figure 2-33.

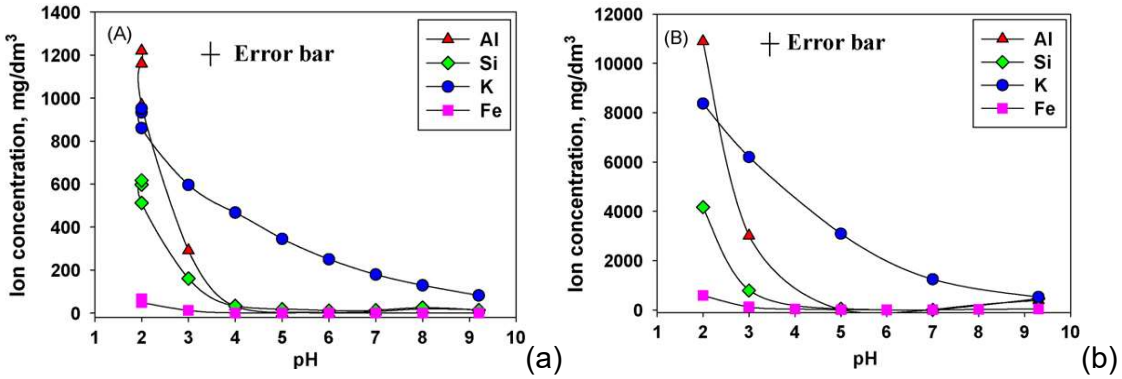

Figure 2-33 - Concentration of Al(III), Si(IV), Fe(III) and K ions leached into solution as a function of pH from muscovite dispersions in 10−3 M KNO3, measured with ICP. For both 8 wt.% (a) and 57 wt.% solid (b) dispersions (Nosrati e. al, 2009)

As shown in Figure 2-33, the leaching of K and Al increases with a decrease of pH. The increase in the percentage of muscovite in the pulp increased the concentration of K and Al ions in solution greatly.

2.8.3.2 Muscovite Behaviour in Flotation

According to Silvester et al. (2013), muscovite does not have inherent floatability but reports strongly to the concentrate.

Muscovite can be readily recovered via flotation using cationic or anionic collectors. Cationic collectors, such as amines like DTAB (Silvester et al., 2013; Nishimura et al.,

2000; Browning, 1973), can recover muscovite because the it has an overall negative charge across the entire pH range (Silvester et al., 2013; Scales et al., 1990). It also can be separated via anionic collectors, like fatty acids (Rao et al., 1995; Gaudin, 1957), and alkyl sulphates over a pH range from 2 to 8 (Sutherland and Wark, 1955).

The use of depressants, such as polysaccharides does not improve the selectivity of muscovite significantly. There is no general agreement on its primary mechanism of recovery. It is an issue that should be analysed case by case (Silvester et al., 2013).

Li et al. (2014) investigated the recovery behaviour of muscovite and the effect of hydrophobic microcrystalline graphite on water recovery through batch flotation tests and contact angle measurements. The batch flotation tests showed a linear relationship between sericite recovery and water for all size fractions tested, which indicates that entrainment is the mechanism of recovery. This evidence is supported by the contact angle measurement, which is 16.78°, which is characteristic of a hydrophilic material.

Li et al. (2014) found that the degree of entrainment of sericite is higher than quartz for the same size fraction. This behaviour is likely to be due to the platy nature of sericite, as demonstrated by Wiese at al. (2015), that has been shown to increase entrainment. The entrainment factor of particles -18 μm was founded to be 0.98 in Li et al. (2014) work.

The results of Li et al. (2014) also showed that the particle size of sericite affected water recovery. The water recovery decreased from 50.16% to 34.99% when the size fraction was increased from -18 μm to -97+74 μm. This phenomenon indicated that the froth containing fine sericite is more stable than with coarse particles. Li et al. (2014) concluded that entrainment of sericite affects the selectivity of graphite. As the particle size goes finer, the enrichment rate was sharply decreased because of the increase of the entrainment of muscovite.

The interaction of sericite and chalcopyrite has been investigated by He et al. (2009). They observed that a hetero-aggregation of sericite and chalcocite occur when both minerals are negatively charged, as indicated by the values of zeta potential between

pH 5 and 11. The presence of hydrolyzed Cu^{2+} ions in solution when pH varies from 5-11 invert the signal of the surface charge of sericite, as indicated by the zeta potential measurements. An increase of shear stress was also observed when the concentration of Cu^{2+} ions rose for pH values higher than 8, as shown in Figure 2-34.

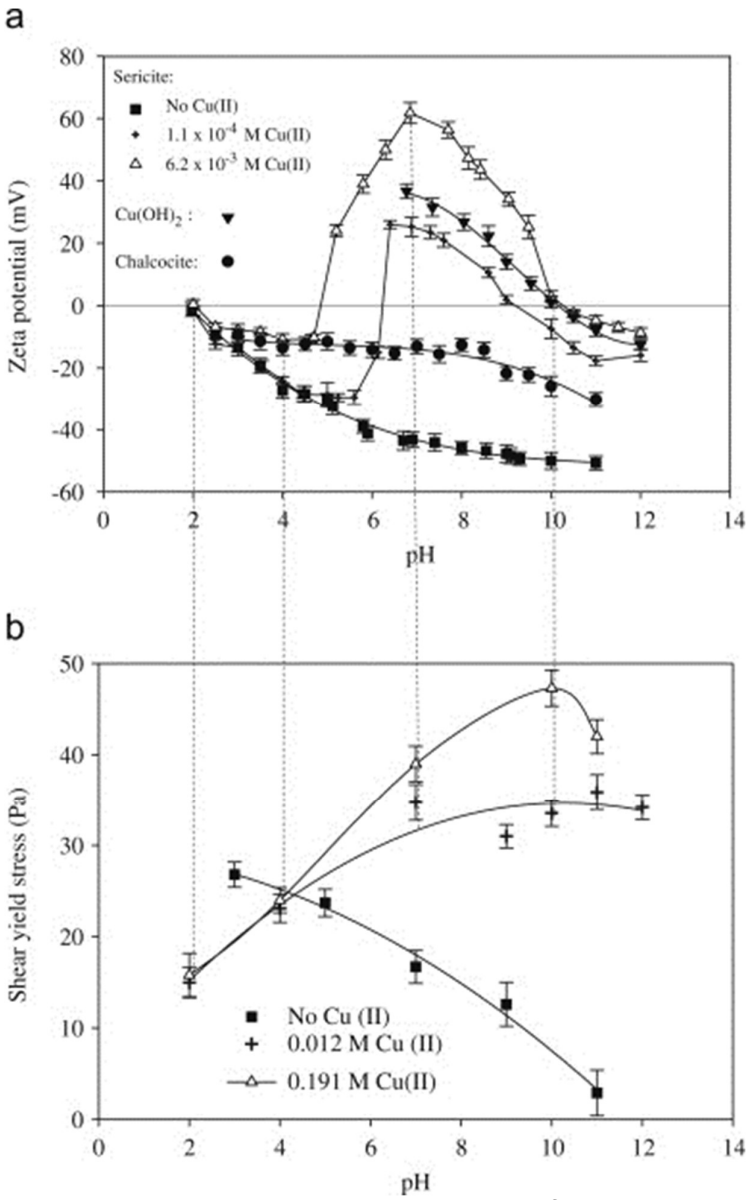

Figure 2-34 – Zeta potential (a) and shear yield stress (b) of sericite in the presence and absence of Cu^{2+} ions (He et al., 2009).

Figure 2-35 illustrates the effect observed by He et al. (2009). The presence of Cu^{2+} ions in solution is due to the oxidation of the chalcocite. An effective solution for the

aggregation problem is to reduce the degree of oxidation of the chalcocite by increasing the pH and introducing nitrogen for flotation.

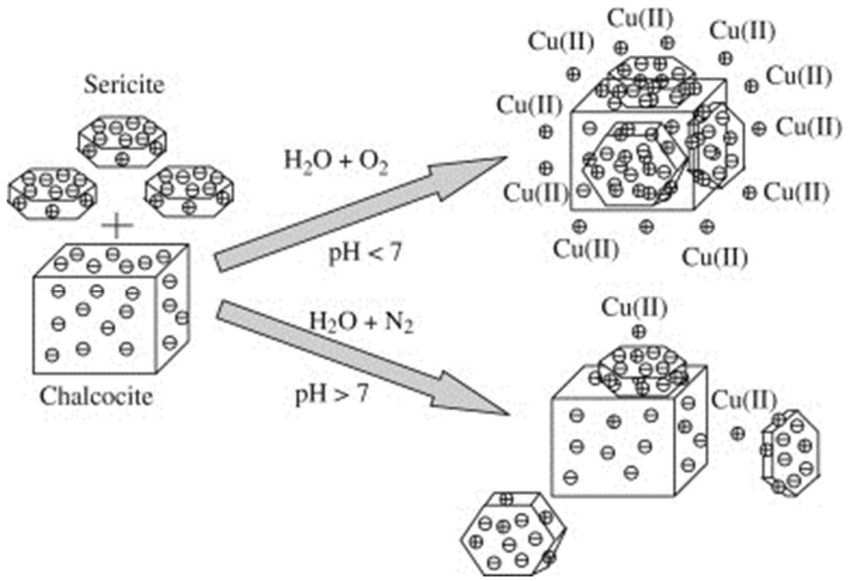

Figure 2-35 – Hetero aggregation of sericite and chalcocite in the presence of Cu^{2+} (He et al., 2009).

2.9 Literature Review Summary and Gaps Identified

It is suspected that the poor flotation rates obtained in Barrick's White Mountain project were due to the high percentage of muscovite in the feed. As such, the literature was reviewed aimed to understand the effect of the presence of muscovite in the flotation of sulfide ores and the factors that affect the flotation performance of pyritic minerals. The objective of the review was to gather information about the effect of the presence of muscovite in flotation, and the factors that drive the flotation performance of pyritic minerals and muscovite, in the context of the flotation conditions of the White Mountain project.

The key finding of the literature review are presented as follows:

1. Muscovite is a micaceous platy phyllosilicate mineral, with high aspect ratio and a high capability for exchanging of ions in solution. It can liberate Al, Si, and K ions to solution by leaching at pH 2 to 9. Because muscovite is a platy mineral,

the surface charge of the face differs from the edges. The isoelectric point is pH 4.6.

2. Muscovite is a hydrophilic mineral. The recovery of muscovite in flotation is due to entrainment. Because of its platy nature, the entrainment of muscovite is higher than spherical minerals.
3. The presence of muscovite in the flotation of copper minerals is associated with a decrease in copper recovery and concentrate grade, an increase in pulp viscosity and flotation of slime coatings.
4. The increase in viscosity with muscovite is a function of the particle size distribution, solids concentration, temperature, chemical factors, and particle aggregation. Increases in viscosity can affect the flotation performance by affecting the degree of energy dissipation in the cell, the bubble rising velocity and the gas hold up.
5. Muscovite forms slime coatings on the surface of chalcocite. The coverage of muscovite increases under acidic pH conditions and high copper concentration.
6. The formation of slimes coatings decreases the flotation rate of chalcopyrite. The detrimental effect of the kaolinite coating on chalcopyrite is exacerbated by the increase of kaolinite proportion in the gangue and at pH below 6. The increase in the percentage of kaolinite led to an increase in pulp viscosity.
7. The presence of hydrophilic ions, such as F, Na, Ca, O, Si, Mg, and K on the chalcopyrite surface decreased its hydrophobicity, consequently affecting the flotation performance.
8. The leaching of phyllosilicates, such as kaolinite and muscovite, can increase the presence of some hydrophilic ions, including Ca and K, in the flotation, which could affect the flotation rate of sulfide minerals.

The gaps identified in the literature review are presented as follows:

1. All the work reporting the effects of muscovite in flotation were done in the context of copper minerals, including chalcopyrite and chalcocite. No literature was found about the effect of the presence of muscovite on arsenopyrite and pyrite.
2. No study was found to quantify the effect of the proportion and size distribution of muscovite in the flotation feed on the flotation rate of arsenopyrite and pyrite

3. The effect of the viscosity, caused by the increase of the proportion of muscovite in the gangue, on the flotation rate of arsenopyrite and pyrite has not been reported in the literature
4. The formation of muscovite slime coating on the surface of arsenopyrite and pyrite has not been investigated
5. No studies using CCRD factorial design were found to investigate the combined effect of the proportion of muscovite, size distribution , %solids of the flotation feed, pH and frother dosage

It will be the objective of this thesis to investigate the effects of muscovite on pyrite and arsenopyrite flotation to determine the reason for the observed results.

Chapter 3

Experimental Method

3 Experimental Method

3.1 Introduction

The objective of this research is to understand whether the presence of muscovite in the flotation feed affects the flotation rate constant of pyrite and arsenopyrite and the mechanisms involved.

This chapter describes the research and experimental method, including sample preparation method and the experimental procedure used to investigate the influence of muscovite in the flotation of pyrite and arsenopyrite.

3.2 Research Method

To address the research hypotheses, the experimental work is divided into two phases:

- Phase 1: Determine whether the presence and the amount of muscovite in gangue are key factors affecting the flotation rate of pyrite and arsenopyrite.
- Phase 2: Identify the mechanisms affecting the flotation rate of pyrite and arsenopyrite.

The initial phase of the research consists of performing a large number of batch flotation tests using a synthetic ore according to the CCRD factorial design. This approach will identify to screen the significant variables, that adversely affect the flotation rate of pyrite and arsenopyrite from the range tested which is the proportion of muscovite in the gangue, percentage of solids in the flotation feed, size distribution of muscovite, frother dosage and pH. The assessment of the significant variables affecting the flotation rates is done through regression analysis that evaluates the statistical significance of the regression terms. The flotation rates used in the regression analysis were calculated through the flotation recoveries of arsenopyrite and pyrite observed in the flotation batch tests. Recovery data of water and muscovite were also collected. The results of this initial phase of the research allow hypothesis 1

(that the presence of a high concentration of muscovite has a detrimental effect on the flotation rate of arsenopyrite and pyrite) to be tested.

The second phase of the research is aimed at identifying the mechanisms by which muscovite affects the flotation rate of pyrite and arsenopyrite. The potential mechanisms investigated are viscosity and/or surface modification via hetero-aggregation and changes in surface chemistry.

The effect of viscosity is investigated by measuring the viscosity of the flotation feed pulp, which allows Hypothesis 2 (that the presence of muscovite affects arsenopyrite and pyrite floatability by changing pulp viscosity) be tested. The viscosity analysis was performed on samples of the flotation feed that were collected during the development of the batch flotation tests of the CCRD factorial design. The effect of pulp viscosity was evaluated through regression analysis that evaluated the statistical significance of the viscosity on the flotation rates of arsenopyrite and pyrite. In addition, an investigation to identify the significant factors from the CCRD factorial design that drive pulp viscosity is included to support the observed effects of viscosity on the flotation rates.

The investigation of the surface modification mechanisms examined both physical surface modification via hetero-aggregation, and chemical modification via the presence of metal ions, collector coverage, and oxidation. Zeta potential measurements were undertaken to investigate if the flotation conditions used promotes hetero-aggregation between muscovite and the pyritic minerals. Time-of-flight resonance-ionisation mass spectrometry (ToF-SIMS) and XPS analysis investigated the presence of metal ions, collector coverage and oxidation on the surface of the pyritic minerals. The results of the zeta potential, ToF-SIMS, and X-ray Photoelectron Spectroscopy (XPS) analysis allows Hypothesis 3 (that the detrimental effect of muscovite in the flotation rate of arsenopyrite and pyrite is due to surface modification of arsenopyrite and pyrite mineral grains) to be tested.

A summary of the steps of the experimental work performed in this research is provided in Figure 3-1.

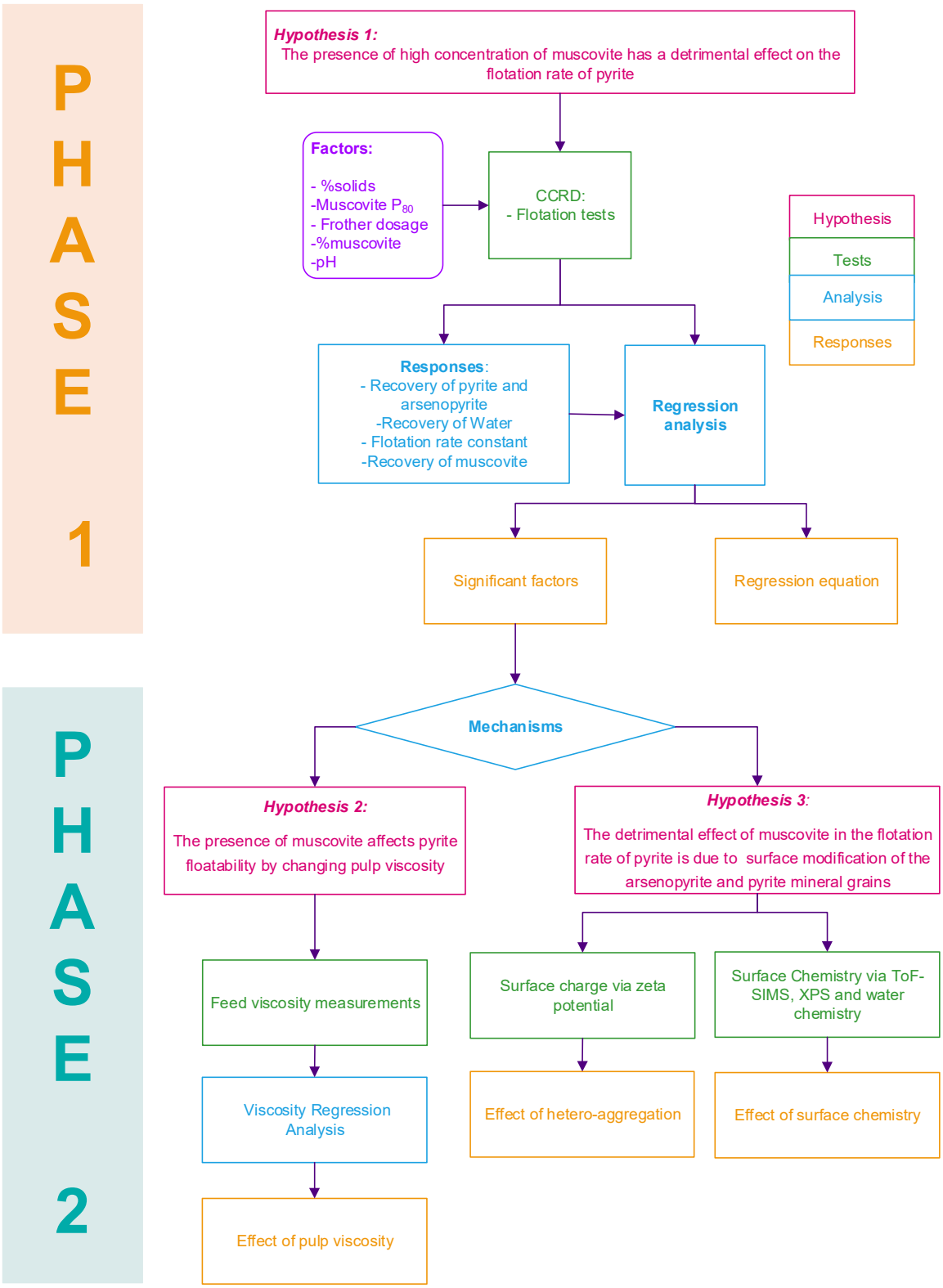

Figure 3-1 – Schematic of the research method

3.2.1 Central Composite Rotatable Design (CCRD) for Flotation Experiments

During the first phase of the research, a central composite rotatable design (CCRD) is the Design of Experiment (DOE) approach used to determine the most important factors that drive the effect of muscovite on the flotation rate of arsenopyrite and pyrite. The CCRD factorial design was selected because of its ability to provide a regression model that can be used to predict and understand the relationship between the factors for the measured response, using a reduced number of experiments.

The CCRD is a surface response method that provides a 3D response surface for the chosen variables, making it possible to build a model and to analyse the interaction between the variables. CCRDs are based on 2-level factorial designs with its origin at the centre and with additional axial points that are apart from the centre at a distance of α. The value of α is selected to provide rotatability to the design. The value of α for rotatability is calculated by:

$$\alpha = 2^{\frac{k}{4}}$$

Where k is the number of factors.

Figure 3-2 shows the structure of a 3-factor CCRD. And Figure 3-3 shows an example of the surface curves generated. (Napier-Munn, 2014).

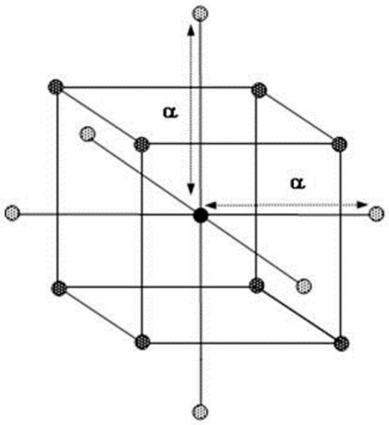

Figure 3-2 – Structure of 3-factor CCRD (Napier-Munn, 2014).

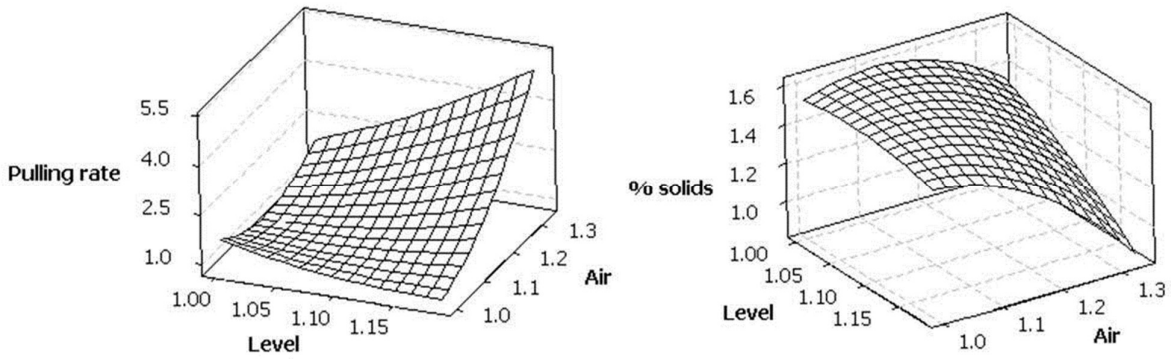

Figure 3-3 – Example of 3D surface response curved generated from a CCRD design (Napier-Munn, 2012)

The objective of the CCRD designed for this research is to understand whether the presence of muscovite affects the flotation rate of arsenopyrite and pyrite and if other factors that drive the flotation behaviour of muscovite and the pyritic minerals affect the flotation kinetics. Five flotation parameters that may affect the flotation behaviour pyrite and arsenopyrite in the presence of muscovite were selected, based on the literature.

The factors evaluated were:

- Frother dosage.
- pH.
- Percentage of muscovite in the synthetic ore.
- P_{80} of muscovite.
- Percentage of solids in the flotation feed.

A full 5 factor central composite rotatable design (CCRD) of experiments was selected for this research. Given the number of factors investigated, the CCRD design required significantly fewer tests than a multilevel factorial design. The full 5-factor CCRD design involved 54 flotation batch tests, rather than 160 tests as required by the multilevel factorial design. The selected CCRD design included repeats and centre point runs. The order of the experiments was blocked to minimise the effect of the length of time taken to complete all tests from the CCRD design. The design was generated in using the commercial statistical software Minitab® version 18 (Minitab, 2019). A detailed list of the tests and conditions is provided in Appendix 1.

Table 3-1 shows the ranges of the factors investigated in the CCRD.

Table 3-1 – Range of the factors tested in the CCRD

Factor / Range	Minimum value	Maximum value
Frother dosage	10 ppm*	30 ppm
pH	4	10
Percentage of muscovite in the synthetic ore	0%	45%
P_{80} of muscovite	50 µm	150 µm
Percentage of solids in the flotation feed	10%	45%

*The frother critical coalescence concentration (CCC) is 8.6 ppm.

These parameters were selected based on operational parameters that could potentially be changed to minimize the deleterious effect of muscovite on the flotation rate of arsenopyrite and pyrite. The flotation rate is also affected by cell parameters, such as geometry, air rate, impeller speed, cell size (Gorain, 1998; Wang, 2016), particle composition, reagent regime, and pulp rheology. Note that equipment and operating parameters, such as airflow, cell geometry, froth height (due to lip height) and impeller speed are not the focus of this thesis.

Table 3-2 lists the objective of testing each of the selected parameters in flotation.

Table 3-2 - Basis of the selection of the parameters tested

CCRD Parameters	Objective
Muscovite P_{80}	Evaluate if the size distribution of muscovite affects the flotation rate of the sulfide minerals
Muscovite proportion (%)	Evaluate the critical components of the gangue in terms of % of muscovite
Frother dosage (ppm)	Evaluate how the increase of gangue entrainment can affect flotation rate without an increase in viscosity
pH	Evaluate how the surface charge of the muscovite affects flotation rate
% solids of the pulp	Evaluate the effect of viscosity or the flotation rate

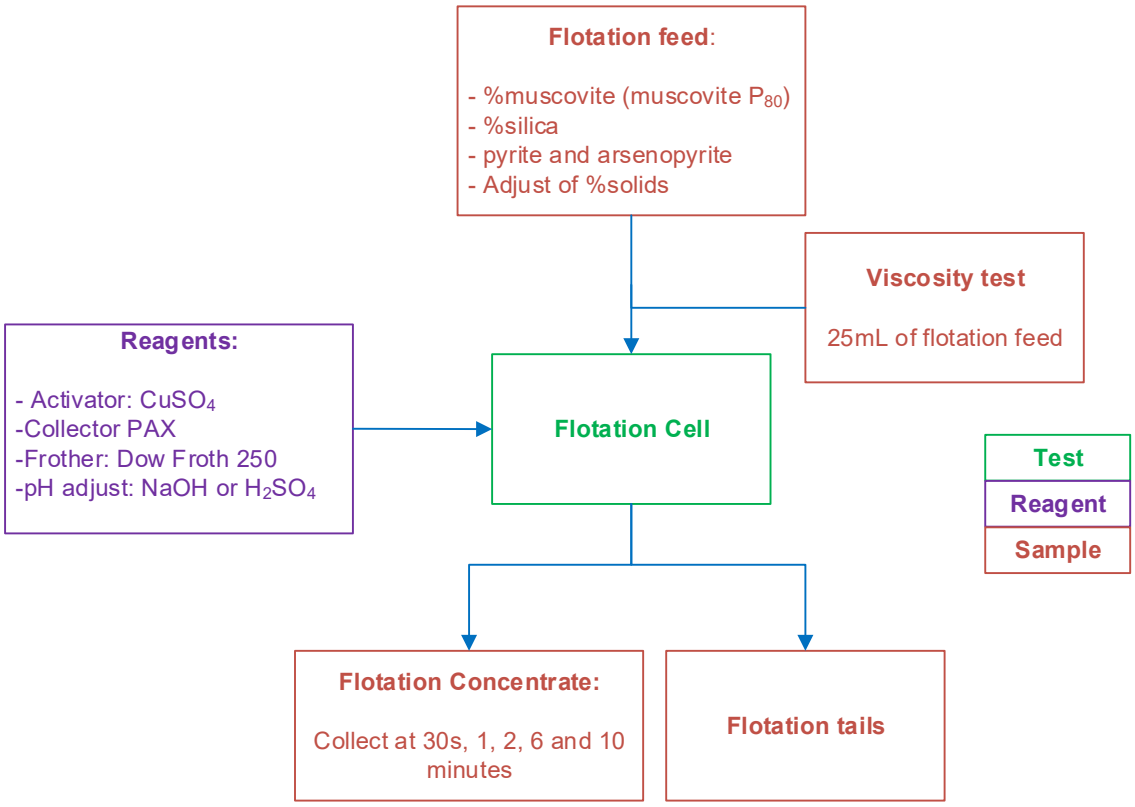

Figure 3-4 – Schematic of the flotation tests of the CCRD

The data measured in each test of the CCRD experiments included timed concentrate and tailings total masses, water content, solids content, and viscosity of the pulp. The recoveries and rate constants of pyrite and arsenopyrite were calculated based on arsenic and sulfur assays. The recovery of muscovite was calculated based on the assays of aluminium. A schematic of the flotation tests of the CCRD program are shown in Figure 3-4. The detailed flotation procedure is presented in Section 3.4.

The collector dosage used in the 5-factor CCRD design was held constant. It is well known that the recovery of pyrite is a function of collector dosage and pH (Fuerstenau, Kuhn and Elgillani, 1968), as shown in Figure 3-5. Because pH is one of the factors evaluated in the CCRD design, an appropriate dosage of collector needed to be selected to keep the recovery of pyrite constant over a wide range of pH values.

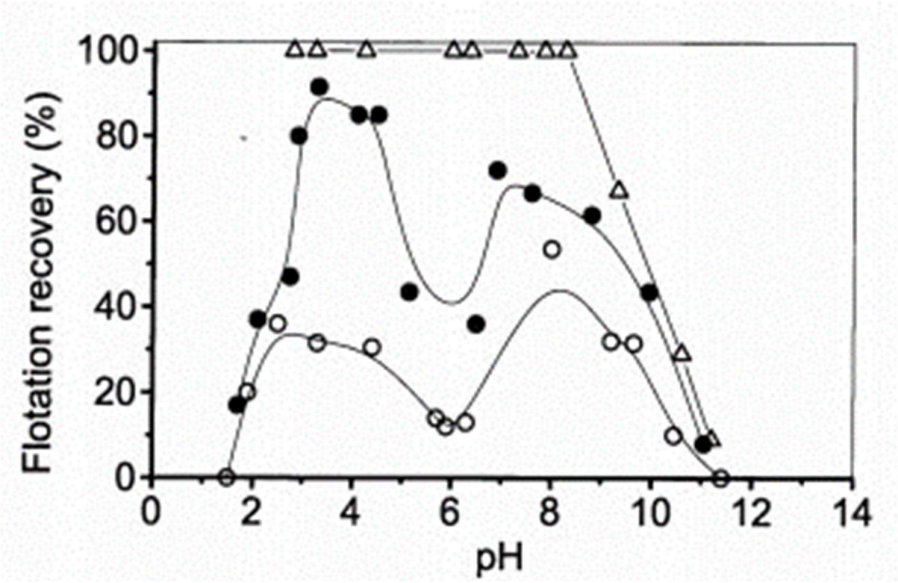

Figure 3-5 – Recovery of pyrite as function of pH with potassium ethyl xanthate of (empty circle) 1 x 10-5 M, (filled circle) 2 x 10-5 M and (triangle) 2 x 10-4 M (Fuerstenau, et al., 2007).

Barrick used potassium amyl xanthate (PAX) as the flotation collector of pyrite and arsenopyrite in the White Mountain project. Therefore, to maintain the conditions of the experiments performed in this research similar to the Barrick flotation test conditions, PAX was selected as the collector. To select the appropriate dosage of potassium amyl xanthate (PAX), an initial 2-factor CCRD experimental design was performed separately. Including the collector dosage as a factor in the full CCRD program would require a 6-factor CCRD which would increase the number of flotation batch tests from 54 to 90. Through performing those tests separately, the total number of tests required to perform the 2-factor and 5-factor CCRD is 68 rather than 90 tests to perform a full 6-factor CCRD design.

This initial 2-factor CCRD design was performed with a synthetic ore. The composition of the synthetic ore used consisted of 35 g of pyrite, 16 g of arsenopyrite and 980 g of silica. The pH was varied from 4 to 7, and the concentration of PAX evaluated was between 30 g/t and 300 g/t. This procedure consisted of 14 flotation tests. Table 3-3 details the pH and the PAX dosage evaluated in these tests.

Table 3-3 – Details of the 2-factor CCRD runs performed to optimise PAX dosage

Run Order	Blocks	pH	PAX dosage (g/t)
1	2	7.0	165
2	2	7.0	30
3	2	4.0	165
4	2	7.0	165
5	2	7.0	300
6	2	10.0	165
7	2	7.0	165
8	1	4.9	260
9	1	7.0	165
10	1	9.1	260
11	1	7.0	165
12	1	4.9	69
13	1	9.1	69
14	1	7.0	165

3.3 Sample Preparation and Characterisation

The study of flotation performance was done using a synthetic ore created by combining pure minerals. The advantage of using a synthetic ore system is that it allows the identification of specific effects of the mineral of interest without the interference of the complex mineralogy of a ‘real’ ore. In addition, the composition of the synthetic mineral mixture can be easily modified, in contrast to real ores.

The mineral composition of the synthetic ore used in this study is designed to approximate the characteristics of the minerals in Barrick’s problematic ore. The sulfide minerals selected for this study, arsenopyrite, and pyrite, are the gold-bearing minerals in the problematic ore from Barrick with slow flotation kinetics. The gangue minerals used are silica and muscovite. Silica is the most abundant gangue mineral in the problematic ore and muscovite is the gangue mineral of interest in this study. Other gangue minerals from Barrick’s problematic ore are not included in this study. Their percentage in the composition of the gangue is replaced by silica in the synthetic ore. This allows the observations of the effect of muscovite on the flotation rates to be made with the exclusion of the interference of other minerals that are not the focus of this research.

The synthetic ore mixture was prepared to create a similar mineral size distribution characteristic to the problematic ore of Barrick. Barrick supplied data of the size characteristics of the sulfide minerals in the problematic ore, and a sample of a reference ore which allowed measurements of the gangue minerals size distribution and liberation characteristics.

This section describes the experimental procedure involved in the sample preparation. Chapter 4 presents the liberation and size distribution analysis completed as part of the sample characterisation procedure.

3.3.1 Reference ore from Barrick

The reference ore of Barrick contained 22% of muscovite by mass, and in this research, the reference ore has been used to provide data for the size distribution and liberation of the gangue minerals of interest, which are muscovite and quartz, at different grind sizes.

The available reference ore sample consisted of a composite sample, totalling 51.6 kg of the ore crushed to −3.35 mm. The samples were representatively split into 1 kg bags.

Representative samples of the ore were split in a riffle splitter and pulverised. The pulverised samples were divided and sent for assay and QXRD to determine elemental and mineral composition.

To assess the liberation characteristics of silica and muscovite in the reference ore, the samples were ground at a range of time intervals to determine the point at which the samples achieved the P_{80} values of 350 µm, 125 µm, and 50 µm. These P_{80} values were chosen to identify the range of liberation stages of the ore. The objective of grinding at different P_{80} values is to observe if there could be an advantage in using a coarser grinding size to facilitate the rejection of muscovite.

After the grinding calibration curve was established, three 1 kg samples were ground to the required P_{80} values, and the products were sized. A representative sample of each size fraction was assayed and sent for mineralogical analysis by MLA to

determine the liberation of muscovite, sulfide minerals and other gangue minerals. The size fractions selected were + 150, - 150 + 75, - 75 + 38, - 38 + 20, - 20 + 10 µm, and - 10 µm. These data are presented in Chapter 4.

3.3.2 Pure mineral samples

3.3.2.1 Pyrite and Arsenopyrite

The pure samples of pyrite used in this work were purchased from GEO Discoveries (Discoveries, 2012) and originated from Peru. They were provided as coarse rocks that required crushing in a Boyd crusher using a closed size setting of 2 mm. The crushed material was screened on an 850 µm sieve with coarse material returned to the crusher. The material finer than 850 µm was split into 35 g subsamples and sealed in individual bags. The bags were stored in the freezer at -18^{o}C to minimise oxidation of the sulfide minerals.

The arsenopyrite was received from GEO Discoveries (Discoveries, 2012) in 2.5 cm cubes, which were crushed in a Boyd crusher to -850 µm and split into 16 g subsamples and sealed in individual bags. The bags were also stored in the freezer at -18^{o}C.

The pyrite and arsenopyrite samples were characterised using the Mineral Liberation Analyser ('MLA') extended back-scatter electron detector ('XBSE') method to determine their purity are presented in Chapter 4.

To prepare the flotation feed prior to each flotation test, pyrite and arsenopyrite were ground together with 75 ml of Brisbane tap water in a 20.5 cm diameter, 23.3 cm long stainless steel rod mill for 5 minutes, using 4 mild steel rods, each 2 cm in diameter and 23.3 cm long. The weight of the grinding media used was 2841 g. The picture of the rod mill used is shown in Figure 3-6.

To minimise contamination between tests, the rods were cleaned by performing a 5 minutes grind using 200 g of silica and 300 ml of tap water.

Preliminary grinding tests were performed at a range of grinding times, to determine the appropriate grinding time to produce pyrite and arsenopyrite with a similar size

distribution to that of the White Mountain ore. The grinding size results are shown in Chapter 4.

Figure 3-6 – Rod mill used for the grinding of pyrite and arsenopyrite

3.3.2.2 *Silica*

The silica samples were purchased as 25 kg bags from Sibelco Australia and did not require crushing. To perform all the flotation tests, approximately 100 kg of silica was required. Four 25 kg bags of Sibelco Silica 60G were blended by performing multiple passes through a rotary Essa splitter. The bags combined in the Essa splitter feeder were split into 8 fractions. The opposite fractions from the split were recombined in the feeder and them re-split. The procedure was repeated three times to ensure thorough blending. The blended sample was subsampled using a rotary sample divider to obtain the amount of silica required for each flotation test.

The size distribution of the silica purchased was compared to the grain size distribution of the silica in the reference ore and the data from White Mountain. No further adjustment of the size distribution of the purchased silica was required. The comparison of the size distribution of the purchased silica with the size distribution of the quartz White Mountain is provided in Chapter 4.

3.3.2.3 *Muscovite*

Muscovite was received from Wards Science® (Ward's Science, 2019) in 1 kg sheets. The size reduction of this material was challenging, requiring multiple steps. The aim was to produce muscovite in different size classes that could be combined in ratios

that would replicate the size distribution which would be expected after grinding of the White Mountain ore. The samples of muscovite were first delaminated using a jaw crusher followed by manual delamination, as shown in Figure 3-7. The delaminated material was comminuted for approximately 2 minutes in a conventional 800 W 2 L 6 blades Sunbeam blender, using the pulse function to generate sheets smaller than 4 cm^2. This material was dry sieved at 850 and 600 μm. This stage of grinding aimed to generate -850+600 μm muscovite for the entire testing campaign, as shown in Figure 3-8.

The remaining delaminated material was comminuted for approximately 2 minutes in a conventional 2000 W 2 L 4 blade Sunbeam blender to generate sheets smaller than 1 mm^2. This blended material was wet sieved at 53 μm and 38 μm, as shown in Figure 3-8. The +53 μm and +38 μm fraction were when dry sieved using 600, 425, 300, 212, 106, 75, 53 and 38 μm screens.

(a) (b)

Figure 3-7 – (a) Muscovite as received from Wards Science® in 1 kg sheets (b) Delaminated muscovite

Figure 3-8 – Muscovite sheets after 2 minutes in the 800 W blender

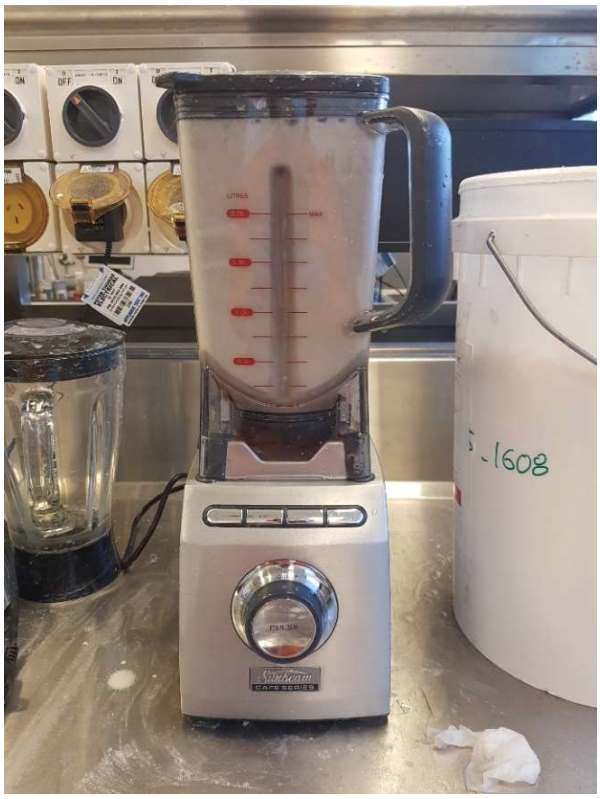

Figure 3-9 - Sunbeam blender 2000 W with 4 blades for the comminution of muscovite

The excess coarse fractions were reground in a laboratory pulveriser for 5 minutes to generate the – 38 µm material. The pulverising procedure was repeated until the required amount of material reported to the – 38 µm fraction. A sample preparation diagram for muscovite is provided in Figure 3-10.

A representative sample of muscovite was submitted for quantitative x-ray diffraction ('QXRD') analysis to determine its mineral composition. Results of this analysis are presented in Chapter 4.

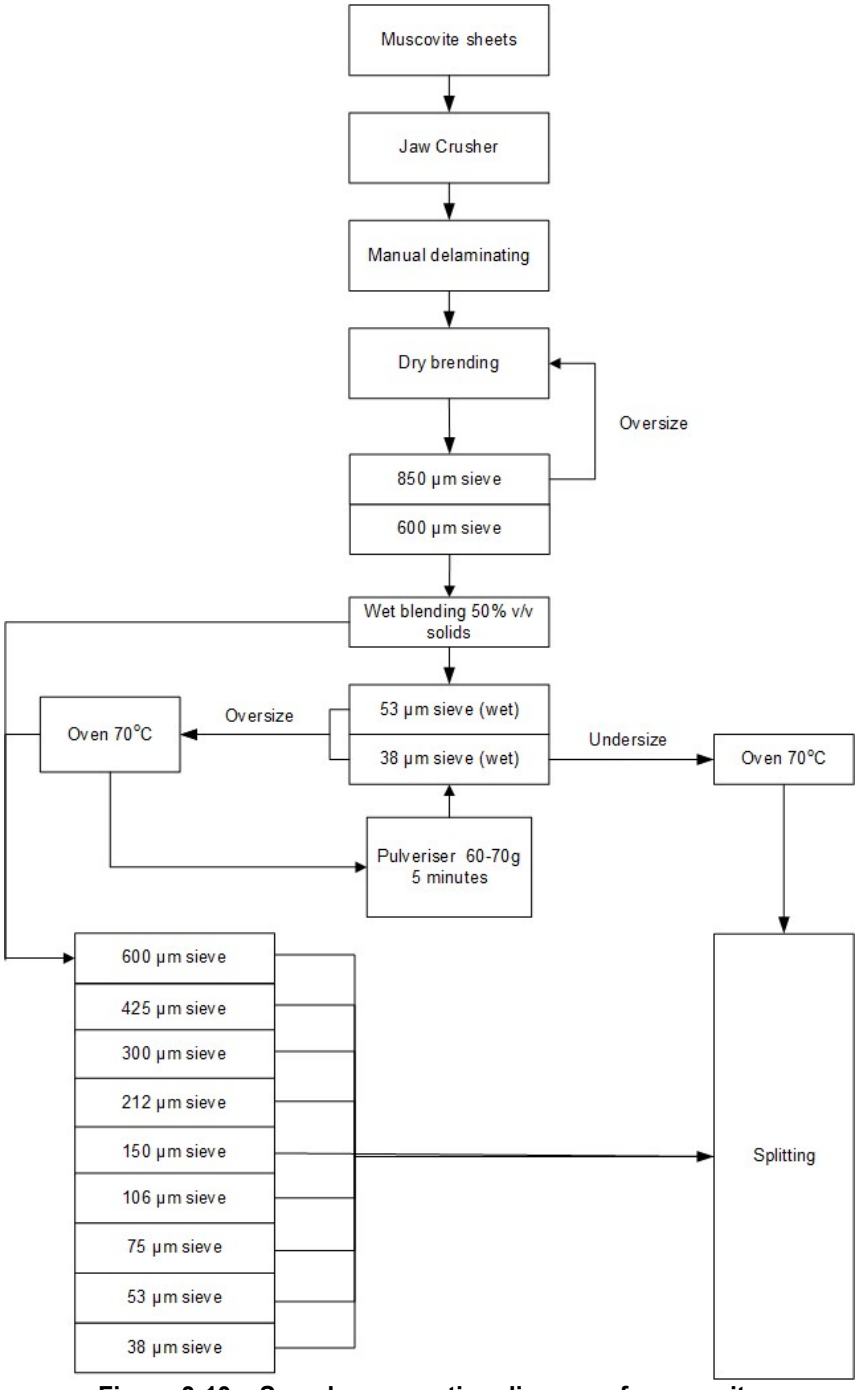

Figure 3-10 – Sample preparation diagram of muscovite

3.4 Flotation Experimental Procedure

3.4.1 Flotation Reagents

The reagents used in the flotation tests were based on the flotation reagents used by Barrick in the White Mountain project. The reagents used by Barrick in the White Mountain project are shown in Table 3-4.

Table 3-4 – Barrick Flotation Reagents (AMEC, 2007)

Type	Reagent	Dosage
Collector	Potassium Amyl Xanthate (PAX)	200 g/t
Activator	$CuSO_4$	100 g/t
Frothers	F549 MIBC (Methyl Isobutyl Carbinol)	5 g/t 95 g/t

The pH adjustment of the slurry of the flotation tests performed for the thesis was made using a 5% weight solution of sodium hydroxide prepared using solid sodium hydroxide from Rowe Scientific, and a 1% volume solution of sulphuric acid 98% from Ajax Chemicals.

100 ml of PAX solution 20 g/L was prepared daily from solid PAX, of 90% purity sourced from Qingdao LNT Chemical CO LTD.

The $CuSO_4$ used in the flotation tests was as a 10 g/L solution from solid $CuSO_4$ from Ajax Finechem (ThermoFisher Scientific, 2019).

Dowfroth 250, a polypropylene glycol-type frother from Dow Chemical Company, was used instead of the mixture of F549 and Methyl Isobutyl Carbinol (MIBC) used in the White Mountain because it has a higher dynamic foamability index (DFI) than MIBC (Laskowski, 2004). The aim was to prevent the froth collapsing and maintain a stable froth throughout the duration of each batch laboratory flotation test. Dowfroth 250 was used undiluted and dosed with a graduated 100 μL pipette. The minimum frother dosage used in the CCRD flotation experiments was 10 ppm, which is above the CCC of Dowfroth 250, that is 8.7 ppm, according to Cho & Laskowski (2002).

All reagent solutions were prepared using Brisbane tap water. The composition of Brisbane tap water, as per the Queensland Urban Utilities (2018) is shown in Table 3-5.

Table 3-5 - Brisbane tap water (Queensland Urban Utilities, 2018)

Element	Aluminium	Chloride	Fe	TDS	Total Hardness
ppm	0.046	62	0.011	290	120

3.4.2 Flotation Procedure

Flotation batch tests were performed to obtain the mineral recovery and water recovery, as a function of time. This information was used to obtain kinetic floatability data.

The mass of pyrite and arsenopyrite in each synthetic ore mixture remained constant at 35 g and 16 g per test, respectively. The quantities of silica and muscovite used in the flotation batch tests were varied according to the desired percentage of solids and the proportion of muscovite to be achieved. Appendix 1 presents the specific amount used in each test. The flotation tests completed in the CCRD were performed using the same operating parameters. All tests were conducted in a 5 L bottom driven laboratory scale flotation cell employing an agitair impeller and stator, run with an impeller speed of 800 rpm, an air rate 11 L/min and a froth depth of 1 cm below the cell lip.

The batch flotation tests were performed according to the following procedure:

1. Clean the rod mill prior to grinding the flotation feed material: add 250 g of cleaning silica and 250 mL of water to the mill. Grind for 5 minutes. Wash mill thoroughly.
2. Pyrite and arsenopyrite grinding: add 35 g of pyrite, 16 g of arsenopyrite and 75 mL of water. Grind for 5 minutes.
3. Measure Eh of pyrite pulp immediately after grinding. Collect the thick pulp in a vial and measure the potential. Wash mill thoroughly.
4. Pre-fill the flotation cell with 2 L of Brisbane tap water.
5. Add Dow Froth 250 using a micropipette to achieve the desired test dosage.

6. Adjust the impeller speed of the cell to 800 rpm.
7. Add dry silica to the cell.
8. Add dry muscovite to the cell.
9. Add the pyrite and arsenopyrite slurry to the cell.
10. Add the remaining amount of water required for the test level.
11. Conditioning for 6 minutes and adjust pH with NaOH for the tests above pH 7 or H_2SO_4 solution for tests below pH 7.
12. Add $CuSO_4$ and condition for 2 minutes.
13. Add PAX and condition for 2 minutes.
14. Turn air to 11 L/min and start stopwatch used to time the test.
15. Collect concentrates at: 0.5, 1, 2, 6 and 10 minutes.
16. The pulp volume in the cell was maintained by the addition of Brisbane tap water pre-conditioned with frother at the same dosage of the given test.
17. Weigh flotation cell which contains tailings and to obtain the wet weights of each product to concentrate containers to calculate the water recovery.
18. The concentrates were filtered, dried and re-weighed to obtain the dry solids mass of each product to calculate the solids recovery and weight %solids.

The flotation cell and the concentrate containers were tared prior to each batch flotation tests.

3.5 Zeta Potential

The zeta potential is a measurement of the surface charge of the minerals involved in flotation. The measurements were carried out to identify the surface charge of pyrite, arsenopyrite, silica and muscovite individually and as a mixture. The zeta potential measurements of the mineral mixture were performed under similar conditions of the centre point runs of the full CCRD, in which the muscovite P_{80} = 100 μm, 22% muscovite and 27% solids. The detailed size distribution of pyrite, muscovite and silica, and used in the zeta potential test can be found respectively in Table 4-4, Table 4-7 and Table 4-9, in Chapter 4.

The zeta potential measurements were performed as a potentiometric titration series using the Colloidal Dynamics Zetasizer, at the Julius Kruttschnitt Mineral Research Centre.

The Colloidal Dynamics ZetaProbe can measure directly samples up to 60% volume, using a patented multi-frequency electroacoustic technology, and operates without entering the particle size of the sample, from a range of 1 nm to greater than 30 μm. The ZetaProbe has no limit on particle size. The instrument automatically compensates for the effect of particle inertia for large particles and has no lower limit in particle size. (Colloidal Dynamics, 2019a; Colloidal Dynamics, 2019b).

Two potentiometric titrations were performed per sample, an acid-to-base, and a base-to-acid pH. The series were conducted over a range of pH values from pH 3 to 11.

3.6 Pulp viscosity

Rheological measurements were performed on the flotation feed slurry using an AR1500EX (from Thermal Analysis, Germany), at the Julius Kruttschnitt Mineral Research Centre, with a CC27/P1-SN10897 vane. This geometry was selected because it can measure more accurately the shear stress at a low shear rate of low solid content slurries. The particles of the slurry tested were 100% passing 850 μm. Rheological measurements were conducted on 25 mL of flotation feed, extracted from the flotation cell using a 30 mL syringe with an aperture of 2 mm, which is larger than the largest particle in the flotation slurry being analysed. The samples of the flotation feed for rheology were collected during the conditioning time after all reagents had been added and prior to the addition of air. The rheology measurement involved adjusting the shear rate at decreasing intervals within the range of 400-0 s^{-1}, over a 60 s time period. For minimising the effect of the slurring settling during the test, the pulp was stirred for 15s at the shear rate of 400 s^{-1} prior to the measurement, and shear stress was taken in decrease intervals. The rheological time dependency of the behaviour of the pulp is not evaluated in this research. Therefore, to minimise this effect, all viscosity measurement was conducted with the same time interval between sample collection and analysis, which was 25 minutes.

3.7 Assaying

The quantities of the minerals present in the concentrates and tailings of the flotation tests were determined via assay of Al, S, and As. Table 3-6 shows the elements assayed and the ratios used to calculate the mineral assays in the synthetic ore.

Table 3-6 – Assayed Elements

Mineral	Formula	Assayed Element	% of Assayed Element in the Mineral (Webmineral 2019a,b,c)
Muscovite	$KAl_2(Si_3Al)O_{10}(OH,F)_2$	Al	20.30
Pyrite	FeS_2	S	53.45
Arsenopyrite	FeAsS	As, S	As = 46.01, S = 19.69

The percentages of each mineral in the streams tested were calculated via element-to-mineral conversions, using the percentage weight of the assayed elements. Silica content was obtained by the difference between the sample mass and the mass of the minerals calculated via the assayed elements because assaying SiO_2 would not distinguish between the content of SiO_2 in muscovite and quartz (silica).

The assay methods used to quantify sulfur, aluminium and arsenic are presented in Table 3-7. All assays were conducted at ALS Global, Brisbane (ALS, 2019).

Table 3-7 – Assaying Method Used

Element	Method description
Total Sulphur	LECO
Arsenic	Aqua regia digestion with ICP-ES finish
Aluminium	Oxidising flux with XRF finish

3.8 Surface analysis

3.8.1 Time of Flight Secondary Ion Mass Spectrometry

The Time of Flight Secondary Ion Mass Spectrometry (ToF-SIMS) instrument used in this study was a model PHI TRIFT V nanoTOF from Physical Electronics Inc, located the Future Industry Institute of the University of South Australia. Mineral particles were mounted on indium foil on a silicon wafer and loaded into the instrument introduction chamber. A pulsed liquid metal gold primary ion gun (LMIG) was used for the analysis

in imaging mode operating at 30 kV energy. “Unbunched” beam settings were used to optimise spatial resolution. Data was acquired for 3 minutes per spot. The typical raster sizes were from 100 x 100 µm to 300 x 300 µm depending on particle sizes.

3.8.2 X-ray photoelectron spectroscopy

X-ray photoelectron spectroscopy (XPS) is a surface-sensitive analytical technique that uses the photoelectric effect to identify and quantify elements on the surface of materials. The instrument focuses an X-ray beam at the target material; photoelectrons are ejected from the atoms of the material with specific kinetic energy depending on their atom of origin. By measuring this kinetic energy, the identity of the original atom is found, and the number of electrons measured at that energy provides quantitative information about the elements (C. Bassel, personal communication, August 15, 2018).

Two spectral regimes can be produced by XPS, survey spectra and high-resolution spectra. The survey spectra allow the identification and quantification of the elements on the surface, while the high-resolution spectra allow the identification and quantification of the chemical environment associated with an element (C. Bassel, personal communication, August 15, 2018).

The XPS instrument used was a Kratos AXIS Ultra DLD spectrometer, at the Future Industry Institute of the University of South Australia. The X-ray was a monochromatic aluminium X-ray running at 225 W with a characteristic energy of 1486.6 eV. The area of analysis (Iris aperture) was a 0.3 mm x 0.7 mm slot; the analysis depth was approximately 15 nm into the surface of the sample. The binding energy range selected was from -10 to 1110 eV. The analysis vacuum was 4 x, 10^{-8} Torr. The electron take-off angle was normal to the sample surface. Spectra were interpreted using the software package CasaXSP. Peak position references are as per the Handbook of X-ray Photoelectron Spectroscopy and the XPS of Polymers Database (C. Bassel, personal communication, August 15, 2018).

3.9 Water Chemistry

The solution samples were prepared to investigate the Al and K leaching from the muscovite in the flotation feed. The leaching tests were conducted using 16.4 g of muscovite, with the size fractions -300/+212 μm, -106/+75 μm, at pH 4 and pH 10. The leaching solution consists of deionised water with pH-regulated with H_2SO_4 and NaOH. The size fractions were leached for 10 minutes (as per the flotation conditioning time) in a beaker agitated in a magnetic agitator, then filtered. The filtrated solution samples were submitted for assay of Cu, K, and Al via ICP – AES, at ALS Global, Brisbane (ALS, 2019). Triplicates of the samples were assayed to ensure the repeatability of the results.

3.10 Froth Stability

According to equation 2-6, the froth stability is directly proportional to the maximum froth height reached in a froth stability column. A number of tests were performed to gain an understanding of how the factors used in the CCRD affected the froth. An extensive study of the effect of all the studied factors of the CCRD is not part of the scope of this research due to time constraints.

The maximum froth height was measured using a transparent flotation column with the same cross-section area as the 5 L cell used in the CCRD experiments. Figure 3-11 shows the device used. The device was built at the Julius Kruttschnitt Mineral Research Centre for these specific measurements. A sample was prepared under a specific set of conditions, and 11 L/min air was then added. The height of the froth was measured after the equilibrium froth height had been reached. The lip was sufficiently tall not to allow spillage of material.

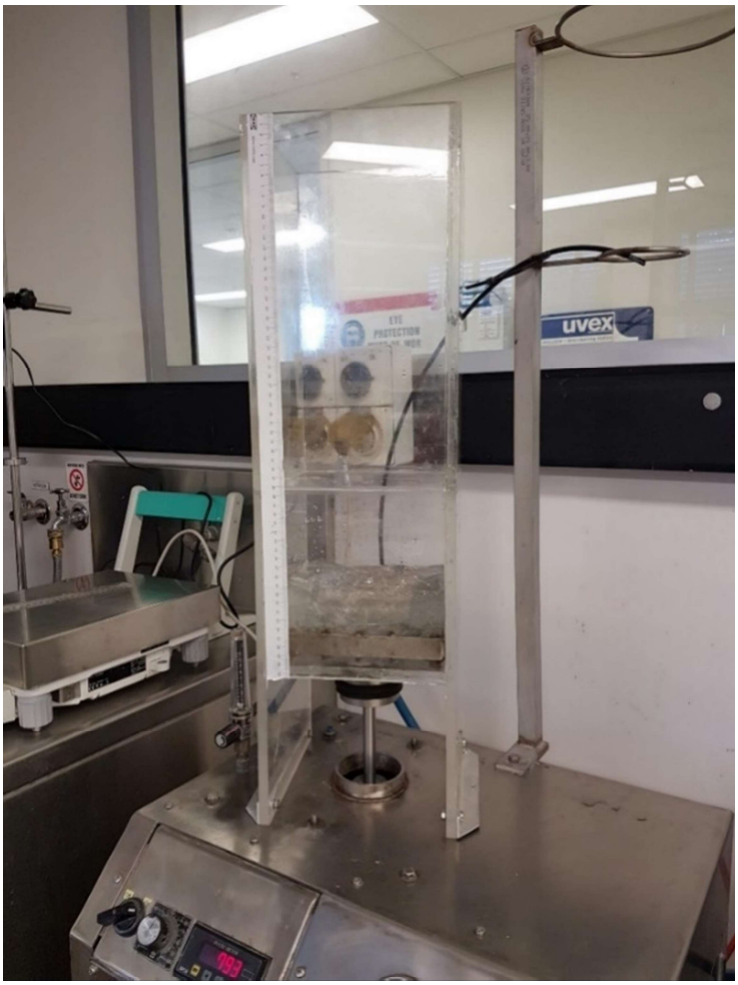

Figure 3-11 – Flotation column used for froth height measurement

Chapter 4

Sample Characterisation for Synthetic Ore Preparation

---

4 Sample Characterisation for Synthetic Ore Preparation

4.1 Introduction

This chapter discusses the basis of the sample preparation of the synthetic ore mixture used in the CCRD. The results of the analyses used to check the quality of the minerals in the synthetic ore, and the results of the preliminary experimental analyses used to characterise the mineral samples prior to preparation of the synthetic ore samples to be used in flotation tests are presented.

It was decided to use a synthetic ore mixture to develop this study because the composition of the mineral mixture could be easily modified by allowing different proportions of muscovite to be tested. It excludes the effect of other gangue minerals that may interact with the pyritic mineral that, which could mask the key effects of muscovite in the ore. Another advantage is that the elemental assays could be used to estimate the mineral content of the muscovite in the products of the flotation batch, reducing the cost significantly. The limitations of using the synthetic ore system include the lack of composite particles that may be playing a major role in the poor performance of the flotation rate in a real ore.

The sample preparation of synthetic ore mixture aims to resemble key characteristics of the real ore of Barrick. For that purpose, Barrick provided mineralogy reports of the problematic ore that could be used to gather the mineral size distribution and liberation of the sulfide mineral, which is used as the basis for the sample preparation of arsenopyrite and pyrite used in the batch flotation tests. In addition, a sample of a reference ore was provided to allow measurements of gangue mineral characteristics, including liberation and mineral size distribution which are used as a basis for the sample preparation of muscovite and silica.

4.2 The reference

The reference ore provided by Barrick is used for measuring the bulk liberation of muscovite, in given grinding sizes, in the absence of information from the problematic White Mountain ore. This section describes the composition of the reference ore, the degree of liberation of silica and muscovite at similar grind sizes to the problematic ore and details the mineral size distribution to be used as a reference to produce pure mineral samples.

4.2.1 Sample characterization

The mineral composition of the reference ore samples was determined via quantitative phase analysis using quantitative X-ray diffraction (QXRD), and the results shown in Table 4-1.

Table 4-1 – Mineral composition of the reference ore from QXRD

Phase	Formula	Weight %
Quartz	SiO_2	35.0
Muscovite	$KAl_2(Si_3Al)O_{10}(OH, F)_2$	30.8
Plagioclase feldspar (labradorite)	$(Na,Ca)(Al,Si)_4O_8$	9.9
K-feldspar (microcline)	$K(AlSi_3O_8)$	9.7
Smectite (montmorillonite)	$Al_2O_3 \cdot 4SiO_2 \cdot xH_2O$	3.5
Fluorite	CaF_2	2.8
Kaolin	$Al_2(Si_2O_5)(OH)_4$	2.2
Cordierite	$Mg_2Al_4Si_5O_{18}$	2.1
Pyrite	FeS_2	2.0
Chlorite	$(Mg,Al,Fe)_6(Si,Al)_4O_{10}(OH)_8$	1.4
Chalcopyrite	CuFeS2	0.5

The QXRD data shows that the reference ore containing 30.8% of muscovite and 35.0% of quartz. The proportion of muscovite in the reference ore is similar to the problematic ore, White Mountain (which is 32.8%). The proportion of quartz is significantly lower than White Mountain (55.2%), due to the presence of other gangue minerals, such as feldspar, which are significantly higher than at White Mountain (3.3%).

4.2.2 Grinding calibration of the reference ore

Two grinding times were selected to produce P_{80} values that would resemble the size distribution of White Mountain reported in Barrick's data, which was 121 µm in the primary grind and 50 µm in the secondary grind. A third P_{80} was introduced to investigate the state of liberation of muscovite at a coarser grind size than presented in the White Mountain data. The objectives of this were to evaluate the liberation of muscovite and silica in the ore at these different particle size distributions and to obtain the grain size distribution of the mineral components in the ore to assist in creating a synthetic version of the flotation feed using pure minerals. Table 4-2 presents the three grinding sizes selected with the respective grinding times.

Table 4-2 – Selected grinding sizes for reference

Grinding time (min)	P_{80} ore (µm)
2	370
10	125
35	55

The coarser grinding size presented in Table 4-2 was selected arbitrarily as approximately three times the primary grinding P_{80} of Barrick's, 125 µm, to follow approximately the same difference between the grinding at P_{80} 50 µm and P_{80} 125 µm. Figure 4-1 displays the size distributions of each grinding time selected.

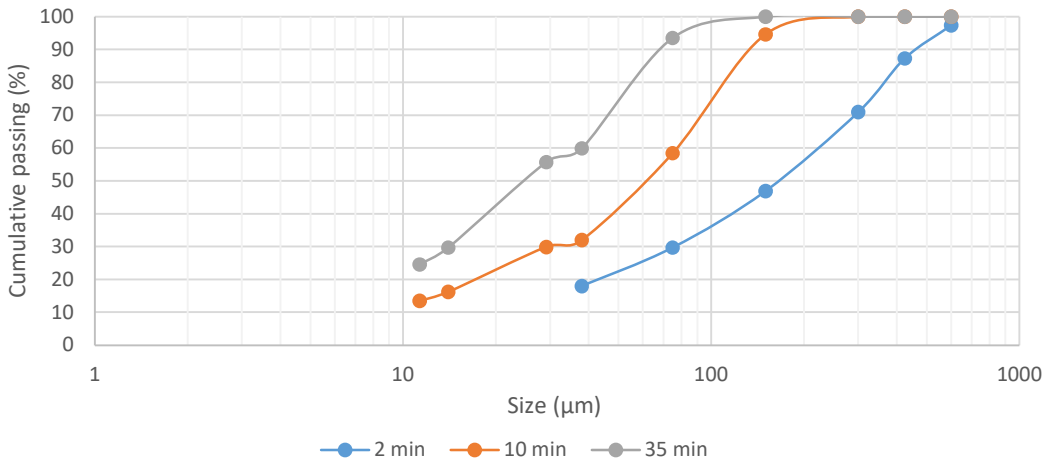

Figure 4-1 – Size distribution of reference ore for the three grinding times

The size distribution of the three grindings indicates that there is no overlapping of size distribution curves obtained. It indicates that the particle size distribution obtained in the three grindings are significantly different, which suggests potential differences in the mineral liberation degree between each grinding.

4.2.3 Liberation by Mineral of Size Fractions

The size fractions of each grinding product were submitted for mineralogical analysis by MLA XBSE to determine the state of liberation of muscovite and quartz. The size fractions analysed were +600 µm, -600+425 µm, -425+300 µm, -300+150 µm, - 150+75 µm, -75+38 µm, -38 µm +C1, C2+C3, C4+C5, -C5, where C1 to C5 correspond to each fraction collected from the cyclosizer cyclones. The equivalent size cut sizes of the cyclosizer fractions were calculated based on the reference ore density, 2.85 g/cm^3. The equivalent sizes are C1 = 29 µm, C3 = 14 µm and C5 = 11 µm. The liberation of the cyclosizer fractions of the 2-minute grind material was not evaluated due to a lack of sufficient sample. In this case, only a combined - 38 µm fraction was analysed.

Figure 4-2 to Figure 4-7 show the liberation by size fraction of muscovite and silica in the reference ore for the grinding sizes presented in Table 4-2. Figure 4-2 to Figure 4-7 were plotted in a way that the sum of the mass percentage of all size fractions in the liberation classes is 100. The liberation tables related to Figure 4-2 to Figure 4-7 are presented in Appendix 2.

Figure 4-2, Figure 4-3 and Figure 4-4 show the mass percentage of muscovite in each size fraction and liberation class.

Figure 4-2 shows that at coarsest grinding size tested, the mass of muscovite in the reference ore concentrate on the liberation classes greater than 90% liberated across all size fractions tested.

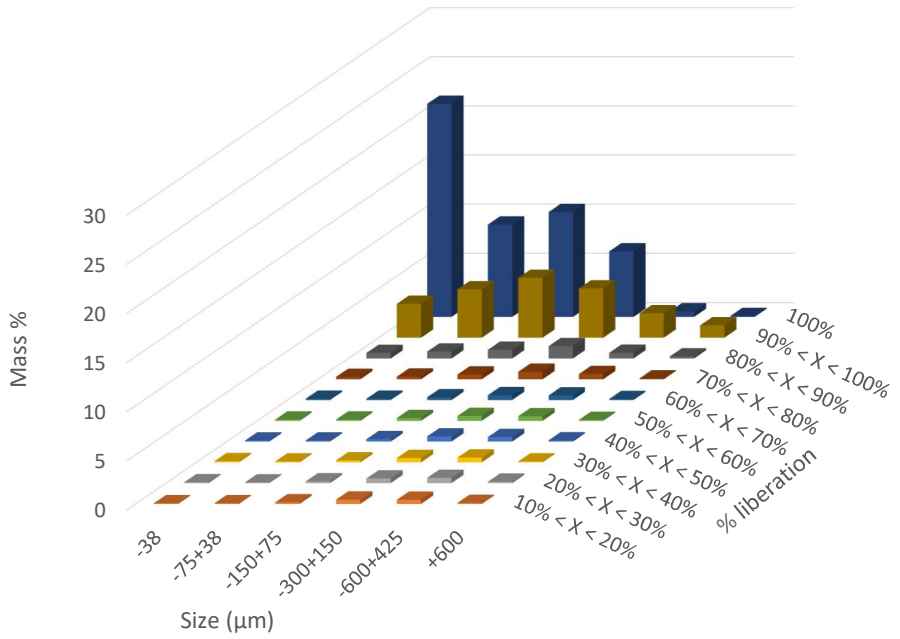

Figure 4-2 - Muscovite bulk liberation of reference ore at 2 minutes, P_{80} 370 µm

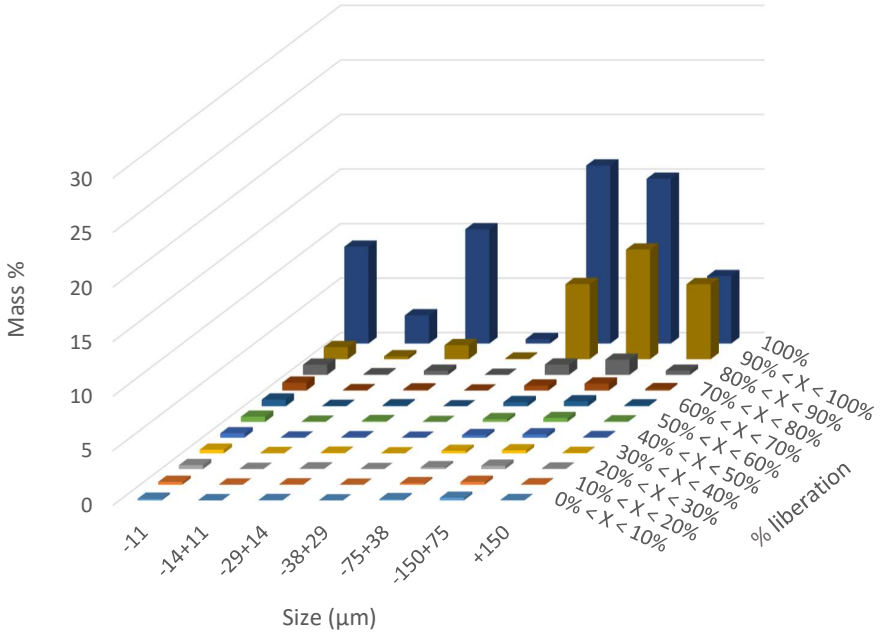

Figure 4-3 – Muscovite bulk liberation of reference ore at 10 minutes, P_{80} 125 µm

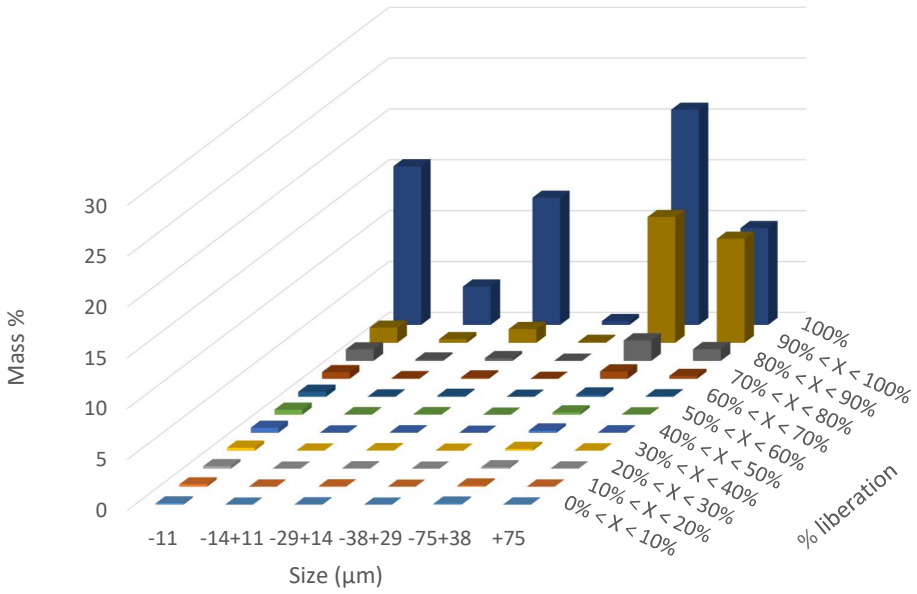

Figure 4-4 - Muscovite bulk liberation of reference ore at 35 minutes, P_{80} 55 µm

Muscovite is well liberated at the three grinding sizes tested because, in Figure 4-2, Figure 4-3 and Figure 4-4 the mass of muscovite concentrates in the liberation classes greater than 90% liberation for all size fractions. Therefore, the degree of liberation of muscovite in Barrick's reference ore is high, greater than 90%.

The liberation of silica in the reference ore sample is shown in Figure 4-5, Figure 4-6 and Figure 4-7.

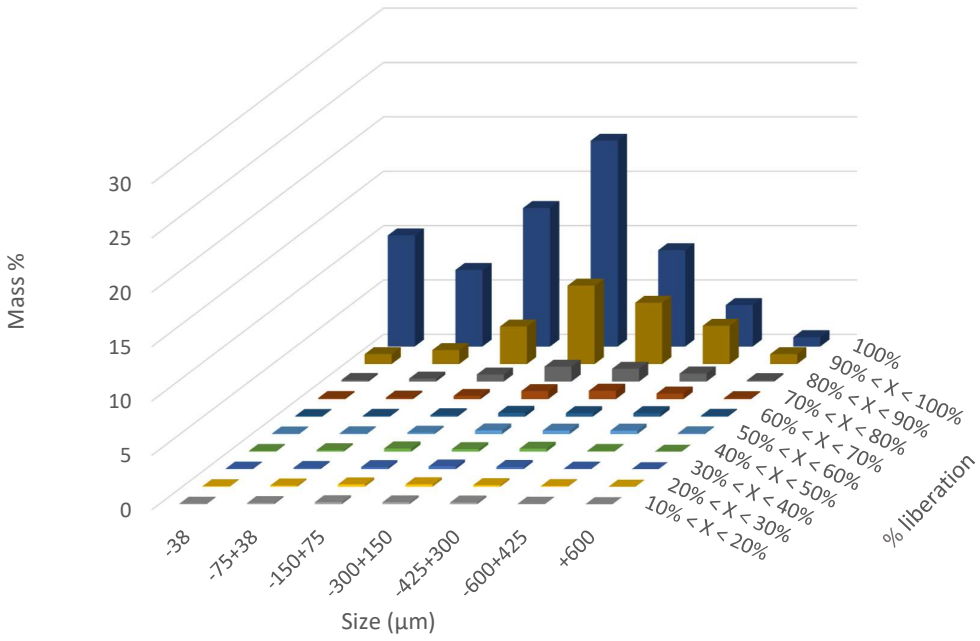

Figure 4-5 - Silica (quartz) liberation of reference ore at 2 minutes, P_{80} 370 µm

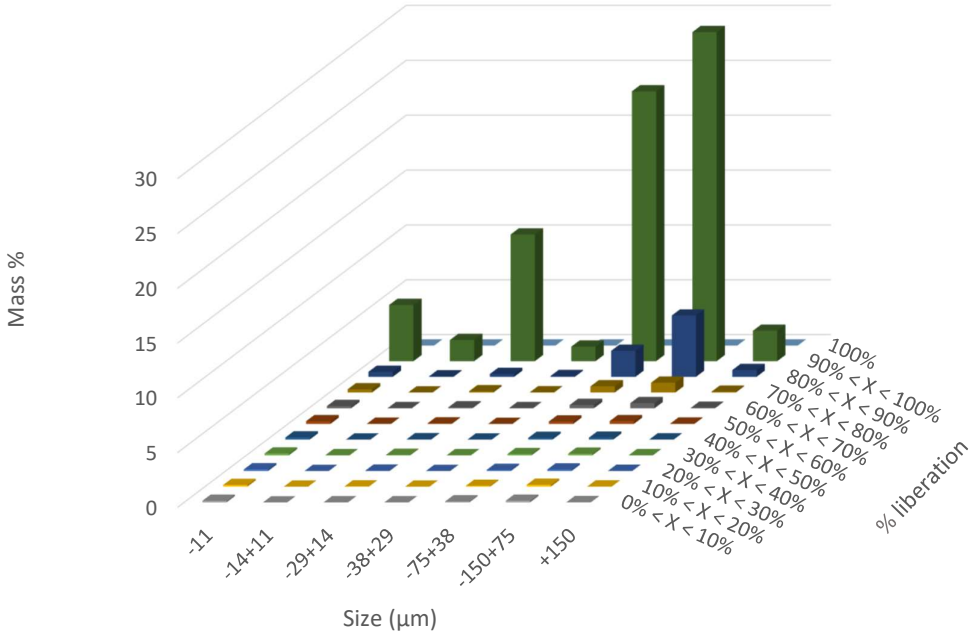

Figure 4-6 - Silica (quartz) liberation of reference ore at 10 minutes, P_{80} 125 µm

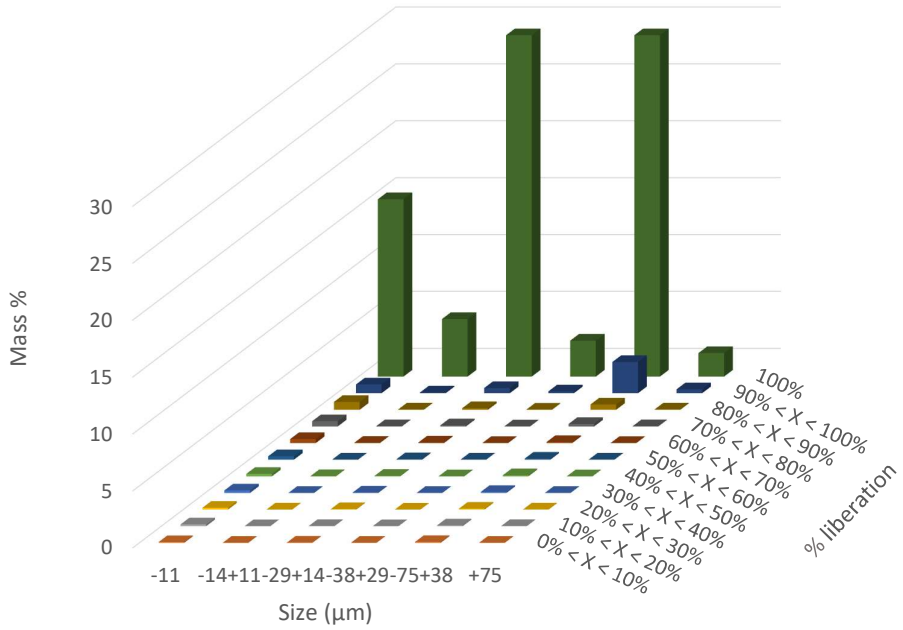

Figure 4-7 - Silica (quartz) liberation of reference ore at 35 minutes, P_{80} 55 µm

Silica is also well liberated at the three grinding sizes tested, as the mass of silica concentrates in the liberation classes greater than 90% liberation for all size fractions, as shown in Figure 4-5, Figure 4-6 and Figure 4-7. A significant improvement of the liberation of silica is noted from Figure 4-5 to Figure 4-6, as the mass of silica in the liberation class of 100% increases.

Figure 4-2 to Figure 4-7 suggested that silica and muscovite are highly liberated (over 90% liberation) at the three grinding sizes of interest. On the basis of that muscovite and silica should present similar liberation characteristics in the problematic ore of Barrick, it is reasonable to use a synthetic ore mixture using pure minerals to represent the real ore, because results would be not be biased due to the presence of composite particles. Therefore, the size distribution of gangue in the synthetic ore mixture is based on the size distribution of fully liberated muscovite and silica in the reference ore.

4.3 Pure Mineral Samples

4.3.1 Pyrite and Arsenopyrite

4.3.1.1 Pyrite and arsenopyrite purity

The purity of pyrite and arsenopyrite samples supplied by GEO Discoveries (GEO Discoveries, 2019) were tested via MLA XBSE to identify and quantify the contamination by other minerals. Figure 4-8 shows the classified MLA XBSE images of pyrite and arsenopyrite.

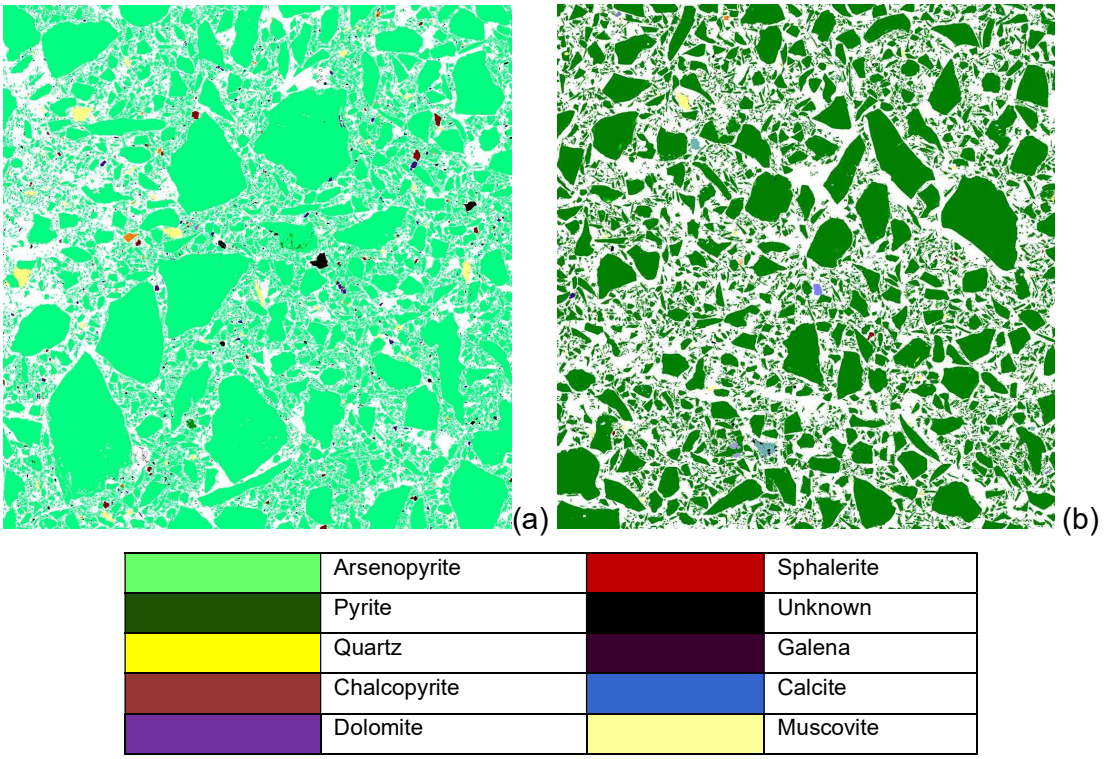

Figure 4-8 – Classified MLA XBSE images. (a) Arsenopyrite (light green), (b) Pyrite (dark green).

The modal mineralogy of the pyrite and arsenopyrite samples, obtained by MLA XBSE, is presented in Table 4-3.

Table 4-3 Composition of Pyrite and Arsenopyrite via MLA XBSE

Pyrite		Arsenopyrite	
Mineral	**%**	**Mineral**	**%**
Pyrite	**98.87**	**Arsenopyrite**	**98.45**
Pyrrhotite	0.35	Galena	0.46
Sillimenite	0.14	Unknown	0.28
Muscovite	0.14	Muscovite	0.21
Quartz	0.10	Sphalerite	0.19
Unknown	0.08	Quartz	0.16
Galena	0.07	Chalcopyrite	0.07
Gypsum	0.06	Pyrite	0.05
Sphalerite	0.05	Sillimenite	0.03
Siderite	0.04	Biotite	0.02
Chalcopyrite	0.03	Chlorite	0.02
Apatite	0.02	Siderite	0.01
Calcite	0.01	Pyrrhotite	0.01
Amphibole	0.01	Plagioclase	0.01
Arsenopyrite	0.01	Amphibole	0.01
Plagioclase	0.01	Calcite	0.01

The MLA XBSE data in Table 4-3 and Figure 4-8 showed that the pyrite and arsenopyrite purchased from GEO Discoveries have high purity levels, over 98%.

4.3.1.2 *Pyrite and arsenopyrite grinding calibration*

The grinding calibration of the samples of pure pyrite and arsenopyrite was primarily designed to determine the grinding time to achieve the target P_{80} and size distribution of the respective minerals in Barrick's White Mountain ore. The size distribution of pyrite, arsenopyrite are based on the QEMSCAN data of White Mountain pilot plant flotation feed from the 2007 campaign provided by Barrick.

Table 4-4 and Figure 4-9 presents the size distribution of arsenopyrite and pyrite samples used in the flotation tests. The grinding curves were produced from a reproducible grinding procedure, which was carried out throughout the testwork program.

Table 4-4 – Size distribution of the samples of pyrite and arsenopyrite used in the flotation tests in cumulative percentage passing

Size (µm)	%Passing Solids	%Passing Arsenopyrite	%Passing Pyrite
150	99.94	99.98	99.93
106	99.60	99.76	99.57
75	97.86	98.51	97.45
53	92.75	93.53	91.84
38	87.30	88.04	85.87
27	62.44	54.00	63.73
19	46.65	38.85	47.22
13	31.86	28.00	30.86
9	21.25	20.52	19.72
7	17.34	16.77	15.76
-7	0.00	0.00	0.00

Figure 4-9 displays the size distribution obtained in the grinding of the pyrite and arsenopyrite for the flotation tests as per Table 4-4.

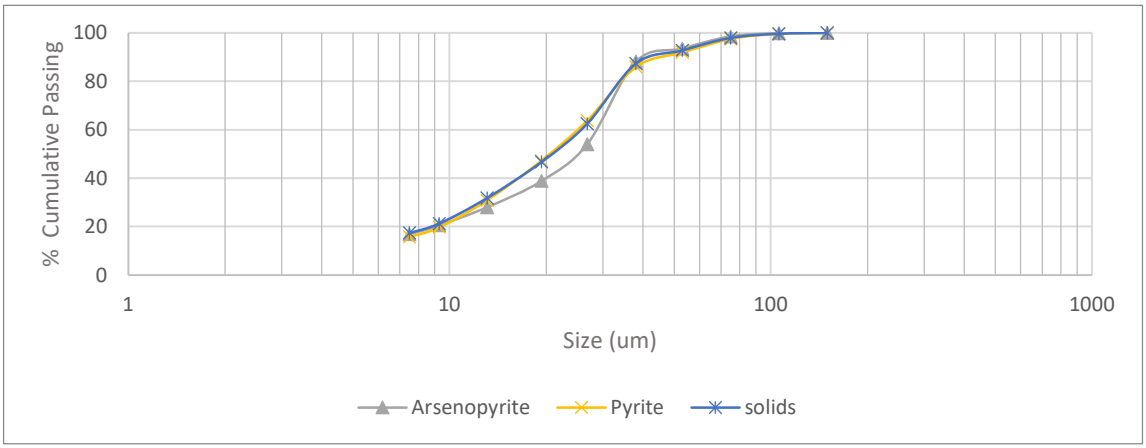

Figure 4-9 – Size distribution of the samples of pyrite and arsenopyrite used in the flotation tests as cumulative percentage passing

The reproducibility of the arsenopyrite and pyrite grinding procedure is shown in Figure 4-10, which displays the cumulative percentage passing of the combined solids. The grinding time selected to achieve those curves is 5 minutes. Grinding times shorter than 5 minutes did not present grinding repeatability.

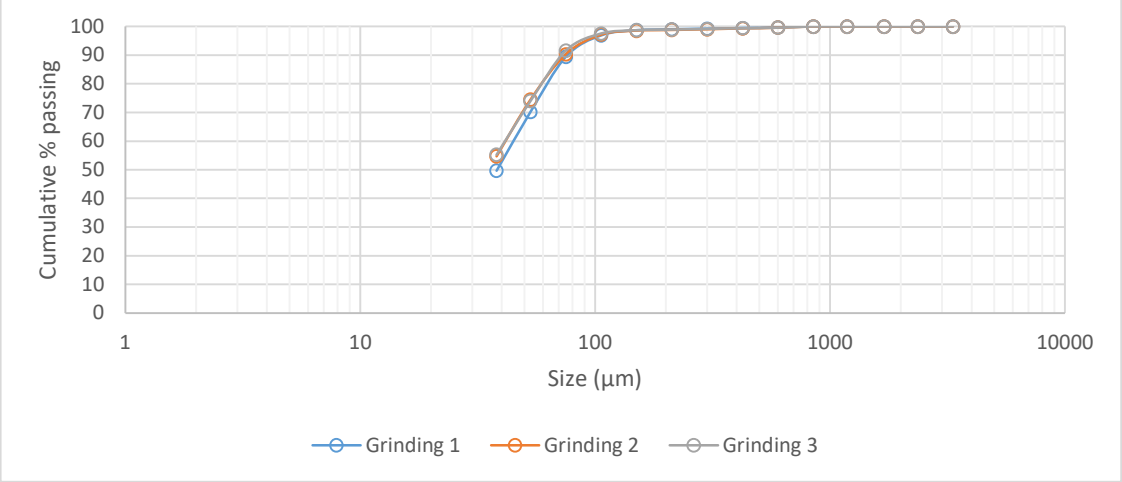

Figure 4-10 – Arsenopyrite and pyrite grinding repeatability

Figure 4-11 compares the size distribution of arsenopyrite and pyrite obtained by grinding procedure with the grain size distribution of arsenopyrite and pyrite in the White Mountain ore.

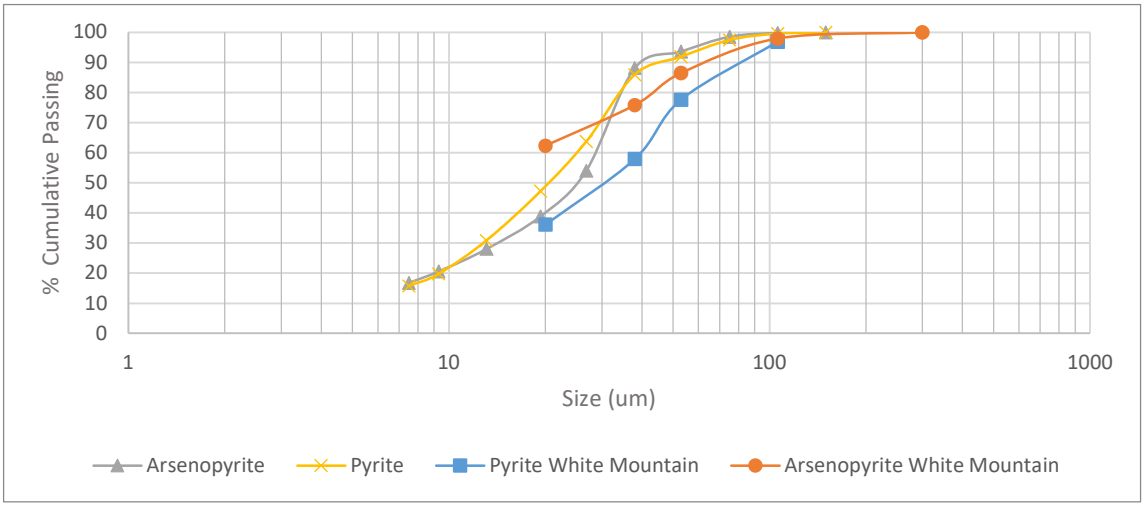

Figure 4-11 - Size distribution of the samples of pure pyrite and arsenopyrite used in the flotation tests compared to the pyrite and arsenopyrite size distribution in the White Mountain ore

It shows that the size distribution obtained by the grinding procedure is finer than the presented at Barrick's ore. Because of the reproducibility limitations of grinding low weight samples in a conventional laboratory-scale rod mill, a finer grinding size of pyrite and arsenopyrite was selected for the flotation tests.

4.3.2 Muscovite

The muscovite sample supplied by Wards Science was tested to identify and quantify any contaminants via QXRD by Sietronics . The XRD patterns were produced using a Bruker-AXS D4 XRD with copper radiation at 40 kV and 30 mA. A graphite monochromator was used in the diffracted beam. Powder mounts were run over a range of 3 to 70°2q, with a 0.02 degree step and a 2 second per step count time. The search/match was carried out using the Bruker Diffracplus Search/Match software and the ICDD PDF-2 database (2006). The quantitative phase analysis was performed using SIROQUANT TM version 4 software.

The QXRD analysis revealed that the sample is 100% muscovite.

The density of muscovite sample supplied measured in a helium pycnometer is 2.90 g/cm^3.

According to, Figure 4-2 to Figure 4-4 muscovite in the reference ore is highly liberated for all grinding times performed. This indicates that the use of pure liberated muscovite in the CCRD experiments provides a valid approximation of the characteristics of muscovite in a real ore.

The size distribution of fully liberated muscovite in reference ore is summarised in Figure 4-12.

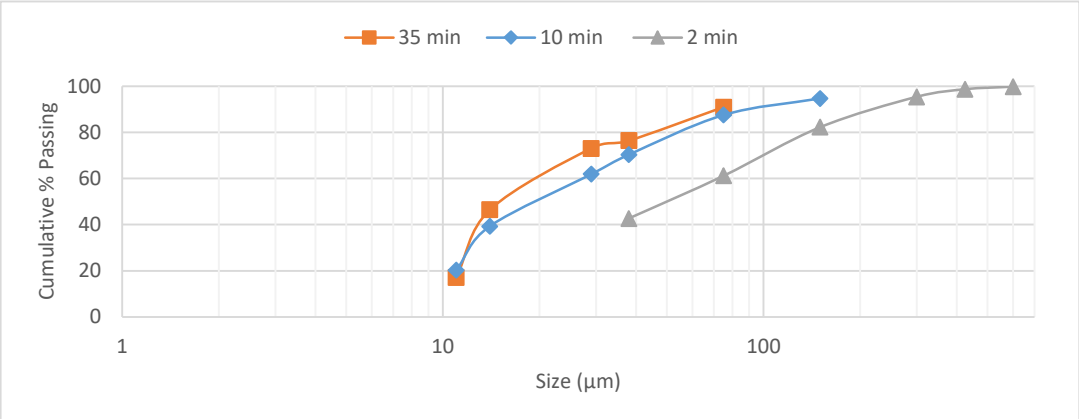

Figure 4-12 – Size distribution of 100% liberated muscovite in reference ore

The P_{80} of muscovite fully liberated in reference ore for each grinding product is shown in Table 4-5.

Table 4-5 – P_{80} Muscovite fully liberated in the reference ore

Grinding time (min)	P_{80} of Muscovite Reference ore (µm)	P_{80} of solids of the reference ore (µm)
2	142	370
10	59	125
35	47	55

The P_{80} of muscovite in the reference ore varies from 47 µm to 142 µm. This data supports the proposed muscovite P_{80} range to be investigated in the CCRD program. A comparison with the size distribution of muscovite in the White Mountain (WM) ore is shown in Figure 4-13.

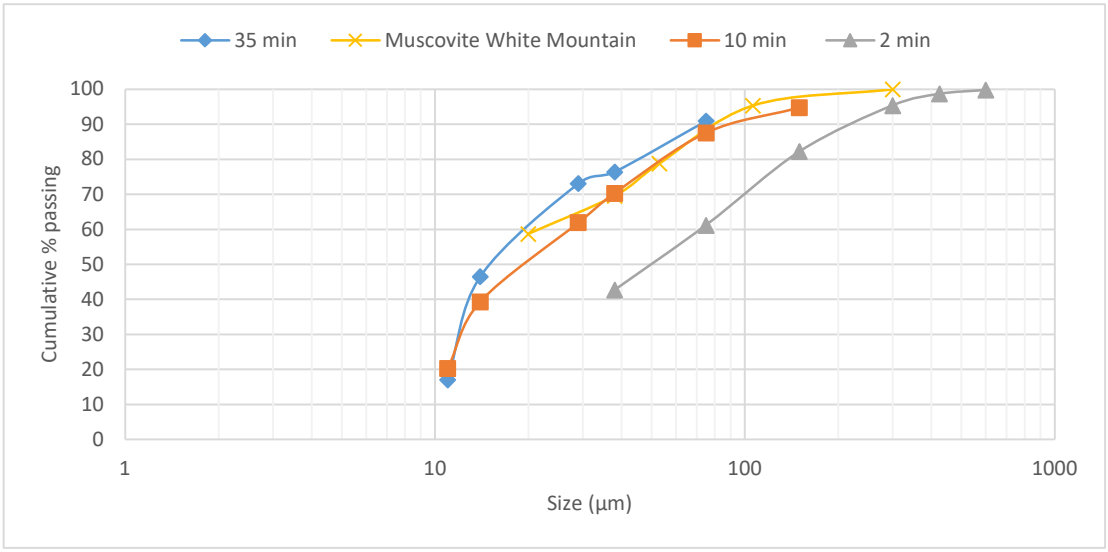

Figure 4-13 – Comparison of the size distribution of muscovite in White Mountain ore to the 100% liberated muscovite in Reference ore

Figure 4-13 shows that the size distribution of the muscovite in White Mountain is similar to the size distribution of that in reference ore, obtained with 10 minutes grinding. It suggests that the properties of muscovite in the White Mountain ore are similar to the reference ore and that the muscovite size distribution in the White Mountain ore is included in the range studied.

The muscovite sample preparation for the CCRD tests is based on the size distribution range presented by the reference ore and White Mountain ore information. The muscovite size distribution in the reference ore is used as a basis to create the muscovite samples for the limiting conditions of P_{80} investigated, 50 µm and 150 µm. The CCRD factorial design investigates 5 levels of each factor tested. The P_{80} values of muscovite were then interpolated using the method described below based on α = 2.38 to provided rotatability to the CCRD design.

The complete size distributions for the interpolated P_{80} values were generated through fitting the muscovite size distributions of White Mountain and the reference ore to a commonly used size distribution function, the Rosin-Rammler equation 4-1. The size distributions of the muscovite presented in Figure 4-13 were fitted using the Rosin-Rammler Distribution (Napier-Munn et al. 1996):

$$Wr = 100\, e^{\left[-\left(\frac{x}{a}\right)^{b}\right]}\% \qquad \text{(Equation 4-1)}$$

Where:

Wr = weight % cumulative retained

x = size

a = size which (100/e) = 36.8% of particles retained

b = constant = slope of plot ln ln (100/Wr) versus ln x

The slope of the plot, parameter b, did not vary widely for the fine grinding between the reference ore and the White Mountain. It differed slightly for the coarse size only. It was decided arbitrarily based on the low variability of b, to use a single value to fit all size curves, which is the White Mountain value. The parameter an of the size curves with P_{80} 50 µm and 150 µm were obtained directly from the size distribution of the reference ore. Those from interpolated P_{80} values were calculated based α to provided rotatability to the CCRD design, and the parameter in the reference ore.

Table 4-6 shows the select Rosin-Rammler parameters used to calculate the size distribution of muscovite by P_{80} value included in the CCRD.

Table 4-6 - Rosin-Rammler parameters used to calculate the complete size distribution of muscovite

P_{80} (µm)	150	121	100	79	50
b	0.7504	0.7504	0.7504	0.7504	0.7504
a (µm)	82	65.0	52.6	40	23

Figure 4-14 shows the Rosin-Rammler fit of the size distribution of muscovite in the reference ore and White Mountain.

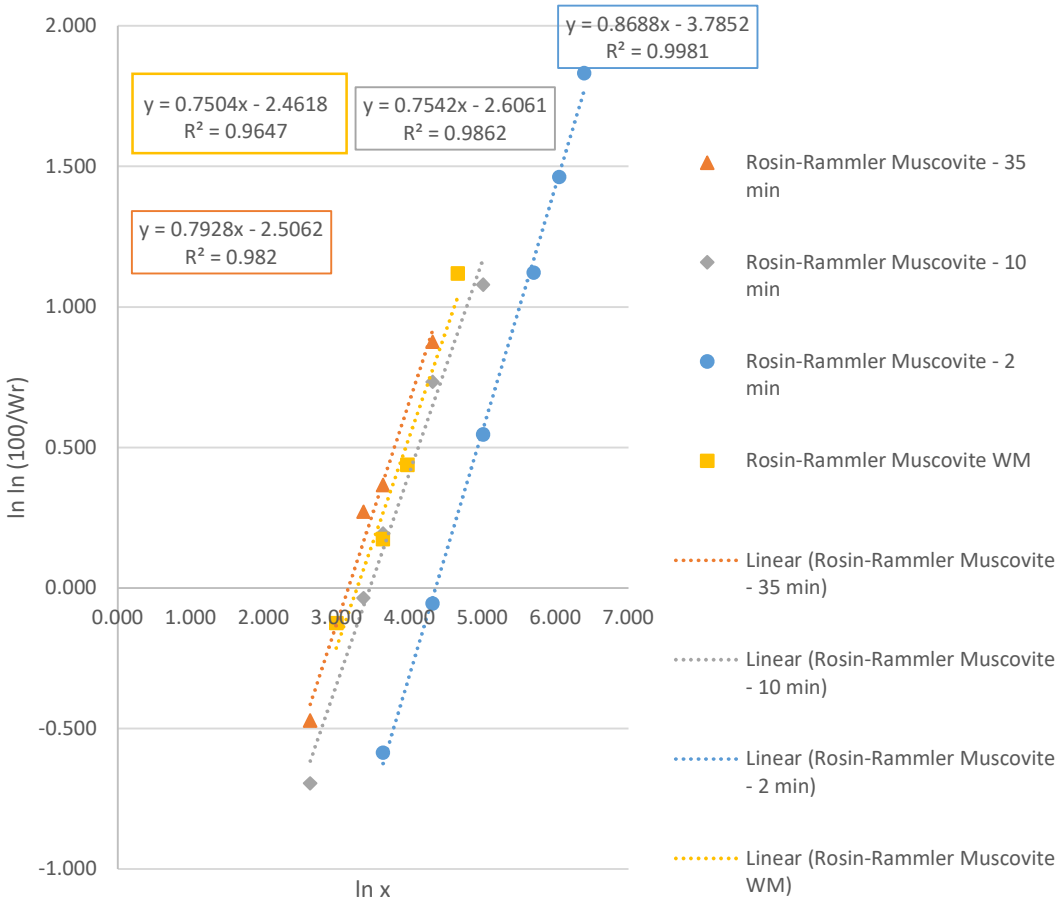

Figure 4-14 – Rosin-Rammler fit of the size distribution of muscovite in the reference ore and White Mountain

Table 4-7 shows the size distribution used to assemble the samples of muscovite for the CCRD tests.

Table 4-7 – Size distribution of muscovite fitted using the Rosin-Rammler method

Percentage Retained Rosin-Rammler calculated						
P_{80} (µm)		**150**	**121**	**100**	**79**	**50**
Size (µm)	**600**	1.17%	0.50%	0.20%	0.05%	0.00%
	425	2.06%	1.17%	0.62%	0.23%	0.01%
	300	3.88%	2.61%	1.66%	0.80%	0.09%
	212	5.93%	4.54%	3.31%	1.98%	0.40%
	150	7.74%	6.55%	5.32%	3.73%	1.18%
	106	9.01%	8.25%	7.28%	5.79%	2.61%
	75	9.50%	9.23%	8.70%	7.63%	4.53%
	53	9.39%	9.56%	9.46%	8.95%	6.57%
	38	8.39%	8.85%	9.10%	9.13%	7.88%
	-38	42.93%	48.75%	54.34%	61.71%	76.72%
Total		**100.00%**	**100.01%**	**99.99%**	**100%**	**99.99%**

To verify if the calculated size distribution presented in Table 4-7 are distributed between the required range, the size curves of muscovite are plotted in conjunction with the reference ore curves, as shown in Figure 4-15.

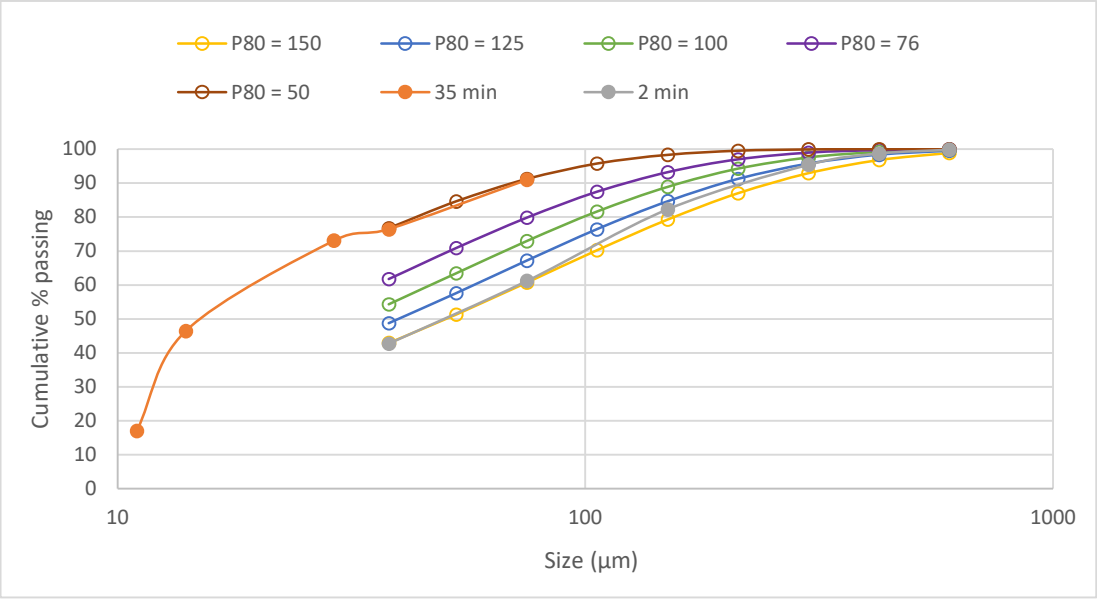

Figure 4-15 – Size distribution of muscovite obtained via Rosin-Rammler and in Reference ore

Figure 4-15 compares the fitted size distributions using the Rosin-Rammler method with the reference data. It shows that the fitted curves fall between the limiting size distributions of reference ore. It indicates that the size distributions obtained via this method are valid to represent the different P_{80} evaluated in the CCRD factorial design.

4.4 Silica

The silica used to create the synthetic ore is Sibelco's Silica Flour 60G, supplied in 25 Kg bags. It is produced from chemically treated, and water washed high purity silica sand. The specific gravity of the product is 2.66.

Table 4-8 shows the composition of the Sibelco's Silica Flour 60G, as provided by the manufacturer. The silica is 99.7% pure. The alumina contaminant present is at a low enough level to not interfere in the interpretation of the flotation assays. This is important, given that aluminium is the assay marker for muscovite.

Table 4-8 – Silica Composition (Sibelco datasheet)

Mineral	Formula	Per cent by Weight
Silica	SiO_2	99.70%
Alumina	Al_2O_3	0.09%
Ferric Oxide	Fe_2O_3	0.02%
Titania	TiO_2	0.02%
Lime	CaO	<0.1%
Loss on Ignition	1000ºC	0.2%

Table 4-9 shows the size distribution of the Sibelco's Silica Flour 60G. The size distribution was obtained via Malvern sizer. The calculated P_{80} of the silica is 95 μm. The size distribution showed that 52% of the silica is below 38 μm.

Figure 4-16 compares the size distribution of the Sibelco silica with the size distribution of silica in the White Mountain ore. The curves are sufficiently similar to allow the use of the silica Sibelco Flour 60G as the quartz component of the flotation samples without size distribution adjustment.

Table 4-9 – Size distribution of silica (Malvern sizer)

Size (µm)	Cumulative %Passing	%Retained
300	**100%**	0%
212	**97%**	3%
150	**92%**	5%
106	**83%**	8.5%
75	**73%**	10%
53	**62%**	11.5%
38	**52%**	10%
24	**40%**	12%
14	**30%**	10%
7	**20%**	10%
1.5	**8%**	12%
0.1	**1%**	7%

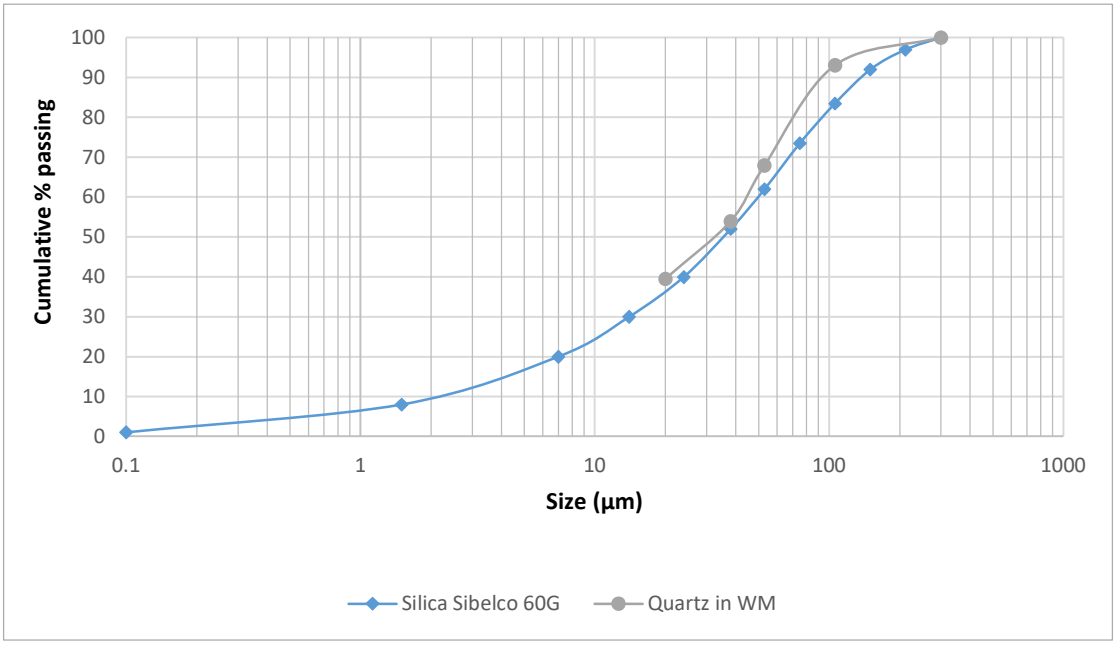

Figure 4-16 – Comparison of the size distribution of the quartz in White Mountain ore with the silica 60G from Sibelco

Chapter 5

DETERMINING THE SIGNIFICANCE OF THE FACTORS ON THE FLOTATION RATE CONSTANT OF ARSENOPYRITE AND PYRITE

---

5 Determining the Significance of the Factors on the Flotation Rate Constant of Arsenopyrite and Pyrite Using a Central Composite Rotatable Design

5.1 Introduction

This chapter presents the key findings from the flotation tests performed using the Central Composite Rotatable Design (CCRD) method. It describes the significant variables affecting the flotation rate constants of arsenopyrite and pyrite found through regression analysis.

The objectives of the full CCRD experiments is to understand which of the variables investigated have a significant effect on the flotation kinetics of arsenopyrite and pyrite and to determine whether muscovite has a deleterious effect on flotation rates.

Therefore, this chapter is focussed on testing *Hypothesis 1,* whether

The presence of a high concentration of muscovite has a detrimental effect on the flotation rate of pyrite.

The Chapter is divided into two parts. The first part presents the results of the preliminary 2-factor CCRD to evaluate the appropriate collector dosage to use in subsequent CCRD tests. The second part describes the analyses of the significant variables affecting the flotation rate of arsenopyrite and pyrite based on the main CCRD program.

5.2 Identifying the Appropriate Collector Dosage for the CCRD

The relationship between the recovery of pyrite, PAX dosage and pH have been reported by Fuerstenau et al. (1968) and Monte et al. (2002).

According to Fuerstenau et al. (1968), the recovery of pyrite is a function of pH and the collector dosage, as shown in Figure 5-1. The collector dosages of PAX presented by Fuerstenau et al. (1968) are between 3 x 10^{-6} and 1 x 10^{-5} M (approximately 8 g/t), without the presence of $CuSO_4$ as the activator.

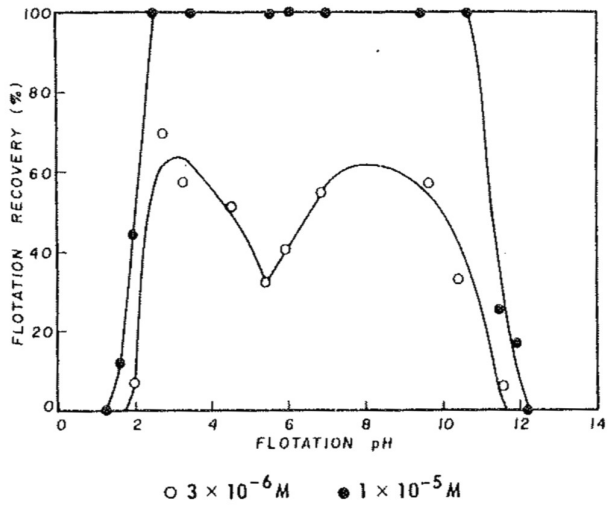

Figure 5-1 – Recovery of pyrite as a function of flotation pH with various additions of potassium amyl xanthate (Fuerstenau et al. 1968)

Monte et al. (2002) observed that the recovery of pyrite and arsenopyrite increased significantly with the PAX concentration, at pH 6.5, using CuSO4, as shown in Figure 5-2. The effect of pH was not investigated.

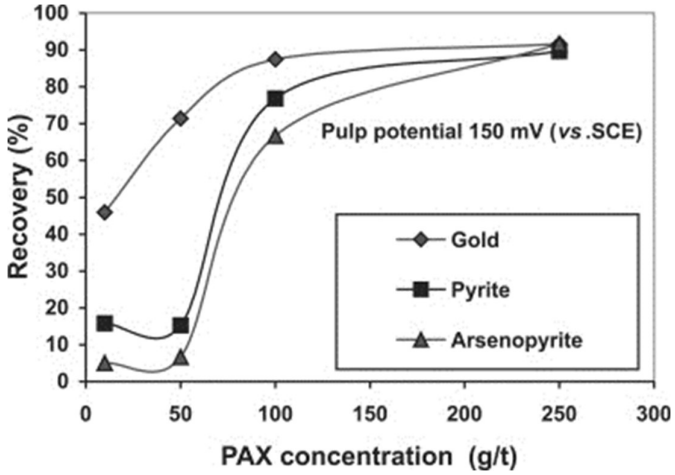

Figure 5-2 - Effect of PAX concentration on the recovery of gold, pyrite and arsenopyrite (Monte et al., 2002)

The observations of Fuerstenau et al. (1968) and Monte et al. (2002) suggested that the interaction of pH and collector dosage could affect the recovery of the pyritic minerals, consequently affecting the flotation rates in CCRD.

The slurry pH included in the main CCRD factorial design as a factor of interest to investigate values that would promote hetero-aggregation of muscovite by changing its surface charge. The effect of the interaction of pH and collector dosage shall be understood and mapped in the developed tests, so it would not mislead the interpretation of the mechanism behind the pH effect.

The collector dosage could be introduced in the CCRD design as a factor. However, this could complicate the evaluation of the mechanism by which pH affects the flotation rate. In addition, it would increase significantly the number of tests required. To develop a 6-factors CCRD factorial design, 90 batch flotation tests are required, instead of 54 for a 5-factors CCRD factorial design, this number was not practical due to time, and sample constraints.

In order to keep the number of tests at a feasible number and to reduce the complexity of the full CCRD experiments, the full CCRD experiments were conducted at a fixed collector dosage. This minimises the effect of the interaction of pH and collector dosage on the recovery and flotation rates of pyrite and arsenopyrite. It simplifies the investigation of the mechanism behind any effect of pH because excludes the possibility of being combined with the effect of the collector dosage.

Thus, a preliminary set of experiments based on a 2-factor CCRD design was performed to determine the optimum concentration of PAX in which the final recovery and the flotation rate constant would present minimal variation over a range of pH from 4 to 10. The concentrations of PAX evaluated were in the range 30 g/t and 300 g/t, and the flotation feed composition was constant at 1.6% arsenopyrite, 3.5% pyrite and 95% silica. Muscovite was not introduced in these tests. The range was selected to include the PAX dosage used in the feasibility study of White Mountain conducted in 2007 (AMEC, 2007a; AMEC, 2007b). Table 5-1 shows the order and conditions of the tests of the 2-factor CCRD design.

Table 5-1 - Preliminary CCRD Test Program

Run Order	Blocks	pH	PAX dosage
1	2	7.0	165
2	2	7.0	30
3	2	4.0	165
4	2	7.0	165
5	2	7.0	300
6	2	10.0	165
7	2	7.0	165
8	1	4.9	260
9	1	7.0	165
10	1	9.1	260
11	1	7.0	165
12	1	4.9	69
13	1	9.1	69
14	1	7.0	165

5.2.1 Evaluation of the Effect of Collector Dosage on the Cumulative Recovery of Arsenopyrite and Pyrite

A total of 14 flotation batch tests were developed according to the 2-factor CCRD design. The cumulative recoveries of arsenopyrite and pyrite other time are shown respectively in Figure 5-3 and Figure 5-4.

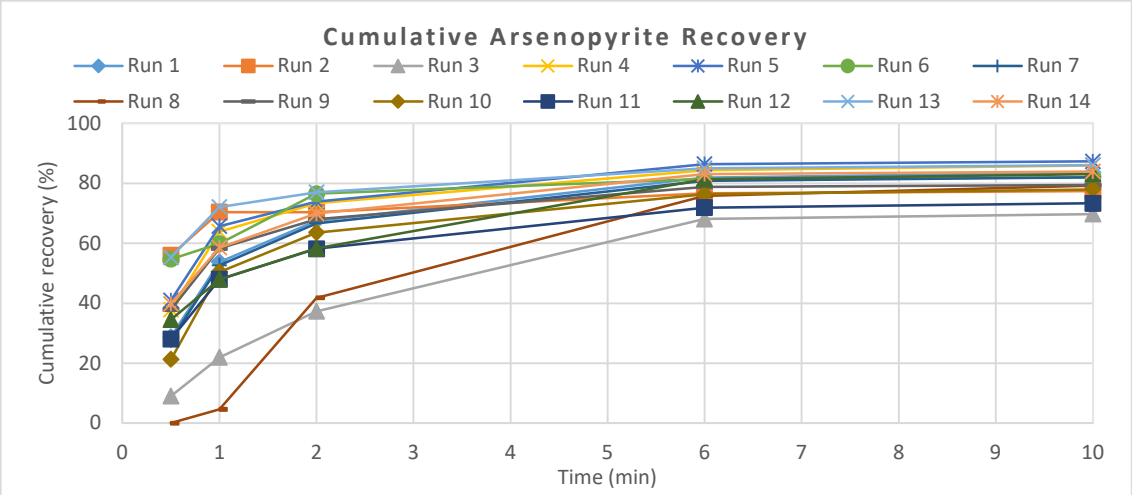

Figure 5-3 – Cumulative recovery of arsenopyrite in the preliminary CCRD

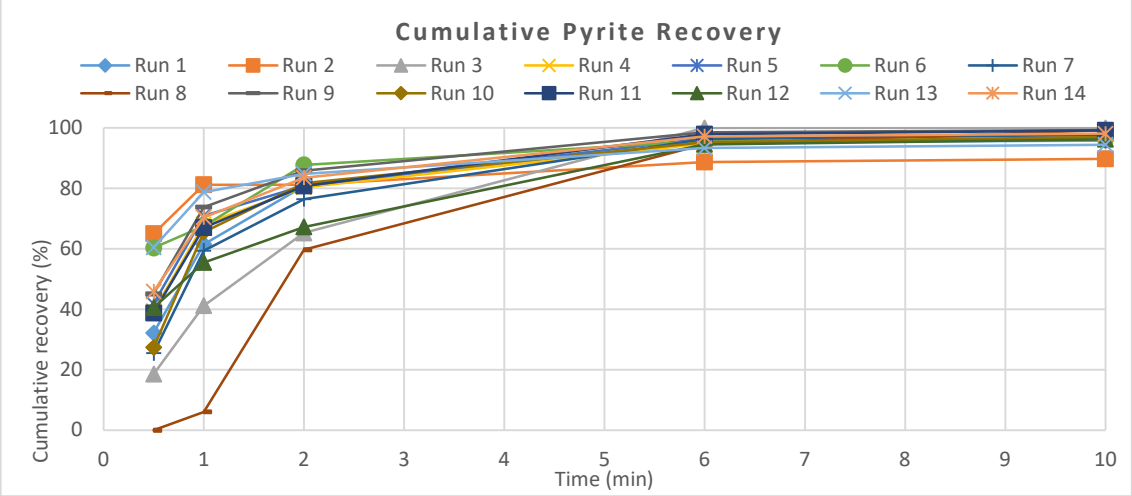

Figure 5-4 - Cumulative recovery of pyrite in the preliminary CCRD

The final recoveries of pyrite at the end of the flotation time are generally higher than the arsenopyrite. The final pyrite recoveries varied between 90% and 100%, while arsenopyrite recoveries varied between 70 and 90%. Arsenopyrite final recoveries show a larger spread of values than pyrite. It suggests that changes in pH and collector dosage may have a more significant effect on the recoveries of arsenopyrite than pyrite.

Regression models for the recovery of pyrite and arsenopyrite were developed to investigate the effect of pH and collector dosage on the recovery of arsenopyrite and pyrite and to estimate the appropriate dosage of PAX to obtain the minimum variation of recovery across the pH range tested.

The models were fitted using the stepwise regression tool of the Minitab® 18 software. The stepwise regression method starts with an empty model and adds terms with P-values that are less than or equal to the specified alpha to remove the term in the model. It excludes all terms with P-values corresponding to an alpha value greater than the chosen value from inclusion in the model. The alpha value of 0.15 was selected arbitrarily for these analyses, and only terms with P-values lower than 0.05 (95% significance) were considered for the regression equations.

Table 5-2 shows the model statistics obtained for the recovery models of pyrite and arsenopyrite. The predictors selected for the regression analyses were: PAX dosage in g/t, pH, the square of PAX concentration in $(g/t)^2$, pH^2 and the interaction term PAX concentration x pH.

Table 5-2 - Model statistics of the pyrite flotation recovery

Model Summary	Standard error	Confidence Interval at 95%	Predictive uncertainty	R^2
Arsenopyrite	-	-	-	-
Pyrite	0.55	1.21%	5.0	32%

The stepwise regression analysis did not return terms for the recovery model of arsenopyrite. Hence, pH and collector dosage are not significant predictors of the final recovery of arsenopyrite. This is unexpected, considering the spread of recoveries observed in Figure 5-3.

The model of recovery of pyrite obtained in equation 5-1 can be used to understand the significance of pH. The coefficient of determination (R^2) for the recovery model of pyrite is too low to provide a good prediction of the final recovery.

The model of the recovery of pyrite is presented in equation 5-1:

$$R_{py} = 99.971 - 0.01551pH^2 \qquad \text{(Equation 5-1)}$$

Where pH is the absolute pH of the test.

The level of significance of the terms of equation 5-1 is presented in Table 5-3.

Table 5-3 Model coefficients statistics of the pyrite flotation recovery

Term	Coefficient	SE of Coefficient	Coded Coefficient	P-value
Constant	99.97	0.368	99.171	0.000
pH^2	-0.015	0.0065	-0.365	0.035

The results of the preliminary CCRD tests indicated that the collector dosage is not a significant factor affecting the recovery of pyrite. The constant and the pH are the most significant predictors of the recovery of pyrite in equation 5-1 because it has the highest coded coefficient absolute value and the lowest P-value. The pH has a

deleterious effect on the recovery of pyrite, as indicated by the negative sign of the pH term.

Comparing the PAX concentrations used by Fuerstenau et al. (1968), which were between 3×10^{-6} and 1×10^{-5} M, to those used in the preliminary CCRD (30 g/t = 3.6×10^{-5} to 300 g/t = 3.8×10^{-4} M), it is expected that the collector dosage would not affect the final recovery of pyrite.

The regression analyses indicated that the PAX concentration from 30 to 300 g/t does not affect the final recovery of the pyrite and arsenopyrite in the pH range studied, from 4 to 10. However, the pH had a deleterious effect on the pyrite recovery. Considering the pH range studied, from pH 4 to 10, the expected variation in pyrite recovery predicted by the model presented in Equation 5-1 is from 99.722% to 98.420%. This variation is expected because the mechanism of formation of dixanthogen and oxidation of pyrite are pH-dependent, thus affecting the recovery and potentially the flotation rate of pyrite.

The flotation rates of arsenopyrite and pyrite were then evaluated to define the most appropriate PAX dosage to conduct the CCRD experiments.

5.2.2 Evaluation of the Effect of Collector Dosage on the Flotation Rate of Arsenopyrite and Pyrite

The flotation rate constants were estimated based on the equation:

$$R = R_{\infty}\left(1 - e^{(-kt)}\right) \qquad \text{(Equation 5-2)}$$

Where R is the flotation recovery at a given time, R_{∞} is the final flotation recovery, t is the flotation time, and k is the flotation rate constant.

The effect of collector dosage and pH in the calculated flotation rate of arsenopyrite and pyrite, for each of the 14 tests, was investigated by regression models obtained using the stepwise regression tool of Minitab® 18 software.

Table 5-4 shows the model statistics of the regression model of the flotation rate constants of pyrite and arsenopyrite.

Table 5-4 - Model statistics of the flotation rate constant

Model Summary	Standard error	Confidence Interval at 95%	Predictive uncertainty	R^2
Pyrite	0.256	0.57	2.21	76%
Arsenopyrite	0.264	0.59	2.16	77%

Table 5-4 shows that the models of the flotation rate constant of pyrite and arsenopyrite presented a high coefficient of determination (R^2) and low predictive uncertainty. Hence, the flotation rate models present a good predictive capacity.

The flotation rate regression equations of arsenopyrite and pyrite are presented as equation 5-3 and 5-4 respectively:

$$k_{aspy} = 1.190 + 0.1563pH - 0.01320PAX + 0.000029PAX^2 \quad \text{(Equation 5-3)}$$

$$k_{py} = -0.605 + 0.367pH + 0.000018PAX^2 - 0.001286pH\ x\ PAX \quad \text{(Equation 5-4)}$$

Where pH is the absolute pH of the test and PAX is the dosage of potassium amyl xanthate in grams per tonne of feed.

The statistics of the coefficient for the flotation rate constant regressions presented by equations 5-3 and 5-4 are shown in Table 5-5 and Table 5-6.

Table 5-5 Model coefficients statistics of the flotation rate constant of arsenopyrite

Term	Coefficients	SE of Coefficient	Coded Coefficients	P-value
Constant	1.19	0.425	1.0498	0.002
pH	0.1563	0.044	0.26	0.005
PAX	-0.0132	0.00364	-0.989	0.005
PAX^2	0.000029	0.000011	0.747	0.021

The stepwise regression method selected pH, PAX dosage and the square of PAX dosage as the most significant predictors of the flotation rate of the arsenopyrite, as shown in Table 5-5 by the P-values of these predictors being lower than 0.05.

The coded coefficients in Table 5-5, showed that the most significant predictor for the regression of the flotation rate constant of arsenopyrite is the constant, followed by the PAX dosage, the square of PAX dosage and pH. The terms with a high absolute value of the coded coefficient are the most significant terms of the model.

These results show that the effect of PAX dosage on the flotation rate of arsenopyrite is greater than the effect of pH. Those effects are not correlated, as no interactive terms such as pH x PAX dosage, are observed in the regression analysis.

It is important to note that, although the pH and PAX dosage were not significant predictors for the final recovery of arsenopyrite, these factors are significant predictors of the flotation rate constant. The results of the analysis show that the effect of the collector dosage on the flotation rate of arsenopyrite is not dependent on the pH.

Table 5-6 Model coefficients statistics of the flotation rate constant of pyrite

Term	Coefficients	SE of Coefficient	Coded Coefficients	P-value
Constant	-0.605	0.407	1.0491	0.019
pH	0.367	0.0778	0.611	0.005
PAX^2	0.000018	0.000008	0.452	0.005
pHxPAX	-0.00129	0.000394	-0.775	0.021

The stepwise regression analysis selected the following as the most significant predictors of the flotation rate of the pyrite: pH, the square of PAX dosage, and the interaction of pH x PAX (as shown in Table 5-6 by the P-values of the predictors lower than 0.05).

The most significant predictors for the pyrite flotation rate constant are the constant, followed by the interaction of pH x PAX dosage, the pH and the square of PAX dosage, as shown by the standardised coefficients in Table 5-6.

The effect of the collector dosage on the flotation rate of pyrite is correlated to the pH, as the interaction term pH x PAX dosage shown to be a significant factor through the regression analysis.

In conclusion, the selection of the appropriate collector dosage should minimise the effect of this interaction on the flotation rate of pyrite, as it is not relevant to the flotation rate of arsenopyrite.

5.2.3 Selecting the Collector Dosage for the Full CCRD Tests

As per Table 5-2 and Table 5-3, the collector dosage is not a predictor of the found recovery of pyrite and arsenopyrite at the end of the flotation test. Thus, the selection of the appropriate collector dosage via recovery analysis is not relevant.

However, the flotation rate constants of arsenopyrite and pyrite are a function of the pH and the PAX dosage, as shown by equations 5-3 and 5-4. Therefore, understanding the effect of collector dosage on the flotation rate constant is essential, as the flotation rate constants of pyrite and arsenopyrite are key characteristics which are the focus of the full CCRD experimental program.

The selection of the optimum collector dosage should be the value at which the variation of the flotation rate constant with the pH is minimal. This is required to minimise the effect of collector dosage in the full CCRD tests.

The selection of collector dosage that presents the minimal variation of the flotation rate constants with pH is made through the analysis of the response surfaces generated by equations 5-3 and 5-4.

The response surface of the flotation rate constant of arsenopyrite is shown in Figure 5-5. It indicates that there is a gradient of variation of the flotation rate constant of arsenopyrite versus the pH throughout the range of collector dosage tested. Clear plateaus of collector dosage, where the flotation rate does not change significantly with the pH were not identified in Figure 5-5.

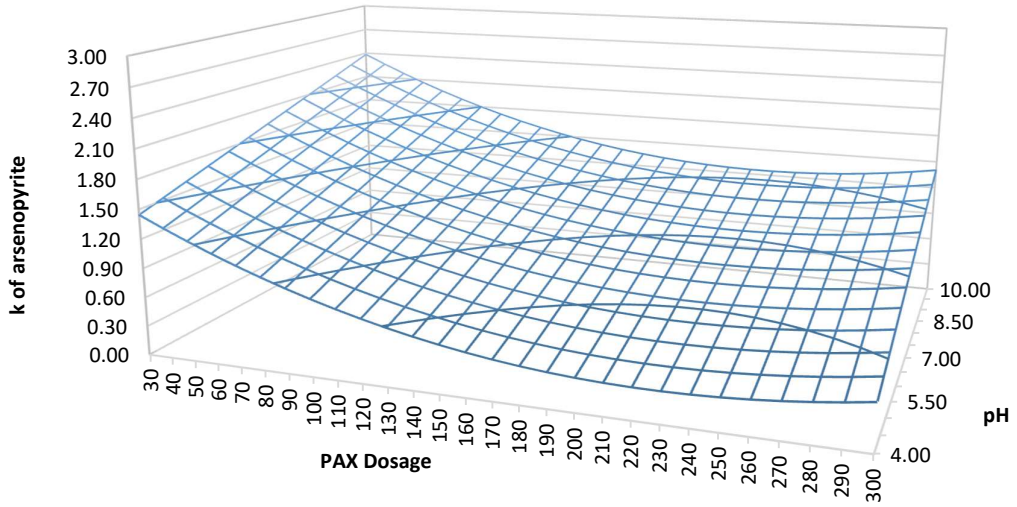

Figure 5-5 – Response surface of the flotation rate constant of arsenopyrite as a function of pH and collector dosage

Figure 5-6 presents a 2D perspective of Figure 5-5, plotting the relationship between flotation rate constant of arsenopyrite and pH at the collector dosages 30 g/t, 165 g /t, and 300 g/t. The confidence intervals at 95% confidence are displayed as error bars.

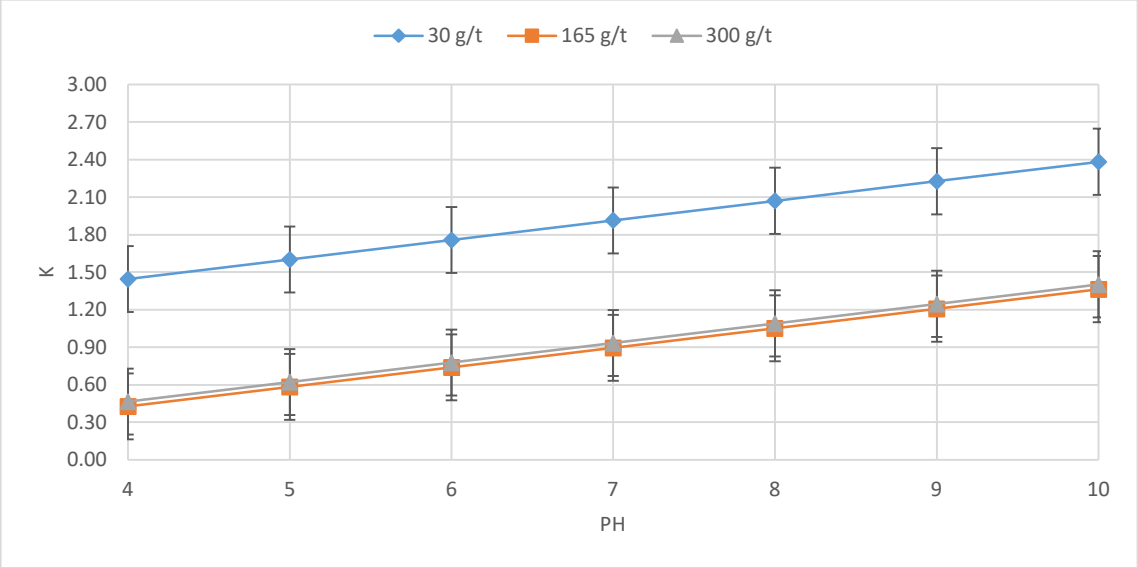

Figure 5-6 - Flotation rate constant of arsenopyrite versus pH for the PAX dosage of 30 g/t, 165 g/t, and 300 g/t.

Through Figure 5-6, it can be observed that there are no significant differences between the flotation rates constants of arsenopyrite at 165 g/t and 300 g/t of PAX. The highest flotation rate constants for arsenopyrite happen at the PAX dosage of 30 g/t. The gradient of variation of the flotation rate constant of arsenopyrite from pH 4 to 10 is approximately the same at all the displayed PAX dosages in Figure 5-6.

Figure 5-7 shows the response surface of the flotation rate constant of pyrite versus pH and PAX dosage. It can be observed that the gradient, by which the flotation rate constant of pyrite increases with the increase of pH, reduces with the increase of PAX dosage. The response surface indicated that at high PAX dosages, the variation of the flotation rate constant of pyrite with the pH is minimum. Therefore, this is the desirable PAX dosage range to use in the full CCRD tests, as the PAX dosage would have a minimal effect on the rate constant due to the variation of pH.

Figure 5-8 presents a 2D perspective of Figure 5-7 displaying the relationship between the flotation rate constant of pyrite and pH at the PAX dosages of 30 g/t, 165 g/t, and 300 g/t.

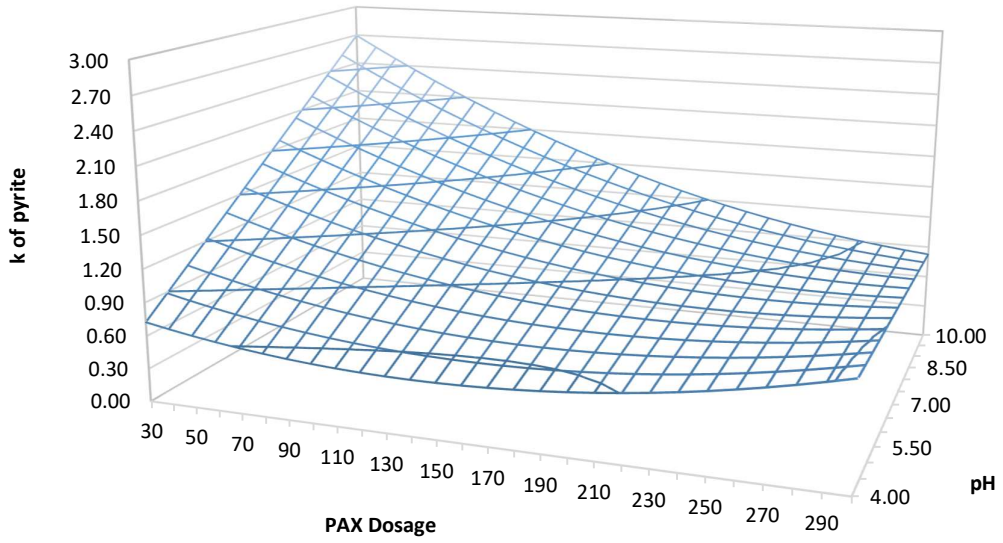

Figure 5-7 – Response surface of the flotation rate constant of pyrite

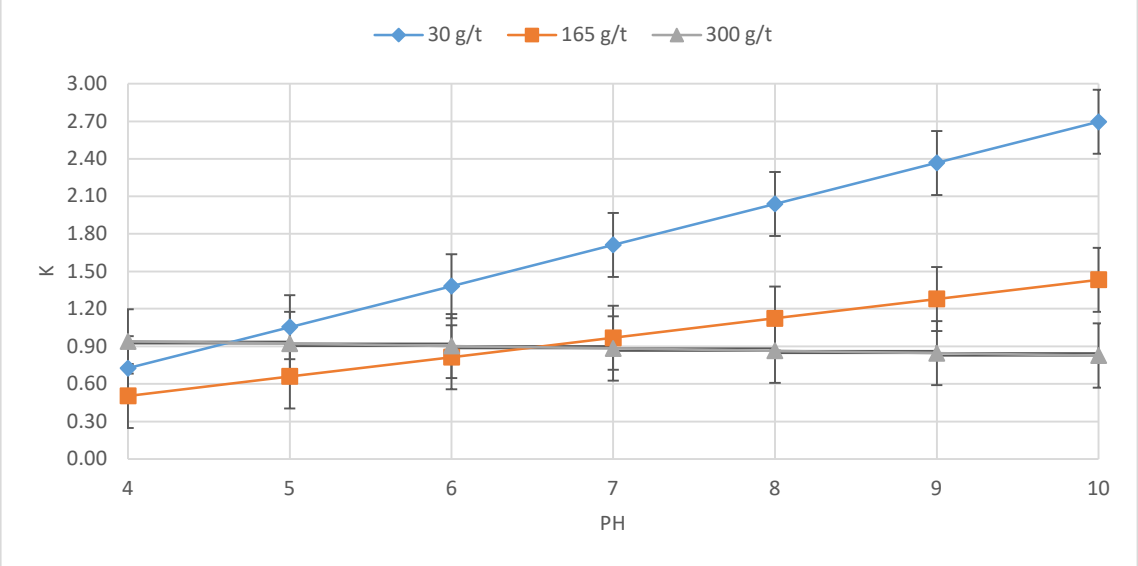

Figure 5-8 - Flotation rate constant of pyrite versus pH for the PAX dosage of 30 g/t, 165 g/t, and 300 g/t.

In Figure 5-8, it is easier to observe the gradient by which the flotation rate constant of pyrite changes with pH due to the variation of the PAX dosage, compared with Figure 5-7. The flotation rate constant of pyrite at the PAX dosage of 300 g/t does not change significantly with pH according to Figure 5-8, because it falls within the 95% confidence intervals.

The PAX dosage of 300 g/t provides a statistically invariable flotation rate constant of pyrite across the pH range tested. Thus, the PAX dosage of 300 g/t is the desirable collector dosage to run the full CCRD experiments.

It is interesting to note that the collector dosage selected in the Barrick's feasibility study of White Mountain is 200 g/t (AMEC, 2007). Barrick's pilot plant campaign tests reported collector dosages up to 500 g/t (SGS, 2007). Based on this observation, the use of high collector dosage in the full CCRD tests would represent better the system of White Mountain.

At 300 g/t, the variation of the flotation rate constant of pyrite with pH was minimal. Despite the evidence that the flotation rate constant of arsenopyrite does not present the same behaviour of the flotation rate constant of pyrite at the PAX dosage of 30 g/t, the variation of the flotation rate constant of arsenopyrite with the pH maintained the

same throughout the range collector dosages tested. In conclusion, any of the PAX dosages tested would have a similar effect on the gradient of the relationship of flotation rate constant of arsenopyrite versus pH. Moreover, the variation of the flotation rate constant of arsenopyrite could not be used as the parameter of selection for the optimum collector dosage of the full CCRD.

This section aimed to minimise the effect of the pH in the mechanisms of activation of arsenopyrite and pyrite and formation of dixanthogen through the evaluation of the collector dosage, considering the work of Fuerstenau et al. (1968) presented in Figure 5-1, that indicates that the increase of the dosage of PAX increased the flotation recovery of the pyrite across a wide range of pH. Thus, it was expected that the evaluation of the collector dosage would present a suitable value by which the effect of the pH, in the range studied, on the mechanism of activation of pyrite and arsenopyrite would be minimised.

Therefore, as the pyrite is in larger proportions in the flotation test and at 300 g/t the variation of the flotation rate constant of pyrite with pH was minimal, the collector dosage used in the full CCRD experiments is 300 g/t.

5.3 Central Composite Rotatable Design (CCRD) of the experiments

The flotation rate is affected by cell parameters, such as geometry, air rate, impeller speed, cell size (Gorain, 1998; Wang, 2016), and by other physical and chemical factors such as particle composition, reagent regime, and pulp rheology. Note that equipment and operating parameters, such as airflow, cell geometry, froth height (due to lip height) and impeller speed are not the focus of this thesis.

As noted in the description of the flotation protocols in Chapter 3, the flotation tests completed in the CCRD utilised constant equipment and operating parameters. All tests were conducted in a 5 L flotation cell, with an impeller speed of 800 rpm, air rate 11 L/min and froth depth 1 cm.

A total of 54 flotation batch tests were completed in the main CCRD factorial design, which included repeat tests to estimate the experimental error.

This section presents the results of the flotation tests in terms of the recoveries, which were the basis of the calculation for the flotation rates, and an analysis of the flotation rates.

5.3.1 Flotation Recovery measurements

There is evidence in the literature that the presence of clays and micas affects the final recovery and rate constant of sulfide minerals (Basnayaka et al., 2017; Forbes et al., 2014). In this research firstly, an assessment of the final recovery of pyrite and arsenopyrite was done to identify if it was affected by any of the factors evaluated in the CCRD. The recovery assessment was made by observing the cumulative recoveries of arsenopyrite and pyrite by time plots, and through the assessment of the final recovery by regression analysis.

The cumulative recoveries of arsenopyrite and pyrite by time plots of all 54 tests of the full CCRD experiments were compiled in Figure 5-9 and Figure 5-10, respectively. As the final recoveries at the time, t=10 minutes seems to be overlapping and are over 95%, the differences in overall recoveries are not easily identified in Figure 5-9 and Figure 5-10. The results suggest that the factors investigated in the CCRD, %solids of the flotation feed, proportion of muscovite in the gangue, pH, frother dosage and muscovite size distribution did not reduce the final recovery of pyrite and arsenopyrite to less than 95%.

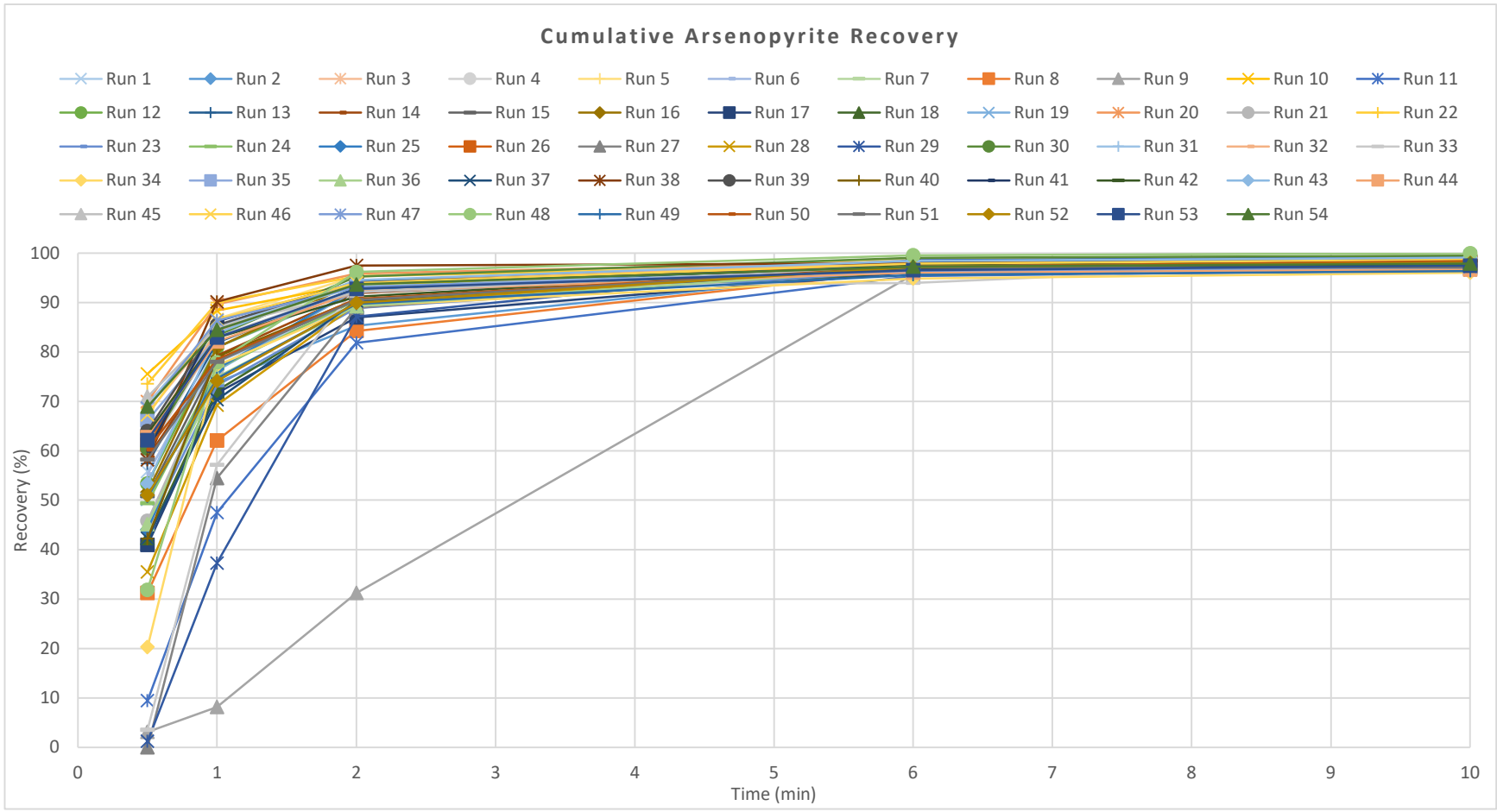

Figure 5-9 – Arsenopyrite Recovery in the 54 Tests of the Full CCRD Design

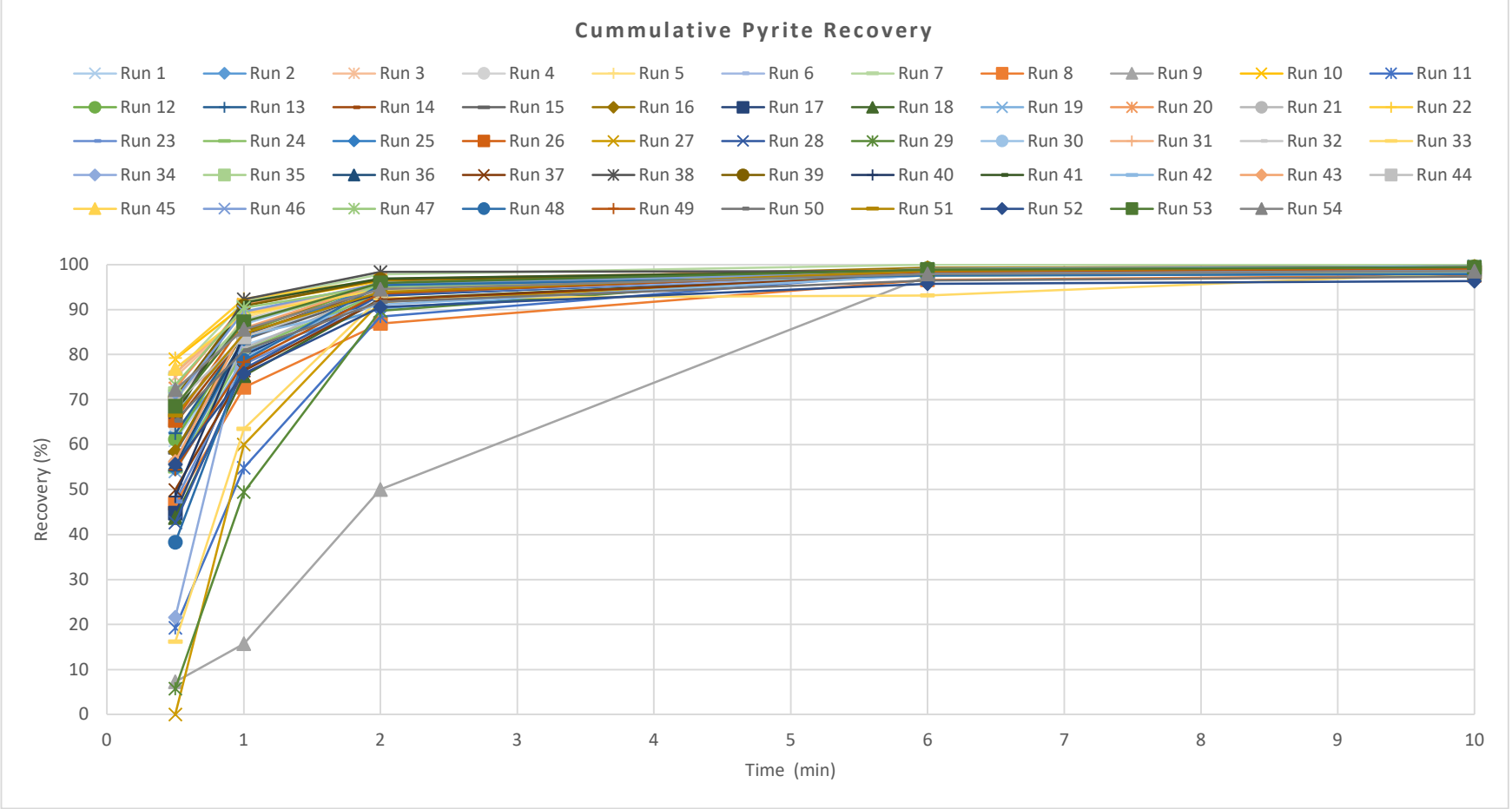

Figure 5-10 - Pyrite Recovery in the 54 Tests of the Full CCRD Design

Figure 5-11 and Figure 5-12 show the final recovery of arsenopyrite and pyrite for each of the tests in the CCRD. The confidence intervals displayed in Figure 5-11 are presented in Table 5-7. The details of the repeatability assessment are presented in Appendix 3.

Table 5-7 – Confidence interval at 95% confidence for arsenopyrite and pyrite flotation recovery

Component	Average Final recovery (%)	95% Confidence Interval
Arsenopyrite	98.15	0.61
Pyrite	98.92	0.33

Table 5-7 shows that the average recovery of arsenopyrite and pyrite are not statistically different, considering the confidence interval at 95% confidence.

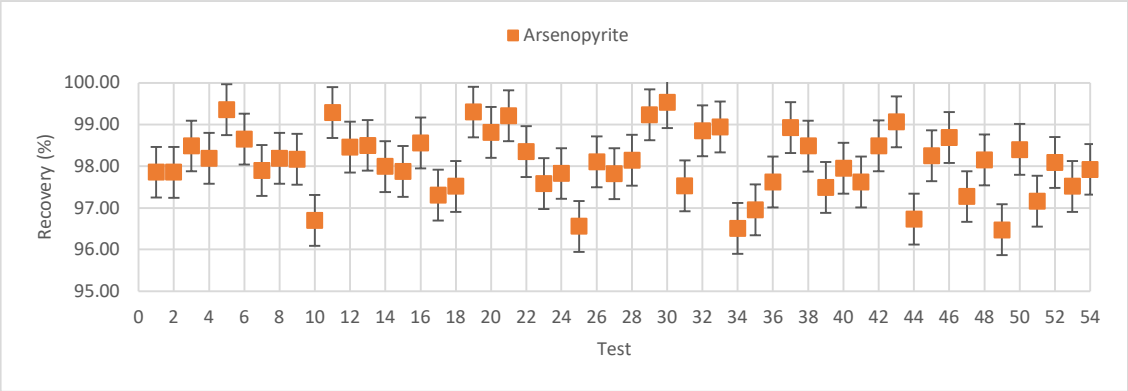

Figure 5-11 – Final recoveries of arsenopyrite in each test of the CCRD

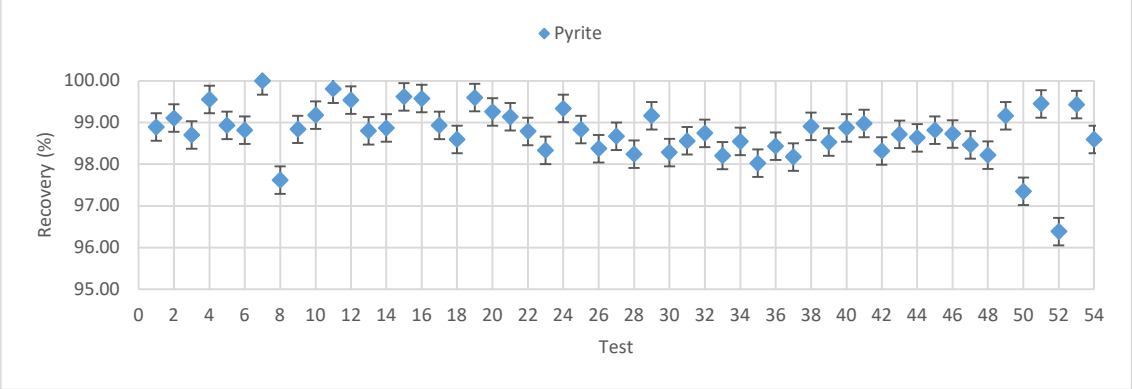

Figure 5-12 – Final recoveries of pyrite in each test of the CCRD

The spread of the recovery data in Figure 5-11 and Figure 5-12 indicates that the factors studied in the CCRD may have affected significantly the final recovery of arsenopyrite and pyrite, at time t = 10 minutes.

The contribution of entrainment for the overall recovery of arsenopyrite and pyrite was calculated based on Savassi (1998) equation, presented in Equation 5-5:

$$R_{ent} = \frac{1-R_{overall}}{1-R_{water}} . ENT_m . R_{water} \qquad \text{(Equation 5-5)}$$

where ENT_m is the degree of entrainment of mineral m, R_{ent} is the recovery of mineral m by entrainment, $R_{overall}$ is the recovery of mineral m by both entrainment and true flotation, and R_{water} is the water recovery. Figure 5-13 shows the calculated recovery of the non-floating component obtained via equation 5-5, the floating component and the final recovery of arsenopyrite and pyrite.

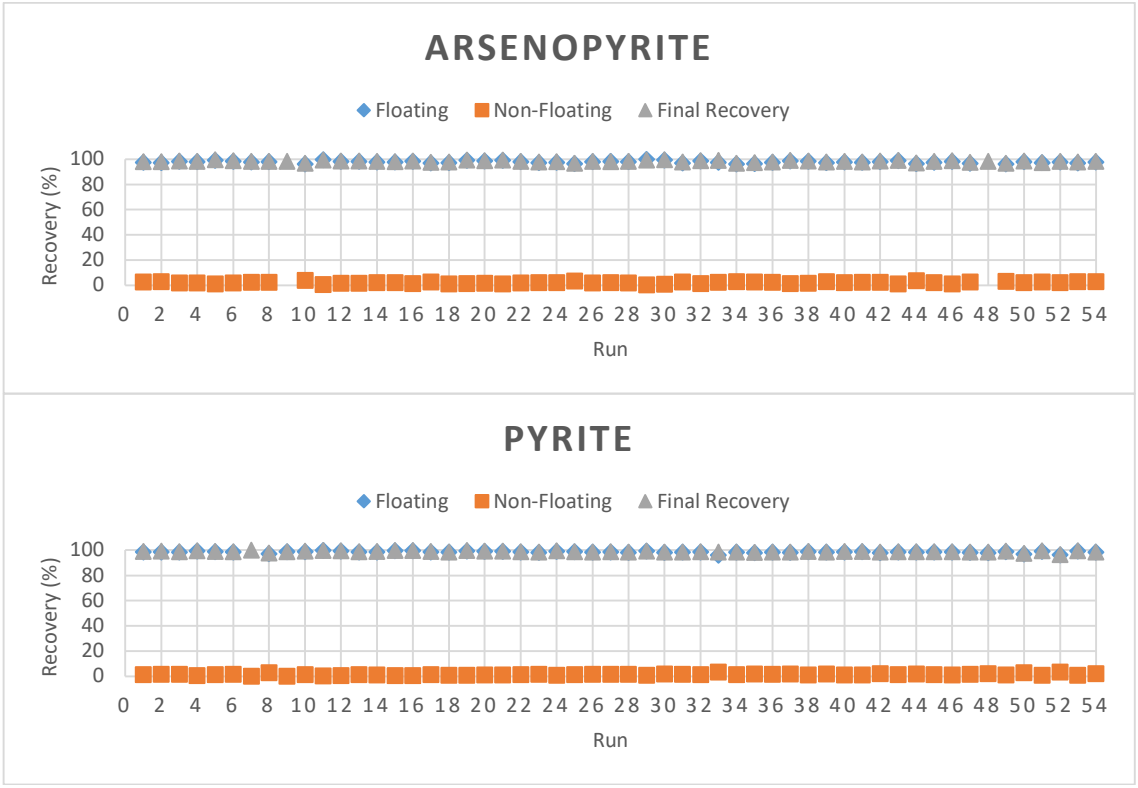

Figure 5-13 - Recovery of arsenopyrite and pyrite non-floating component obtained via equation 5-5, floating component and the final experimental recovery of arsenopyrite and pyrite

The calculation of the recovery of the non-floatable component, entrainment, of arsenopyrite and pyrite indicated in Figure 5-13 that are insignificant for the overall recovery. In addition, the recovery of the floatable component is equivalent to the final measured recovery. Therefore, the recovery by entrainment of pyrite and arsenopyrite are not significant to the final recovery.

Regression models of the final recovery of pyrite and arsenopyrite were developed to assess which factors affecting recovery were the most significant. The models were fitted using the stepwise regression tool of Minitab® 18. The alpha value of 0.15 was selected arbitrarily for these analyses, and only terms with P-values lower than 0.05 (95% significance) were considered for the regression equations.

The predictors selected for testing the effect on the final recovery of arsenopyrite and pyrite are pH, %Muscovite, Frother, %Solids, P_{80}, pH^2, %$Muscovite^2$, $Frother^2$, %$Solids^2$, P_{80}^2, pH * muscovite, pH * Frother, pH * %solids, pH * P_{80}, %Muscovite * frother, %Muscovite * %Solids, %Muscovite * P_{80}, Frother * %Solids, Frother*P_{80}, Solids*P_{80}, and the measured viscosity of the flotation feed pulp at 100 s^{-1} measured in mPa.s.

The stepwise regression analyses returned the following models for the recovery of arsenopyrite and pyrite:

Equation 5-6, recovery of arsenopyrite:

$$R_{aspy} = 98.205 - 0.01629\, pH^2 + 0.1355\, Frother \times \%Solids \quad \text{(Equation 5-6)}$$

Equation 5-7, recovery of pyrite:

$$R_{py} = 99.23 - 5.87\, \%Solids^2 \quad \text{(Equation 5-7)}$$

The statistics of the two regressions models are shown in Table 5-8.

Table 5-8 - Model statistics of the flotation final recovery

Model Summary	Standard error	Confidence Interval at 95%	Predictive uncertainty	R^2
Pyrite	0.59	1.36	19.36	12.9%
Arsenopyrite	0.73	1.68	30.56	22.6%

The results in Table 5-8 show that the models of the final recovery of arsenopyrite and pyrite present high standard error and predictive uncertainty in addition to a low coefficient of determination (R^2). The recovery models have limited predictive capacity but are useful to indicate the significant factors affecting the recovery.

Table 5-9 shows the model coefficients of the final recovery of arsenopyrite.

Table 5-9 Model coefficients statistics of the final recovery of arsenopyrite

Term	Coefficient	SE of Coefficient	P-value
Constant	98.205	0.473	0.00
pH^2	-0.016	0.006	0.007
Frother*%solids	0.1355	0.059	0.026

According to Table 5-9, the constant, pH^2 and the interaction Frother x %solids are significant predictors of the recovery of arsenopyrite in equation 5-6. The pH has a negative effect on the recovery, while the interaction term Frother x %solids has a positive effect. Contrary to the observation in Section 5.2, pH is a prediction of the flotation recovery of arsenopyrite in the system containing muscovite. The effect of pH in the recovery can be due to another mechanism other than the effect of the chemisorption of xanthate, given that no effect was observed in the system in the absence of muscovite.

The level of significance of the terms of equation 5-7 is presented in Table 5-10.

Table 5-10 Model coefficients statistics of the final recovery of pyrite

Term	Coefficient	SE of Coefficient	P-value
Constant	99.23	0.0804	0.00
%Solids2	-5.87	0.0812	0.01

According to Table 5-10, the constant and the $\%Solids^2$ are the most significant predictors of the recovery of pyrite in equation 5-7. The $\%Solids^2$ has a negative effect.

The deleterious effect of the increase of the term %Solids^2 in the recovery of pyrite could be due to the increase of pulp viscosity

The range of variation of the recoveries of arsenopyrite and pyrite due to the effects of viscosity, pH, frother dosage and %solids are shown in Table 5-11.

The range of variation of the recoveries presented on Table 5-11 is similar to the confidence intervals of recoveries present in Table 5-8.

Table 5-11 Model coefficients statistics of the final recovery of pyrite

Recovery	Maximum	Minimum
Arsenopyrite	99.8	96.7
Pyrite	99.0	97.6

5.4 Evaluation of the Flotation Rate Constant of Arsenopyrite and Pyrite

This section assesses the effect of the flotation factors tested on the flotation rate of arsenopyrite and pyrite. The analyses are performed through regression analyses that aim to identify the significant factors affecting the flotation rates. The models obtained through the regression analysis are not used for prediction.

5.4.1 Repeatability of the Flotation Rate Constant Estimate through the Experiments

The reproducibility of the flotation tests in the full CCRD design was assessed via 10 repeats of the centre point. The flotation operation conditions in the repeat tests were 35 g of pyrite, 16 g of arsenopyrite, 20 ppm of Dowfroth 250, 300 g/t of PAX, 27.5% w/w solids. The repeats were performed as part of the main body of the full CCRD design. The tests were performed in blocked order, which minimises the effect of the length of time to complete the experimental program. Due to operational problems during the tests, one of the 10 repeat tests was rejected. The objective of the repeats was to estimate the experimental error of the flotation rate constant.

Table 5-12 shows the average arsenopyrite and pyrite flotation rate observed in the 9 repeat tests, the confidence interval and the percentage of error (confidence interval) represented as the percentage of the average.

The results show that the average flotation rate constant of pyrite is higher than arsenopyrite. The confidence interval of the pyrite is wider than the arsenopyrite. The experimental error of the flotation constant rate of arsenopyrite is 8.4%, and the pyrite is 11.7%.

Table 5-12 – Experimental confidence interval at 95% level of confidence for arsenopyrite and pyrite flotation rate

Component	Average k_i	Standard Deviation	95% Confidence Interval*	% of the variation of confidence interval compared to the average
Arsenopyrite	1.67	0.18	0.14	8.4
Pyrite	1.83	0.28	0.21	11.7

5.4.2 Flotation Rate constant measurements

The flotation batch tests were performed using a pure mineral system, consisting of single mineral liberated particles. The system does not contain composite particles. Therefore, a single flotation rate is evaluated.

Figure 5-14 shows the distribution of the rates across the 54 tests of the CCRD. The error bars represent the confidence interval at 95% level of confidence.

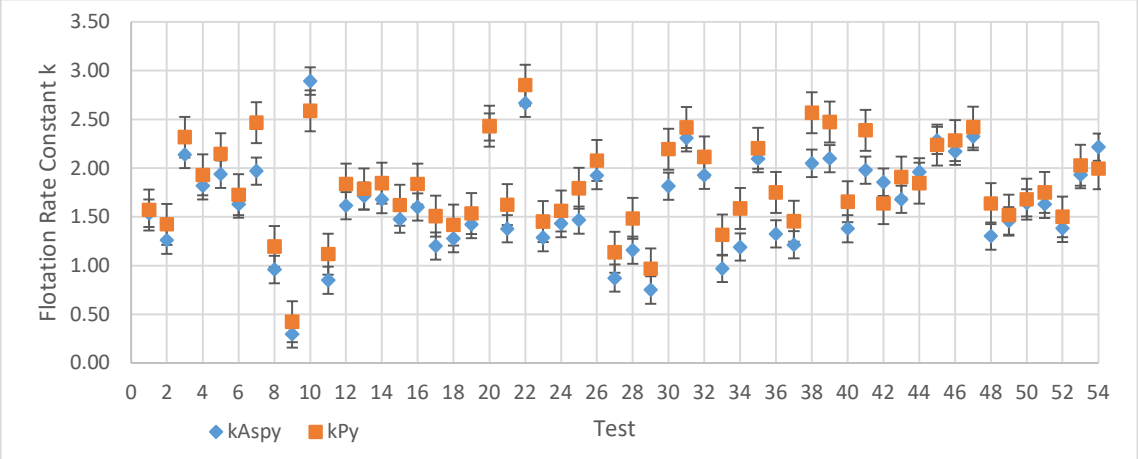

Figure 5-14 – Arsenopyrite and Pyrite Flotation Rates in each test in the Full CCRD tests

The results presented in Figure 5-14, show that the differences between the flotation rate of arsenopyrite and pyrite across the 54 tests are greater than the confidence interval at 95% confidence. This indicates that the variation of the flotation rate across the tests is real and that the factors studied in the CCRD affected the flotation rate of both minerals.

5.4.3 Flotation Rate Constant Regression Analysis

The significance of the variables was assessed via CCRD analysis and the regression model tools in Minitab® 18. The main advantage of using a CCRD for the experiments versus a factorial design is that a CCRD is able to identify the significant variables and to provide a model of the behaviour of the system.

For the development of the model, a stepwise analysis was done. The stepwise analysis eliminated all non-significant terms at a 95% level of confidence from the model. The models obtained through the regression analyses are used solely to identify the level of significance of the factors and their potential interactions, providing a comprehensive understanding of the effect of the factors investigated on the flotation rates.

The stepwise analysis evaluated the five factors of the CCRD factorial design. The candidate terms of the stepwise analysis for the regression model of arsenopyrite and pyrite were:

- Single terms: pH, %muscovite, frother (ppm), %solids w/w, P_{80}, %solids (v/v).
- Quadratic terms: pH^2, $muscovite^2$, $frother^2$, $\%solids^2$ w/w, P_{80}^2.
- Two-way interaction terms: pH x %muscovite, pH x frother, pH x %solids (w/w), pH x P_{80}, %muscovite x frother, %muscovite x %solids (w/w), %muscovite x P_{80}, frother x %solids (w/w), frother x P_{80}, %solids (w/w) x P_{80}.

Where the terms are as follows:

- The frother is the dosage in ppm. E.g., 30 ppm, then frother = 30.

- %solids: the percentage value expressed as a range from 0 to 1. Eg: 20% solids, %solids = 0.2.
- %muscovite: is the percentage of muscovite in the gangue, expressed as a range from 0 to 1. Eg: 12% muscovite, %muscovite = 0.12.
- P_{80}: P_{80} of muscovite in μm.
- pH: the absolute value of pH.

5.4.4 The regression model of arsenopyrite flotation rate

The regression model for the flotation rate of the arsenopyrite is represented by the regression equation 5-8:

$$k_{aspy} = 1.127 + 0.00739\ pH\ x\ frother - 0.01881\ \%solids\ x\ P_{80} \quad \text{(Equation 5-8)}$$

5.4.4.1 Goodness-of-fit of the arsenopyrite regression model

The model summary of the regression model for the flotation rate of arsenopyrite is given in Table 5-13.

Table 5-13 – Arsenopyrite Model Statistics Summary

S	R^2	Predictive uncertainty
0.38	43%	8.4

The coefficient of determination R^2 in Table 5-13 shows that only 43% of the data is explained by the model presented on equation 5-8. The low R^2 presented by the regression analysis can be due to experimental factors which were not controlled, such as the composition of the ions in the tap water composition used in the flotation batch tests and temperature. The standard deviation of the model is given by the term S (Minitab 18 Support, 2018), which is used to assess the goodness of the model, by comparing the term S with the standard deviation of the experimental data. This showed that the standard deviation of the flotation rate constant of the arsenopyrite is 0.18.

Figure 5-15 shows the measured versus predicted plot for the arsenopyrite flotation rate constant. The points shown in Figure 5-15 are randomly distributed and

reasonably following the diagonal line (where the experimental value is equal to the predicted value). The distribution of the points on both sides of the diagonal line indicates that the experimental data is responding to the variables evaluated in the CCRD with reasonable accuracy. Therefore, despite the low R^2 presented on Table 5-13, the model presented in equation 5-8 is adequate to describe the system.

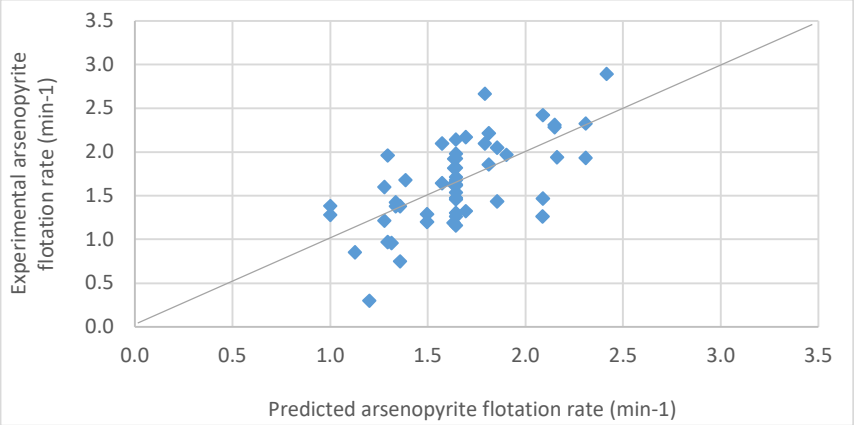

Figure 5-15 – Measured versus Predicted Plot for the Arsenopyrite Flotation Rate Constant

5.4.4.2 Significant factors which affect the flotation rate constant of arsenopyrite

Table 5-14 shows the model coefficients and P-values of the significant factors that affect the flotation rate of arsenopyrite.

Table 5-14 – Arsenopyrite Model Coefficients

Term	Coefficient	SE Coefficient	Coded Coefficient	P-value
Constant	1.1270	0.2770	1.6528	0
pH x frother	0.00739	0.00144	0.2687	0
%solids x P_{80}	-0.01881	0.00611	-0.1613	0.003

The significance of the terms in the regression is determined by the in P-values. As the results of the analysis in Table 5-14 show, all terms in the model have a level of significance higher than 95%, as all P-values are lower than 0.05. The order of significance to the model is given by the absolute value of the coded coefficients. The coded coefficients on Table 5-14 were obtained by running the stepwise regression using predictors standardised by subtracting the mean and dividing by the standard deviation.

The most significant factors affecting the flotation rate constant of arsenopyrite, as shown in Table 5-14 are, in order of significance, the constant, the interaction pH x frother followed by the interaction %solids x P_{80}.

The proportion of muscovite in the gangue does not affect the flotation rate constant of arsenopyrite directly, as it does not appear as a significant term in Table 5-14. However, the size distribution of muscovite is a significant term as an interaction with the percentage of solids. The term %solids x P_{80} is negative, which suggests that the increase in the percentage of solids and the P_{80} of muscovite have a deleterious effect on the flotation rate of arsenopyrite. The increase of % of solids could be related to an increase in viscosity.

The deleterious effect of the increase of muscovite P_{80} is counter-intuitive because it is expected that fine muscovite would have a greater deleterious effect on the flotation rate of arsenopyrite through an increase in the viscosity and the probability of slime coatings formed on the surface of arsenopyrite.

The interaction effect of pH x frother is positive. The increase of pH and frother dosage has a positive effect on the flotation rate constant of arsenopyrite, which is two times greater than the negative effect of the interaction %solids x P_{80}. Therefore, an increase in frother dosage and pH can compensate for the deleterious effect of an increase of %solids and muscovite P_{80}.

The effect of pH could be linked to a change of hydrophobicity through oxidation or the presence of hydrophilic ions in the double-layer of arsenopyrite. The effect of the frother dosage could be liked with an increase of froth stability. Note that all experiments of the CCRD were run with frother concentration above the critical coalescence concentration of Dowfroth 250, which suggests that the reduction if bubble size and the increase of the bubble-particle collision probability is not likely to be the mechanism by which the increase of frother dosage is affecting the flotation rates. The effect of pH and frother dosage will be discussed in detail in Chapter 7.

5.4.5 The regression model of Pyrite

The regression model for the flotation rate of the pyrite is represented by the regression equation 5-9:

$$k_{Py} = 1.484 + 2.45\ \%\text{muscovite}^2 + 0.00571\ \text{pH x Frother} - 0.02206\ \%\text{solids x } P_{80}$$

(Equation 5-9)

5.4.5.1 Goodness-of-fit of the pyrite regression model

The model summary is given in Table 5-15.

Table 5-15 – Pyrite Model Summary

S	R^2	Predictive uncertainty
0.35	44%	7.3

The coefficient of determination in Table 5-15 shows that 46% of the data is explained by equation 5-9. The value of S in Table 5-15 is relatively similar to the standard deviation of k_{py} in the repeats, which is 0.28 and as a result. It suggests that the error of the flotation rate of the pyrite model is similar to the experimental error. It suggests that the model have a good predictive capacity.

Figure 5-16 shows the measured versus predicted plot for the pyrite flotation rate.

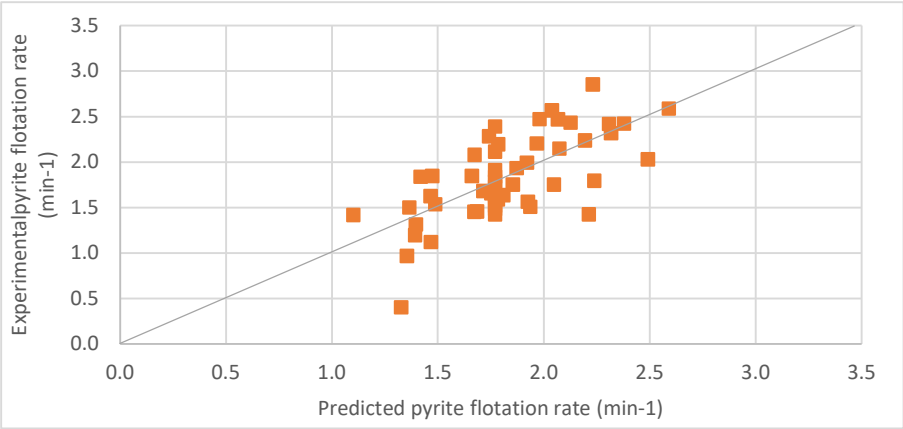

Figure 5-16 - Measured versus Predicted Plot for the Pyrite Flotation Rate

The points shown in Figure 5-16 are randomly distributed and reasonably following the diagonal line (where the experimental value is equal to the predicted value). The distribution of the points on both sides of the diagonal line indicates that the experimental data is responding to the variables evaluated in the CCRD with reasonable accuracy.

The regression model of the pyrite flotation rate presented similar trends to the regression model of arsenopyrite. It suggests that those minerals present similar kinetic behaviour in the flotation conditions investigated.

5.4.5.2 Significant factors affecting the flotation rate of pyrite

Table 5-16 shows the model coefficients and P-value of the significant factors that affect the flotation rate constant of pyrite.

Table 5-16 – Pyrite Model Coefficients

Term	Coefficient	SE Coefficient	Coded Coefficient	P-value
Constant	1.484	0.269	1.8245	0
%muscovite^2	2.45	1.23	0.0975	0.052
pH x frother	0.00571	0.00135	0.2074	0
%solids*P_{80}	-0.02206	0.00571	-0.1892	0

The results presented in Table 5-16 shows that all 5 factors tested in the CCRD were significant at a 95% level of significance to the flotation rate of pyrite. The most significant terms for the regression are the constant followed by pH x frother, %solids x $P_{80,}$ and %muscovite^2. The P-value of the interaction %muscovite^2 is slightly higher than 0.05. It could be considered not significant at a level of confidence of 95%. However, because it is in the borderline of the level of significance, it was decided to include it in the regression analysis. It suggests that the percentage of muscovite in the gangue is the least significant parameter for the flotation rate constant of pyrite.

Analysing the regression data of arsenopyrite and pyrite, it indicated that the percentage of muscovite in the gangue has little or no influence on the flotation kinetics. On the other hand, the size distribution of muscovite has a significant effect combined with the percentage of solids. The effect of the interaction %solids x P_{80} is

deleterious to the flotation rate constant because it is a negative term. The interaction pH x frother is beneficial to the pyrite rate constant.

The increase in % of solids could be related to an increase in viscosity. The viscosity is discussed in more details in Chapter 6.

The similarity of the regression terms suggests that the flotation rates of pyrite and arsenopyrite are affected by the same mechanisms.

5.5 The Effects of the Investigated Factors on the Flotation Rates

The CCRD analysis allowed the calculation of the individual effect of the factors on the flotation rate constants of arsenopyrite and pyrite. Figure 5-17 presents the plots of the individual effect of the factors on the flotation rate constants of arsenopyrite and pyrite. These plots were obtained by averaging the responses for all tests that contain the given factor.

The following observations can be drawn from Figure 5-17:

- pH: the flotation rates increase with the increase of pH of the pulp, peaking around pH 8, with a slight decrease from pH 8 to 10. The relationship between flotation rate and pH is non-linear.
- Muscovite proportion (%): the increase of the proportion of muscovite in the gangue mixture from 0% to approximately 22% decreases the flotation rate of arsenopyrite and pyrite but increases the flotation rate when the % of muscovite increases from 22% to 45%. The confidence intervals at 95% showed that muscovite proportion in the gangue has a low significance to the flotation rate.
- Frother dosage: the increase of frother dosage increases the flotation rate across the whole range tested, which is from 10 ppm to 30 ppm.
- %solids: the increase of % solids has a deleterious effect on the flotation rate for both pyrite and arsenopyrite.
- P_{80} of muscovite: the flotation rate decreases with increase in P_{80} of muscovite from 50 μm to 100 μm. The flotation rates of pyrite and arsenopyrite do not change significantly from the muscovite P_{80} 100 μm to 150 μm.

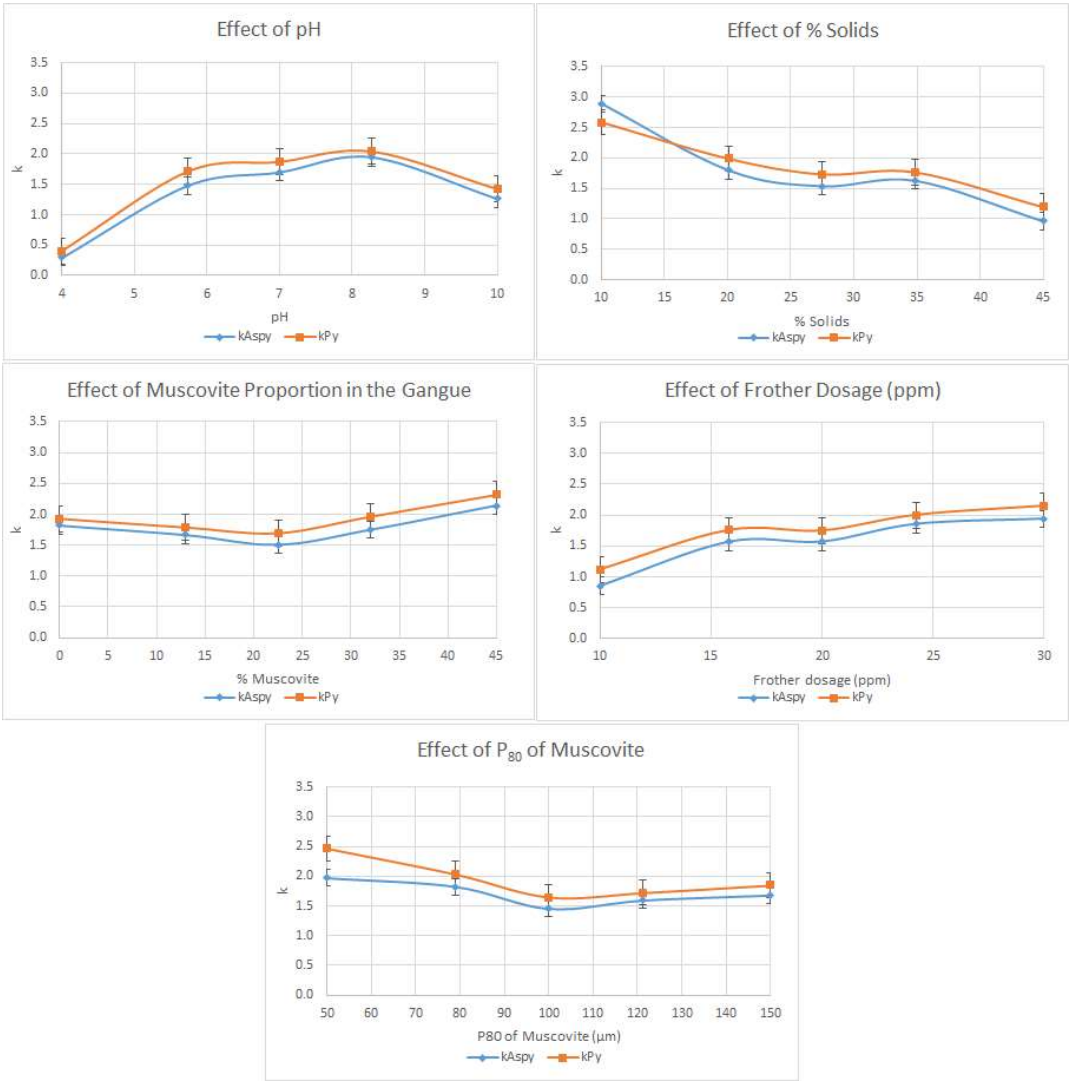

Figure 5-17 - Effect of the Individual Factors on the Flotation Rate of Arsenopyrite and Pyrite

The trends presented in Figure 5-17 are similar for the two sulfide minerals in regards to the effect of each factor on the flotation rate constant. This behaviour is expected because the regression equations 5-8 and 5-9 presented the same terms.

The effects showed in Figure 5-17 gives a simplified view of the effect of the invested factors on the flotation rate because they do not account for interactions. The interaction terms are the most significant to the flotation kinetics, as indicated by the stepwise regression analyses. The interaction terms are better displayed in 3-D response surface plots, which are shown in the following section.

5.6 Response Surface of the Flotation Rate Constant of Pyrite and Arsenopyrite

The interactions pH x frother and %solids x P_{80} were found to be significant to the flotation rate constant of arsenopyrite and pyrite. The term muscovite^2 was only significant to the flotation rate constant of pyrite. The effect of the interaction terms can be visualised in the surface response plots presented in this section.

Response surfaces for the flotation rate constant of arsenopyrite and pyrite as a function of the significant factors of the full CCRD were plotted using the regression equations 5-8 and 5-9. Despite their limited predictive capability, the empirical models of the flotation rate constant are useful to understand the behaviour of the system.

5.6.1 Response Surface of the Flotation Rate Constant of Arsenopyrite

The response surfaces of the arsenopyrite flotation rate constant are shown in Figure 5-18 and Figure 5-19.

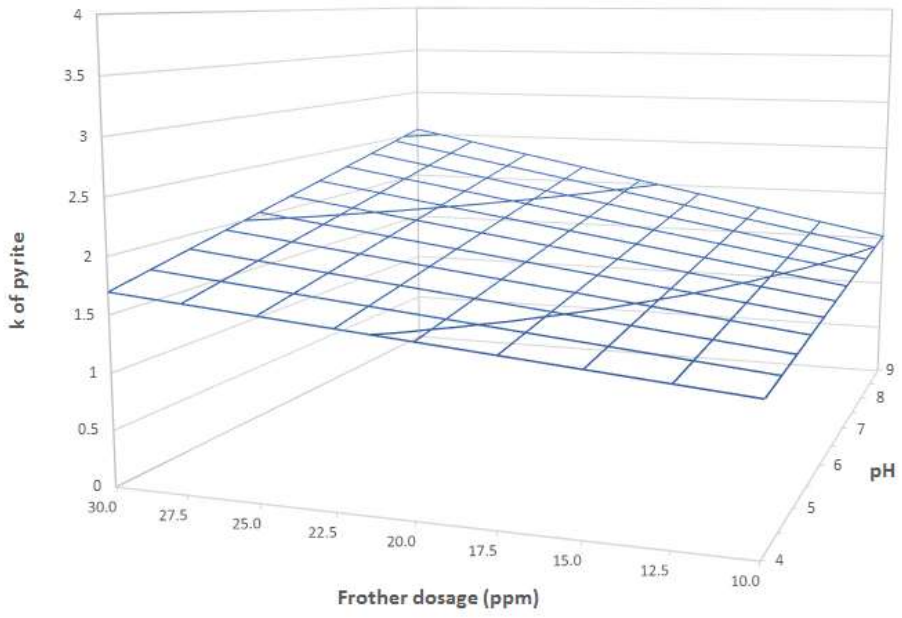

Figure 5-18 - Arsenopyrite flotation rate response surface of the interaction pH x frother, at muscovite P_{80} 100 µm, 27% solids.

Figure 5-18 shows the effect of the interaction pH x frother. The response surface in this figure was plotted at the centre point conditions: muscovite P_{80} 100 µm, 27% solids. The equation 5-8 showed that the interaction pH x frother has a positive effect on the flotation rate of arsenopyrite. The positive effect of the interaction pH x frother can be observed by the lift of the surface in the region of high pH and high frother dosage in Figure 5-18. Because the term pH x frother is linear, the surface does not present curvature.

The effect of pH on the flotation rate of arsenopyrite could be due to surface modification by oxidation which reduces the floatability of the mineral. The highest flotation recoveries of arsenopyrite should occur at pH 4-5 (Valdivieso et al., 2006; Sirkeci, 2000 and Gaudin, 1957). The pH could also modify the surface charge of the muscovite and promote slime coating of arsenopyrite, which could be deleterious to the flotation kinetics.

The pH of the flotation can also affect froth stability. Sheni et al. (2018), in their study using a sample of Platinum Group Metal (PGM) ore, suggested that the increase of pH increases froth stability. The hydrophobicity of the particles plays an important role in the froth stability as highly hydrophobic particles can destabilise the froth (Farrokhpay, 2011; Zanin et al., 2009).

Because the regression equation for arsenopyrite flotation rate (equation 5-8) shown that pH x frother is a significant term and both factors affect froth stability, it could be indicating that the mechanism by which this interaction affects the flotation kinetics is through the froth stability.

As per equation 5-8, the interaction %solids x P_{80} has a negative effect on the flotation rate of arsenopyrite. The increase of the percentage of solids or the muscovite P_{80} would move the surface presented in Figure 5-18 down, parallel to the original position of the surface. The opposite happens by decreasing the %solids or the P_{80} the surface presented would move up. The proportion of muscovite in the gangue does not affect the flotation rate of arsenopyrite. Therefore, the response surface in Figure 5-18 remains the same for all muscovite proportions.

Figure 5-19 shows the effect of the interaction %solids x P_{80}. The response surface is plotted for pH 7 and frother dosage 20 ppm. The term %solids x P_{80} is negative in equation 5-8; therefore, the increase of %solid or/and P_{80} has a deleterious effect on the flotation rate constant. This effect is observed through the drop of the flotation rate constant with the simultaneous increase of the %solids x P_{80}. The response surface shown in Figure 5-19 does not present curvature.

An increase of pH and or frother dosage would lift the response surface, and the decrease of pH and or frother dosage would drop the response surface on Figure 5-19.

According to Figure 5-18 and Figure 5-19, the maximum flotation rate constant of arsenopyrite would be observed at pH 10, frother dosage of 30 ppm, 10% solids and muscovite of P_{80}, independent of the percentage of muscovite in the gangue.

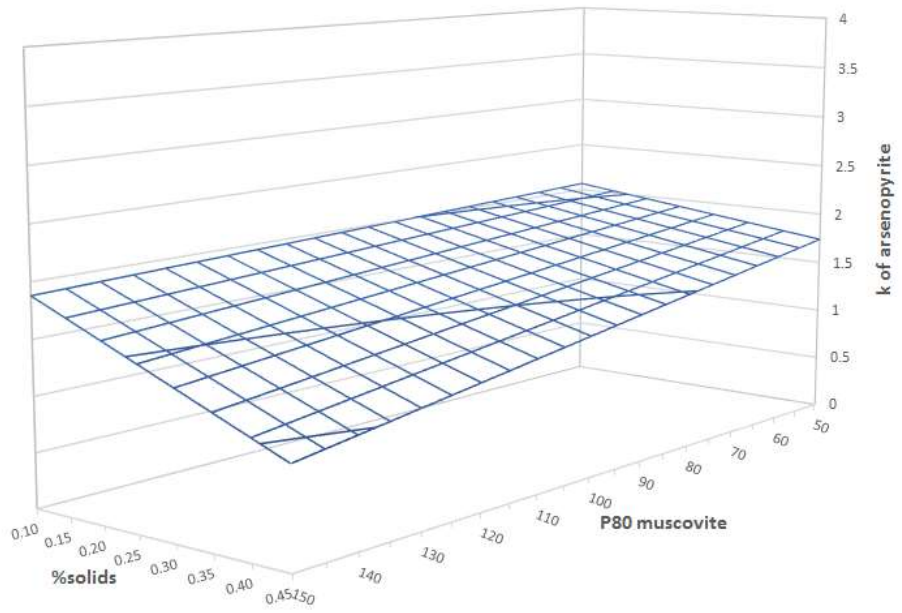

Figure 5-19 – Arsenopyrite flotation rate response surface of the interaction term %solids x P_{80}, at pH 7, frother dosage 20 ppm.

Based on the literature, the percentage of solids of the pulp and muscovite size distribution are factors that are expected to affect the viscosity of the pulp, consequently affecting the flotation performance. An increase in %solids and a

decrease of muscovite P_{80} could cause an increase in the pulp viscosity, that would appear in turn to be the cause of the deleterious effect on the flotation kinetics.

The literature also indicates that the formation of hetero-aggregation of muscovite and the pyritic minerals could lead to poor flotation kinetics. This mechanism may be suggested by a decrease of the flotation rates with the increase of fines in the pulp (low muscovite P_{80}). However, in the results of this research, the increase of muscovite P_{80} is deleterious to the flotation rate, rather than the decrease of particle size. This appears to contradict the explanation for the effect of the muscovite particle size to be due to an increase of pulp viscosity, or the formation of slime coating on the surface of arsenopyrite.

The underlying cause of the deleterious effect of the size distribution of muscovite on the flotation kinetics is not yet clear. The magnitude of this effect appears to be amplified by the effect of the %solids, as the regression equation presents those factors as a single interaction term.

5.6.2 Response Surface of the Flotation Rate Constant of Pyrite

The response surfaces of the pyrite flotation rate are shown in Figure 5-20 to Figure 5-27. Figure 5-20 shows the effect of the interaction pH x frother on pyrite flotation rate, which is positive according to equation 5-9. The flotation rate increases with the increase of the pH and frother dosage. This trend is similar to the arsenopyrite flotation rate response surface presented in Figure 5-18.

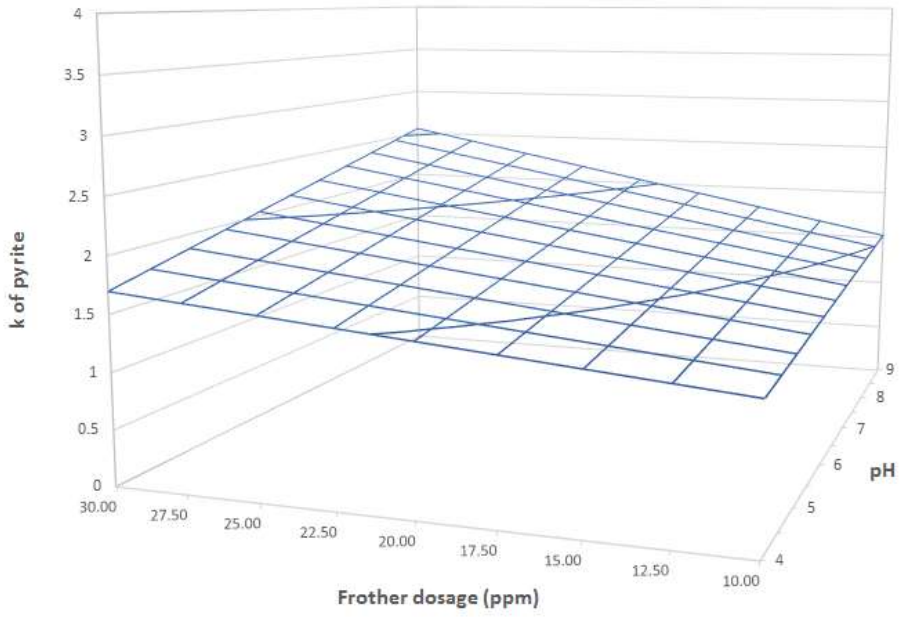

Figure 5-20 - Pyrite flotation rate response surface of the interaction pH x frother, at muscovite P_{80} 100 µm, 27% solids, and 22% muscovite.

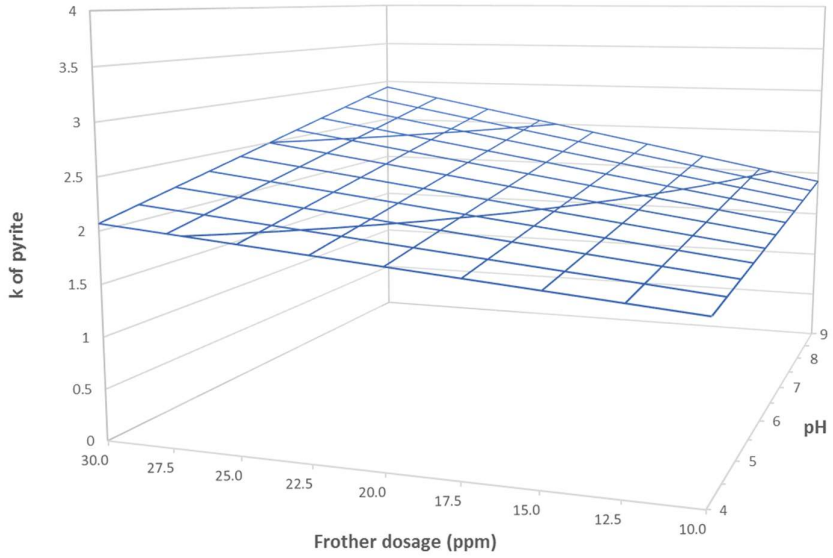

Figure 5-21 - Pyrite flotation rate response surface of the interaction pH x frother, at muscovite P_{80} 100 µm, 27% solids and 45% muscovite

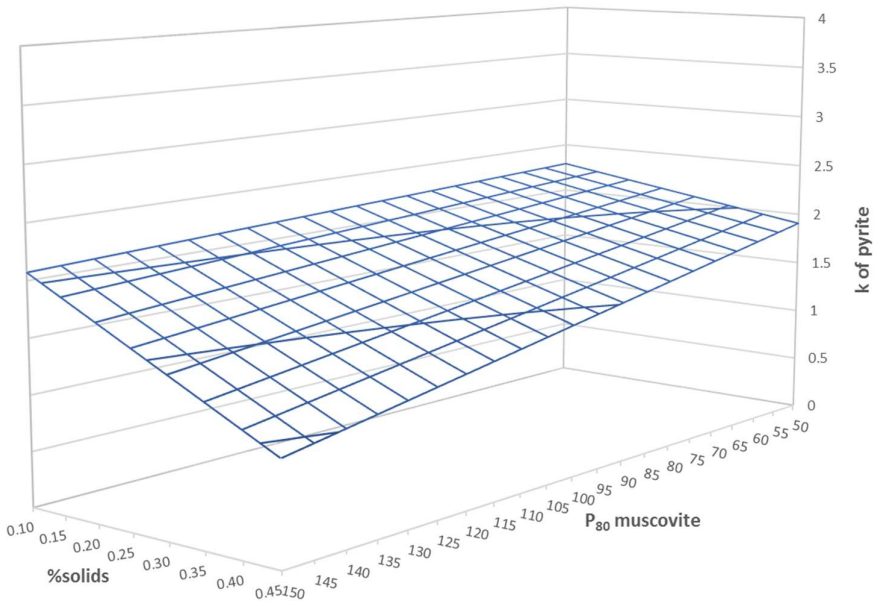

Figure 5-22 - Pyrite flotation rate response surface of the interaction term %solids x P_{80}, at pH 7, frother dosage 20 ppm, 22% muscovite.

Figure 5-22 shows the effect the interaction %solids x P_{80}. The term %solids x P_{80} is negative in equation 5-9; therefore, the increase of %solid and/or P_{80} has a deleterious effect on the flotation rate.

Figure 5-20 and Figure 5-22 show that pyrite and arsenopyrite presented similar response surface shapes in regards to the terms pH x frother and %solids x P_{80}. The key difference between the behaviour of pyrite and arsenopyrite in regard to the pH x frother and %solids x P_{80} terms is that pyrite flotation rate is affected by the presence of muscovite.

Therefore, the potential causes for the effect of the interactions pH x frother and %solids x P_{80} on the flotation rate of pyrite may be the same of the presented for the arsenopyrite, given the similar behaviour of the flotation rate constant to these variables.

In the regression equation for the flotation rate of pyrite, the increase of the proportion of muscovite suggests a positive effect on the flotation rate constant of pyrite. The

increase of muscovite proportion increases the flotation rate of pyrite by moving the response surface in Figure 5-21 and Figure 5-23 up without changing its shape.

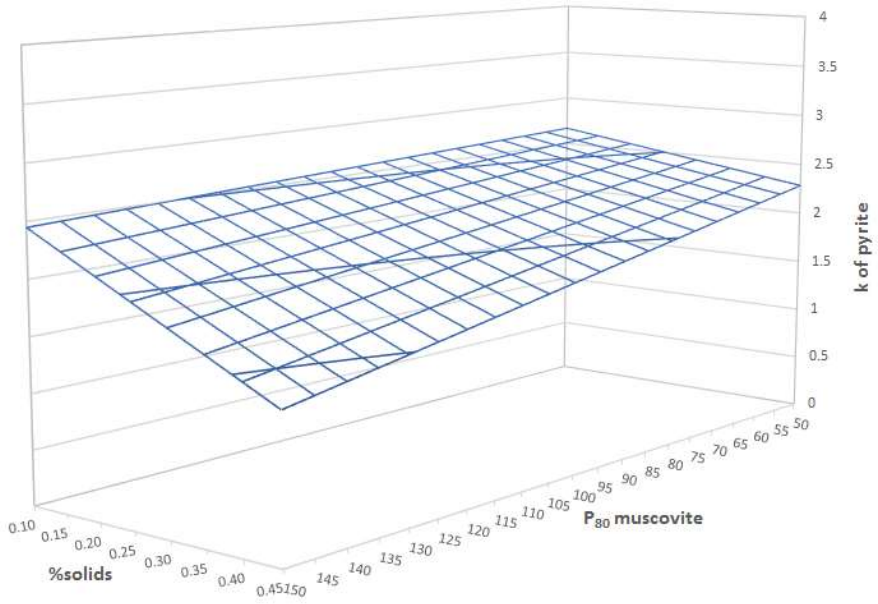

Figure 5-23 - Pyrite flotation rate response surface of the interaction term %solids x P_{80}, at pH 7, frother dosage 20 ppm, 45% muscovite

The term for the proportion of muscovite term in equation 5-9 is quadratic, which introduces curvature to the response surface. The muscovite proportion is not part of any interaction terms in equation 5-9. Therefore, the response surfaces, including the muscovite term can be presented versus the other four significant factors of the CCRD, as shown in Figure 5-24 and Figure 5-27.

Figure 5-24 shows the response surface of the pyrite flotation rate as a function percentage of muscovite in the gangue and pH. The curvature due to the quadratic term for the muscovite proportion can be observed in Figure 5-25, Figure 5-26 and Figure 5-27. Because of the positive relationship of the muscovite term in equation 5- 9, the increase of muscovite proportion leads to an increase in the flotation rate. The graph presented in Figure 5-24 is plotted at muscovite P_{80} 100 µm, 27% solids and frother dosage 20 ppm. Changing the muscovite P_{80} and % solids would

move the surface up or down to a parallel position and would not change the relationship %muscovite versus pH. The alteration of the frother dosage would intensify the effect of pH because the effect of pH is a function of the frother dosage.

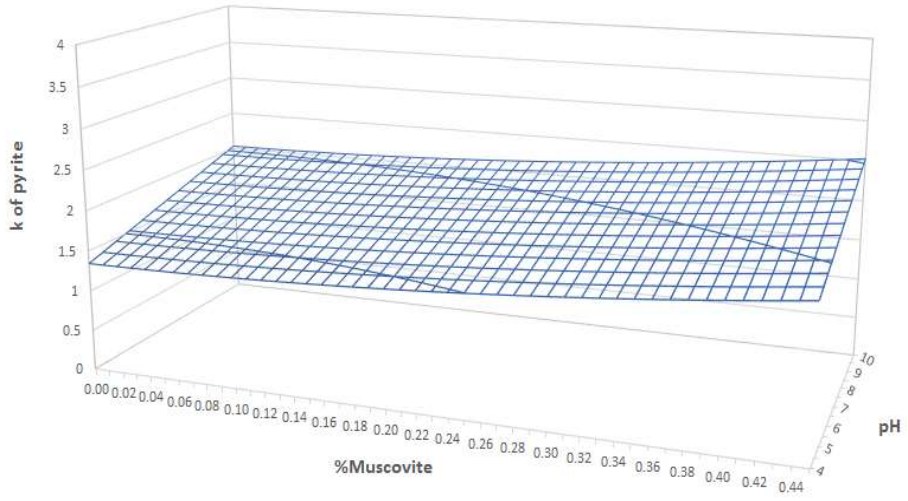

Figure 5-24 - Pyrite flotation rate response surface of the pH versus the percentage of muscovite, at muscovite P_{80} 100 µm, 27% solids and frother dosage 20 ppm

Figure 5-25 shows the response surface of pyrite flotation rate for the percentage of muscovite in the gangue versus muscovite P_{80}. The major effect on the flotation rate is caused by the P_{80} of muscovite, rather than of the proportion of muscovite. The increase of muscovite proportion leads to an increase in the flotation rate, independent of the effect of the muscovite size distribution. The presented graph in Figure 5-25 is plotted at muscovite pH 7, 27% solids and frother dosage 20 ppm. Changing the pH and frother dosage would move the surface up or down to a parallel position. The alteration of the frother dosage would intensify the effect of muscovite P_{80} because the effect of P_{80} is a function of the percentage of solids.

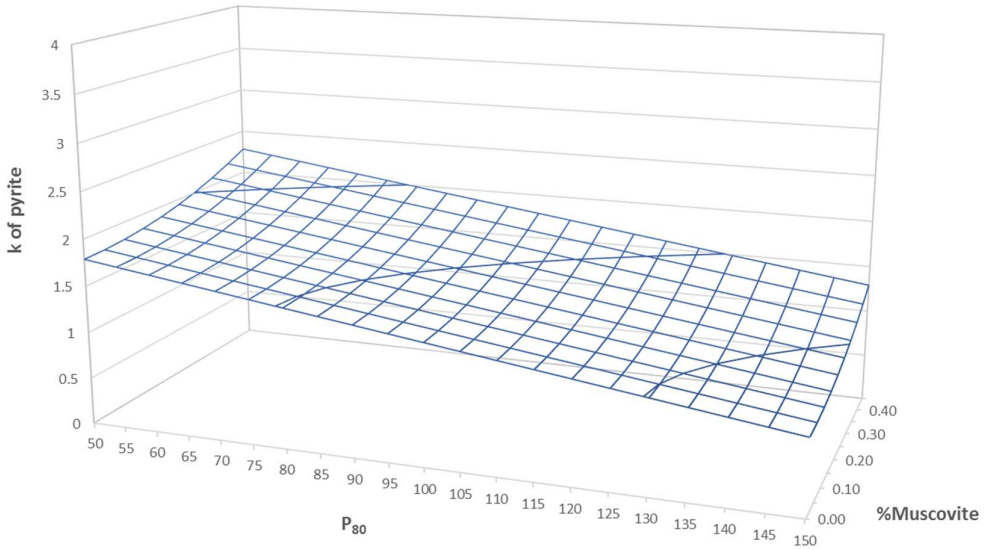

Figure 5-25 - Pyrite flotation rate response surface of the muscovite P_{80} versus percentage of muscovite, at 27% solids, pH 7 and frother dosage 20 ppm

Similar observations from Figure 5-25 applies to Figure 5-26. Figure 5-26 shows the response surface of pyrite flotation rate of percentage of muscovite versus muscovite percentage of solids. The surfaces in Figure 5-25 and Figure 5-26 presented similar shapes. Comparing the effect of %solids versus muscovite P_{80}, the effect of the latter is greater than the former, as the decline of the flotation rate is steeper in Figure 5-25 than in Figure 5-26.

Figure 5-27 shows the response surface of pyrite flotation rate as a function of the percentage of muscovite in the gangue and frother dosage. It can be observed that the dominant effect on the flotation rate constant in Figure 5-27 is caused by frother dosage, instead of the proportion of muscovite.

Figure 5-27 was plotted at muscovite P_{80} 100 µm, pH 7 and 27% solids. The effect of changing muscovite P_{80} and percentage of solids would move the surface up or down, while a change of pH would intensify the effect of frother dosage.

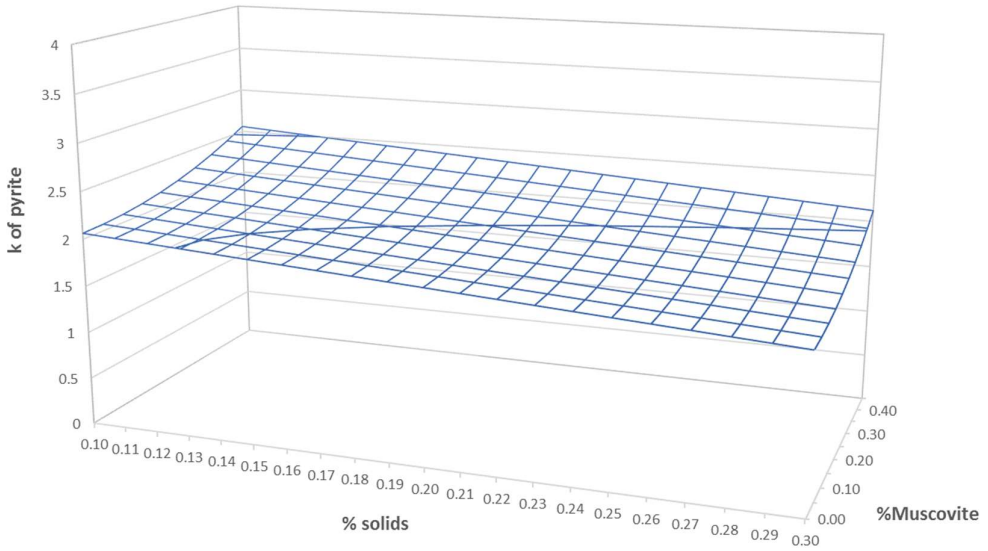

Figure 5-26 - Pyrite flotation rate response surface of the percentage of solids versus the percentage of muscovite, at muscovite P_{80}, pH 7 and frother dosage 20 ppm

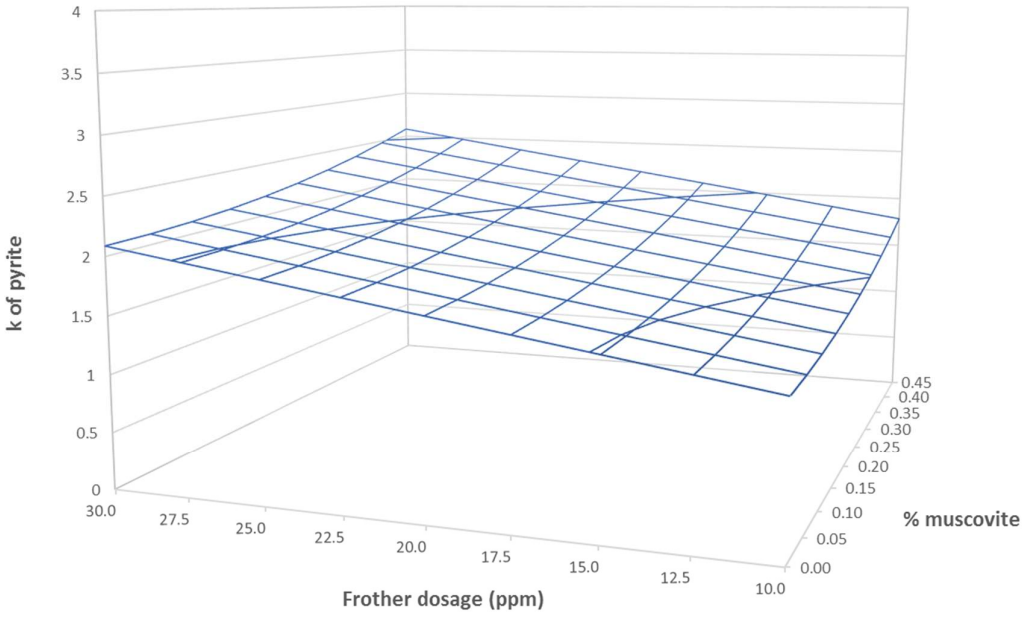

Figure 5-27 - Pyrite flotation rate constant response surface of the percentage of solids versus the percentage of muscovite, at muscovite P80 100 µm, pH 7 and 27% solids.

As shown in Figure 5-20 to Figure 5-27, the effect of muscovite proportion on the flotation rate constant appears to be less significant than the effect of the other factors. this is because the proportion of muscovite term in equation 5-9 is less significant than the other terms.

5.7 Conclusions

This chapter has discussed the outcomes of the CCRD experimental program in terms of the factors that affected the flotation rates of arsenopyrite and pyrite.

The regression analysis indicated that the flotation rate of arsenopyrite and pyrite are affected by the interactions of pH with frother and %solids with muscovite P_{80}.

The effect of the interaction pH with frother is positive in both the arsenopyrite and pyrite flotation rate model, which means an increase of the flotation rate constant when either pH or frother dosage increased. This effect of pH can be related to the hydrophobicity of the pyritic minerals studied. The hydrophobicity is related to the level of particle oxidation, activator and collector coverage at a given pH. The effect of the pH could also be linked to froth stability. Chapter 7 examines the surface oxidation, collector and activator coverage based on the results from the XPS and ToF-SIMS analyses. The effect of the frother dosage could be related to froth stability and bubble size, which is discussed further in Chapter 7.

The effect of the interaction of %solids with muscovite P_{80} is negative in the arsenopyrite and pyrite flotation rate model, which means that the flotation rate decreased when either the percentage of solids or muscovite P_{80} increased. The increase in %solids could be increasing pulp viscosity, and this could be the mechanism by which the %solids is affecting the flotation rates. However, the underlying mechanism which the effect of the size distribution of muscovite is not clear from the results of the CCRD.

The positive effect of the interaction between pH and frother on the flotation rate of arsenopyrite is twice the deleterious effect of the interaction between %solids and muscovite $P_{80,}$ as shown by the coded coefficients in Table 5-14. In relation to the

pyrite flotation rate, the positive effect of the interaction between pH and frother is equal to the magnitude of the %solids and muscovite P_{80} interaction, according to the coded coefficients in Table 5-16.

The results indicated that the proportion of muscovite in the gangue does not affect the flotation rate of arsenopyrite. On the other hand, it has a small positive effect of the flotation rate constant of pyrite. However, the effect of the proportion of muscovite on the flotation rate constant of pyrite is half the magnitude of the term pH x frother, as per the coded coefficients in Table 5-16.

Although the proportion of muscovite has no effect on the arsenopyrite flotation rate and minimal effect on the flotation rate of pyrite, the size distribution of muscovite has a significant deleterious effect. Because a coarse size distribution of muscovite particles is associated with the detrimental effect of the flotation rate constant, slime coatings are less likely to be observed in the system. Zeta potential measurements were undertaken to assess whether the formation of slime coatings is likely to be occurring in a given pH range, and the results of these analyses are described in Chapter 7.

The increase in the percentage of solids in the flotation feed has a detrimental effect on the flotation rate constant of both arsenopyrite and pyrite. The percentage of solids effect is associated with the muscovite P_{80} in the interaction term %solids x muscovite P_{80} in equations 5-8 and 5-9.

The first hypothesis of this research stated that:

The presence of high concentrations of muscovite has a detrimental effect on the flotation rate of pyrite and arsenopyrite.

Based on the evidence from the results of the flotation tests in the full CCRD presented in this chapter, the proportion of muscovite in the gangue appears to have no effect on the flotation rate of arsenopyrite, and a positive effect with low significance on the flotation kinetics of pyrite.

Despite the fact that the proportion of muscovite has no deleterious effect, the increase of the size distribution of muscovite has a deleterious effect on the flotation rate constant of arsenopyrite and pyrite. The deleterious effect of the increase in muscovite particle size appears to be amplified by the percentage of solids. To investigate the mechanisms by which those factors affect the flotation rate. Zeta potential measurement and ToF-SIMS analysis are undertaken, and the results of these analyses are presented in Chapter 7.

Chapter 6

Investigating the Effect of Pulp Viscosity

---

6 Investigating the Effect of Pulp Viscosity

6.1 Introduction

This chapter investigates the mechanisms by which the variables studied in the CCRD experiments affect the flotation rate of pyrite and arsenopyrite. Based on previous research published in the literature, it was expected that the presence of muscovite could have a deleterious effect on the flotation rate of pyrite and arsenopyrite by causing a change in pulp viscosity (Farrokhpay et al., 2013, Ndlovu, 2013).

The results presented in this chapter allow Hypothesis 2 (that the presence of muscovite affects arsenopyrite and pyrite floatability by changing pulp viscosity) to be tested and provides a discussion of the significant factors affecting the viscosity of the pulp.

6.2 Investigating the Effect of Pulp Viscosity

The effect of feed pulp viscosity on the flotation of arsenopyrite and pyrite is expected to be observed in the CCRD by changing the percentage of solids of the pulp, increasing the percentage of muscovite in the gangue, and increasing the content of fines as - 38 µm particles by changing the P_{80} of the muscovite.

An increase in the percentage of solids and a decrease in muscovite P_{80} are expected to increase pulp viscosity (Shi & Napier-Mann, 1995), resulting in a detrimental effect on the flotation rate constant. Other factors, such as the chemical environment and temperature, can also affect the rheology of pulp (Shi & Napier-Mann, 1995). A strong rheology effect was expected to be observed as the output of the CCRD, given that the factors studied are expected to cause large changes in the pulp viscosity.

6.2.1 Pulp Viscosity Measurements

All 54 CCRD tests had the flotation viscosity of the feed measured. The results of these measurements presented as flow curves the flotation feed pulp are shown in

Figure 6-1. The list of conditions in each of the 54 tests is presented in Appendix Table 2, in Appendix 1.

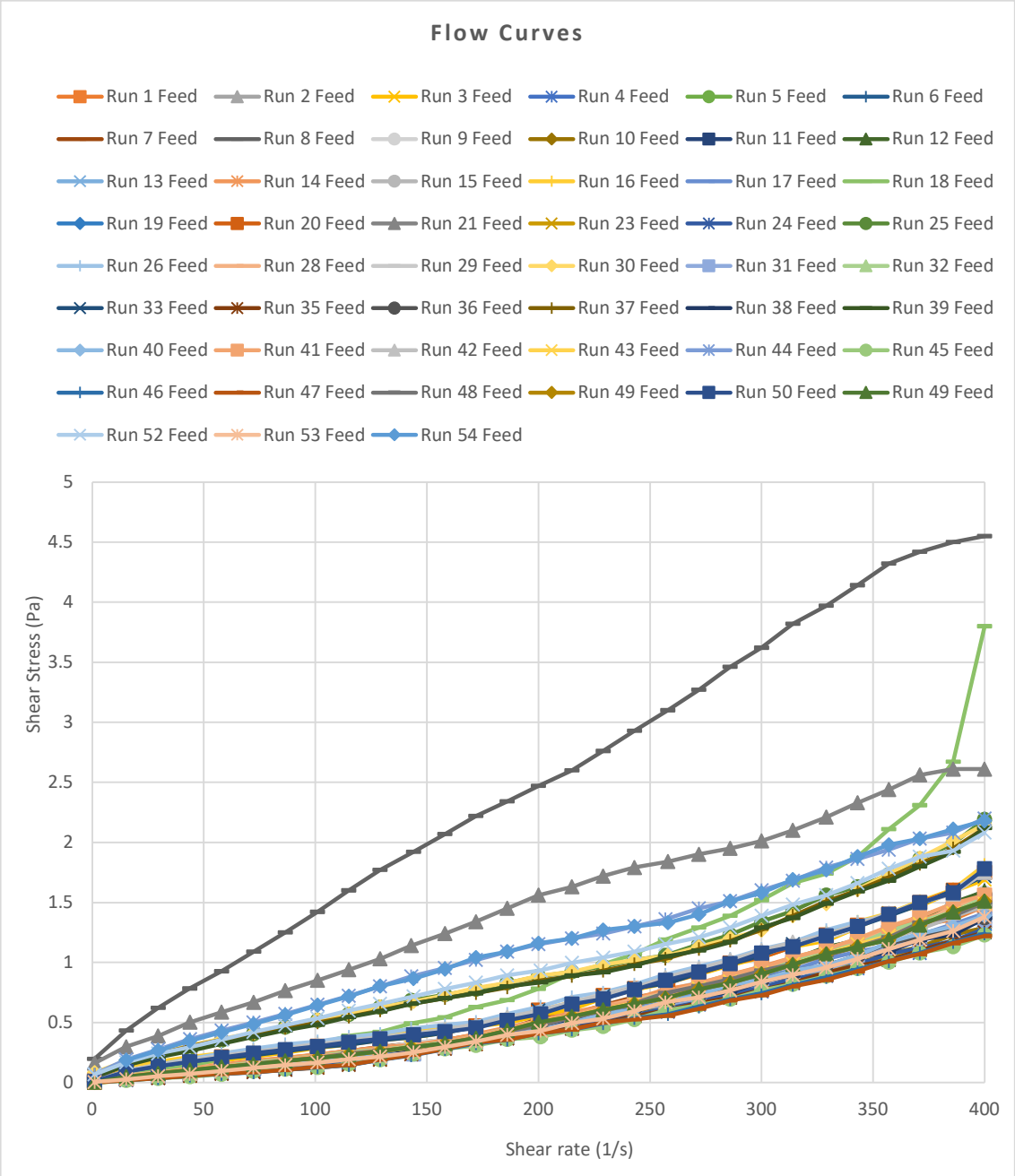

Figure 6-1 –Shear Rate versus Shear Stress of the flotation feed of the CCRD test

The characteristic rheological behaviour of the flotation feed pulp is shear thickening since in Figure 6-1 the shear stress increases with the shear rate. Shear thickening

occurs only in moderately to highly concentrated multi-phase mixtures, which are usually observed to have yield stress as well. Shear thickening does not occur in typical clay suspensions, but the presence of an additional coarse solid phase at high enough concentration may produce this effect (Forbes and Chyss, 2017).

From the literature, the shear stress versus shear rate relationship of pure muscovite slurry follows the Bingham plastic model, which is a linear relationship. The fitted yield stress is the Bingham yield stress (Farrokhpay et al. 2013; Ndlovu, 2013; Ndlovu et al., 2014).

The curves presented in Figure 6-1 were fitted to the data using Excel®, and the equation of the curves are presented in Appendix 4. All tests fitted a second-order polynomial equation, which is characteristic of a dilatant fluid. However, the polynomial relationship does not have a physical meaning other than the constant, which is the yield stress of the pulp.

Figure 6-2 shows the measured viscosity of the flotation feed pulp at the shear rate of 100 s^{-1} for all 54 flotation tests in the main CCRD.

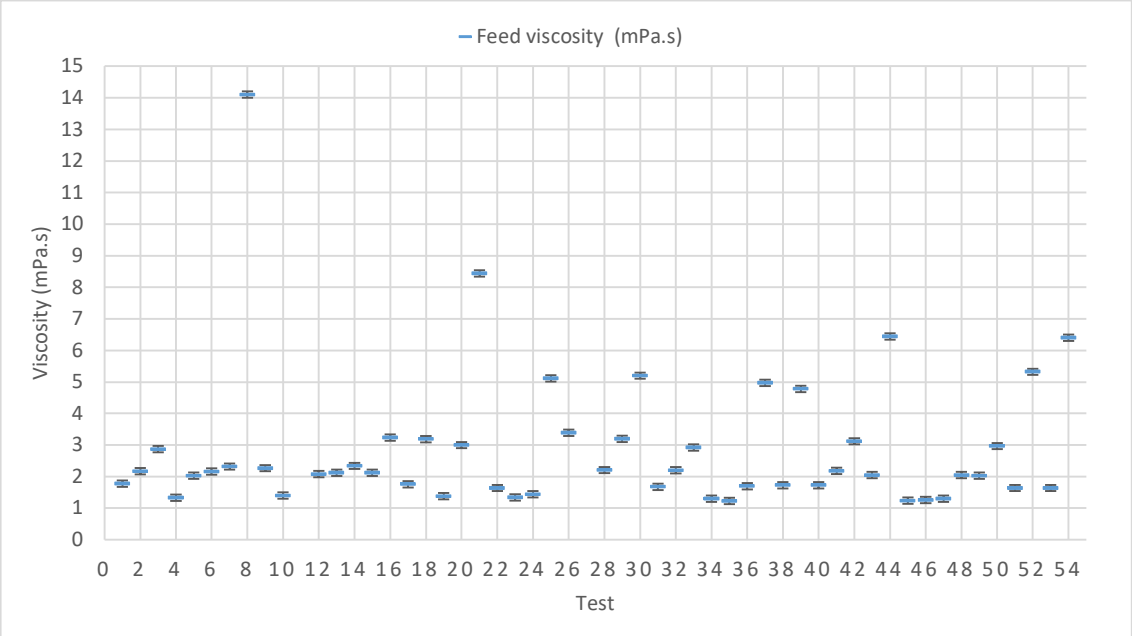

Figure 6-2 – Apparent viscosity of the flotation feed pulp at the shear rate of 100 s^{-1} (viscosity of centre point and confidence interval at 95% confidence: 2.08±0.1 Pa)

The error bars represent the confidence interval at 95% confidence. The confidence interval was calculated based on the repeat tests executed as part of the CCRD program. The viscosity measurement error was calculated through the centre point repeats provided in the CCRD. The average viscosity of the flotation feed pulp at the shows the measured viscosity of the flotation feed pulp at the shear rate of 100 s^{-1} is 2.09 mPa.s, and the confidence interval is 0.1 mPa.s.

The spread of the flotation feed viscosity shown in Figure 6-2 suggested that significantly different viscosity levels were achieved in the CCRD; therefore, an effect of viscosity may be observed in the system.

6.2.2 Pulp Viscosity Regression Analysis

The viscosity of each test of the CCRD was measured at the shear rate of 100 s^{-1}. The shear rate of 100 s^{-1} was selected as the best point to estimate the shear stress of the pulp, based on the literature. According to Ralston et al. (2007), the value of 100 s^{-1} could be the average shear rate in a flotation cell. The viscosity, given by the shear stress divided by the shear rate, was added as an extra predictor on the stepwise regression analysis of flotation rate of arsenopyrite and pyrite.

In Chapter 5 the regression analysis of the flotation evaluated the five factors of the CCRD, including pH, frother dosage, muscovite P_{80}, the proportion of muscovite and %solids of the flotation feed. In these new regressions, the stepwise analysis evaluated the five factors of the CCRD and the measured viscosity of the flotation feed of each test. The viscosity was selected to be part of the stepwise regression analysis to identify if it would present as an independent term not related to the percentage of solids in the regression equation. The percentage of solids was modified in the CCRD experiments to be the proxy for viscosity. However, the mechanism, which the percentage of solids affects, the flotation rate constant can be different from the increase of viscosity. By having both terms in the stepwise regression, this difference can be observed.

Therefore, the candidate terms of the stepwise analysis for the regression model of arsenopyrite and pyrite were:

- Single terms: pH, %muscovite, frother (ppm), %solids w/w, P_{80}, viscosity, pulp density, %solids (v/v).
- Quadratic terms: pH^2, $muscovite^2$, $frother^2$, $\%solids^2$ w/w, P_{80}^2, $viscosity^2$, pulp x $density^2$.
- Two-way interaction terms: pH x %muscovite, pH x frother, pH x %solids (w/w), pH x P_{80}, %muscovite x frother, %muscovite x %solids (w/w), %muscovite x P_{80}, frother x %solids (w/w), frother x P_{80}, %solids (w/w) x P_{80}, viscosity x pH, viscosity x %solids (v/v), viscosity x %muscovite, viscosity x frother, viscosity x P_{80}.

Where the terms are as follows:

- The frother is the dosage in ppm. E.g., 30 ppm, then frother = 30.
- %solids: the percentage value expressed as a range from 0 to 1. Eg: 20% solids, %solids = 0.2.
- %muscovite: is the percentage of muscovite in the gangue, expressed as a range from 0 to 1. Eg: 12% muscovite, %muscovite = 0.12.
- P_{80}: P_{80} of muscovite in μm.
- pH: the absolute value of pH.
- Viscosity: viscosity of the flotation feed in mPa.s measured at a shear rate of 100 s^{-1}.
- Pulp density: calculated pulp density in kg/L based on the pure minerals' density.

The stepwise regression analysis, including viscosity as a predictor, returned the same regression models presented in Chapter 5 equations 5-8 and 5-9. Surprisingly this indicated that the viscosity is not a significant factor affecting the flotation rate of arsenopyrite and pyrite. This result was unexpected because the models generated by the data analysis from the CCRD indicated that the increase in % solids decreases

the flotation rates. Therefore, it suggested that the mechanism behind the increase in the percentage of solids would be a change in pulp viscosity.

However, the regression analysis of the final recovery of pyrite indicated that the viscosity of pulp has a deleterious effect on the recovery, as shown in equation 6-1:

$$R_{py} = 99.057 - 0.1020\ viscosity \quad \text{(Equation 6-1)}$$

The level of significance of the terms of the equation 6-1 is presented in Table 6-1

Table 6-1 Model coefficients statistics of the final recovery of pyrite

Term	Coefficient	SE of Coefficient	P-value
Constant	99.057	0.133	0.00
Viscosity	-0.10	0.0368	0.0008

According to Table 6-1, the constant and the viscosity are the most significant predictors of the recovery of pyrite in equation 6-1. The viscosity has a negative effect. Comparing equation 6-1 to equation 5-7, the viscosity term in equation 6-1 is replacing the term $\%Solids^2$ in equation 5-7. It may suggest the deleterious effect of the percentage of solids in equation 5-7 is related to the effect of the viscosity.

To verify if the viscosity calculated at the shear rate of 400 s^{-1} is more adequate to be used in this thesis, the regression analysis in Minitab was repeated using the new viscosity values calculated at a shear rate of 400 s^{-1}. The regression analysis using the viscosity values calculated at the shear rate of 400 s^{-1} returned the same regression models presented in Chapter 5 equations 5-8 and 5-9. It indicated that the use of a shear rate of 400 s^{-1} or 100 s^{-1} does not change the conclusion that pulp viscosity does not have a significant effect on the flotation rate of pyrite and arsenopyrite.

The analyses presented in this chapter aim to investigate the significant factors that affect the pulp viscosity and understand if the effect of viscosity is embedded in other factors that have a significant effect on the flotation rates of arsenopyrite and pyrite.

6.2.2.1 Pulp Viscosity Regression Analysis

To understand the drivers of pulp viscosity, an empirical relationship is proposed based on the factors studied in the CCRD. Due to the change in rheological behaviour of the system in the given conditions of the CCRD, the pulp viscosity is evaluated at a shear rate of 100 s^{-1}.

The assessment of the empirical relationship between the pulp viscosity and the CCRD factors is done through stepwise regression analysis. The model generated by the regression analysis was used to obtain insightful information about the drivers of flotation feed pulp viscosity. The candidate terms selected for the stepwise regression analysis of pulp viscosity were pH, %muscovite, frother dosage (ppm), muscovite P_{80}, %solids (v/v), pulp density, %passing 38 μm. The quadratic and two-way interaction terms were also included in the regression.

The fitted equation for the pulp viscosity at the shear rate of 100 s^{-1} is shown in equation 6-2:

$$\textit{Pulp viscosity @ 100 } s^{-1} = 9.309 - 2461\ \%solids\ (v/v) - 0.03330\ pH^2 - 3539\ \%solids^2 + 2327\ density*\%solids + 3.44\ pH*\%solids - 15.68\ (\%\ passing\ 38\ \mu m)^2$$

(Equation 6-2)

Where:

- %solids: the volumetric percentage (v/v) value expressed as a range from 0 to 1. Eg: 20% solids, %solids = 0.2. The percentage of solids by volume was calculated based on the percentage of solid by mass and the volumes of the individual minerals and the water. The range tested from 0.04 to 0.23.
- Density = pulp density in kg/L, range tested from 1.13 to 1.97.
- %passing 38 μm = mass fraction of the gangue (silica and muscovite combined) passing 38 μm expressed as a range from 0 to 1, the range tested from 0.096 to 0.4320.
- pH: the absolute value of pH, range tested from 4 to 10.

The pulp viscosity model summary is shown in Table 6-2.

Table 6-2 – Shear Stress Model Summary

S	R^2	Predictive Uncertainty
0.38	96.9%	23.5

The coefficient of determination (R^2) in Table 6-2 shows that 96.9% of the data is explained by the regression model presented in equation 6-2. The model coefficients and P-values of the significant factors that affect the shear stress are shown in Table 6-3.

Table 6-3 – Pulp Viscosity Model Coefficients

Term	Coefficient	Standard Error Coefficient	Coded Coefficient	P-value
Constant	9.309	0.896	2.7664	0
%solids (v/v)	-2461	228	-87.11	0
pH^2	-0.0333	0.00892	-0.581	0.001
%solids^2 (v/v)	-3539	413	-32.54	0
density x %solids(v/v)	2327	229	120	0
pH x %solids (v/v)	3.44	1.05	0.985	0.002
(%passing 38 μm)^2	-15.68	5.52	-0.2513	0.007

Table 6-3 showed the terms %solids (v/v), %solids^2 (v/v), density x %solids(v/v), %passing 38 μm x pH were significant at a 95% level of significance to the flotation feed pulp viscosity.

The most significant terms for the regression are density x %solids(v/v) followed by %solids(v/v), %solids^2 (v/v), constant, pH x %solids (v/v), pH^2 and (%passing 38 μm)^2, according the absolute values of the coded coefficient.

6.2.3 Pulp Rheology Discussion

The regression analysis presented in Table 6-3 suggests that the main driver of the viscosity of the flotation feed pulp is the interaction term pulp density x %solids (v/v). The term is positive; therefore, the increase of pulp density led to an increase in pulp

viscosity. The pulp density of the present system is a function of the percentage of solid by mass, the density of the minerals in the pulp and the density of the water.

Silica and muscovite present the largest mass proportion of the gangue. The density of those minerals is reasonably similar. The density of the silica provided by Sibelco is 2.66 g/cm^3, while muscovite density is 2.90 g/cm^3. Therefore, the effect of pulp density observed is likely not be due to the variation of the proportion of muscovite in the gangue, given the similarity of the densities of muscovite and silica.

In addition, the concentration of $CuSO_4$, PAX, and frother present in solution are not sufficiently high to increase the density of the liquid phase of the pulp (Laliberté, 2007).

It suggested that the percentage of solids by mass should be the major contributor to the density of the pulp because the density of muscovite and silica are very similar. The relationship between solids concentration and pulp density is linear, as indicated by Figure 6-3.

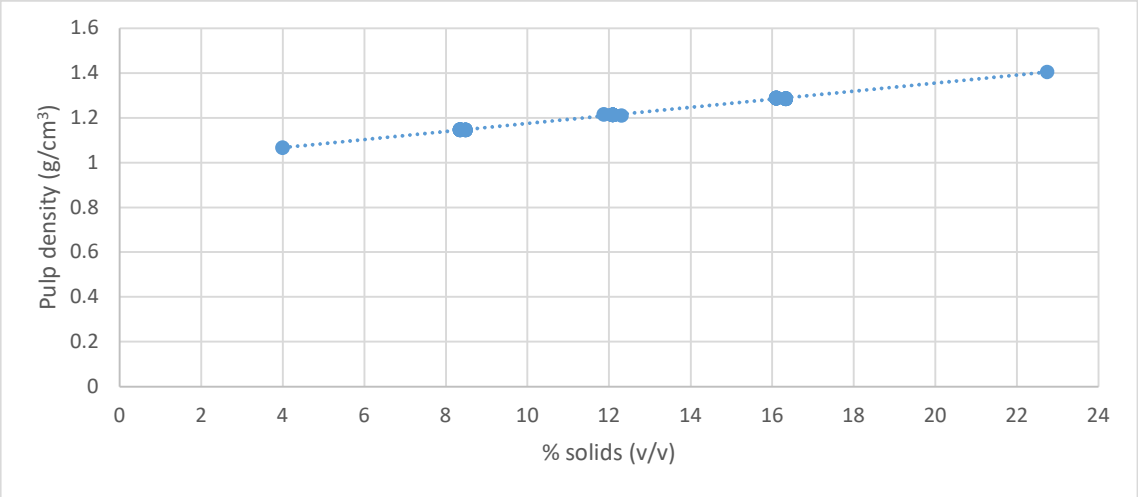

Figure 6-3 – Relationship between solids concentration and pulp density

The terms %solids (v/v) and %solids^2 (v/v) are negative. The relationship between the percentage of solids and pulp viscosity was obtained as main effect plot, to compare with the negative relationship observed by the regression analysis. The main effect plot of the effect of the percentage of solids on the viscosity is shown in Figure 6-4.

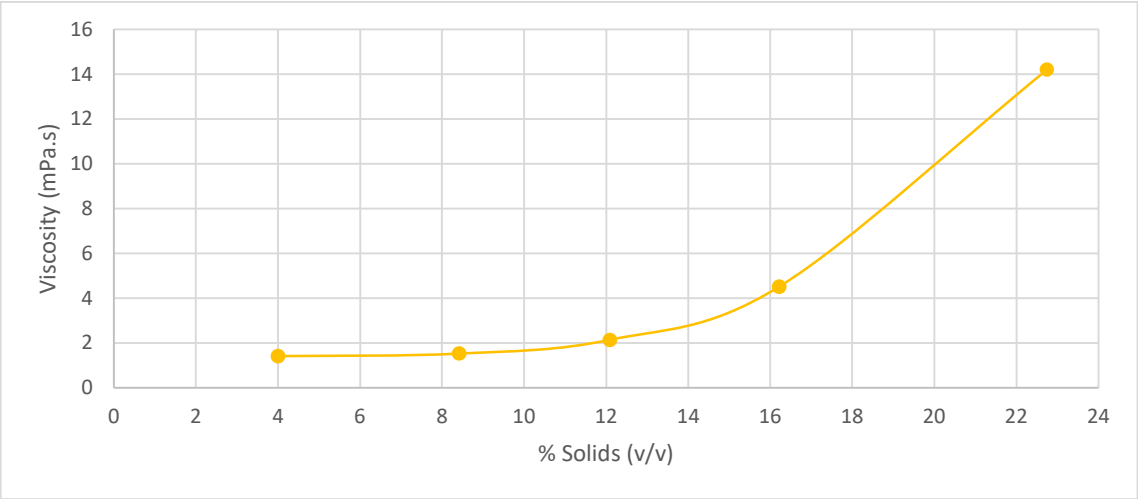

Figure 6-4 – Effect of the percentage of solids on the viscosity

Figure 6-4 indicates that the viscosity increases with the percentage of solids and that the relationship between the percentage of solids and pulp viscosity is non-linear. Therefore, it suggests that the negative sign of the terms %solids (v/v) and %solids^2 (v/v) are introducing curvature in the regression model.

The regression analysis classifies the interaction pH x %solids (v/v), and pH^2 (as a negative term) as significant terms affecting pulp viscosity. The effect of pH on pulp viscosity might be due to modification of the solids surface charge that promotes agglomeration or dispersion of the pulp. These interactions occur due to van der Waals forces of attraction or repulsion between the particles (Chhabra, 2010). The viscosity of suspensions is highly dependent on those inter-particle forces (Ndlovu, 2013).

The degree of coagulation or dispersion of the particles is a resultant of the net inter-particle force (VT), which is a combination of the van der Waals attractive forces (VA) and the repulsive forces of the particle double layer (VR), as per the DLVO theory (Derjaguin and Landau, 1941; Verwey and Overbeek, 1948). The formation of aggregates, the degree of coagulation and attraction between the particles can lead to an increase in viscosity. In addition, the opposite, repulsion between the particles can occur (Ndlovu, 2013; Johnson et al., 2000; Laskowski and Pugh, 1992), as shown in Figure 6-5.

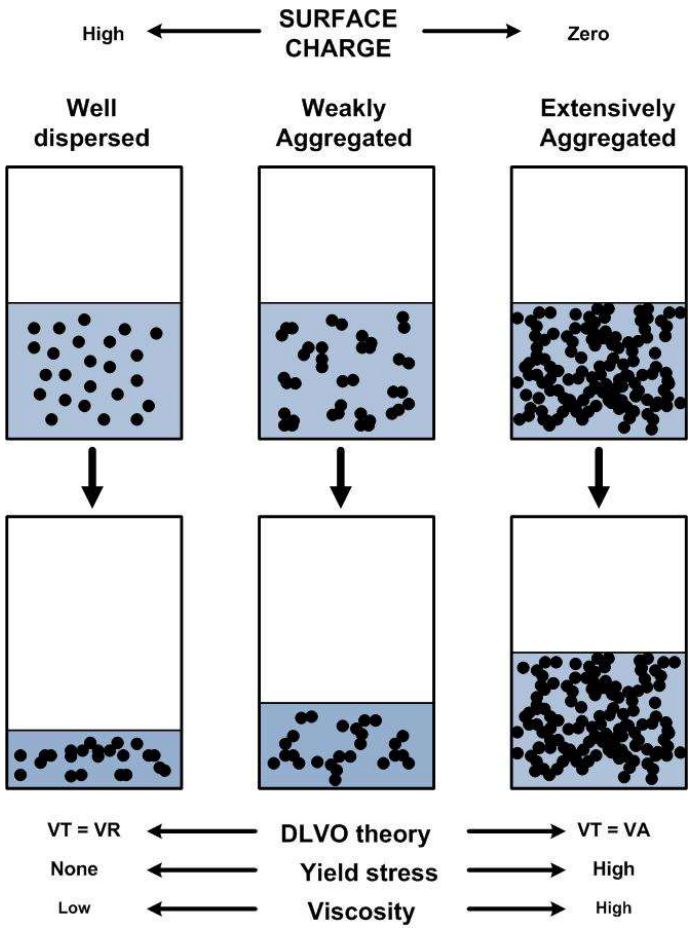

Figure 6-5 – Representation of the relationship between surface charge and rheological properties (Laskowski and Pugh, 1992 cited by Ndlovu, 2013)

It was expected that, by increasing the proportion of muscovite in the flotation feed, pulp viscosity would increase, resulting in a decrease of flotation rate. The regression analysis the pulp viscosity did not include the proportion of muscovite in the gangue as a predictor, which suggested that it does not affect the pulp viscosity significantly. In addition, the regression analysis of the flotation rate in Chapter 5 indicated that the proportion of muscovite does not affect the flotation rate of arsenopyrite and has low significance to the flotation rate of pyrite. This suggests that hypothesis 2: '*The presence of muscovite affects pyrite and arsenopyrite floatability by changing pulp viscosity'* is not supported by the results of the regression analysis presented in this chapter, as the proportion of muscovite does not affect pulp viscosity.

However, the percentage of solids, which is the main predictor of the pulp viscosity, does have a significant deleterious effect on the flotation rate of arsenopyrite and pyrite. Hence, because the percentage of has a deleterious effect on the flotation rates and it is the main predictor of pulp viscosity, it suggested that increase of viscosity may be the mechanism by with the increase of the percentage of solids affects the flotation rates.

According to Ralston et al. (2007), the slurry viscosity affects both the energy dissipation profile through the cell and bubble rise velocity. Hence, it will directly affect the bubble-particle collision frequency. The effect of percentage of solids observed in Figure 5-17 could be due to the “crowding effect” of the gangue, affecting the mobility of the pyrite, arsenopyrite, and air in the pulp, therefore, decreasing the probability of collision of the sulfide minerals with the bubbles and decreasing the bubble-raising velocity. This may be a possible explanation for the deleterious effect of the %solids of the flotation on the flotation kinetics of arsenopyrite and pyrite.

The relative velocity between the particle and the bubble can be considered as a factor of the detachment energy. Another possible effect of the percentage of solids on the flotation rate of arsenopyrite and pyrite is the increase of bubble detachment probability due to the shear between loaded bubbles and gangue (Wang, 2016).

Alternatively, the lack of a statistical correlation of between viscosity and flotation rates may suggest that the mechanism behind the deleterious effect of the interaction %solids x P_{80} on flotation kinetics, is not solely due to the viscosity effect caused by the increase of the percentage of solids. The deleterious effect of the increase of muscovite P_{80} is not well understood and is investigated in Chapter 7.

6.2.4 Pulp Rheology Analysis Conclusions

The following conclusions can be drawn from the pulp rheology analysis presented in this chapter:

1. The regression analysis of the flotation rates including the measured pulp viscosity as a predictor indicated that the viscosity does not have a

significant effect on the flotation rates; however, the percentage of solids, which is the driver of the increase in pulp viscosity does have a deleterious effect on the flotation kinetics.

2. The regression analysis of the pulp viscosity suggested that the proportion of muscovite in the gangue does not affect the pulp viscosity significantly. In addition, the regression analysis of the flotation rate in Chapter 5 indicated that the proportion of muscovite does not affect the flotation rate of arsenopyrite and has low significance to the flotation rate of pyrite. This suggests that hypothesis 2: '*The presence of muscovite affects pyrite and arsenopyrite floatability by changing pulp viscosity*' is not supported by the results of the regression analysis presented in this chapter, as the proportion of muscovite does not affect pulp viscosity.
3. The mechanism by which the percentage of solids affects the flotation rate of arsenopyrite and pyrite may be due to the increase of viscosity, and/or another mechanism that involved the P_{80} of muscovite because the measured viscosity did not present a statistical correlation with the flotation rates.

Chapter 7

Investigating the Effect of Surface Modification on the Flotation Rate

---

7 Investigating the Effect of Surface Modification on the Flotation Rate

7.1 Introduction

This chapter investigates the mechanisms by which the variables studied in the CCRD experiments affect the flotation rate of pyrite and arsenopyrite. The data presented in this chapter allows Hypothesis 3 ('*The detrimental effect of muscovite in the flotation rate of pyrite is due to surface modification of pyrite and arsenopyrite mineral grains'*) to be tested.

The evidence presented aims to understand whether surface modification via hetero-aggregation or chemical modification is the dominant mechanism affecting the floatability of the pyritic minerals.

According to the observations of the main effect plots and the regression analyses in Chapter 5, more than one mechanism could be affecting the flotation rate of pyrite and arsenopyrite. To decouple these mechanisms, this chapter investigates the role of hetero-aggregation (presented in section 7.3), surface chemistry (section 7.4), and reagents (specifically frother and pH modifier, in section 7.5) on the flotation rate of pyrite and arsenopyrite.

7.2 Investigating the Effect of Hetero-Aggregation on the Flotation Rate

He et al. (2009) observed the presence of hydrolysed Cu^{2+} ions in solution from the oxidation of the chalcocite inverts the sign of the surface charge of muscovite, resulting in hetero-aggregation of muscovite on the surface of chalcocite. In the system studied in this research, pyrite and arsenopyrite are intentionally activated by Cu^{2+} ions from the addition of copper sulfate to the flotation feed. The presence of Cu^{2+} ions on the surface of pyrite and arsenopyrite could promote the hetero-aggregation of pyrite and/or arsenopyrite and muscovite.

The presence of a muscovite coating on the pyrite and arsenopyrite particles could be detected by:

- The decrease of final recovery of pyrite and/or arsenopyrite.
- The decrease of final recovery of pyrite and/or arsenopyrite with the increase of muscovite fines.
- Zeta potential tests indicating aggregation of the muscovite particles with pyrite and arsenopyrite.
- Increase in viscosity at a given pH.

The CCRD results presented in Chapter 5 showed that, at the range of conditions tested, no decrease of final pyrite and arsenopyrite recovery was observed, nor the decrease of flotation rate, with an increase the proportion of muscovite fines in the system, as shown in Figure 7-1. Contrarily, the flotation rate of pyrite and arsenopyrite increase with the decrease of muscovite particle size. The mechanism behind this effect is not yet understood.

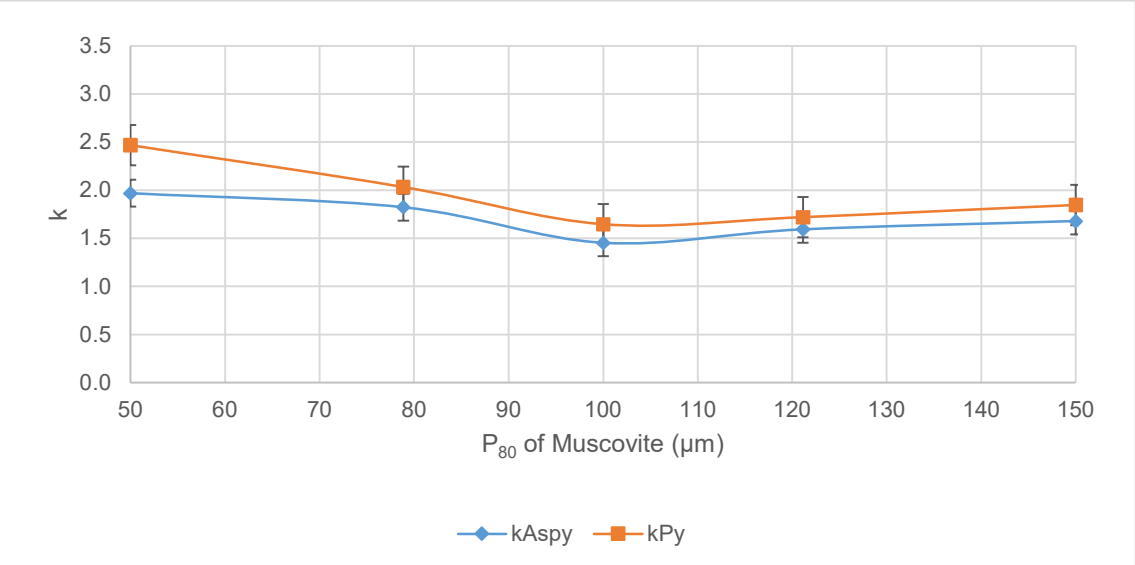

Figure 7-1 – Effect of muscovite P_{80} on the flotation rate of arsenopyrite and pyrite, at the CCRD centre point conditions: pH 7, 27.5% solids, 22.5% of muscovite in the gangue and muscovite P_{80} 100 µm.

In addition, the pulp viscosity regression, presented in Chapter 6, suggested that the increase of muscovite fines and pH appears to increase pulp dispersion, which suggests a decrease of pulp viscosity.

The increase of the flotation rate with the decrease of the size distribution of muscovite indicated that hetero-aggregation of the muscovite and pyritic mineral is not likely to be the cause of the poor kinetic performance.

This section presents the zeta potential measurements to assess the possibility of hetero-aggregation between muscovite and pyrite and arsenopyrite particles via zeta potential analysis.

7.2.1 Zeta Potential Analysis

The zeta potential describes the charging behaviour of the solid-liquid interface (Luxbacher, 2014). The magnitude of the zeta potential indicates the degree of electrostatic repulsion between particles in suspension (Greenwood & Kendall, 1999). Aggregation and electrostatic attraction between particles are characterised by zeta potential values equal or close to zero. The greater the distance of the zeta potential value from zero, the greater is the repulsion between the particles (Ndlovu, 2013).

Zeta potential analysis is a technique for the measurement of the surface charge of minerals and has been used in this work to measure the surface charge of pyrite, arsenopyrite, silica and muscovite minerals, individually and as a mixture.

A series of potentiometric titration was conducted over a range of pH values between pH 3 and 11 to identify the pH range of potential aggregation between muscovite and pyrite/arsenopyrite particles. The pH range of the titrations covered the same the pH range as the CCRD tests.

Muscovite is a plate-like anisotropic mineral, for which the charge of the edges differs from that of the flat surface. Hence the value of zeta potential measured represents an average charge of the whole particle. (Forbes et al., 2014; Ndlovu, 2013).

The zeta potentials of pyrite, arsenopyrite, muscovite and silica minerals were measured individually via potentiometric titration. NaOH and H_2SO_4 were used as the pH modifiers in the ZetaProbe. The results are shown in Figure 7-2. The zeta potential measurements were performed under conditions to the flotation tests undertaken in the CCRD. Therefore, the background electrolyte consisted of 100 g/t of $CuSO_4$ and 300 g/t of PAX. The measurements of silica and muscovite were done at 27.5% solids, which is the solids content of the centre point of the CCRD. The size distribution of the silica used is presented in Table 4-9, and the muscovite is in Table 4-7, P_{80} 100 µm.

The measurement of the pyrite and arsenopyrite was done using 5g of each of the minerals ground separately. The grinding consisted of 35g of pyrite and 16g arsenopyrite ground separately in a laboratory rod mill for 5 minutes in 75 mL of Brisbane tap water. This method of grinding pyrite and arsenopyrite does not account for the galvanic interactions amongst the sulfide minerals in the mill and may have achieved a finer size distribution than the grinding for the flotation tests. However, it was the best approach to test the zeta potential of the sulfide minerals individually.

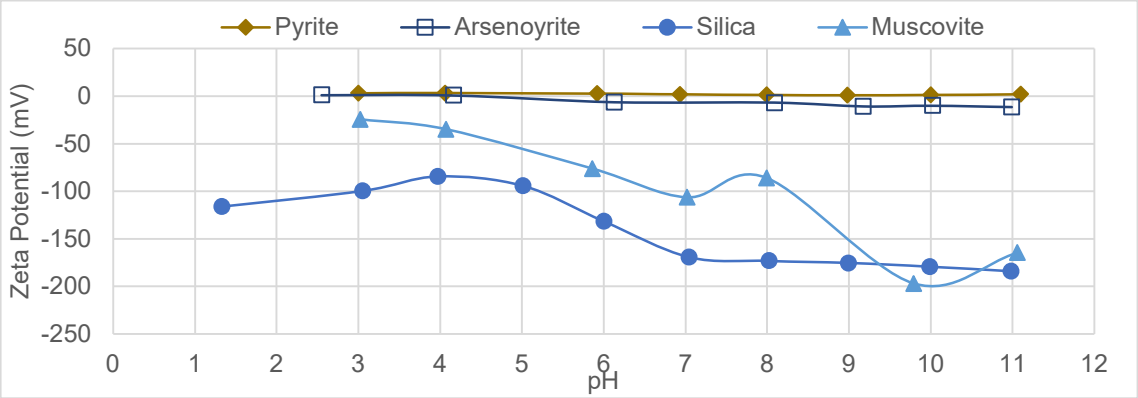

Figure 7-2 - Zeta potential of pyrite, arsenopyrite, muscovite and silica

According to the results in presented Figure 7-2, the zeta potential of pyrite is neutral over the whole pH range tested. The zeta potential of arsenopyrite is similar but slightly negative. The zeta potentials of muscovite and silica are highly negative compared to the sulfide minerals. The zeta potential of muscovite becomes less negative with decreasing pH and tends to net-zero potential below pH 4, where the poor kinetics

performance of the pyritic minerals was observed in the CCRD. The tendency to attain the net-zero potential in the acidic region of the pH spectrum, indicates favourable conditions for agglomeration, as shown in Figure 7-3. Therefore, according to Figure 7-2, the pH region that could favour the formation of hetero-aggregation by muscovite coating pyritic minerals is around pH 3-4.

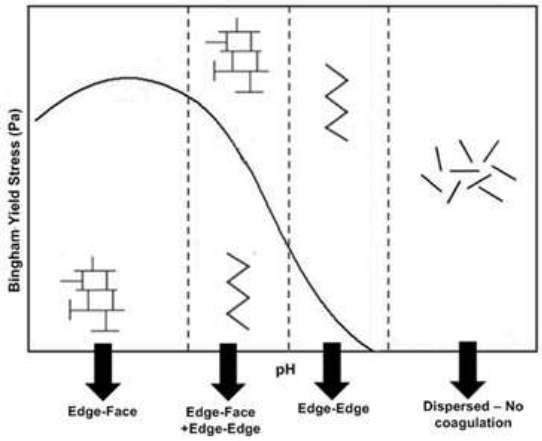

Figure 7-3 – Reproduced from Figure 2-28 - Schematic representation of the modes of particle interaction inhomogeneous mineral suspensions as a function of pH and Bingham yield stress (Rand and Melton (1977) cited by Ndlovu, 2013).

The muscovite isoelectric point was not detected in the zeta potential measurements in Figure 7-2. In addition, the zeta potential values showed in Figure 7-2 are high when compared to He et al. (2009) and Ndlovu (2013). Ndlovu (2013) measured the isoelectric point of muscovite around pH 4.6; however, this was obtained for a different background electrolyte, NaCl solution. In this research, the zeta potential conditions mimicked the flotation feed conditions, using $CuSO_4$ and PAX as the background electrolyte.

The presence of cations and anions from the electrolyte can change the magnitude and sign of the zeta potential considerably. For example, previous studies have found that the presence of sulphate ions increased the negative charges of sulphide minerals (Bulut and Yenial, 2016). The additional presence of collector in the measurements performed in this thesis is likely to have a more complex effect on zeta potential, however, in order to understand the overall effects in the real system, it is important to

make these measurements in the same conditions as the flotation testwork. The zeta potential results are strongly dependent and variable with the water chemistry and minerals present in the pulp, and therefore, cannot be directly compared with measurements performed under different conditions.

An extended investigation of the mechanisms leading to the high zeta-potential of the muscovite and silica and the effects of $CuSO_4$ and PAX would be helpful work but was not part of the scope of this thesis.

The zeta potential of muscovite presented in Figure 7-2 represents the average zeta potential of muscovite at P_{80} 100 µm. To investigate if a particular size fraction would potentially be more likely to coat the pyritic minerals, the zeta potential of each size fraction of muscovite is measured, and the results of these analyses are shown in Figure 7-4. The potentiometric titrations presented in Figure 7-4 were obtained using 10g of muscovite in the designated size fraction, 100 g/t of $CuSO_4$ and 300 g/t of PAX as the background electrolytes and NaOH and H_2SO_4 was used as the pH modifiers.

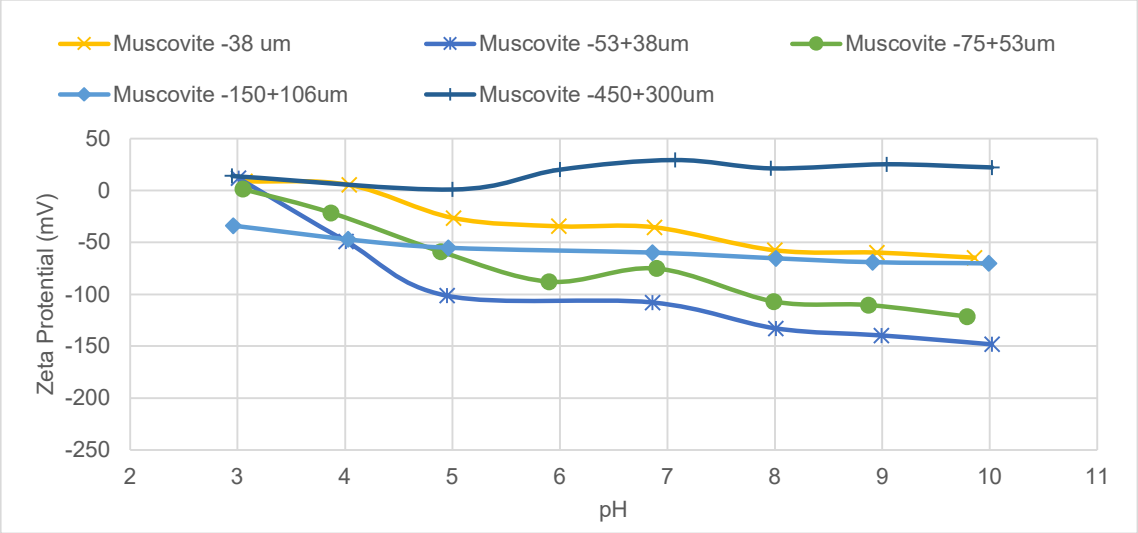

Figure 7-4 – Zeta potential by the size of muscovite

In Figure 7-4, the average zeta potential of muscovite -38 µm is positive below pH 4-3, which reinforces the possibility of coating. The muscovite at the size fraction of - 450/+300 µm presented a positive zeta potential value through the investigated pH

range. The zeta potential value of muscovite from pH 5-10 appears to decrease, with the increase in muscovite particle size, with the exception of the material at - 38 µm. This behaviour can be expected due to the anisotropic nature of muscovite.

The interactions between the minerals were observed by comparing the zeta potentials of the individual minerals with the zeta potential of the mixtures. If the zeta potential of the mixture is overlapping the zeta potential of an individual component, this component is coating the other (Yu et al., 2017; Forbes et al., 2014).

As suggested by the data presented in Figure 7-2 and Figure 7-4, the most likely pH region to observe hetero-aggregation would be between pH 3-4. To confirm the likelihood of formation presence of muscovite coatings on the pyrite surface at pH 4, the zeta potential of the individual minerals at pH 4 was compared to the mineral mixture, containing pyrite, muscovite and silica, according to the method proposed by Yu et al. (2017). This method compared the calculated zeta potential of the mixture obtained via the weighted average of the zeta potential of the single minerals, to measured zeta potential of the mixture. The calculation is as follows:

Zeta potential (mixture) = Wt%Mineral A x (Mineral A measured zeta potential) + ... + Wt%Mineral N x (Mineral N measured zeta potential).

The comparison is provided in Table 7-1 and Figure 7-5. Arsenopyrite was not included in the test because of the limitation of subsampling representative amounts of this mineral for the test. Therefore, the conclusions are drawn sorely for pyrite.

Table 7-1 presented the measure zeta potential of the minerals of interest (pyrite, muscovite and silica) and the mixture, which was prepared with the same proportion as the minerals of the flotation test performed at pH 4, consisting of 22.5% of muscovite at P80 = 100 µm and 27% solids. The background electrolytes were $CuSO_4$ and PAX, the pH was adjusted with H_2SO_4.

Table 7-1 - Zeta potentials of the individual minerals (measured) and mixture (calculated) at pH 4

Measured potential		
Mineral or mixture	**Zeta potential**	**pH**
Pyrite	0.89	4
Muscovite	-28.88	4
Silica	-94.32	4
Pyrite + Muscovite +Silica	-103.2	4
Calculated potential based on the individual minerals		
Mineral or mixture	**Zeta potential**	**pH**
Pyrite + Muscovite +Silica	-81.68	4

Figure 7-5 is a graphic representation of the zeta potential values presented in Table 7-1. The formation of gangue coating on pyrite would be indicated in Figure 7-5 by the zeta potential of the mineral mixture overlapping/approaching the zeta potential of muscovite (coating of muscovite) or silica (coating of silica). Figure 7-5 also presents the calculated zeta potential of the mixture based on the zeta potential of the individual minerals and its proportions in the mixture.

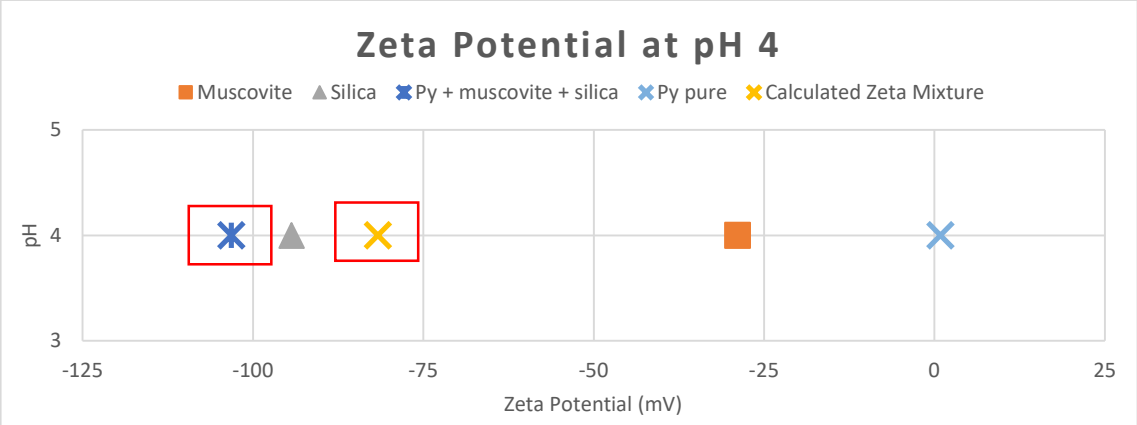

Figure 7-5 – Zeta potential of the mineral mixture, individual minerals and calculated zeta potential of the mixture

As shown in Figure 7-5, the zeta potential of the mixture does not overlap with the gangue zeta potential. Moreover, the zeta potential of the mixture (-103 mV) is more negative than would be expected (-82 mV). This indicates that the system is dispersed. Therefore, no evidence of hetero-aggregation is found under flotation conditions.

7.2.2 Hetero-Aggregation Analysis Conclusions

The following conclusions can be drawn from the zeta potential analysis:

1. The most likely pH range to observe hetero-aggregation of muscovite and pyrite would be pH 4-3; however, the zeta potential analysis of the mineral mixture under the same flotation conditions does not indicate hetero-aggregation at pH 4.
2. The low flotation rates observed at pH 4 compared to pH 10 cannot be explained by the formation of slime coating of muscovite or silica on the surface of the pyrite.

Therefore, there is no strong evidence to confirm that hetero-aggregation of fine particles of muscovite has a deleterious effect on the flotation rate of pyrite and arsenopyrite in this system.

7.3 Investigating the Effect of Surface Chemistry on the Flotation Response

This section presents the results of the surface chemistry analyses from via ToF-SIMS and XPS analysis of pyritic minerals. The ToF-SIMS analysis consisted of a qualitative investigation of the presence of metal ions and collector on the surface of the pyritic minerals. The XPS analysis presents complementary information about the state of oxidation of the arsenopyrite and pyrite.

7.3.1 Sample Preparation for the Surface Analysis

To investigate the mechanism by which the proportion of muscovite, the muscovite P_{80} and pH affect the flotation rate, a 3-factor factorial experiment was undertaken to provide flotation feed samples for surface analysis via ToF-SIMS and XPS techniques. The factors investigated were pH, muscovite size distribution and proportion of muscovite in the feed. Table 7-2 lists the tests of the 3-factor factorial experiment and the range of the factors investigated.

Table 7-2- Three-factor factorial experiment for surface analysis

Test	pH	The ratio of %Muscovite/%Silica (in the gangue)	P_{80} of Muscovite (µm)
S1	10	0/100	-
S2	10	45/55	50
S3	4	45/55	50
S4	4	0/100	-
S5	10	45/55	150
S6	4	45/55	150

The reagents added in tests S1 to S6 were PAX at 300 g/t, Dowfroth 250 at 20 ppm and 100 g/t of $CuSO_4$. The reagent regime in the 3-factor factorial experiment reflects the centre point of the CCRD tests.

The samples of the flotation feed were collected after the reagents had been added and 10 minutes conditioning time completed. Air was not injected in the feed pulp prior to the collection of the samples. Approximately 20 mL of feed samples collected in plastic vials were snap-frozen in liquid nitrogen and stored at -18 ^oC for transport.

7.3.2 ToF SIMS Results

The aim of the surface analysis by ToF-SIMS was to identify the species present on the surface of sulfide minerals that promotes its hydrophobicity, such as collector, and Cu activator, and also the presence of hydrophilic metal ions originated from the gangue, which are Si, Al, K ions.

ToF-SIMS is a qualitative analysis technique that reports relative changes in abundance of a given ion on the outer 1-2 layers of atoms of the surface of a particle, measured as normalised ion intensity (Vizcarra, 2010; Boulton et al., 2003). The ToF-SIMS analysis was done in a particle by particle basis. A minimum of 15 particles was analysed for gathering the spectrum data of each sample, as per Table 7-3.

Table 7-3 – Number of Particles Analysed by ToF-SIMS

Test	S1	S2	S3	S4	S5	S6
Number of particles	24	21	21	22	21	15

The results are presented as normalised ion intensity with the respective error bars (95% confidence interval). The ions selected for analysis of the positive SIMS were Fe, Cu, Si, Al, K. The C_3H_7 species was also included to account for the collector molecule fragment, because the whole molecule of the collector, because $C_6H_{11}KOS_2$ was not identified, as shown in Figure 7-6.

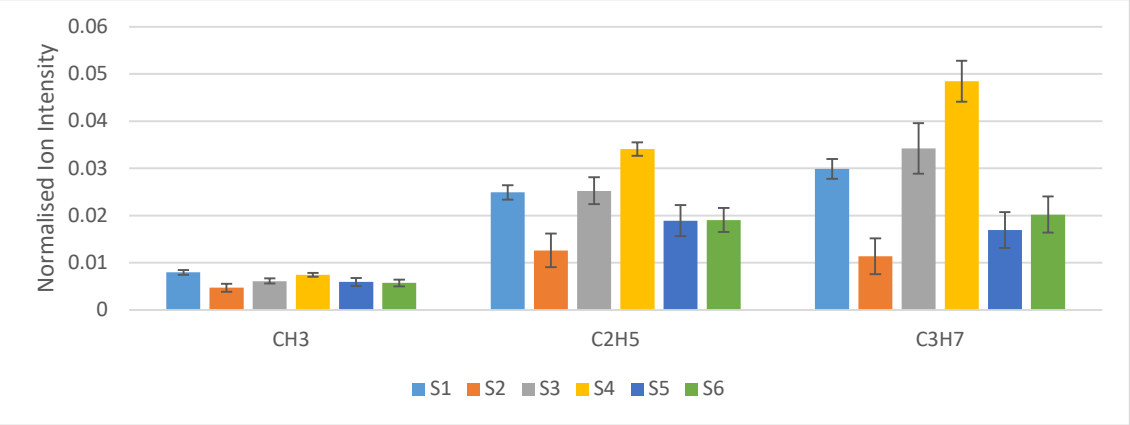

Figure 7-6 – Normalised ion intensity of the organic fragments of the collector identified in the ToF-SIMS analysis

The elements analysed through the negative SIMS were O, S, and SiO_2. In the synthetic ore used in this work, Fe and S are related exclusively to the surface of the pyrite (FeS_2), while Al and K relate to the composition of muscovite ($KAl_3Si_3O_{10}(OH)_2$). The K can also be related to the collector PAX, which can be observed through tests S1 and S4, in the absence of muscovite. Cu accounts for the $CuSO_4$ added to the system. Si can be related to both silica and muscovite. Arsenic presented a very low normalised ion intensity, which could not be comparable with the other ions. As a result, the arsenopyrite could not be distinguished from pyrite in the ToF-SIMS analysis. For simplification, the results are commented in relation to pyrite.

7.3.2.1 Tests in the absence of muscovite

Tests S1 and S4 were performed at pH 10 and pH 4, respectively, in the absence of muscovite. The normalised ion peak intensity with 95% confidence intervals of Fe, Cu, Al, K and C_3H_7 in the flotation feed with no added muscovite is shown in Figure 7-7.

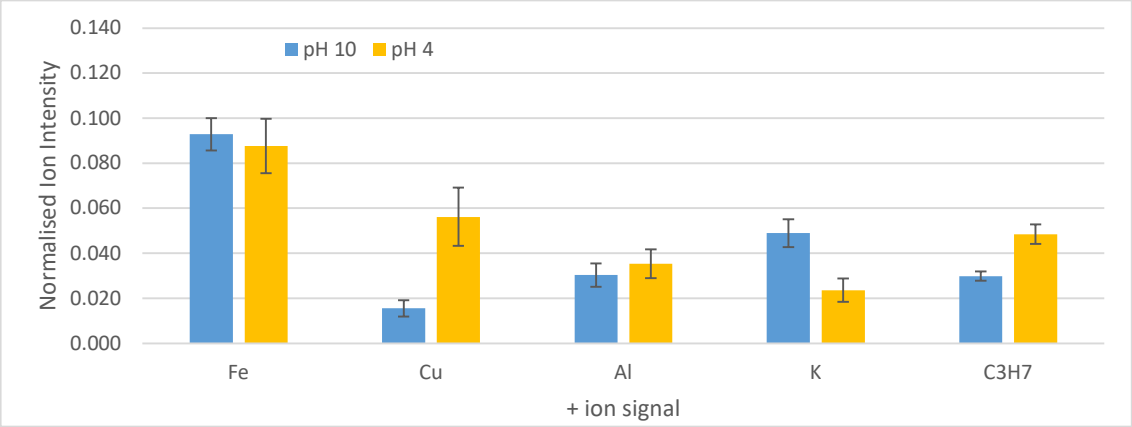

Figure 7-7 – Statistical comparison of ToF-SIMS normalised intensities for pyrite particles at pH 4 and pH 10. Error bars represent 95% CI.

The surface analysis results shown in Figure 7-7 indicated that the pH level does not affect the ion intensities of the Fe and Al. The main differences between pH 4 and 10 are observed in Cu, K, and collector (C_3H_7). In the absence of muscovite, Al ions are not expected to have notable ion intensity, as these ions originated from muscovite. The presence of K can be related to the collector PAX.

The Al observed on the surface of pyrite at the tests run in the absence of muscovite are likely to have originated from the tap water used in the flotation and Al contamination of silica and pyrite, as no muscovite or another source of Al was added to S1 and S4. The silica used contains 0.09% Al_2O_3. Pyrite samples have 0.08% of Al, while arsenopyrite contains 0.06%, which are originated from the contamination of phyllosilicate minerals (as shown in Table 4-3). The flotation tests were performed using Brisbane tap water, which contains 0.046 mg/L of aluminium (Queensland Urban Utilities, 2018).

The sources of K observed on the surface of pyrite could originate from the Brisbane tap water used in the experiment and the collector. Liu and Peng (2014) reported 3.16 mg/L of K in Brisbane tap water. However, no information about traces of K found in Brisbane tap water was supplied by Queensland Urban Utilities (2018). The signal of K does not follow the same trend of Al; therefore, the difference observed is assumed to be due to the collector PAX ($CH_3(CH_2)_4OCS_2K$) dissolution in water, as no other source of K was identified.

The levels of Al and K observed in Figure 7-7 sets minimum baseline levels of those ions in the system in comparison with the system with muscovite.

The concentration of Cu ions on the surface of pyrite at pH 4 is significantly higher than at pH 10. The normalised ion intensity of Cu on the surface of pyrite at pH 4 is approximately 3 times higher than at pH 10. The ion intensity of the collector fragment C_3H_7 on the surface of the pyrite at pH 4 is significantly higher than at pH 10. It indicates a higher copper activation of the pyrite surface and consequently, higher collector coverage at pH 4 when compared to pH 10.

7.3.2.2 The effect of muscovite P_{80} at pH 10

The effect of the presence of muscovite on the surface chemistry of the pyrite can be observed by comparing the normalised ion intensities of Fe, Cu, Si, Al, K, O, S, and C_3H_7, for the two levels of pH investigated. The normalised ion intensities on the surface of pyrite at pH 10 are shown in Figure 7-8.

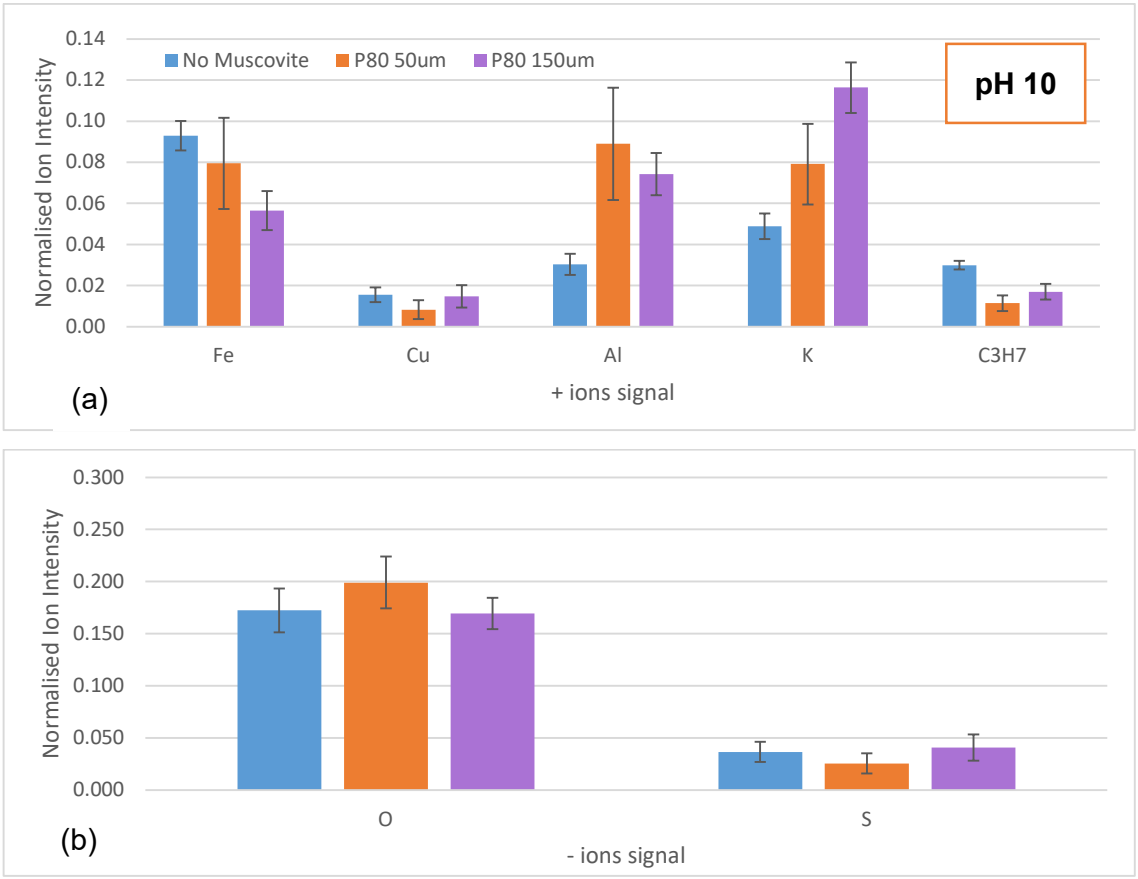

Figure 7-8 –ToF-SIMS normalised ion intensities for pyrite particles at pH 10. (a) Positive ions. (b) Negative ions. Error bars represent 95% CI.

Overall, according to the results presented Figure 7-8(a), it appears that the presence of muscovite leads to a decrease in Fe and C_3H_7 and an increase of Al and K levels on the surface of pyrite. The size distribution of muscovite affects the levels of Fe, Cu, K and C_3H_7 on the surface of pyrite.

No significant differences were observed in the O and S signals, as presented in Figure 7-8(b).

The level of Fe on the surface of pyrite seems to decrease with an increase of particle size of muscovite, as indicated by the normalised ion intensity on Figure 7-8(a). The test with muscovite at P_{80} 50 µm, appears to have more Fe on the surface of pyrite than a test at muscovite P_{80} 150 µm; however, test with muscovite at P_{80} 50 µm has a large data spread, as indicated by the error bars.

The size distribution of muscovite appears to affect the level of Cu on the surface of the pyrite. The level of Cu appears to be lower in the presence of muscovite at P_{80} 50 μm compared to muscovite at P_{80} 150 μm. It indicates that the size distribution of muscovite could be affecting the level of pyrite activation at pH 10.

The same trend is observed in the collector fragment ion intensity signal. The level of collector (C_3H_7) coverage on the surface of the pyrite appears to be lower when muscovite at P_{80} 50 μm is present, compared to muscovite at P_{80} 150 μm.

The intensity of K ions on the surface of pyrite when muscovite is present increases significantly compared to the baseline observed in the absence of muscovite. The level of K on the surface of pyrite is higher when muscovite size distribution is coarse (P_{80} 150 μm).

The increase of K on the surface of pyrite appears to follow the decrease of Fe. It may suggest that K ions in solution could affect the level of Fe ions on the surface of pyrite.

The mean level of Al on the surface of pyrite when finer muscovite (P_{80} 50 μm) is present seems to be higher than when coarse muscovite (P_{80} 150 μm) is present. However, this difference is not statistically significant, at 95%.

7.3.2.3 The effect of muscovite P_{80} at pH 4

The levels of Fe, Cu, Si, Al, K and C_3H_7 (normalised ion intensities) on the surface of pyrite at pH 4 are shown in Figure 7-9.

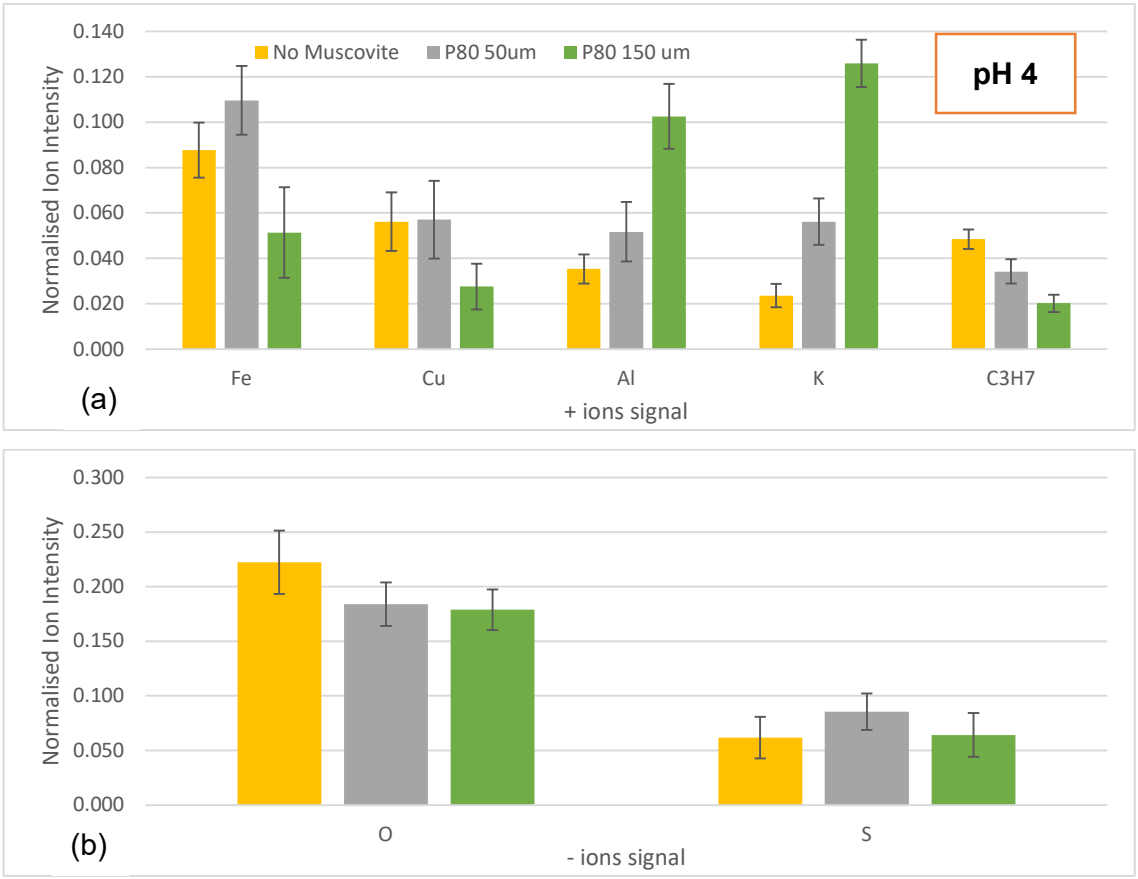

Figure 7-9 - ToF-SIMS normalised ion intensities for pyrite particles at pH 4. (a) Positive ions. (b) Negative ions. Error bars represent 95% CI.

Overall, according to Figure 7-9(a), it appears that the presence of muscovite leads to a decrease in C_3H_7 and an increase of Al and K levels on the surface of pyrite. The size distribution of muscovite affects the levels of Fe, Cu, Al, K and C_3H_7 on the surface of pyrite. However, no statistically significant changes were observed in Figure 7-9(b).

The levels of Al and K on the surface of pyrite appears to increase when muscovite is present at pH 4. The levels of K appear to increase significantly with the increase of muscovite size. The level of Al appears to increase significantly when coarse muscovite (P_{80} 150 µm) is present.

The level of Fe on the surface of pyrite seems to increase when muscovite at P_{80} 50 µm is present. The Fe ion intensity appears to decrease considerably in the

presence of coarse muscovite (P_{80} 150 μm), as suggested by the normalised ion intensity in Figure 7-9 (a).

There are no significant differences between the levels of Cu in the absence of muscovite and presence of finer muscovite (P_{80} 50 μm), contrary to the behaviour observed at pH 10, in which the level of Cu appears to decrease. The levels of Cu decreased significantly in the presence of coarse muscovite (P_{80} 150 μm). Therefore, the trends presented in Figure 7-9(a) suggests that the size distribution of muscovite appears to affect the activation of pyrite at pH 4.

The collector (C_3H_7) coverage on the surface of the pyrite appears to decrease with the increase of the levels of K and Al observed. The extent of this decrease in coverage depends on the size distribution of muscovite. As muscovite size distribution gets coarser, a lesser coverage of collector on the surface of pyrite was observed.

At pH 10, it seems that fine muscovite was more detrimental to the activation of pyrite and collector coverage. At pH 4, the coarse muscovite appears to be more detrimental to the activation by Cu and collector coverage. As well as at pH 10, the presence of coarse muscovite at pH 4 decreases the exposure of Fe in the surface of pyrite. However, the exposure of Fe increased in the presence of fine muscovite at pH 4.

7.3.3 XPS Results

The XPS technique does not analyse the surface of specific particles. It analyses the atomic percentages of the chemical species present in the bulk sample surface (Vizcarra, 2010) quantitatively.

The surface analysis by the XPS presented in this section investigates the level of oxidation of the pyritic minerals, quantifies the presence of hydroxides and detects collector levels on the sample. Arsenic was not visible in the surface analysis due to the low grade of arsenopyrite in the flotation feed. Therefore, the conclusions of the surface analysis are valid only for pyrite.

7.3.3.1 Tests in the absence of muscovite

The effect of pH in the floatability of pyrite can be observed comparing the level of oxidation of pyrite in tests 1 and 4 through the Fe spectra. Table 7-4 compares information on the high-resolution spectrum of Fe 2p of pH 10 versus pH 4. Tests 1 and 4 were conducted in the absence of muscovite.

Table 7-4 - High-resolution spectrum of Fe 2p in the absence of muscovite

Binding Energy (eV)		**710.46**	**712.74**	**715.29**
Test	**pH**	**FeS+ FeO**	**Fe_2O_3**	**FeOOH**
S1	**10**	59.08	31.86	9.06
S4	**4**	61.76	23.89	14.35

According to Table 7-4, the proportion of FeS+ FeO is similar at pH 4 and pH 10. The percentage of Fe_2O_3 appears to increase from pH 4 to pH 10, while the proportion of FeOOH seems to decrease. Therefore, it suggests that pyrite is more oxidised at pH 10 than at pH 4.

7.3.3.2 The effect of the presence and P_{80} of muscovite

Table 7-5 compares the high-resolution spectrum of Fe 2p between samples 1, 2 and 5 at pH 10.

Table 7-5 – High-resolution spectrum of Fe 2p at pH 10

Binding Energy (eV)			**710.46**	**712.74**	**715.29**
Test	**% Muscovite**	**P_{80} of Muscovite**	**FeS+ FeO**	**Fe_2O_3**	**FeOOH**
1	0	-	59.08	31.86	9.06
2	45	50	54.71	24.11	8.85
5	45	150	38.35	32.95	22.86

Table 7-5 suggested that the presence of fine muscovite did not affect greatly the levels of FeS+ FeO and FeOOH observed. The level of FeOOH appears to increase with the increase of the particle size of muscovite. The level of Fe_2O_3 seems to decrease with the reduction of the size distribution of muscovite.

The signal for the binding energy of the organic C-O bond, referent to the collector, in the high-resolution spectra of the O 1s for the tests conducted at pH 10 is shown in Table 7-6.

Table 7-6 - High-resolution spectrum of O 1s at pH 10

Binding Energy (eV)			531.90
Test	**% Muscovite**	**P_{80} of Muscovite**	**Organic C-O**
1	0	-	44.59
2	45	50	35.68
5	45	150	34.50

The atomic intensity of the collector, shown in Table 7-6, appears to decrease when muscovite is present. This result aligns with the observations of the ToF-SIMS in Figure 7-8 (a).

Table 7-7 compares the high-resolution spectrum of Fe 2p between samples 4, 3 and 6 at pH 4.

Table 7-7 - High-resolution spectrum of Fe 2p at pH 4

Binding Energy (eV)			710.46	712.74	715.29
Test	**% Muscovite**	**P_{80} of Muscovite**	**FeS+ FeO**	**Fe_2O_3**	**FeOOH**
4	0	-	61.76	23.89	14.35
3	45	50	44.55	27.93	14.89
6	45	150	57.37	21.39	18.06

Table 7-7 suggests that the presence of fine muscovite decrease levels of FeS+ FeO and increase the levels of Fe_2O_3. The level of FeOOH observed seems not to be affected by the presence of muscovite.

The signal for the binding energy of the organic C-O bond, referent to the collector, in the high-resolution spectra of the O 1s for the tests conducted at pH 10 is shown in Table 7-8.

Table 7-8 - High-resolution spectrum of O 1s at pH 4

Binding Energy (eV)			531.90
Test	**% Muscovite**	**P_{80} of Muscovite**	**Organic C-O**
4	0	-	43.93
3	45	50	36.76
6	45	150	31.36

The atomic intensity of the collector, showed in Table 7-8, appears to decrease with the presence of muscovite, as well as the effect shown in Table 7-6. This result aligns with the observations of the ToF-SIMS in Figure 7-9(a).

7.3.4 Muscovite Leaching Tests

The CCRD analyses indicated that the size distribution of muscovite affects the flotation rate of pyrite, leaching tests were conducted on the muscovite to identify the species leached by size fraction. The leaching tests were conducted using 16.4 g of muscovite, with the size fractions -300/+212 μm, -106/+75 μm, at pH 4 and pH 10. The size fractions were leached for 10 minutes (as per the flotation conditioning time) in a beaker agitated in a magnetic agitator, then filtered. The leaching solution consists of deionised water with pH-regulated with H_2SO_4 and NaOH. Triplicates of the filtrated solution samples were submitted for assay of Cu, K, and Al to ensure repeatability of the results.

7.3.5 Muscovite Leaching Results

The assay results of the leaching of the size fractions of muscovite are presented in Figure 7-10 and Figure 7-11. The standard deviation of the assays is shown in Table 7-9 and Table 7-10. Because of the small number of repeat samples for the assays of the muscovite leaching, it was chosen to discuss the error of the assays as standard deviation instead of the confidence interval.

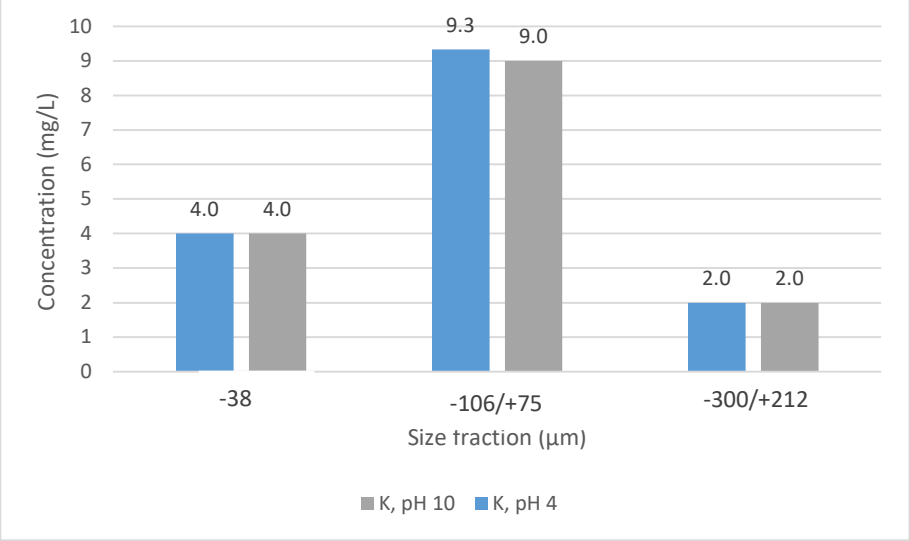

Figure 7-10 – Average potassium concentration in solution from muscovite leaching under the pH conditions of flotation

Table 7-9 – Standard deviation of K assays from the muscovite leaching tests

Size fraction	-300/+212 µm	-106/+75 µm	-38 µm
pH 4	0.0	0.6	0.0
pH 10	0.0	0.0	0.0

According to Figure 7-10 and the standard deviation analysis in Table 7-9, the dissolution of potassium does not depend on pH. The highest dissolution of K from the muscovite occurs at the size fraction -106/+75 µm, followed by – 38 µm and - 300/+212 µm.

The differences observed in assays values of the size fractions – 38 µm and - 300/+212 µm were not significant, because they are within the experimental error. The standard deviation of the K assays for the size fraction - 106/+75 µm is 0.6, which indicates that the assays at pH 4 and 10 are statistically the same; therefore, the results of these tests indicated that the dissolution does not depend on pH, but the particle size.

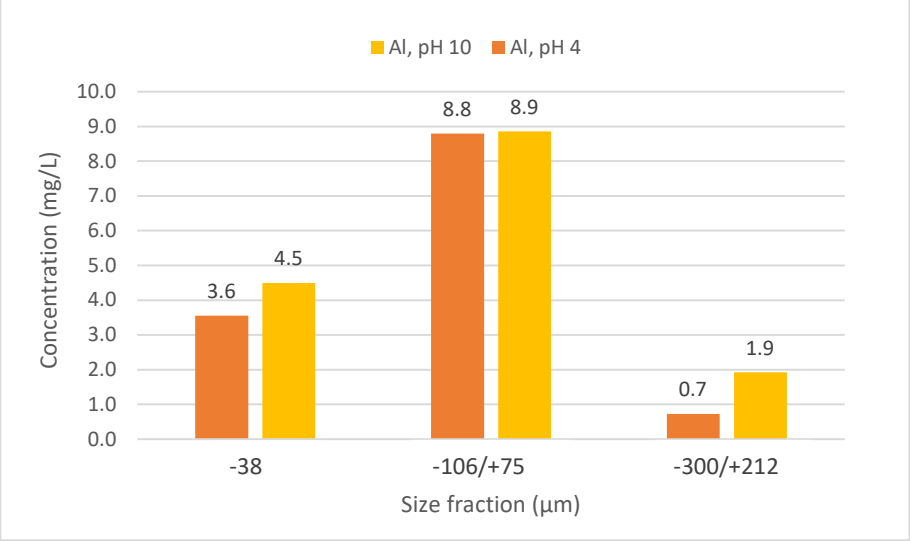

Figure 7-11 – Average aluminium concentration in solution from muscovite leaching under the pH conditions of flotation

Table 7-10 – Standard deviation of Al assays from the muscovite leaching tests

Size fraction	-300/+212 µm	-106/+75 µm	-38 µm
pH 4	0.1	1.3	0.7
pH 10	0.2	0.4	0.8

According to Figure 7-11, the highest dissolution of Al to solution occurs at the size fraction -106/+75 µm, followed by - 38 µm and -300/+212 µm. The dissolution of aluminium to solution follows the pattern of potassium, as per Figure 7-10.

Comparing the standard deviation in Table 7-10, the effect of pH is not significant for the aluminium leaching of the size fractions - 106/+75 µm and - 38 µm. However, at the size fraction -300/+212 µm, the higher pH 10 enhanced the leaching of aluminium.

The leaching analysis in Figure 7-10 and Figure 7-11 showed that the leaching of K and Al from muscovite is size-dependent. Comparing the average concentration of aluminium and potassium in solution versus pH, the size fractions - 106/+75 µm and - 38 µm present similar values for both pH values tested. The size fraction - 300/+212 µm present similar concentration of Al and K in solution at pH 10. The concentration of K is higher than Al at pH 4.

The K atoms are located on the faces of muscovite, while Al on the edges. Maslova et al. (2004) described that the aspect ratio of muscovite is approximately 20, as the ratio of the surface area of basal to edge face. It was expected that given the high aspect ratio of muscovite, the leaching of Al would be associated with the edges, while K with the faces. The leaching of the K and Al indicates that the anisotropic nature of the muscovite affects the flotation by releasing ions into the solution. The proportion of K and Al leached to the solution were similar in all size fractions. However, no distinction amongst the size fractions can be associated to the leach of K or Al exclusively.

The size fraction - 106/+75 µm liberated the highest concentrations of K and Al to the solution in all leaching tests conducted. Therefore, in the flotation tests, the effect of muscovite P_{80} due to the increase of Al and K ions to the solution could be related to the amount of the size fraction - 106/+75 µm present in the flotation feed pulp.

The percentage of -106/+75 µm in the muscovite size distributions used in the flotation tests to collect samples for the surface analysis via ToF-SIMS and XPS are shown in Table 7-11.

Table 7-11 – Percentage of the size fractions used in the leaching tests in the size distributions of muscovite used in flotation tests

P_{80}/Size fraction µm	-300/+212 µm	-106/+75 µm	-38 µm
P_{80} = 150 µm	1.2	9.5	42.9
P_{80} = 50 µm	0.0	4.5	76.7

Table 7-11 showed that the muscovite at P_{80} 150 µm has two times more muscovite in the size fraction -106/+75 µm than muscovite at P_{80} 50 µm. Furthermore, more K and Al are available in solution at the tests that muscovite is present at a coarse size distribution.

7.3.6 Surface Analysis Discussion

ToF-SIMS analysis suggested that the presence of the muscovite in the flotation feed leads to a reduction of Cu coverage on the surface of pyrite, resulting in less collector on the surfaces. In addition, the increase of the particle size of muscovite leads to an increase of K and Al on the surface of pyrite.

The effect of the presence of muscovite in the surface chemistry of pyrite appears to be size-dependent, as shown by the ToF-SIMS analyses in comparing the ion intensities of the tests containing fine muscovite (P_{80} 50 µm) versus coarse muscovite (P_{80} 150 µm).

At both pH levels observed, the increase of the particle size of muscovite in the pulp increased the levels of K^+ on the surface of pyrite. In addition, the ToF-SIMS analyses suggested that the increase in particle size of muscovite decreases the level of Cu and collector on the surface of pyrite. Muscovite has the capacity to exchange K and Al ions from the surfaces for ions available in an aqueous solution, including Fe and Cu (Nosrati et al., 2012; Nosrati et al., 2009). Given the capacity of muscovite exchange Fe and Cu ions in solution for K, it may suggest that the muscovite may uptake Cu ions from the solution, which might be the cause for the lower levels of Cu on the surface of pyrite.

The potassium ions are located on the faces of muscovite, while aluminium originates at edges (Forbes & Chryss, 2017; Ndlovu et al., 2014). It suggests that the effect of the faces of muscovite, loaded with K, is observed when the coarse muscovite (P_{80} 150 µm) is present, as more K is transferred to the pyrite surface. The effect of the muscovite edge seems to be more prominent when fine muscovite is present (P_{80} 50 µm). The effect can be observed by the higher Al intensity on the pyrite compared with coarse muscovite.

The water chemistry tests, comparing the amount of Al and K leached from different size fractions of muscovite, showed that the muscovite at P_{80} 150 µm liberates much more K and Al ions to a solution than muscovite at P_{80} 50 µm. Moreover, more K and Al are available for adsorption at the surface of pyrite when muscovite at P_{80} 150 µm is present in the flotation feed. However, the water chemistry tests did not provide sufficient evidence to support the suggestion that the effect of the edges of muscovite is observed when muscovite at P_{80} 50 µm is present. Nor the effect of the face, when muscovite at P_{80} 150 µm is present because there were no differences on the levels of Al and K leached to the aqueous phase on the size fractions tests.

The CCRD showed that the increase in the size distribution of the muscovite leads to a decrease in flotation rate. This decrease in flotation rate is aligned with the observations in the ToF-SIMS results by the reduction of Cu and C_3H_7 coverage on the surface of the pyrite and the increase of K and Al. Potassium and aluminium are hydrophilic species, the increase of K and Al concentration on the surface of pyrite reduces it hydrophobicity resulting in slower flotation rates.

Table 7-4 showed the XPS results for the samples in the absence of muscovite at pH 4 and pH 10 aiming to indicate the differences in the oxidation of pyrite that is leading to flotation behaviour at pH 4 and 10. According to Table 7-4, the level of Fe_2O_3 on the pyrite at pH 10 is higher than at pH 4. In addition, the ToF-SIMS results presented in Figure 7-7, shows that at pH 10, the levels of Cu and collector on the surface of pyrite are lower at pH 10 than at pH 4. The formation of Fe_2O_3 layer on pyrite surface at high pH should prevent sulfide-collector interaction, which is a common industry practice to use high pH to depress fresh pyrite in many other sulfide separations. However, it does not explain the behaviour observed in the CCRD. Therefore, it can't be concluded that the reason for the poor floatability is the high levels of Fe_2O_3.

7.3.7 Surface Chemistry Analysis Conclusions

The following conclusions can be drawn from the surface analysis via ToF-SIMS and XPS:

1. The level of oxidation of pyrite at pH 10 is higher than at pH 4. Lesser Cu and collector coverage are observed at pH 10 than at pH 4. Therefore, the flotation rates at pH 10 should be slower than at pH 4, contrary to the data presented in the CCRD.
2. The increase in flotation rate with the increase of pH is not due to the surface chemistry of the pyrite.
3. The increase in particle size of muscovite increases the levels of K^+ on the surface of pyrite. In addition, the increase in particle size of muscovite decreases the level of Cu and collector on the surface of pyrite. Moreover, the increase of muscovite particle size in the flotation feed is detrimental to the flotation rate, as observed by the CCRD.

4. The extent of the detrimental effect of those ions is indicated to be size-dependent, as muscovite at P_{80} 150 µm liberates much more K and Al ions to a solution than muscovite at P_{80} 50 µm
5. The presence of muscovite did not overwrite the effect of pH. It amplified the oxidation effect of the pH.

7.3.8 Conclusions of the Effect of Surface Modification on the Flotation Rate

This chapter investigated the potential mechanisms by which the variables studied in the CCRD experiments affect the flotation rate of pyrite and arsenopyrite, which allows Hypothesis 3 to be tested:

The detrimental effect of muscovite in the flotation rate of pyrite is due to surface modification of pyrite and arsenopyrite mineral grains

The nature of surface modification investigated in this thesis consisted of hetero-aggregation and surface chemistry modification.

The zeta potential analysis was conducted to verify the hetero-aggregation between the pyritic minerals and muscovite. The analyses suggested that the most likely range of pH to observe hetero-aggregation of fine particles of muscovite are pH 3-4. However, the analyses of the zeta potential of the mixture under the same flotation conditions of the centre point of the CCRD does not indicate hetero-aggregation at pH 4.

In addition, even if hetero-aggregation of the fine particle was likely to be occurring, it doesn't have an effect on the flotation rate of pyrite and arsenopyrite, because the CCRD analysis showed that the flotation rate increases with the decrease of muscovite particle size. Therefore, the flotation rate of arsenopyrite and pyrite is not affected by hetero-aggregation.

The regression analysis in Chapter 5 indicated that the proportion of muscovite in the feed is not deleterious to the flotation rate of arsenopyrite and has a minor effect on the flotation rate of pyrite. However, it is suggested that the increase of the P_{80} of

muscovite combined with the increase of %solids is deleterious to the flotation rate of arsenopyrite and pyrite.

The ToF-SIMS analyses suggested that when muscovite is present, the increase in particle size of muscovite increases the levels of K and Al on the surface of pyrite and decreases the level of Cu and collector at the levels of pH tested pH 4 and 10. These observations align with the observations of the CCRD analysis that showed a decrease of the flotation rate of arsenopyrite and pyrite with the increase of muscovite particle size.

This indicates that the detrimental effect of muscovite is due to surface chemistry modification of pyrite and arsenopyrite caused the Al and K ions, which originate from muscovite leaching. The extent of the detrimental effect of those ions is indicated to be size depended, as muscovite at P_{80} 150 µm releases much more K and Al ions into solution than muscovite at P_{80} 50 µm. Moreover, more K and Al are available for adsorption at the surface of pyrite when muscovite at P_{80} 150 µm is present in the flotation feed.

The XPS results indicated the level of Fe_2O_3 on the pyrite at pH 10 is higher than at pH 4. The formation of Fe_2O_3 layer on the pyrite surface at high pH should prevent sulfide-collector interaction. In addition, the ToF-SIMS showed that at pH 10, the levels of Cu and collector on the surface of pyrite are lower at pH 10 than at pH 4, which indicated that at high pH the floatability of pyrite should be lower. However, it is contrary to the observations of the CCRD. Therefore, it could not be concluded that the effect of pH in de CCRD is due to oxidation through the formation Fe_2O_3 leading to the poor floatability.

As the CCRD regression analyses showed that the deleterious effect of muscovite P_{80} is dependent on the increase of %solids. It suggests that the percentage of solids ‘amplifies’ the deleterious effect of muscovite in the surface chemistry of the pyritic minerals. In the set of tests completed in the CCRD, the percentage of muscovite in the pulp increases proportionally to the percentage of solids. This would suggest that more muscovite is available for leaching in the pulp, leading to a significant increase

in the concentration of Al and K ions, which may be the reason for the amplifying effect of the %solids.

Therefore, hypothesis 3, that the detrimental effect of muscovite in the flotation rate of arsenopyrite and pyrite is due to surface modification is partially supported by the evidence presented in this chapter.

7.4 Other Factors Affecting the Flotation Rate: Frother Dosage and pH

7.4.1 Introduction

The regression analysis of the CCRD from Chapter 5 showed that the flotation rate of arsenopyrite and pyrite increases with the interaction denoted by the product of frother dosage and pH, as shown in Figure 7-12.

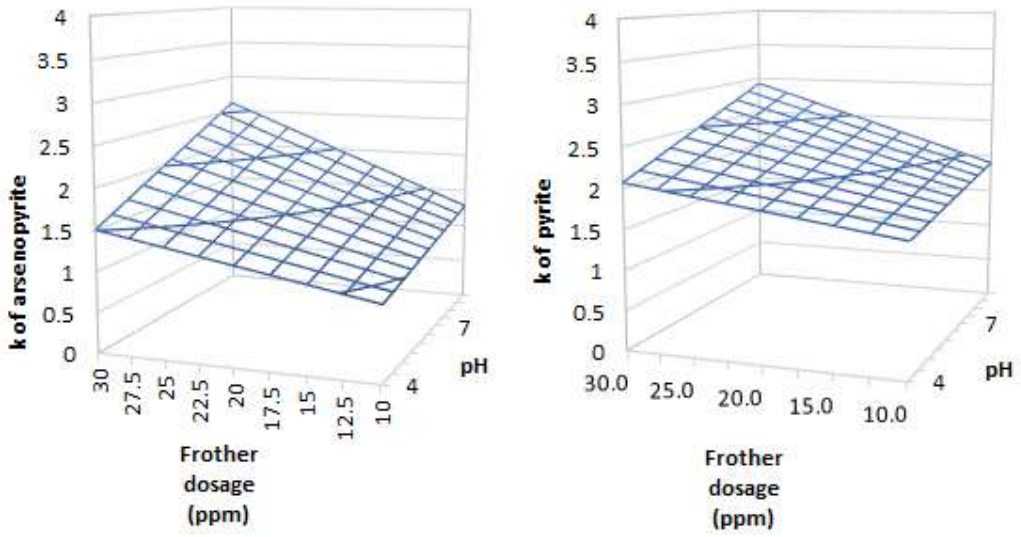

Figure 7-12 – Effect of pH and frother dosage on the flotation rate constant of arsenopyrite and pyrite

The potential causes for the poor flotation kinetics at low pH included the formation of slime coating of muscovite on the surfaces of pyrite and arsenopyrite, and/or chemical

modification of the surface of the pyritic mineral that would decrease the hydrophobicity, consequently, reducing the flotation rates.

The zeta potential analysis indicated that it was most likely to observe the formation of slime coatings of muscovite on the pyritic minerals is at pH 4. However, the measurements of the zeta potential of the mineral mixture at pH 4 indicated that the system is dispersed at this pH. Therefore, it suggests that the low flotation rates observed at pH 4 are not the formation of a slime coating on the pyritic minerals.

The surface analysis via XPS and ToF-SIMS indicated that the level of oxidation of pyrite at pH 10 is higher than at pH 4. Lesser Cu and collector coverage are observed at pH 10 than at pH 4. Therefore, the flotation rates at pH 10 should be slower than at pH 4, contrary to the results observed in the CCRD.

Because the surface analyses via zeta potential, XPS and ToF-SIMS suggested that the causes of the low flotation kinetics of the pyritic minerals at low pH are not due to surface modification mechanisms that would reduce the hydrophobicity of the pyritic minerals, it suggests other factors are causing this response. One possible cause is that the pH is actually affecting froth stability. This is reinforced by the suggestion shown by the regression equation that the interaction term pH x frother is significant because both factors are affecting the froth stability.

This section aims to verify the effect of pH and frother on the froth phase.

7.4.2 Effect of pH on the Froth Height and its Effect on the Flotation Rate

Throughout the execution of the CCRD flotation tests, froth height differences were observed visually. Due to limitations of the flotation cell used, the froth height was not recorded as part of the flotation experiments.

To understand the effect of pH on the froth stability, froth height measurements were conducted at selected pH conditions. Ideally, the froth height measurements should be performed using a factorial design that would include the evaluation of the effect of frother dosage, pH, the proportion of muscovite and muscovite P_{80} and %solids.

However, due to time constraints and limited muscovite samples available, the froth height measurements were performed in the absence of muscovite, at selected pH conditions.

Because no concentrate is collected in the froth height tests, the flotation conditions selected to perform these tests should be the same conditions of flotation batch-test performed previously, so the froth height measured could be compared to the flotation rates of pyrite and arsenopyrite from those tests.

7.4.2.1 Froth Height Measurement

The froth height was measured, in the absence of muscovite, at pH 4, 7 and 10, using the conditions of the flotation tests in the preliminary CCRD stage: 30 ppm of Dowfroth 250, 100 g/t of $CuSO_4$, 165 g/t of PAX (collector dosage as per the centre point of the preliminary CCRD) and 20% of solids.

Although Figure 5-6 and Figure 5-8, in Chapter 5, indicated there are differences between the effects of the pH on the flotation kinetics using 165 g/t and 300 g/t of PAX, the flotation rates obtained directly from the experimental data, of the preliminary CCRD (at 165 g/t of PAX) and CCRD (300 g/t of PAX), are following similar trends with the increase of pH, as suggested in Figure 7-13.

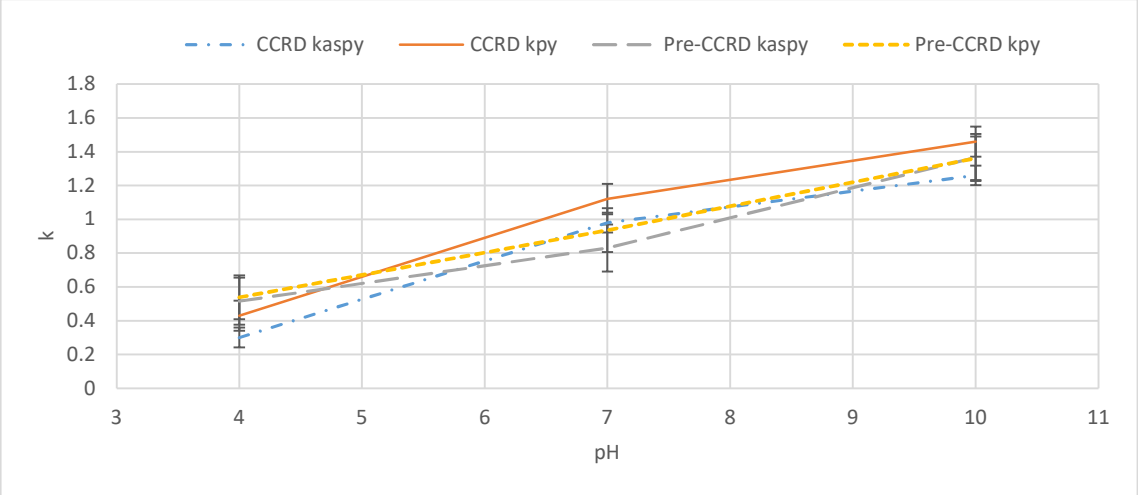

Figure 7-13- Flotation rates of arsenopyrite and pyrite versus pH

The overlap of the trends and confidence intervals suggests that the effect of the collector dosage on the rates was not very significant. Therefore, the selected flotation conditions to evaluate the froth height should be sufficient to detect significant differences in the froth due to the pH.

Two tests with silica only (absence of pyrite and arsenopyrite) were run at pH 4 and pH 10 as a blank test to distinguish the effect of the hydrophobicity of the pyrite and arsenopyrite on the froth stability.

The maximum froth height was measured in a custom-made flotation column with the same cross-section area of the flotation cell used in the flotation tests campaign. The same impeller stator mechanism used in the flotation test campaign was adopted in the column to replicate the conditions of the previous flotation tests.

Figure 7-14 shows the maximum froth height of the tests without sulfides. The maximum froth height at pH 4 is 3 cm and at pH 10 is 15 cm. The height of the froth increases with the pH independently of the presence of sulfides.

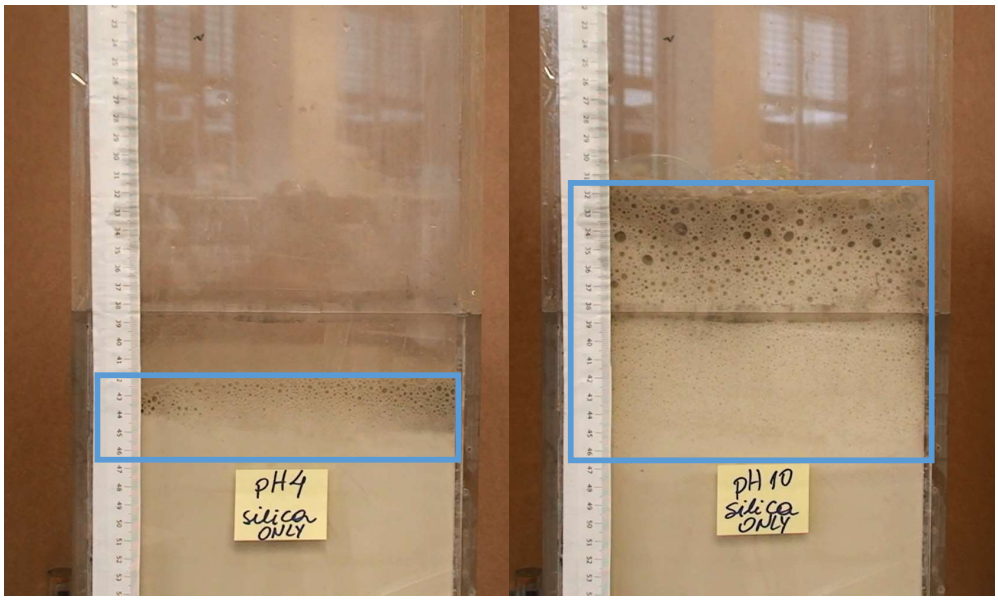

Figure 7-14 –Froth height of silica at pH 4 and pH 10, 30 ppm of Dowfroth 250, 100 g/t of CuSO4, 165 g/t of PAX and 20% solids

Dark solids appeared to contaminate the froth in Figure 7-14. Those dark solids reporting to the froth phase during tests with silica only could be a precipitate of copper xanthate that would form upon mixing of xanthate with copper sulfate, as the cell was carefully cleaned between tests, discarding the possibility of residues from other experiments.

Figure 7-15 shows the maximum froth height of the tests which include arsenopyrite and pyrite, at pH 4, 7 and 10.

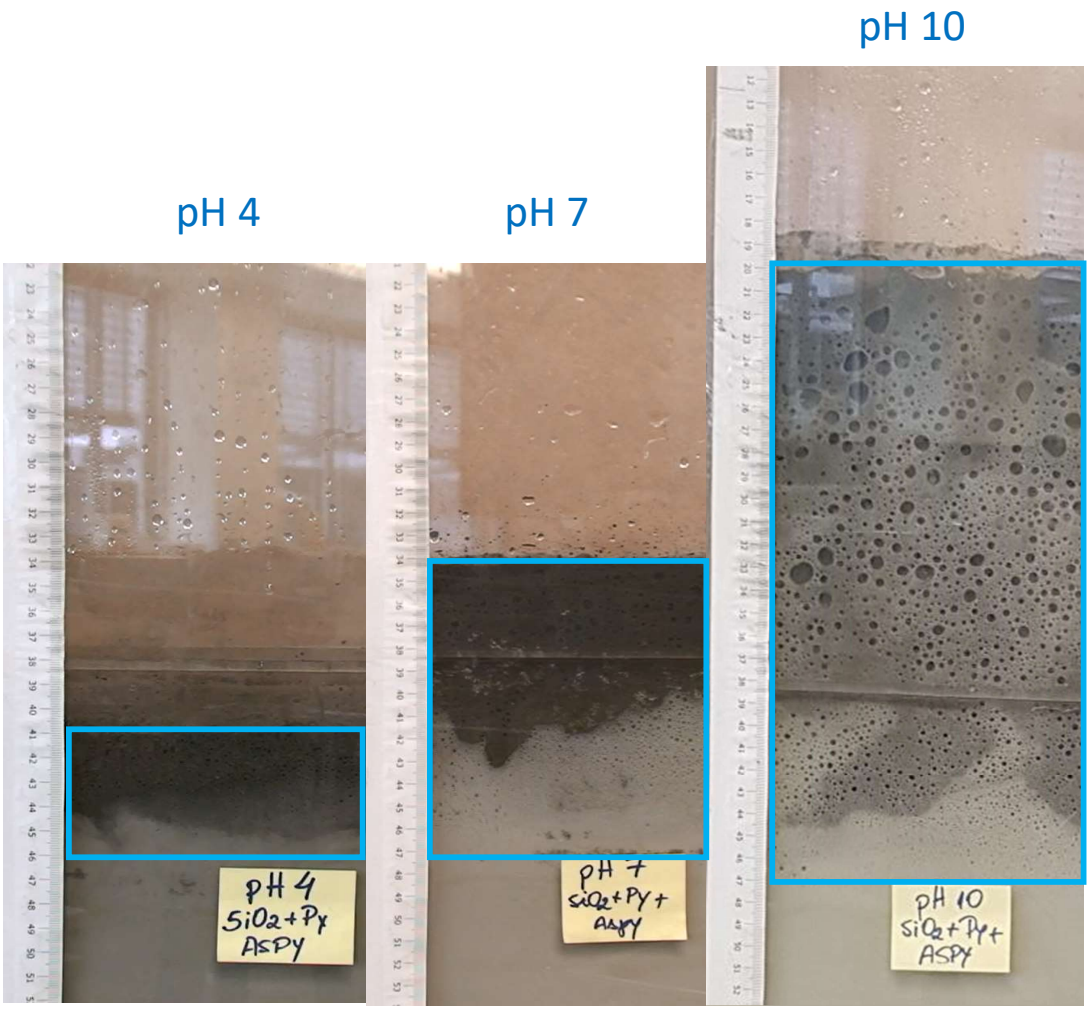

Figure 7-15 - Froth height of the system pyrite, arsenopyrite and silica at pH 4, 7 and 10, 30 ppm of Dowfroth 250, 100 g/t of CuSO4, 165 g/t of PAX and 20% solids

Table 7-12 shows the maximum froth height at pH 4, 7 and 10.

Table 7-12 – Froth height versus pH

pH	Maximum Height (cm)	Eh
4.24	4.7	279
7.14	12	210
10.01	27	77

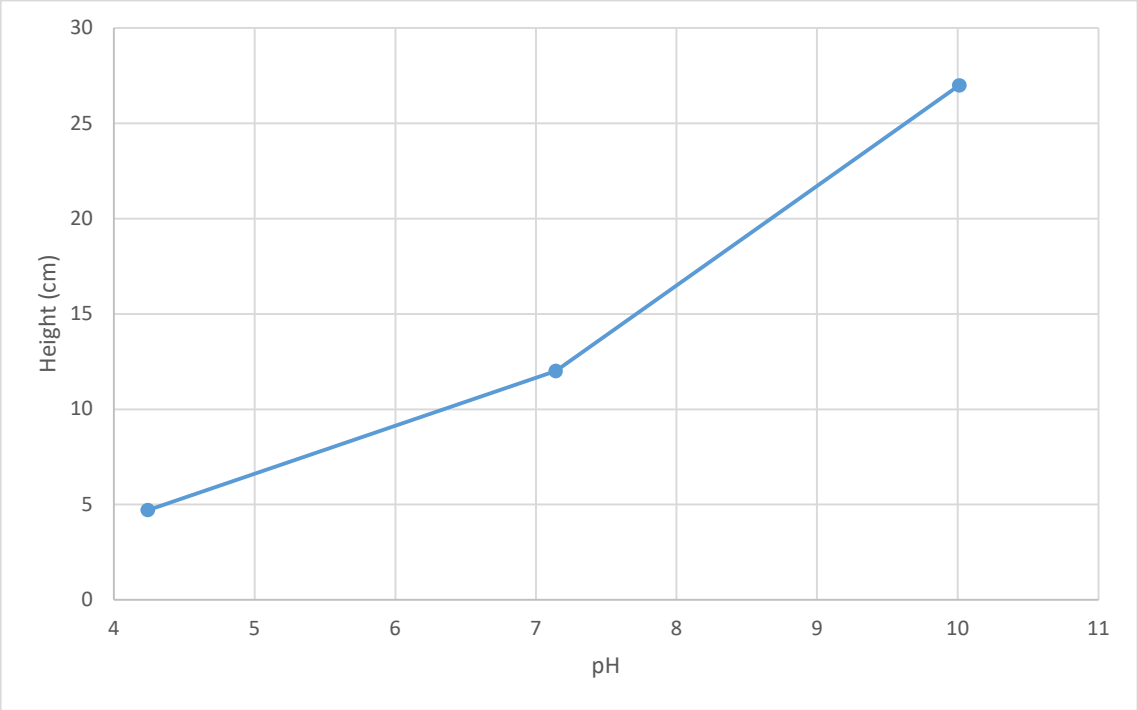

Figure 7-16 - Froth height versus pH

The froth height significantly increased with the pH, as shown by Figure 7-15 and Table 7-12. Figure 7-15 shows the graphic representation of Table 7-12.

Low froth heights were visually observed throughout the completion of flotation tests at tests conducted at low pH, and high froth height at high pH tested, which were confirmed by the measured data, in Figure 7-15.

Prior to the froth height tests presented on Figure 7-14 and Figure 7-15, a sighter test was performed in a standard flotation cell, using silica and frother, in the exclusion of PAX and $CuSO_4$, to identify if the pH and frother would be in interacting to increase the froth depth or volume. Those tests suggested that the froth height or volume increases with the rise in pH, as shown in Figure 7-17.

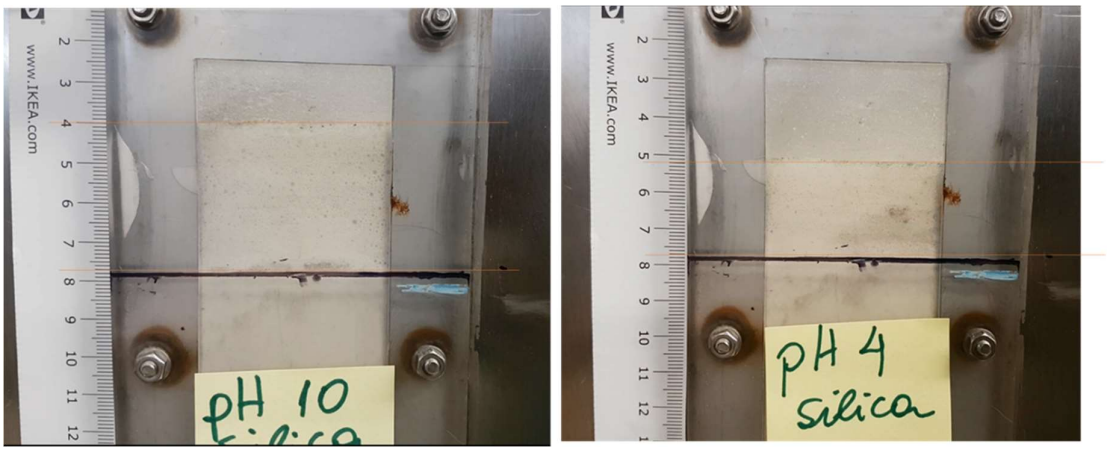

Figure 7-17 - Froth height of silica in the flotation cell used to perform the CCRD test at pH 4 and 10, using 30 ppm of Dowfroth 250 and 20% solids

The froth height measurements for pH values over 7 were not very accurate using a conventional flotation cell because the froth overflowed through the lip. The complete profile of froth depth versus pH measured in the conventional flotation cell using silica and frother in the absence of PAX and $CuSO_4$ is shown in Figure 7-18, which suggests that even in the absence of PAX and $CuSO_4$, the froth height increased with the increase of pH.

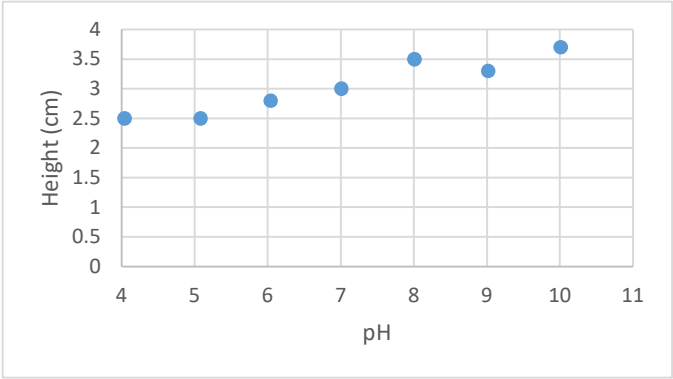

Figure 7-18 - Froth height of silica in the conventional flotation cell used to perform the CCRD test versus pH, using 30 ppm of Dowfroth 250 and 20% solids

The difference of froth depth in Figure 7-15 was not as prominent in Figure 7-18, which could be due to the precipitation of copper xanthate. However, those sighter tests in Figure 7-18 indicated that the effect of pH on the froth height is other than the

difference been related to the chemical instability of xanthate at low pH versus high pH because no xanthates were present.

The mechanism causing the froth height to rise could be the adsorption of frother molecules on the surfaces of silica. However, the tests presented in the scope of this thesis are not able to confirm this mechanism.

The froth height test was repeated in a two-phase system to verify if the pH was changing the surface tension of the water-air interface. The two-phase system test, with water and frother and water and flotation reagents, was performed in an aerated measuring cylinder, using a fixed dosage of frother, 30 ppm. The froth depth obtained in the two-phase is shown in Figure 7-19.

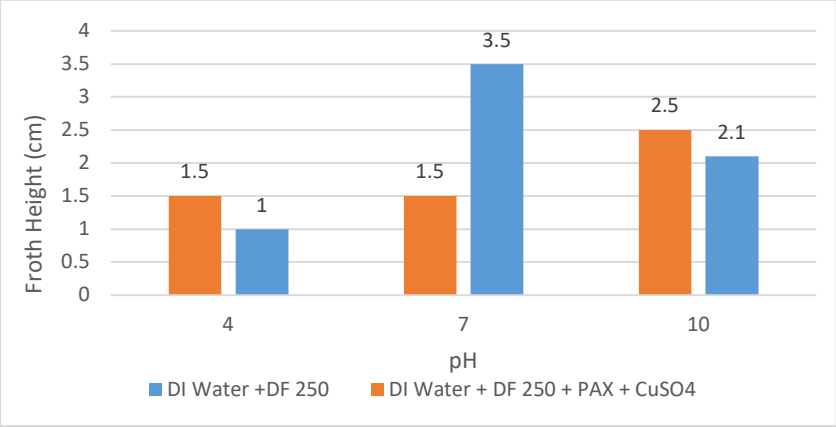

Figure 7-19 – Froth depth measured in the two-phase system using deionised water and flotation reagents

It was observed a visual difference of froth height across the range of pH tested in the two-phase (air-solution) system that could suggest a modification of the surface tension with the pH. Interestingly, no precipitate was observed in the system with PAX and $CuSO_4$, which suggests that the solids observed in Figure 7-15, could be impurities.

These are extremely complex systems, and yet the conclusions from these tests could be enriched with more investigation. The study of the froth phase was outside the scope of the thesis.

7.4.2.2 Comparison of the Flotation Rate and the Froth Height Measurement

Figure 7-20 compares the increase of the froth height with the flotation rate of pyrite and arsenopyrite at pH 4, 7 and 10. The flotation rates shown in Figure 7-20 corresponded to the rates using 165 g/t of PAX, 30ppm of Dowfroth 250, 27% solids, in which no muscovite was added in those tests. It seems that the froth height and the flotation rate versus pH follow the same trend, suggesting that the flotation rate increased with the froth height.

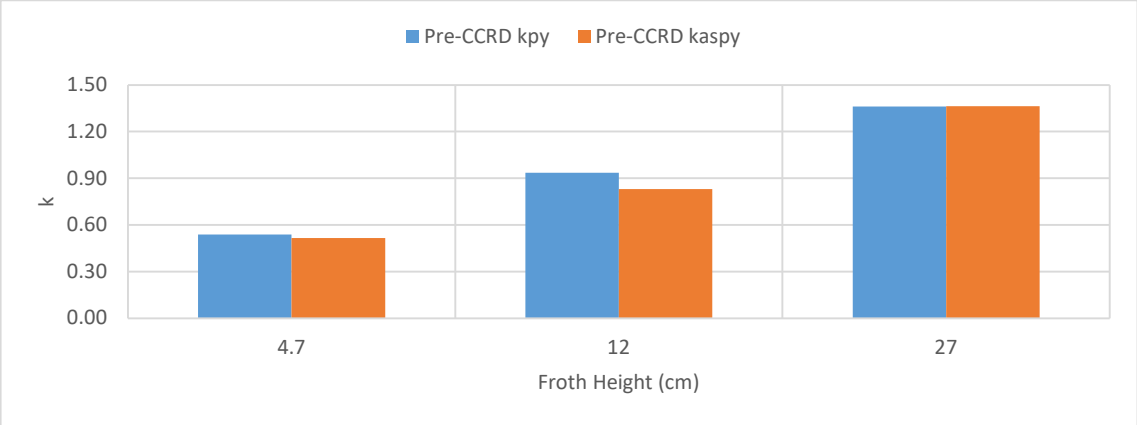

Figure 7-20 – Flotation rate in the of pyrite and arsenopyrite at pH 4, 7 and 10, at 30ppm of Dowfroth 250 and 300 g/t of PAX, versus froth height

In the absence of froth height tests with muscovite, the water recovery at the first concentrate is used as a proxy for the froth height because it gives an indication of the volume of froth recovered at the beginning of the tests. The mass of water pulled at the first concentrate from the CCRD tests performed at 27% solids, 22.5% of muscovite in the gangue, 30 ppm of frother and 300 g/t of PAX is shown in Figure 7-21.

It suggests that the froth height at the tests conducted at the CCRD, using 300 g/t of PAX, 30 ppm of frother, at 27% solids and 22.5% of muscovite in the gangue, increased with the increase of pH because of the increase of froth height is also associated with the increase of water recovery.

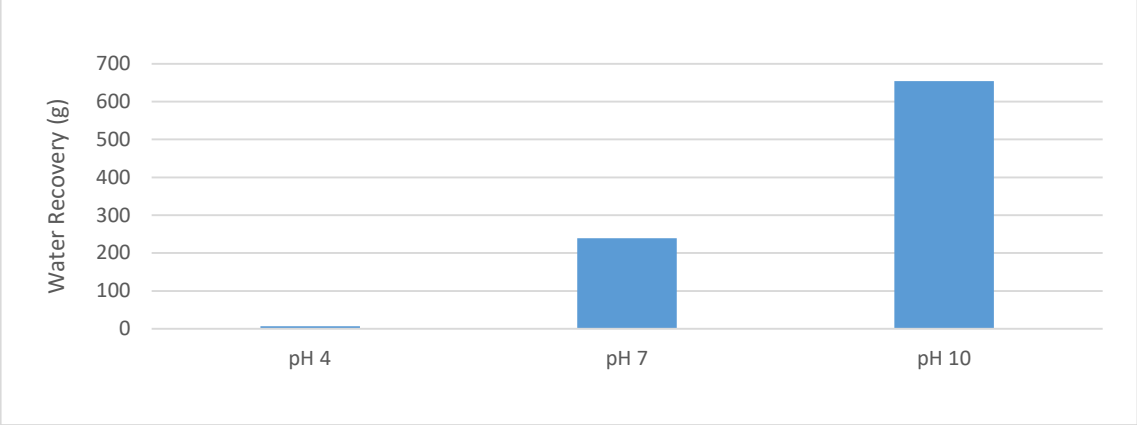

Figure 7-21 – Water recovery in the first concentrate (0.5 minutes) in the CCRD tests, in the presence of 22.5% of muscovite in the gangue composition

7.4.2.3 Conclusions on the Effect of pH

The increase of pH led to an increase of froth stability, thus the increase of froth height. Consequently, an increase in flotation kinetics was observed.

The increase of froth height with pH observed in the experiments developed in this study align with the observation of Sheni et al. (2018), which observed an improvement in froth stability with pH, on the study of the froth stability in a PGM ore, using frother Senfroth 516, which is also a polyglycol frother (Ngoroma, 2015), and NaOH as the pH modifier.

According to Ata et al. (2009), the maximum froth stability is achieved when the froth phase is loaded with moderately hydrophobic particles. The ToF-SIMS analysis showed that at pH 4, pyrite has the highest collector coverage, compared to pH 10. The lowest froth height observed was at pH 4. Froth collapsing was not observed in the experiments. As per Figure 7-15, at pH 4, a visible froth phase with 4.7 cm is observed. The high hydrophobicity of the pyrite and arsenopyrite particles at pH 4 was not sufficient to destroy the froth phase, but it may affect the froth stability due to the low froth height observed.

Moreover, the experiments conducted could not properly differentiate the mechanism by which it affects froth stability between the high hydrophobicity of pyrite and the decrease of the surface tension of the interface air-liquid. The froth height obtained in

the two-phase system suggests that the decrease of the surface tension of the interface air-liquid is likely to be a significant mechanism. However, further studies are required to understand the effect of the hydrophobicity of the pyritic minerals and the increase of pH and frother dosage on the surface tension of the interfaces.

Froth transport and viscosity were not inferred as part of the main experimental program as it was outside the scope of work in the original experimental design. Those factors could potentially be related to flotation performance and should be investigated as future work.

The effect of the presence of muscovite in the froth stability was not studied due to the limited availability of pure mineral samples. However, the water recovery analysis of the first concentrate at the flotation test with 22.5% muscovite in the gangue composition showed that the water recovery increases with the pH, which is an indication that froth height rises with pH, similarly to the tests presented in the absence of muscovite.

7.4.3 The Effect of Frother Dosage on the Flotation Rate

The effect of the frother dosage on the flotation rate of arsenopyrite is pH-dependent, as shown in Figure 7-12. The froth height tests performed suggested that the increase of pH led to an increase of froth stability, thus the increase of froth height. Consequently, an increase in flotation kinetics was observed.

The increase of pyrite and arsenopyrite kinetics with the increase of frother dosage is not due to the concentration of frother reaching the critical bubble coalescence concentration (CCC), as it was set above the CCC in all flotation tests performed. The minimum frother dosage used in the CCRD flotation experiments was 10 ppm, which is above the CCC of Dowfroth 250, that is 8.7 ppm, according to Cho & Laskowski (2002).

According to Gupta et al. (2006), froth stability increases with the pH because of the high surface activity of polyglycol frothers. This statement agrees with the froth height

increase observed with the increase of pH at the experiments performed in the previous section.

Subrahmanyam & Forssberg (1988), cited by Aktas et al. (2008), indicate that the surface tension of the air-liquid is lowered by frothers to produce stable bubbles. Johansson & Pugh (1991) observed an increase of maximum froth height and a decrease of surface tension with the increase of frother dosage, using a polyglycol frother.

The flotation experiments were conducted using Dowfroth 250, which is a polyglycol frother and an increase of the froth height was observed with the pH. It can be speculated that the enhancement of froth stability reduces the probability detachment of pyrite and arsenopyrite particles followed by drainage into the pulp, which could be linked to higher flotation rates.

The two-phase froth height test indicated that the pH affects the surface tension as it changed the froth height. However, surface tension analysis was not conducted as part of this research. Therefore, the mechanism by which pH and frother act on the froth stability could not be confirmed as the reduction of surface tension.

7.4.3.1 Effect of Frother Dosage Conclusions

The regression analysis indicates that the most significant term for the increase of the flotation rates of arsenopyrite and pyrite is the multiplication term pH x frother dosage.

The literature indicated that froth stability increases with the pH because of the high surface activity of polyglycol frothers. In addition, surface tension decreases with the increase of frother dosage when a polyglycol frother, which is related to an increase of maximum froth height. Therefore, it suggests the more stable bubbles are formed.

It can be speculated that positive effect of the term pH x frother dosage on the flotation rates of arsenopyrite and pyrite is due to the combined effect of the frother and pH on the decrease of the surface tension of the liquid interface that produces stable bubbles, reducing the probability of particle drainage and perhaps detachment.

Chapter 8

Conclusions and Future Work

---

8 Conclusions and Future Work

8.1 Introduction

The research undertaken in this thesis aimed to understand how muscovite affects the flotation rate of pyrite and arsenopyrite and to understand the conditions that would minimise the effect of muscovite on the flotation rates of the pyritic minerals. The effects of muscovite on the flotation kinetics of arsenopyrite and pyrite were investigated by performing flotation batch tests using a CCRD design. The results from the CCRD were analysed using regression analysis to identify the key variables affecting the flotation rate. Measurements of viscosity, ToF-SIMS and XPS surface analysis, muscovite leachability and froth stability were conducted to investigate the underlying mechanism of the significant effects observed through the regression analysis.

The conclusions drawn from the results of this research are presented in this chapter. The conclusions are discussed in the context of the hypotheses, which the research set out to test. These hypotheses are:

Hypothesis 1:

The presence of high concentration of muscovite has a detrimental effect on the flotation rate of arsenopyrite and pyrite.

Hypothesis 2:

The presence of muscovite affects arsenopyrite and pyrite floatability by changing pulp viscosity

Hypothesis 3:

The detrimental effect of muscovite in the flotation rate of arsenopyrite and pyrite is due to surface modification of pyrite and arsenopyrite mineral.

8.1.1 The Effect of Muscovite Content in the Gangue on Pyrite and Arsenopyrite Flotation Rates

The results of the 54 flotation experiments performed in the CCRD showed that there was very little difference in the final recovery of arsenopyrite and pyrite achieved in all tests but that there were discernible differences in the flotation rates.

Regression analyses of the factors studied in the CCRD, %muscovite by weight in the gangue, %solids, frother dosage (ppm), P_{80} of muscovite in gangue and pH were performed to assess which of these factors affected the flotation rate of arsenopyrite and pyrite at a level of significance of 95%.

The results of the regression analysis indicated that the factors that significantly affected the kinetics of arsenopyrite and pyrite were the interactions of pH with frother and of %solids with muscovite P_{80}. The positive effect of interactions of pH with frother is the most significant, followed by the deleterious effect of the interaction %solids with muscovite P_{80}. The similarity of the regression models for pyrite and arsenopyrite indicates that the two minerals present analogous flotation kinetics.

The regression analysis of the arsenopyrite flotation rate indicated that the proportion of muscovite in the gangue has no effect on the flotation rate of arsenopyrite. In the case of pyrite, the effect of the proportion of muscovite in the flotation feed on the flotation kinetics of pyrite is not deleterious and has low significance, according to the regression. Therefore, the hypothesis that the high concentration of muscovite has a detrimental effect on the flotation rate of arsenopyrite and pyrite appears not to be supported.

Despite the fact that the proportion of muscovite has no deleterious effect, the increase of the size distribution of muscovite does have a deleterious effect on the flotation rate constant of both arsenopyrite and pyrite. The deleterious effect of the increase in muscovite particle size appears to be amplified by the increase in the percentage of solids.

In conclusion, the although the regression analysis indicated that the proportion of muscovite is not significant to the flotation kinetics, the increase of muscovite particle size has a deleterious effect, which appears to be amplified by the %solids of the pulp. Moreover, the hypothesis that the high concentration of muscovite has a detrimental effect on the flotation rate of arsenopyrite and pyrite is partially supported because the increase in muscovite size distribution has a deleterious effect on the flotation kinetics of the pyritic minerals.

8.1.2 The Effect of Muscovite on Pulp Viscosity

When the viscosity of the flotation feed slurry was included as a factor in the flotation rate regression analysis, the regression analysis results indicated that the pulp viscosity is not a significant factor affecting to the flotation rate of arsenopyrite and pyrite.

However, although viscosity appears not to affect the flotation rate of arsenopyrite and pyrite, the increase of %solids does have a deleterious effect. Since the solids content of a slurry is known to affect viscosity, a regression analysis was run to investigate the most significant factors affecting the pulp viscosity.

The results of this analysis indicated that the proportion of muscovite in the gangue does not significantly affect the pulp viscosity. In addition, the regression analysis of the flotation rate indicated that the proportion of muscovite does not affect the kinetics of arsenopyrite significantly. This suggests that Hypothesis 2 is not supported, because the proportion of muscovite does not affect pulp viscosity significantly, according to the regression analysis.

The percentage of solids, which also has a deleterious effect on the flotation rate, appears to be the most significant factor affecting pulp viscosity. It could suggest that the deleterious effect of the percentage of solids in the flotation rate is due to the increase in viscosity.

However, because the pulp viscosity was not shown to be a significant factor on the regression analysis of the flotation rates, it is suggested that the mechanism by which

the increase of the percentage of solids is deleterious to the flotation rate is not solely the increase of viscosity and further work is required in this area.

8.1.3 The Effect of Muscovite on the Flotation of Pyrite and Arsenopyrite Through Modification of Particle Surfaces

The nature of surface modification investigated in this thesis consisted of hetero-aggregation and surface chemistry modification.

Analyses of zeta potential were conducted to verify the presence of hetero-aggregation between the pyritic minerals and muscovite and the results of the zeta potential measurements of the mixture under the same flotation conditions as the centre point of the CCRD did not indicate the presence of hetero-aggregation at pH 4. The CCRD analysis of the flotation results showed that the flotation rate increases with the decrease of muscovite particle size, which suggested that the flotation rate of arsenopyrite and pyrite is not likely to be affected by hetero-aggregation, as this is an effect caused by fine particles.

The surface analyses from ToF-SIMS and XPS suggested that the increase in particle size of muscovite is related to an increase of the levels of K and Al on the surface of pyrite and a decrease of the level of Cu and collector. This suggests that an increase in the levels of K and Al on the surface leads to lower adsorption of activator and collector with a subsequent decrease of particle hydrophobicity of pyritic minerals.

The origin of Al and K ions in the pulp is the muscovite leaching, which is size-dependent, as there is evidence that muscovite at P_{80} 150 µm releases more K and Al ions to a solution than muscovite at P_{80} 50 µm.

This suggests that an underlying reason for the deleterious effect of the interaction term %solids x muscovite P_{80} could be the increase in K and Al ions on the pyritic minerals surfaces. As the percentage of solids increases, more muscovite is available for leaching in the pulp and less solution is available to dilute those ions; therefore, the concentration of K and Al ions increases significantly, leading to adsorption on the sulfide surfaces and a decrease of flotation kinetics. It can be speculated that this

effect is more significant than the effect of the increase in the proportion of muscovite alone.

Therefore, the hypothesis that the detrimental effect of muscovite in the flotation rate of arsenopyrite and pyrite is due to surface modification of pyrite and arsenopyrite mineral is supported.

8.1.4 Conclusions of the Effect of Frother Dosage and pH

The regression analysis of the flotation rate showed that the most significant factor of the increase of the flotation rate of arsenopyrite and pyrite is the term frother dosage x pH.

The ToF-SIMS analysis showed that at pH 4, pyrite has the highest collector coverage, compared to pH 10 and therefore is likely to be in its most hydrophobic condition. This seems to be contradicted by the flotation rates, which were the lowest observed in the experimental program. The zeta potential analyses indicated that the lowest rates observed were not due to the formation of slime coating on the surfaces of the sulfide minerals studied.

The lowest froth height in the experimental program was observed at pH 4, and it is possible that the high hydrophobicity of the pyrite and arsenopyrite at this pH may be destabilizing the froth. However, because froth height measurements with silica only indicated an increase of the froth height with the pH, it can be speculated that the decrease of the surface tension of the air-liquid interface is likely to be a significant mechanism.

The literature suggests that froth stability increases with the pH are linked to the high surface activity of polyglycol frothers. It appears that surface tension decreases with the increase of frother dosage when a polyglycol frother is used, which is related to an increase of maximum froth height. Therefore, it suggests the more stable bubbles are formed.

It can be speculated that the positive effect of the interaction term pH x frother dosage on the flotation rates of arsenopyrite and pyrite is due to the combined effect of the frother and pH on the decrease of the surface tension of the liquid interface that produces stable bubbles, reducing the probability of particle drainage and perhaps detachment.

8.2 Contributions to Knowledge

The literature suggested that that clay and micas affected the flotation performance by increasing pulp viscosity and hetero-aggregation, which represents physical mechanisms. The studies found in the literature were performed on copper minerals, including chalcopyrite and chalcocite. No studies were found in the literature about the effect of muscovite on pyrite and arsenopyrite flotation performance and kinetics.

This research presents as a contribution to knowledge the investigation of viscosity and hetero-aggregation effect of muscovite on arsenopyrite and pyrite. It indicated that those physical effects are not significant to the flotation kinetics of arsenopyrite and pyrite, contrary to research published in the literature for copper minerals.

Another contribution to the knowledge of this research is the demonstration of the effect of the size distribution of muscovite in the flotation rate of arsenopyrite and pyrite due to a surface chemistry effect, specifically the release into the solution of Al and K ions that affect the hydrophobicity of the pyritic minerals. The observed increase of the flotation kinetics with the decrease of muscovite size distribution appears to be counter-intuitive because the decrease of particle size is expected to mean more liberation of Al and K, contrary to the observation of the leaching tests.

No other study has been reported to investigate the effect of muscovite on the flotation rate of pyrite and arsenopyrite using a CCRD design. The investigation of the factors presented in the regression analyses is novel to the literature.

8.3 Suggestions for Future work

The regression analysis presented in this work showed that the most significant terms for the kinetics of arsenopyrite and pyrite are pH x frother dosage and %solids x muscovite $P_{80.}$ According to the conclusions presented in the previous section, it appears that the deleterious effect of the term %solids x muscovite is due to the modification of the surface chemistry of the pyritic minerals, and the positive effect of the term pH x frother dosage appears to be an effect of froth stability.

The surface analysis presented in Chapter 7 indicated that underlying mechanism of the contribution of the muscovite size distribution presented a suggestion for the mechanism by which the %solids of the pulp is playing a role on the chemical mechanism of the effect of muscovite. However, no supporting evidence was available to support the hypothesis of the effect of %solids of the pulp in the surface chemistry of arsenopyrite and pyrite. Further work is required to clarify the role of the %solids of the pulp.

The results presented by this research using a synthetic ore with muscovite as the problematic gangue (given the inert behaviour of silica) indicated that the deleterious effect of the gangue is by chemical modification of pyrite surface by metal ions, Al and K, originating from the muscovite. Considering that gangue minerals can affect the surface chemistry of pyritic minerals leading to poor flotation kinetics, more work is required to understand the behaviour of other gangue minerals from Barrick's problematic ore, such as calcite and feldspars that could also be modifying the surface chemistry of the pyritic minerals through F, Ca, Mg, Na, Cl and carbonates ions.

The selected froth height tests performed suggested that the increase in pH leads to an increase in froth stability. The increase in frother is known to increase froth stability by reducing surface tension. An investigation of surface tension was not conducted as part of this research. Therefore, further studies are required to understand the effect of the hydrophobicity of the pyritic minerals and the increase of pH and frother dosage on the surface tension of the interfaces.

Froth transport and viscosity were not included as part of the experimental program as it was outside the original scope of work. Those factors could potentially be related to flotation performance and should be investigated as future work.

The effect of the presence of muscovite on froth stability was not studied due to the limited availability of samples. Further work is required to understand the effect of muscovite on froth stability.

Chapter 9

References

9 References

Abramov, A. A. (1964). 'Sericite flotation with anionic and cationic collectors', *Tsvet. Metall*., 7, (6), 22–29.

Adams, M. D. (2005). *Advances in gold processing*. Amsterdam, Netherlands: Elsevier.

Adams, M. D. (2016). Summary of gold plants and processes. In M. D. Adams (Ed.), *Gold Ore Processing: project development and operations* (pp. 961-984). Amsterdam, Netherlands: Elsevier.

Aktas, Z., Cilliers, J. J., & Banford, A. W. (2008). Dynamic froth stability: particle size, airflow rate. *International Journal of Mineral Processing*, 87, 65-71.

Alexander, D. J., & Collins, D. A. (2008). A methodology for measuring the floatability of ores - the floatability index test. *Metallurgical Plant Design and Operating Strategies* (pp. 261-272). Perth: AusIMM.

Alexander, D. J., Runge, K. C., Franzidis, J.-P., & Manlapig, E. V. (2000). The application of multi-component floatability models to full-scale flotation circuits. *Seventh Mill Operators' Conference* (pp. 167-177). Kalgoorlie: AusIMM.

Allaby, M. (Ed.). (2015). A Dictionary of Geology and Earth Sciences (4th ed.). Oxford University Press.

ALS (2019). Retrieved from: https://www.alsglobal.com/

AMEC. (2007a). *Design Criteria*. Provided by Barrick Gold Corporation.

AMEC. (2007b). *Feasibility Study Report, Section 5*. Provided by Barrick Gold Corporation.

AMEC. (2011). *White Mountain Gold Project, NI 43 101 Technical Report on Second Updated Feasibility Study*. Retrieved from https://www.sedar.com/.

Amelunxen, P. & Runge, K. (2013). Innovations in froth flotation modelling and testing. *Innovations in Minerals Processing Symposium*. (pp. 24-27). Denver Colorado USA: SME Annual Meeting.

American Geological Institute. (1997). *Dictionary of Mining, Mineral, and Related Terms.* Alexandria, Virginia, USA: American Geological Institute and Society for Mining, Metallurgy and Exploration, Inc.

AMTEL. (2007). *Process Mineralogy of White Mountain Ores: Deleterious elements in PP testwork products*. Provided by Barrick Gold Corporation.

Angove, J. (2005). Metallurgical testwork: gold processing options, physical ore properties and cyanide management. In M. Adams, & B. Wills (Eds.), *Advances in gold ore processing.* (pp. 97-107). Perth, WA, Australia: Elsevier. doi:10.106/S167-4528(05)15004-2.

Ashley, K. J. (2002). Sampling a mineral deposit for feasibility studies. In A. L. Mular, D. N. Halbe, D. J. Barratt (Eds.), *Mineral processing plant, design. Practice and control proceedings* (Vol. 1, pp. 25-36). Littleton, Colorado, USA: SME.

Ata S., Ahmed N. & Jameson G.J. (2003). A study of bubble coalescence in flotation froths. *International Journal of Mineral Processing*, 72 (1), 255-266.

Barrick. (2014). Projects. Retrieved from Barrick: http://www.barrick.com/operations/projects/default.aspx

Basnayaka, L. Subasinghe, N. & Albijanic, B. (2017). Influence of clays on the slurry rheology and flotation of a pyritic gold ore. *Applied Clay Science*, 136, 230-238.

Beloglazov, K.F. (1939) Tsvet. Metally No. 9, 70.

Bergaya, F., & Lagaly, G. (2013). General Introduction: Clays, Clay Minerals, and Clay Science. In *Handbook of Clay Science Developments in Clay Science* (pp. 1-19). Oxford, UK: Elsevier Ltd.

Bikerman, J. Foams. Springer-Verlag, Berlin (1973).

Browning, J. S. (1973) Mica beneficiation', Bulletin no. 662, US Bureau of Mines, Washington, DC, USA.

S. Brunauer & P.H. Emmett, E. Teller (1938). Absorption of gases in multimolecular layers J. *American Chemistry Society.,* 60 (2), 309-319.

Brigattia, M., Galán, E., & Theng, B. (2013). Structure and Mineralogy of Clay Minerals. *Handbook of Clay Science Developments in Clay Science*. (pp. 21-81). Oxford, UK Elsevier Ltd.

Brindley, G. W. (1951). X-Ray Identification and Crystal Structures of Clay Minerals. *Acta Crystallographica*, 4(3), 287.

Brito e Abreu, S. (2010). Correlation of ToF-SIMS surface analysis with particle hydrophobicity and flotation (Doctoral dissertation, University of South Australia, Adelaide, Brisbane).

Brito e Abreu, S., Brien, C., & Skinner, W. (2010). ToF-SIMS as a new method to determine the contact angle of mineral surfaces. *Langmuir Article, the ACS journal of surfaces and colloids,* 26 (11), 8122-8130.

Bulled, D., & McInnes, C. (2005). Flotation Plant Design and Production Planning Through Geometallurgical Modelling. *Centenary of Flotation Symposium,* (pp. 809-814). Brisbane: AusIMM.

Bulut, G., & Yenial, Ü. (2016). Effects of major ions in recycled water on sulfide minerals flotation. *Minerals & Metallurgical Processing*, *33*(3), 137–143.

Butcher, A. (2010). A Practical Guide to Some Aspects of mineralogy that Affect Flotation. *Flotation Plant Optimisation, Spectrum Series 16.* (pp. 83-93). Carlton: AusIMM.

Chandra, A. P., & Gerson, A. R. (2009). A review of the fundamental studies of the copper activation mechanisms for selective flotation of the sulfide minerals, sphalerite and pyrite. *Advances in Colloid and Interface Science,* 145 (1), 97-110.

Cheng, T. W., & Holtham, P. (1995). The particle detachment process in flotation. *Minerals Engineering*, 8 (8), 883-891.

Chesworth, W. (2008). *Encyclopedia of Soil Science*. Berlin: Springer.

Chhabra, R. P. (2010). Non-Newtonian Fluids: An Introduction. Retrieved from: http://www.physics.iitm.ac.in/~compflu/Lect-notes/chhabra.pdf.

Cho, Y. S., & Laskowski, J. S. (2002). Effect of flotation frothers on bubble size and foam stability. *International Journal of Mineral Processing*, 64 (2), 69-80.

Chryssoulis, S. L., & McMullen, J. (2005). Mineralogical investigation of gold ores. *Advances in Gold Ore Processing.* (pp. 21-72). San Diego: Elsevier.

Cline, J. S., Hofstra, J. L., Muntean, J. L., Tosdal, R. M., & Hickey, K. A. (2005). Carlin-Type Gold Deposits in Nevada: Critical Geologic Characteristics and Viable Models. Retrieved from: https://pyrite.utah.edu/fieldtrips/SEGFnevada2007/Readings/General_CTD/Cline2005.pdf.

Colloidal Dynamics (2019)a. How do the Zetaprobe and Acustosizer II measure zeta potential and particle size?. Retrieved from http://www.colloidal-dynamics.com/docs/CD_measurement_techniques.pdf.

Colloidal Dynamics (2019)b. Zetaprobe. Retrieved from http://www.colloidal-dynamics.com/docs/ZetaProbe_Data_Sheet.pdf.

Connelly, D. (2011). High clay ores: a mineral processing nightmare part 2. Retrieved from: https://www.linkedin.com/pulse/cdms-designs-wet-sticky-clay-ores-damian-connelly/.

Christenson, H. K., & Thomson, N. H. (2016). The nature of the air-cleaved mica surface. *Surface Science Reports*, 71(2), 367-390.

Crozier, R. D. (1992). *Flotation: theory, reagents and ore testing*. Oxford: Pergamon.

Cruz, N., Peng, Y., Farrokhpay, S., & Bradshaw, D. (2013). Interactions of clay minerals in copper–gold flotation: Part 1 – Rheological properties of clay mineral suspensions in the presence of flotation reagents. *Minerals Engineering*, *50-51*(C), 30–37.

de Poel, W., Pintea, S., Drnec, J., Carla, F., Felici, R., Mulder, P. & Vlieg, E. (2013). Muscovite mica: flatter than a pancake. *Surface Science*, 619, 19-24.

de Poel, W., Vaessen, S. L., Drnec, J., Engwerda, A. J., Townsend, E. R., Pintea, S. & Vlieg, E. (2017). Metal ion-exchange on the muscovite mica surface. *Surface Science*, 665, 56-61.

Derjaguin, B. V., & Dukhi, S. S. (1961). Theory of Flotation of Small and Medium Size Particles. *Transactions of the Institution of Mining and Metallurgy*, 43 (1-4), 221-246.

Derjaguin, B.V. & Landau, L. (1941), Theory of stability of strongly charged lyophobic sols and the adhesion of strongly charged particles in solution of electrolytes, *Acta Physiochem* 14, 633-662.

Dippenaar, A. (1982). The Destabilization of Froth by solids. I. The Mechanism of Film Rupture. *International Journal of Mineral Processing*, 9 (1), 1-14.

Discoveries, G. (2012). Geo Discoveries. Retrieved from Geo Discoveries: http://www.geodiscoveries.com.au/.

Duan, J., Fornasiero, D., & Ralston, J. (2003). Calculation of the flotation rate constant of chalcopyrite particles in an ore. *International Journal of Mineral Processing*, 72 (1), 227-237.

Duarte, A. C., & Grano, S. R. (2007). Mechanism for the recovery of silicate gangue minerals in the flotation of ultrafine sphalerite. *Minerals Engineering*, 20(8), 766-775.

Dunstan, G. (2014). Overview - Ore Reserve Estimation. In Mineral Resource and Ore Reserve Estimation. *The AusIMM Guide to Good Practice, Monograph 30*. Carlton, Victoria, Australia: AusIMM.

Evans, C. (2010). Development of a Methodology to Estimate Flotation Separability from Ore. (Doctoral dissertation, University of Queensland, Brisbane, Australia).

Evans, C. L., & Morrison, R. D. (2016). Mineral Liberation. *Process Mineralogy* (pp. 219-233). Indooroopilly: Julius Kruttschnitt Mineral Research Centre.

Fairbanks, E. E. (1981). Gangue minerals. *Encyclopedia of Earth Science. Boston*, MA: Springer.

Farrokhpay, S. (2011). The Significance of Froth Stability in Mineral Flotation — A Review. *Advances in Colloid and Interface Science*, 166 (1) 1-7.

Farrokhpay, S., & Bradshaw, D. (2012). Effect of Clay Minerals on the Froth Stability on Mineral Flotation: A Review. *Proceedings of the XXVI IMPC*, (pp. 04601-04611).

Farrokhpay, Saeed, & Ndlovu, Bulelwa. (2013). Effect of phyllosilicate minerals on the rheology, colloidal and flotation behaviour of chalcopyrite mineral. *Chemeca 2013: Challenging Tomorrow,* 733-739.

Farrokhpay, S., Bradshaw, D., & Dunne, R. (2013). Rheological investigation of the flotation performance of a high clay containing gold ore from Carlin Trend. *World Gold Conference*. (pp.333-340).

Farrokhpay, S., Ndlovu, B., & Bradshaw, D. (2014). Characterising the deleterious effect of phyllosilicate minerals on the copper flotation via froth stability analysis. *Proceedings of the XXVII IMPC.* (pp 46-53).

Farrokhpay, S & Zanin, M. (2012) An investigation into the effect of water quality on froth stability. *Advanced Powder Technology,* 23(4), 493-497.

Finch, J. A., & Dobby, G. S. (1990). *Column Flotation*. New York, USA: Pergamon Press.

Forbes. E. & Chryss, A. (2017). Fundamentals of Clays Surface and Colloid Science, and Rheology. *Clays in the minerals processing value chain*. (pp. 81-110). CSIRO: Cambridge University Press.

Forbes, E., Davey, K. J., & Smith, L. (2014). Decoupling rheology and slime coatings effect on the natural flotability of chalcopyrite in a clay-rich flotation pulp. *Minerals Engineering*, 56, 136-144.

Franchi, M., Ferris, J. P., & Gallori, E. (2003). Cations as mediators of the adsorption of nucleic acids on clay surfaces in prebiotic environments. *Origins of Life and Evolution of the Biosphere*, 33 (1), 1-16.

Fraser, K.S., Walton, R.H., & Wells, J.A.(1991). Processing of refractory gold ores. *Minerals Engineering, 4 (7),* 1029-1041.

Fuerstenau, M. C., Jamerson, G., & Yoon, R. (2007). *Froth Flotation, A Century of Innovation*. Littleton: SME.

Fuerstenau, M. C., Kuhn, M. C. & Elgillani, D. A. (1968). The role of dixanthogen in xanthate flotation of pyrite. *Transactions Society of Mining Engineers of AIME*, 241, 148-156.

Fuerstenau, M. C., Miller, J. D., & Kuhn, M. C. (1985). *Chemistry of flotation*. New York: Society of Mining Engineers.

Galvin, K., & Iveson, S. (2014). Gravity separation and flotation of fine particles using the Reflux Classifier platform. *XXVII International Mineral Processing Congress*. (pp. 1-11).

Gaudin, A.M, Groh, J.O.& Henderson, H.B. (1931) Effect of particle size on flotation. *AIME, Tech. Publ.*, 414 (1931), 3-23.

Gaudin, A.M.(1957). *Flotation*. New York, USA: McGrawHill Book Co.

GEO Discoveries (2019). Retrieved from https://www.geodiscoveries.com.au/

Gorain, B. (1998). The effect of bubble size surface area flux on the kinetics of flotation and its relevance to scale-up (Doctoral dissertation, University of Queensland, Brisbane, Australia)

Grafe, M., McFarlane, A., & Klauber, C. (2017). Clays and the minerals processing value chain (MPVC). *Clays in the minerals processing value chain*. (pp. 1-80). CSIRO: Cambridge University Press.

Greenwood, R., & Kendall, K. (1999). Electroacoustic studies of moderately concentrated colloidal suspensions. *Journal of the European Ceramic Society*, 90, 479-488.

Grupta, A. K., Banerjee, P.K., Mishral, A., Sathish & Pradip, P. (2006). Frother characterization with two-phase foam system. *Proceedings of the International Seminar on Mineral Processing Technology.* (pp. 279 – 290).

Hadler, K., Greyling, M., Plint, N., & Cilliers, J. J. (2012). The effect of froth depth on air recovery and flotation performance. *Minerals Engineering*, 36-38, 248-253.

Harris, P. J. (1982). Principles of flotation: mineral-water interfaces and the electrical double layer. Johannesburg: South African Institute of Mining and Metallurgy.

Harrison, K. (2018, December 17). Potassium Amyl Xanthate. Retrieved from 3DChem.com - Chemistry, Structures & 3D Molecules: http://www.3dchem.com/pax.asp

Harvey, P.A., Nguyen, A.V., Jameson, G.L. & Evans, G.M. (2005). Influence of sodium dodecyl sulphate and Dowfroth frothers on froth stability. *Minerals Engineering*, 18 (3), 18-311.

He, M., Addai-Mensah, A., & Beattie, D. (2009). Sericite-chalcocite mineral particle interactions and hetero-aggregation (sliming) mechanism in aquelous media. *Chemical Engineering Science*, 64 (13), 3083-3093.

He, S., Fornasiero, D., & Skinner, W. (2005). Correlation between copper-activated pyrite flotation and surface species: effect of pulp oxidation potential. *Minerals Engineering*, 18 (12), 1208-1213.

Hosseini, P. (2010). Exploring energy usage in comminution and media wear using steel wheel abrasion test. Retrieved from:

http://digitool.library.mcgill.ca/webclient/StreamGate?folder_id=0&dvs=1548666072599~472.

Hudson Institute of Mineralogy. (2016, February 8th). Mindat.org. Retrieved from Mindat.org: www.mindat.org/min-2815.html.

Hudson Institute of Mineralogy. (2018). Pyrite. Retrieved from Mindat: https://www.mindat.org/min-3314.html

Igusti-Ngurah, A. (1989). Effect of bubble size distribution on the flotation rate of complex ore in froth flotation column (Master dissertation, University of Wooloongong, Wooloongong, Australia).

Jamerson, G. J., & Allum, P. (1984). A survey of bubble size in industrial flotation cells. Unpublished report.

Janetski, N. D., Woodburn, S. I., & Woods, R. (1977). An electrochemical investigation of pyrite flotation and depression. *International Journal of Mineral Processing*, 4 (3), 227-239.

Jiang, Z.W. & Holtham, P.N. (1986). Theoretical model of collision between particles and bubbles in flotation. Trans. Inst. Min. Metall. (London), 9, C187-C194

JKTech. (2007). Flotation Circuit Analysis of the White Mountain Pilot Plant Campaign, Final Report. Brisbane. Confidential report.

Johansson, G. & Pugh, R.J. (1991). The influence of particle size and hydrophobicity on the stability of mineralized froths. *International Journal of Mineral Processing*, 34, 1-21.

Johnson, N. W. (1972). The Flotation Behaviour of Some Chalcopyrite Ores (Doctoral dissertation, The University of Queensland, Brisbane, Australia).

Johnson, S.B., Franks, G.V., Scales, P.J., Boger, D.V. & Healy, T.W. (2000). Surface chemistry–rheology relationships in concentrated mineral suspensions, *International Journal of Mineral Processing*, 58 (1), 267-304.

Johnson, N. W. (2005). A Review of the entrainment mechanism and its modelling in industrial flotation process. *Centenary of Flotation Symposium* (pp. 487-496).

Johnson, N. W., McKee, D. J., & Lynch, A. J. (1974, September). Flotation rates of nonsulfide minerals in chalcopyrite flotation process. *Transactions*, pp. 204-209.

Kawatra, S. K.& Eisele, T.C. (2001). Froth Flotation - Fundamental Principles. Retrieved from:http://www.chem.mtu.edu/chem_eng/faculty/kawatra/Flotation_Fundamentals.pdf.

King R.P. (2012). Flotation. In *Modeling and Simulation of Mineral Processing Systems* (2nd Edition, pp. 1–2). Society for Mining, Metallurgy, and Exploration (SME). Retrieved from https://app.knovel.com/hotlink/pdf/rcid:kpMSMPSE02/id:kt00A92ZE8/modeling-simulation-mineral/flotation?kpromoter=Summon.

Klimpel, R.& Isherwood, S., (1991). Some industrial implications of changing frother chemical structure. *International. Journal of Mineral Process*. 33 (1) 369-381.

Klimpel, R. R. (1984). Froth Flotation: The Kinetic Approach. International Conference on Mineral Science and Technology. *Proceedings of Mintek 50* (pp. 1-26).

Laliberté, M. (2007). Model for calculating the viscosity of aqueous solutions. *Journal of Chemical Engineering Data*, 52 (2), 321-335.

Lane, G., Whittering, R., & Jeffery, D. (2012). Benchmarking versus test work - how should you manage process risk. *Project evaluation conference* (pp. 49-52). Melbourne: AusIMM.

Laskowski, J.S. & Pugh, J.S.(1992) - Dispersion stability and dispersing agents. *Colloid Chemistry in mineral processing*. (pp. 151-161). Amsterdam, Netherlands: Elsevier Science Publishers B.V..

Laskowski, J. S. (2004). Testing Flotation Frothers. *Physicochemical Problems of Mineral Processing*, 38, 13-22.

Lauder, D. W., Mavotoi, M., & Glatthaar, J. W. (2003). Fluorine removal from Ok Tedi copper/gold concentrates. *8th Mill Operator's Conference* (pp. 203-209). Townsville: AusIMM.

Leiro, J. A., Torhola, M., & Laajalehto, K. (2017). The AFM Method in Studies of Muscovite Mica and Galena Surfaces. *Journal of Physics and Chemistry of Solids*, 100, 40-44.

Lewis, P. J. (2014). Metallurgical Input to the Determination of Ore Reserves*. Mineral Resources and Ore Reserve Estimation, *The AusMM Guide of Good Practice, Monograph 30* (pp. 433-441). Carlton: AusIMM.

Lewis, R. (1971). Mineral Research Laboratory progress report.

Li, H., Feng, Q., Yang, S., Ou, L., & Lu, Y. (2014). The entrainment behaviour of sericite in microcrystalline graphite flotation. *International Journal of Mineral Processing*, 127, 1-9.

Lunt, D., & Weeks, T. (2005). Process flowsheet selection. *Advances in gold ore processing* (pp. 73-95). Perth, WA, Australia: Elsevier. doi:10.1016/S0167-4528(05)15003-0

Luxbacher, T. (2014). *The Zeta Potential for Solids Surface Analysis*. Austria: Anton Paar GmbH.

Malhotra, D., Taylor, P., Spiller, E., & LeVier, M. (2009). *Recent Advances in Mineral Processing Plant Design*. Englewood: SME.

Manutchehr-Danai, M. (2008). *Dictionary of Gems and Gemology*. Springer.

Marsden, J. O., & Iain House, C. (2006). *The Chemistry of Gold Extraction*. Littleton, Colorado, USA: SME.

Maslova, M., Gerasimova, V., & Forsling, L. (2004). Surface Properties of Cleaved Mica. *Colloid Journal, 66*(3), 322-328.

McCarthy, P. (2014). Why Feasibility Studies Fail. *Risk Management Seminar.* Perth: AusIMM.

Meffre, S., Large, R. R., Steadman, J. A., Gregory, D. D., Stepanov, A. S., Kamenetsky, V. S., Scott, R. J. (2016). Multi-stage enrichment processes for large gold-bearing ore deposits. *Ore Geology Reviews*, 76, 268-279.

Michaud, D. (2015, September 24). Carlin-Type Gold Deposit. Retrieved from: https://www.911metallurgist.com/blog/carlin-type-gold-deposit.

Minitab (2019). Retrieved from: http://www.minitab.com/en-us/.

Minitab 18 Support (2018). Retrieved from: http://support.minitab.com/en-us/minitab/18/

Monte, M. B. M., Dutra, A. J. B., Albuquerque, C. R. F., Tondo, L. A. & Lins, F. F. (2002). The influence of the oxidation state of pyrite and arsenopyrite on the flotation of an auriferous sulphide ore. *Minerals Engineering*, 15 (12), 1113-1120.

Moslemi, H., Gharabaghi, M. (2017). A review on electrochemical behavior of pyrite in the froth flotation process. *Journal of Industrial and Engineering Chemistry,* 47, 1-18.

Nagaraj, D. (2005). Reagent selection and optimization—the case for a holistic approach. *Minerals Engineering,* 18(2), 151-158.

Napier-Munn, T. J. (2012, November). The CCRD Experimental Design. JKTech e-Newsletter.

Napier-Munn, T. J. (2014). *Statistical Methods for Minerals Engineers*. Indooroopilly, QLD: Julius Kruttschnitt Mineral Research Centre.

Napier-Munn, T. J., Morrell, S., Morrison, R. D., Kojovic, T (1996). *Mineral Comminution Circuits Their Operation and Optimisation*. Indooroopilly, QLD: Julius Kruttschnitt Mineral Research Centre.

Ndlovu, B. (2013). The effect of phyllosilicate mineralogy and surface charge on the rheology of mineral slurries (doctoral dissertation, University of Cape Town, Cape Town, South Africa).

Ndlovu, B., Becker, M., Forbes, E., Deglon, D., & Franzidis, J.-P. (2011). The influence of phyllosilicate mineralogy on the rheology of mineral slurries. *Minerals Engineering*, 24 (12) 1314-1322.

Ndlovu, B., Farrokhpay, S., & Bradshaw, D. (2013). The effect of phyllosilicate minerals on mineral processing industry. *International Journal of Mineral Processing*, 125, 149-156.

Ndlovu, B., Forbes, E., Farrokhpay, S., Becker, M., Bradshaw, D., & Deglon, D. (2014). A preliminary rheological classification of phyllosilicate group minerals. *Minerals Engineering*, 55, 190-200.

Nesset, J.E.& Finch, J.A., (2013). Correcting bubble size measurement for frother concentration in the McGill Bubble Size Analyzer. *Proceedings of the Materials Science & Technology (MS&T) Water and Energy in Mineral Processing*. (pp. 1824-1840).

Ngoroma, F. (2015). Retrieved from: https://open.uct.ac.za/bitstream/handle/11427/13752/thesis_ebe_2015_ngoroma_f.pdf?sequence=1.

Nguyen, A. V., & Ejtemaei, M. (2017). Kinetic studies of amyl xanthate adsorption on bubble attachment to Cu-activated sphalerite and pyrite surfaces. *Minerals Engineering*, 112, 36-42.

Nosrati, A., Addai-Mensah, J., & Skinner, W. (2009). pH-mediated interfacial chemistry and particle interactions in aqueous muscovite dispersions. *Chemical Engineering Journal*, 152 (2), 406-414.

Nosrati, A., Addai-Mensah, J., & William, S. (2012). Muscovite clay mineral particle interactions in aqueous media. *Powder Technology*, 219, 228-238.

Owusu, C., Brito e Abreu, S., Skinner, W., Addai-Mensah, J., & Zanin, M. (2014). The influence of pyrite content on the flotation of chalcopyrite/pyrite mixtures. *Minerals Engineering*, 55, 87-95.

Peng, Y., Grano, S., Fornasiero, D.& Ralston, J. (2017). Control of grinding conditions in the flotation of galena and its separation from pyrite. *International Journal of Mineral Processing*, 70 (1), 67-82.

Perkins, T., Siliezar, J., Yahyaei, M., & Vos, F. (2015). Glencore Ernest Henry Mining. Brisbane: AMIRA P9P.

Rand, B. & Melton, I.E. (1977). Particle interactions in aqueous kaolinite suspensions: I. Effect of pH and electrolyte upon the mode of particle interaction in homoionic sodium kaolinite suspensions, *Journal of Colloid and Interface Science*, 60 (2), 308-320.

Ralston, J., Fornasiero, D., & Mishchuk, N. (2001). The hydrophobic force in flotation-a critique. *Colloids and Surfaces A: Physicochemical and Engineering Aspects*, *192*(1-3), 39–51. https://doi.org/10.1016/S0927-7757(01)00715-4.

Ralston, J., Fornasiero, D., Grano, S., Duan, J., & Akroyd, T. (2007). Reducing uncertainty in mineral flotation—flotation rate constant prediction for particles in an operating plant ore. *International Journal of Mineral Processing*, 84 (1), 89-98.

Rao, K. H., Cases, J. M., Barres, O., Forssberg, K. S. (1995). Flotation, electrokinetic and FT-IR studies of mixed anionic/cationic collectors in muscovite-biotite system, *Mineral processing: recent advances and future trends*, (ed., Mehrotra S P, Shekhar R), 29–44; New Delhi, Allied Publishers.

Rickard, T. A., & Ralston, Oliver C. (1917). *Flotation*. Mining and Scientific Press. Retrieved from http://hdl.handle.net/2027/nyp.33433090915061.

Sandoval-Zambrano, G. E. (2013). Development of a novel strategy to estimate flotation recovery as a function of particle size and mineral liberation (Doctoral dissertation, University of Queensland, Brisbane, Australia).

Sandoval-Zambrano, G. & Montes-Atenas, G. (2012). Errors in the estimation of size-by-liberation flotation rate constants. *Minerals Engineering,* 27-28, 1-10.

Savassi, N. O., Alexander, D. J., Franzidis, J. P., & Manlapig, E. V. (1998). An empirical model for entrainment in industrial flotation plants. *Minerals Engineering*, 11 (3), 243-256.

Savassi, O. N. (1998). Direct Estimation of the Degree of Entrainment and the Froth Recovery if Attached Particles in Industrial Cells (Doctoral dissertation, University of Queensland, Brisbane, Australia).

Savassi, O. N., Alexander, D. J., Johnson, N. W., Manlapig, E. V., & Franzidis, J. P. (1997). Measurement of Froth Recovery of Attached Particles in Industrial Cells. Proceedings of the Sixth Mill Operators Conference. (pp. 149-155). Melbourne: AusIMM.

Shabalala, N. P., Harris, M., Leal Filho, L. S., & Deglon, D. A. (2011). Effect of Slurry Rheology on Gas Dispersion in a Pilot-Scale Mechanical Flotation Cell. *Minerals Engineering*, 24 (13), 1448-1453.

Sheni, N., Corin, K., & Wiese, J. (2018). Considering the effect of pulp chemistry during flotation on froth stability. *Minerals Engineering*, 116, 15-23.

Shi, F. N. & Napier-Munn, T. J. (1995). A model for slurry rheology. *International Journal of Mineral Processing,* 47 (1-2), 103-123.

Schoeman, J. J. (1989). Mica and Vermiculite in South Africa. *Journal of The South African Institute of Mining and Metallurgy*, 89, 1-12.

Sirkeci, A.A. (2000). The flotation separation of pyrite from arsenopyrite using hexyl thioethylamine as collector. *International Journal of Mineral Processing*, 60 (3), 263-276.

SGS. (2007a). Pilot Plant Products - White Mountain Log Sheets. Unpublished report.

SGS. (2007b). The mineralogical characteristics of pilot plant streams from The White Mountain Project. Ontario: Barrick. Unpublished report.

Silvester, E. J., Heyes, W. J., Bruckard, W. J., & Woodcock, J. T. (2013). The recovery of sericite in flotation concentrates. *Mineral Processing and Extractive Metallurgy*, 120 (1), 10-14.

Subrahmanyam T.V.& Forssberg E. (1988). Froth stability, particle entrainment and drainage in flotation: a review. *International Journal of Mineral Processing*, 23 (1), 33-53.

Sutherland, K. L. (1948). Kinetics of the Flotation Process. *The Journal of Physical Chemistry*, 52 (2), 394-425.

Sutherland, K. L., & Wark, I. W. (1955). *Principles of flotation*. Melbourne: Australasian Institute of Mining and Metallurgy.

Tabatabaei, R. H. (2011). The Causes for the Poor Flotation Performance of a Double-Refractory Gold Ore (Doctoral dissertation, University of Queensland, Brisbane, Australia)

Tabatabaei, R. H., Nagaraj, D. R., Vianna, S., & Napier-Munn, T. J. (2014). The Effect of Non-Sulphide Gangue Minerals on the Flotation of Sulphide Minerals from Carlin-Type Gold Ores. *Minerals Engineering*, 60, 26-32.

Tan, S.N., Pugh, R.J., Fornasiero, D. & Ralston, J., (2005). Foaming of polypropylene glycols and glycol/MIBC mixtures. Minerals Engineering, 18 (2), 179-188.

Tao, D.P.; Richardson, P.E.; Luttrell, G.H. & Yoon, R.-H. (2003). Electrochemical studies of pyrite oxidation and reduction using freshly-fractured electrodes and rotating ring-disc electrodes. *Electrochimica Acta*, 48 (24), 3615-3623.

Tao, D.P. & Li, Y. Q. (1994). The incipient oxidation of pyrite. *Colloids and Surfaces*, 93, 229-239.

Tapley, B., & Yan, D. (2003). The Selective Flotation of Arsenopyrite from Pyrite. *Minerals Engineering*, 16 (11), 1217-1220.

Thella, J. (2018). The influence of mineralogy and surface chemistry on flotation of Cortez complex carbonaceous double refractory gold ore (Doctoral dissertation, University of Queensland, Brisbane, Australia).

ThermoFisher Scientific (2019). Retrieved from: http://www.ajaxfinechem.com/.

Trahar, W. J. (1981). A rational interpretation of the role of particle-size in flotation. *International Journal of Mineral Processing*, 8 (4), 289-327.

Valdivieso, L., Escamilla, C. O. & Orozco, P. L. (1994). Flotation of arsenopyrite using xanthates as the collector. *GEOMIMET XXI Epoca*, 190, 9-20.

Valdivieso, A. L, Lopez, A. A. S. & Song, S. (2005). On the cathodic reaction coupled with the oxidation of xanthates at the pyrite/aqueous solution interface. *International Journal of Mineral Processing*, 77, 154-164.

Valdivieso, A.L., López, A.A.S., Escamilla, C.O & Fuerstenau, M.C (2006). Flotation and depression control of arsenopyrite through pH and pulp redox potential using xanthate as the collector. *International Journal of Mineral Processing*, 81 (1), 27-34.

van Olphen, H. (1951). Rheological phenomena of clay sols in connection with the charge distribution on the micelles. *Discussions of the Faraday Society*, 1951, 11, 83– 96.

Vaughan, D. J., & Pattrick, R. A. (1995). *Mineral Surfaces*. London: Chapman & Hall.

Verwey, E.J.W. & Overbeek, J.T.G. (1948). *Theory Stability of Lyophobic Solids.* Amsterdam, Elsevier.

Vianna, S. S. (2004). The effect of particle size, collector coverage, and liberation on the floatability of galena particles in an ore (Doctoral dissertation, University of Queensland, Brisbane, Australia).

Vinnett, L., Yianatos, J., & Alvarez, M. (2014). Gas dispersion measurements in mechanical flotation cells: Industrial experience in Chilean concentrators. *Minerals Engineering*, 57, 12–15.

Vizcarra, T. G. (2010). The effect of comminution mechanism on particle properties: consequences for downstream flotation performance (Doctoral dissertation, University of Queensland, Brisbane, Australia).

Voigt, S., Szargan, R., & Suoninen, E. J. (1994). Interaction of copper (II) ions with pyrite and its influence on ethyl xanthate adsorption. *Surface and Interface Analysis*, 21 (8), 526-536.

Walklate, J. R., & Heram, H. (2008). The development of a metallurgical flowsheet to treat tails. *Journal of The South African Institute of Mining and Metallurgy*, 108 (1), 45-53.

Wang, X. H., Forssberg, K.S.E. & Bolin, N.J. (1989). Activation of arsenopyrites by copper (II) ions. *Scandinavian Journal of Metallurgy*, 18, 288-294.

Wang, X. H. (1995). Interfacial electrochemistry of pyrite oxidation and flotation. *Journal of Colloid Interface Science*, 171 (2), 413-428.

Wang, L. (2016). Entrainment of fine particles in flotation. (Doctoral dissertation, University of Queensland, Brisbane, Australia).

Wang, L., Hu, Y., Liu, J., Sun, Y., & Sun, W. (2015a). Flotation and adsorption of muscovite using mixed cationic-nonionic surfactants as collector. *Powder Technology*, 276, 26-33.

Wang, L., Runge, K., & Peng, Y. (2015b). Entrainment modelling. AMIRA P9P Sponsor meeting. Brisbane: JKMRC.

Ward's Science (2019). Retrieved from https://www.wardsci.com/store/.

Webmineral. (2019, January 18)a. Retrieved from Arsenopyrite Mineral Data: http://webmineral.com/data/Arsenopyrite.shtml#.XACahTgzaM8.

Webmineral. (2019, January 18)b . Retrieved from Muscovite Mineral Data: http://webmineral.com/data/Muscovite.shtml#.XEEvtFUzaM8.

Webmineral. (2019, January 18)c. Retrieved from Pyrite Mineral Data: http://webmineral.com/data/Pyrite.shtml#.XEEwpFUzaM8.

Welby, S. D., Vianna, S. M., & Franzidis, J. P. (2010). Assigning Physical Significance to Floatability Components. *International Journal of Mineral Processing*, 97 (1), 59-67.

Welsby, S. D. (2009). On the interpretation of floatability using the bubble load. (Doctoral dissertation, University of Queensland, Brisbane, Australia).

Whincup, P. (2010). Guidelines for mineral process plant development studies. *Mineral Processing and Extractive Metallurgy,* 119 (4), 191-198.

White, M. E., & Harrington, I. (2014). Feasibility Studies - Scope and Accuracy*. *Mineral Resources and Ore Reserve* Estimation, *The AusIMM Guide of Good Practice, Monograph 30*, (pp. 507-518). Carlton: AusIMM.

Wiese, J., Becker, M., Yorath, G., & O'Connor, C. (2015). An investigation into the relationship between particle shape and entrainment. *Minerals Engineering*, 83, 211-216.

Wightman, E., & Sandoval, G. (2011). Attributing Physical Significance to floatability parameters. AMIRA P9O Final Technical Report , 357-377.

Williams, E., & Dardengo, E. (2011). A phased approach to test programs to meet feasibility study requirements. Eighth international heavy minerals conference (pp. 375-382). Perth: AusIMM.

Wills, B. A & Finch, J. A. (2016). *Will's mineral processing technology: an introduction to the practical aspects of ore treatment and mineral recovery*. Oxford, UK: Elsevier.

Wills, B. A (1988). *Mineral processing technology*. Oxford, UK: Elsevier.

Woods, R. (2003) Electrochemical potential controlling flotation. *International Journal of Mineral Processing*, 72 (1), 50–57.

Xu, D., Ametov, I., & Grano, S. R. (2011). Detachment of coarse particles from oscillating bubbles—The effect of particle contact angle, shape and medium viscosity. *International Journal of Mineral Processing*, 101 (1), 50–57.

Yianatos, J., & Contreras, F. (2010). Particle entrainment model for industrial flotation cells. *Powder Technology*, 197 (3), 260–267.

Yu, Y., Ma, L., Cao, M. & Liu, Q. (2017). Slime coatings in froth flotation: A review. *Minerals Engineering*, December, 114, 26-36.

Zhang, W., Zhou, X., & Finch, J. A. (2012). Determining independent control of dual-frother systems – Gas holdup, bubble size and water overflow rate. *Minerals Engineering*, *39*, 106–116. https://doi.org/10.1016/j.mineng.2012.08.008.

Zhang, Yahui, Cao, Zhao, Cao, Yongdan, & Sun, Chuanyao. (2013). FTIR studies of xanthate adsorption on chalcopyrite, pentlandite and pyrite surfaces. *Journal of Molecular Structure*, *1048*, 434–440. https://doi.org/10.1016/j.molstruc.2013.06.015.

Zanin, M., Wightman, E., Grano, S. R., & Franzidis, J. P. (2009). Quantifying contributions to froth stability in porphyry copper plants*. International Journal of Mineral Processing*, 91 (1), 19-27.

Appendix 1

CCRD Extended Plan

Appendix Table 1 - – Preliminary CCRD Test Program

RunOrder	Blocks	pH	PAX dosage
1	2	7.00	165.00
2	2	7.00	30.00
3	2	4.00	165.00
4	2	7.00	165.00
5	2	7.00	300.00
6	2	10.00	165.00
7	2	7.00	165.00
8	1	4.88	260.46
9	1	7.00	165.00
10	1	9.12	260.46
11	1	7.00	165.00
12	1	4.88	69.54
13	1	9.12	69.54
14	1	7.00	165.00

Appendix Table 2 - Full CCRD Test Program

RunOrder	Blocks	pH	%Solids	Muscovite proportion in %	Frother Dosage (ppm)	P_{80}	Muscovite mass (g)	Silica mass (g)
1	2	7.00	27.50	22.50	20.00	100.00	375.7	1235.7
2	2	10.00	27.50	22.50	20.00	100.00	375.7	1235.7
3	2	7.00	27.50	45.00	20.00	100.00	754.1	863.0
4	2	7.00	27.50	0.00	20.00	100.00	0.0	1605.7
5	2	7.00	27.50	22.50	30.00	100.00	375.7	1235.7
6	2	7.00	27.50	22.50	20.00	100.00	375.7	1235.7
7	2	7.00	27.50	22.50	20.00	50.00	375.7	1235.7
8	2	7.00	45.00	22.50	20.00	100.00	712.0	2341.5
9	2	4.00	27.50	22.50	20.00	100.00	375.7	1235.7
10	2	7.00	10.00	22.50	20.00	100.00	120.2	395.4
11	2	7.00	27.50	22.50	10.00	100.00	375.7	1235.7
12	2	7.00	27.50	22.50	20.00	100.00	375.7	1235.7
13	2	7.00	27.50	22.50	20.00	100.00	375.7	1235.7
14	2	7.00	27.50	22.50	20.00	150.00	375.7	1235.7
15	1	7.00	27.50	22.50	20.00	100.00	375.7	1235.7
16	1	5.73	34.90	12.99	15.77	78.87	291.5	1874.0
17	1	5.73	20.10	32.01	15.77	78.87	369.8	745.1
18	1	5.73	34.90	12.99	15.77	121.13	291.5	1874.0

RunOrder	Blocks	pH	%Solids	Muscovite proportion in %	Frother Dosage (ppm)	P_{80}	Muscovite mass (g)	Silica mass (g)
19	1	5.73	20.10	12.99	15.77	121.13	149.8	962.8
20	1	8.27	34.90	12.99	24.23	78.87	291.5	1874.0
21	1	5.73	34.90	32.01	24.23	121.13	721.2	1453.1
22	1	8.27	20.10	32.01	15.77	78.87	369.8	745.1
23	1	5.73	20.10	12.99	15.77	78.87	149.8	962.8
24	1	5.73	20.10	12.99	24.23	78.87	149.8	962.8
25	1	8.27	34.90	32.01	24.23	78.87	721.2	1453.1
26	1	5.73	34.90	12.99	24.23	78.87	291.5	1874.0
27	1	7.00	27.50	22.50	20.00	100.00	375.7	1235.7
28	1	7.00	27.50	22.50	20.00	100.00	375.7	1235.7
29	1	5.73	34.90	12.99	24.23	121.13	291.5	1874.0
30	1	5.73	34.90	32.01	24.23	78.87	721.2	1453.1
31	1	8.27	20.10	32.01	24.23	121.13	369.8	745.1
32	1	7.00	27.50	22.50	20.00	100.00	375.7	1235.7
33	1	8.27	34.90	12.99	15.77	121.13	291.5	1874.0
34	1	8.27	20.10	12.99	15.77	121.13	149.8	962.8
35	1	8.27	20.10	12.99	15.77	78.87	149.8	962.8
36	1	5.73	20.10	32.01	24.23	121.13	369.8	745.1
37	1	5.73	34.90	32.01	15.77	78.87	721.2	1453.1
38	1	5.73	20.10	32.01	24.23	78.87	369.8	745.1
39	1	8.27	34.90	32.01	15.77	78.87	721.2	1453.1
40	1	5.73	20.10	32.01	15.77	121.13	369.8	745.1
41	1	7.00	27.50	22.50	20.00	100.00	375.7	1235.7
42	1	8.27	34.90	12.99	24.23	121.13	291.5	1874.0
43	1	7.00	27.50	22.50	20.00	100.00	375.7	1235.7
44	1	8.27	34.90	32.01	15.77	121.13	721.2	1453.1
45	1	8.27	20.10	12.99	24.23	121.13	149.8	962.8
46	1	5.73	20.10	12.99	24.23	121.13	149.8	962.8
47	1	8.27	20.10	12.99	24.23	78.87	149.8	962.8
48	1	7.00	27.50	22.50	20.00	100.00	375.7	1235.7
49	1	7.00	27.50	22.50	20.00	100.00	375.7	1235.7
50	1	8.27	34.90	12.99	15.77	78.87	291.5	1874.0
51	1	8.27	20.10	32.01	15.77	121.13	369.8	745.1
52	1	5.73	34.90	32.01	15.77	121.13	721.2	1453.1
53	1	8.27	20.10	32.01	24.23	78.87	369.8	745.1
54	1	8.27	34.90	32.01	24.23	121.13	721.2	1453.1

Appendix 2

Reference Liberation Data

Appendix Table 3 - – Muscovite liberation of Reference ore at 2 minutes, P_{80} 370 µm

Size (µm)	Liberation class										
	0% < X < 10%	10% < X < 20%	20% < X < 30%	30% < X < 40%	40% < X < 50%	50% < X < 60%	60% < X < 70%	70% < X < 80%	80% < X < 90%	90% < X < 100%	100%
+600	0.1	0.1	0.1	0.1	0.1	0.1	0.1	0.1	0.2	1.3	0.1
-600+425	0.4	0.4	0.5	0.5	0.5	0.5	0.5	0.5	0.6	2.5	0.6
-425+300	0.4	0.5	0.5	0.5	0.5	0.6	0.6	0.7	0.9	3.6	1.7
-300+150	0.4	0.4	0.5	0.4	0.5	0.5	0.5	0.8	1.3	5.0	6.7
-150+75	0.1	0.2	0.2	0.2	0.2	0.3	0.3	0.5	0.9	6.1	10.7
-75+38	0.1	0.1	0.1	0.1	0.1	0.1	0.1	0.3	0.7	4.9	9.4
-38	0.1	0.1	0.1	0.1	0.1	0.1	0.1	0.2	0.6	3.4	21.7

Appendix Table 4 - Muscovite liberation of Reference ore at 10 minutes, P_{80} 125 µm

Size (µm)	Liberation class										
	0% < X < 10%	10% < X < 20%	20% < X < 30%	30% < X < 40%	40% < X < 50%	50% < X < 60%	60% < X < 70%	70% < X < 80%	80% < X < 90%	90% < X < 100%	100%
+150	0.0	0.0	0.0	0.0	0.0	0.1	0.1	0.1	0.4	6.9	6.2
-150+75	0.2	0.3	0.3	0.3	0.3	0.4	0.5	0.6	1.4	10.1	15.1
-75+38	0.1	0.1	0.2	0.2	0.2	0.3	0.4	0.5	1.0	6.9	16.3
-38+29	0.0	0.0	0.0	0.0	0.0	0.0	0.0	0.0	0.0	0.1	0.4
-29+14	0.0	0.0	0.1	0.1	0.0	0.1	0.1	0.1	0.4	1.3	10.5
-14+11	0.0	0.0	0.0	0.0	0.0	0.0	0.0	0.0	0.1	0.3	2.6
-11	0.2	0.3	0.4	0.3	0.4	0.5	0.6	0.7	0.9	1.1	8.9

Appendix Table 5 - Muscovite liberation of Reference ore at 35 minutes, P_{80} 50 µm

Size (µm)	Liberation class										
	0% < X < 10%	10% < X < 20%	20% < X < 30%	30% < X < 40%	40% < X < 50%	50% < X < 60%	60% < X < 70%	70% < X < 80%	80% < X < 90%	90% < X < 100%	100%
+75	0.0	0.0	0.0	0.0	0.0	0.0	0.0	0.3	1.2	10.2	9.5
-75+38	0.1	0.1	0.1	0.2	0.2	0.2	0.2	0.7	2.0	12.4	21.2
-38+29	0.0	0.0	0.0	0.0	0.0	0.0	0.0	0.0	0.0	0.1	0.4
-29+14	0.0	0.0	0.0	0.0	0.0	0.1	0.1	0.1	0.3	1.4	12.5
-14+11	0.0	0.0	0.0	0.0	0.0	0.1	0.0	0.1	0.1	0.4	3.8
-11	0.1	0.2	0.2	0.3	0.5	0.5	0.5	0.7	1.1	1.5	15.6

Appendix Table 6 - Pyrite liberation of Reference ore at 2 minutes, P_{80} 370 µm

Size (µm)	Liberation class										
	0% < X < 10%	10% < X < 20%	20% < X < 30%	30% < X < 40%	40% < X < 50%	50% < X < 60%	60% < X < 70%	70% < X < 80%	80% < X < 90%	90% < X < 100%	100%
+600	0.0	0.0	0.0	0.0	0.0	0.0	0.0	0.0	0.1	4.0	0.3
-600+425	0.0	0.0	0.0	0.0	0.0	0.0	0.0	0.0	0.1	10.3	1.5
-425+300	0.0	0.0	0.0	0.1	0.1	0.0	0.0	0.2	0.8	19.9	3.6
-300+150	0.0	0.0	0.0	0.0	0.1	0.0	0.0	0.3	0.3	13.4	13.9
-150+75	0.0	0.0	0.0	0.0	0.0	0.0	0.0	0.1	0.1	3.0	11.5
-75+38	0.0	0.0	0.0	0.0	0.0	0.0	0.0	0.0	0.1	0.8	5.3
-38	0.0	0.0	0.0	0.0	0.0	0.0	0.0	0.0	0.0	0.2	9.0

Appendix Table 7 - Pyrite liberation of Reference ore at 10 minutes, P_{80} 125 µm

Size (µm)	Liberation class										
	0% < X < 10%	10% < X < 20%	20% < X < 30%	30% < X < 40%	40% < X < 50%	50% < X < 60%	60% < X < 70%	70% < X < 80%	80% < X < 90%	90% < X < 100%	100%
+150	0.0	0.0	0.0	0.0	0.0	0.0	0.0	0.0	0.0	1.2	2.6
-150+75	0.0	0.0	0.0	0.0	0.0	0.0	0.1	0.1	0.3	9.3	35.0
-75+38	0.0	0.0	0.0	0.0	0.0	0.0	0.1	0.1	0.1	2.5	23.1
-38+29	0.0	0.0	0.0	0.0	0.0	0.0	0.0	0.0	0.0	0.3	6.6
-29+14	0.0	0.0	0.0	0.0	0.0	0.0	0.0	0.0	0.0	0.0	8.8
-14+11	0.0	0.0	0.0	0.0	0.0	0.0	0.0	0.0	0.0	0.0	1.5
-11	0.2	0.1	0.1	0.0	0.0	0.0	0.0	0.1	0.1	0.1	6.9

Appendix Table 8 - Pyrite liberation of Reference ore at 35 minutes, P_{80} 50 µm

Size (µm)	Liberation class										
	0% < X < 10%	10% < X < 20%	20% < X < 30%	30% < X < 40%	40% < X < 50%	50% < X < 60%	60% < X < 70%	70% < X < 80%	80% < X < 90%	90% < X < 100%	100%
+75	0.0	0.0	0.0	0.0	0.0	0.0	0.0	0.0	0.0	0.6	2.5
-75+38	0.0	0.0	0.0	0.0	0.0	0.0	0.0	0.2	0.5	4.6	31.8
-38+29	0.0	0.0	0.0	0.0	0.0	0.0	0.0	0.0	0.0	0.2	16.1
-29+14	0.0	0.0	0.0	0.0	0.0	0.0	0.0	0.0	0.0	0.2	19.6
-14+11	0.0	0.0	0.0	0.0	0.0	0.0	0.0	0.0	0.0	0.1	2.8
-11	0.1	0.1	0.1	0.1	0.1	0.1	0.1	0.0	0.1	0.2	18.9

Appendix Table 9 - Silica (quartz) liberation of Reference ore at 2 minutes, P_{80} 370 µm

Size (µm)	Liberation class										
	0% < X < 10%	10% < X < 20%	20% < X < 30%	30% < X < 40%	40% < X < 50%	50% < X < 60%	60% < X < 70%	70% < X < 80%	80% < X < 90%	90% < X < 100%	100%
+600	0.0	0.0	0.1	0.1	0.1	0.1	0.1	0.1	0.1	0.9	0.9
-600+425	0.1	0.2	0.1	0.2	0.3	0.3	0.3	0.5	0.7	3.5	3.8
-425+300	0.1	0.2	0.2	0.3	0.2	0.3	0.3	0.8	1.2	5.6	8.9
-300+150	0.1	0.2	0.2	0.2	0.3	0.3	0.3	0.7	1.4	7.2	18.9
-150+75	0.1	0.1	0.1	0.1	0.1	0.1	0.1	0.3	0.7	3.5	12.7
-75+38	0.0	0.1	0.1	0.1	0.1	0.1	0.1	0.1	0.3	1.3	7.0
-38	0.0	0.0	0.1	0.0	0.1	0.1	0.1	0.1	0.2	0.9	10.2

Appendix Table 10 - Silica (quartz) liberation of Reference ore at 10 minutes, P_{80} 125 µm

Size (µm)	Liberation class										
	0% < X < 10%	10% < X < 20%	20% < X < 30%	30% < X < 40%	40% < X < 50%	50% < X < 60%	60% < X < 70%	70% < X < 80%	80% < X < 90%	90% < X < 100%	100%
+150	0.0	0.0	0.0	0.0	0.0	0.0	0.0	0.1	0.6	2.8	0.0
-150+75	0.2	0.2	0.1	0.1	0.2	0.3	0.5	0.9	5.6	36.5	0.0
-75+38	0.1	0.1	0.1	0.1	0.2	0.2	0.3	0.6	2.4	24.6	0.0
-38+29	0.0	0.0	0.0	0.0	0.0	0.0	0.0	0.0	0.1	1.3	0.0
-29+14	0.0	0.0	0.0	0.0	0.0	0.1	0.1	0.1	0.3	11.6	0.0
-14+11	0.0	0.0	0.0	0.0	0.0	0.0	0.0	0.0	0.1	1.9	0.0
-11	0.1	0.2	0.1	0.2	0.2	0.3	0.2	0.3	0.5	5.1	0.0

Appendix Table 11 - Silica (quartz) liberation of Reference ore at 35 minutes, P_{80} 50 µm

Size (µm)	Liberation class										
	0% < X < 10%	10% < X < 20%	20% < X < 30%	30% < X < 40%	40% < X < 50%	50% < X < 60%	60% < X < 70%	70% < X < 80%	80% < X < 90%	90% < X < 100%	100%
+75	0.0	0.0	0.0	0.0	0.0	0.0	0.0	0.0	0.0	0.3	2.1
-75+38	0.1	0.1	0.1	0.1	0.1	0.1	0.1	0.2	0.5	2.7	33.4
-38+29	0.0	0.0	0.0	0.0	0.0	0.0	0.0	0.0	0.0	0.2	3.2
-29+14	0.0	0.0	0.0	0.0	0.0	0.0	0.1	0.1	0.1	0.5	31.3
-14+11	0.0	0.0	0.0	0.0	0.0	0.0	0.0	0.0	0.0	0.1	5.1
-11	0.1	0.2	0.2	0.2	0.2	0.3	0.4	0.5	0.7	0.8	15.6

Appendix 3

Flotation Recovery Repeatability in the Full CCRD Program

Flotation Reproducibility in the Preliminary CCRD for Identifying the Appropriate Collector Dosage

The flotation reproducibility in the preliminary 2-factor CCRD was assessed via 6 repeats of the centre point. The repeats were performed as part of the main body 2-factor CCRD in blocked order, which minimises the effect of length of experiments.

The objective of performing the repeats was to estimate the experimental error. The reproducibility of the flotation tests performed was evaluated as:

- Cumulative mass recovery of solids and water.
- Cumulative component recovery based on assays.
- Flotation rate of arsenopyrite and pyrite.

The flotation operation conditions in the repeat tests were 35 g of pyrite, 16 g of arsenopyrite, 1112 g of silica, 30 ppm of Dowfroth 250, 165 g/t of PAX, 20% w/w solids.

Appendix Table 12 shows the average solids recovery, the confidence interval and the percentage of error (confidence interval) represented as the percentage of the average.

Appendix Table 12 - Confidence interval at 95% level of confidence for solids cumulative mass recovery (%)

Concentrate (min)	Average Total % Recovery Solids	95% Confidence Interval Solids % Recovery	% of confidence interval compared to the average
0.5	2.28	0.42	18.31
1	4.14	0.43	10.27
2	5.20	0.41	7.92
6	6.94	0.45	6.46
10	7.68	0.47	6.09

As shown in Appendix Table 12, after 10 minutes of collection of concentrate, the error associated with the total mass recovered to the concentrate is 6%. Appendix Figure 1 shows the graphic representation of the confidence intervals. High and low confidence interval trends were selected for display of the error instead of error bars because, in batch flotation tests, error associated with each concentrate is different.

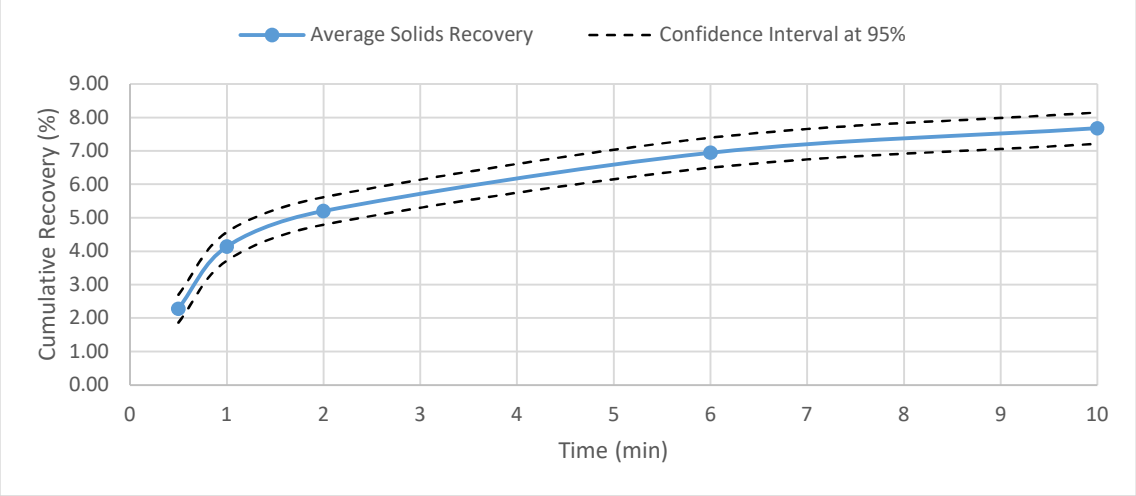

Appendix Figure 1 – Average cumulative solids recovery and the 95% confidence intervals

Appendix Table 13 shows the c represented as the percentage of the average. After 10 minutes of concentrate collection, the error associated with the total mass of water recovered to the concentrate is 9%.

Appendix Table 13 - Confidence interval at 95% level of confidence for water cumulative mass recovery (%)

Concentrate (min)	Average Total Water % Recovery	95% Confidence Interval Water % Recovery	% of Confidence Interval compared to the average
0.5	1.18	0.36	30.04
1	2.73	0.48	17.56
2	4.00	0.61	15.14
6	9.69	1.00	10.29
10	15.58	1.40	9.01

Appendix Figure 2 shows the graphic representation of the confidence intervals.

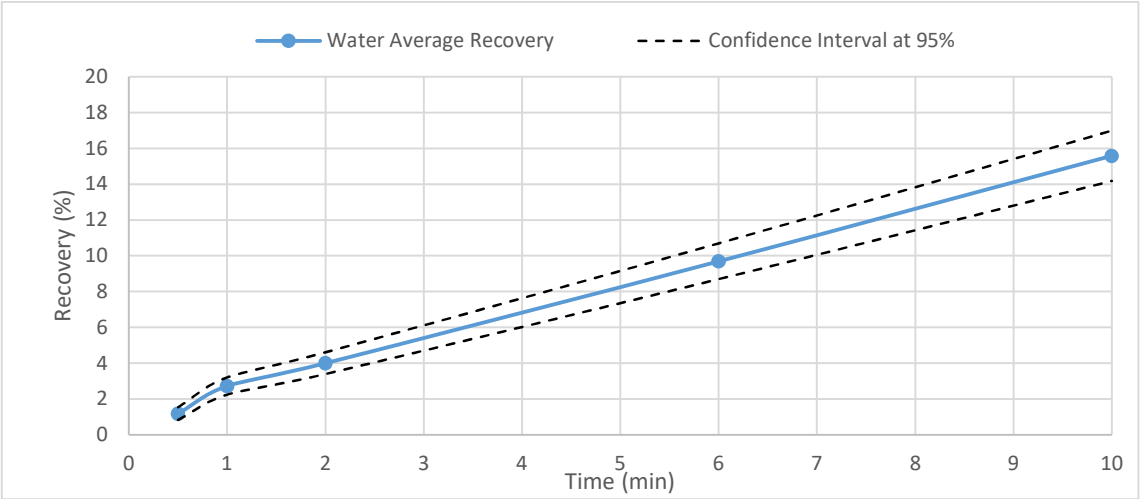

Appendix Figure 2 - Confidence interval at 95% level of confidence for water cumulative mass recovery (%)

Appendix Table 14 shows the average recovery for arsenopyrite, the confidence interval and the percentage of error (confidence interval) represented as the percentage of the average. The error values for recovery of arsenopyrite varied from 0.5 to 18%. The values are in the normal error range according to Sandoval-Zambrado and Montes-Atenas (2012).

Appendix Table 14 - Confidence interval at 95% level of confidence for arsenopyrite cumulative % recovery

Concentrate (min)	Average Total % Recovery Arsenopyrite	95% Confidence Interval Arsenopyrite % Recovery	% of the variation of Confidence Interval compared to the average
0.5	39.75	7.06	17.77
1	67.36	5.48	8.14
2	80.84	2.99	3.70
6	96.70	0.40	0.41
10	98.13	0.48	0.49

Appendix Figure 3 shows the graphic representation of the confidence intervals.

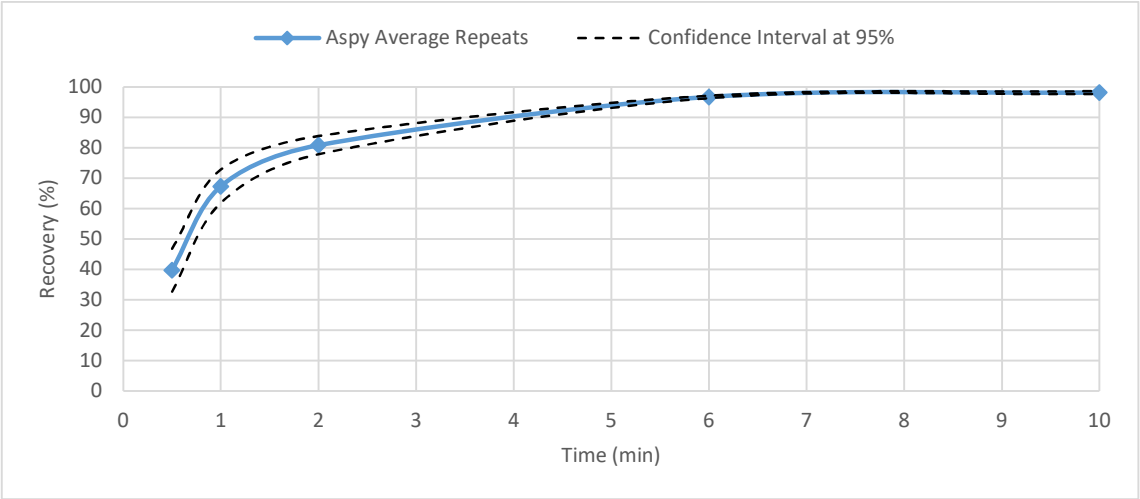

Appendix Figure 3 - Confidence interval at 95% level of confidence for arsenopyrite cumulative % recovery

Appendix Table 15 shows the average pyrite recovery, the confidence interval and the percentage of error (confidence interval) represented as the percentage of the average. The error values for recovery of pyrite varied from 0.3 to 20%.

Appendix Table 15 - Confidence interval at 95% level of confidence for pyrite cumulative % recovery

Concentrate (min)	Average Total % Recovery Pyrite	95% Confidence Interval Pyrite % Recovery	% of Variation of Confidence Interval Compared to the Average
0.5	38.82	7.79	20.07
1	67.84	5.09	7.50
2	82.55	2.99	3.63
6	98.19	0.86	0.88
10	99.46	0.30	0.30

Appendix Figure 4 shows the graphic representation of the confidence intervals.

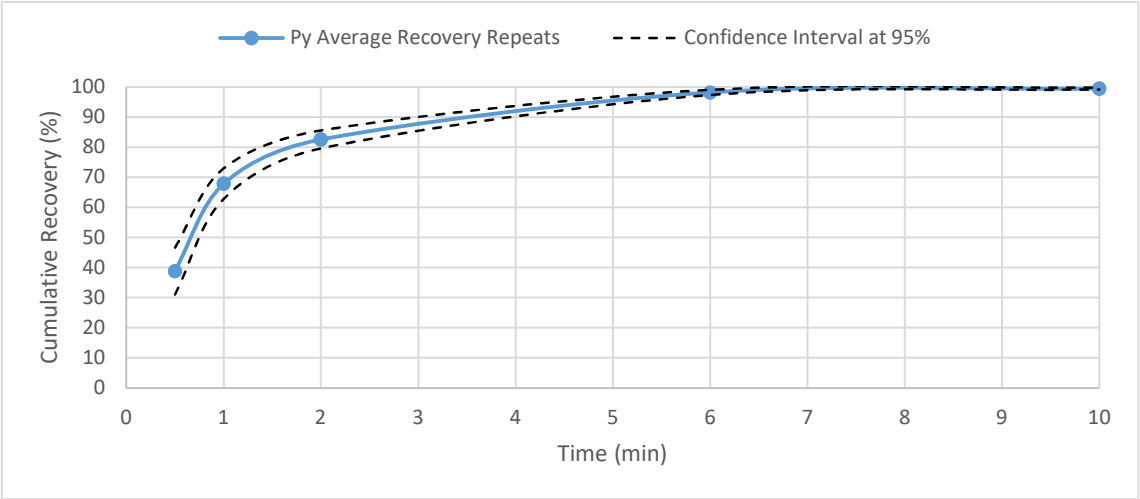

Appendix Figure 4 - Confidence interval at 95% level of confidence for pyrite cumulative % recovery

Appendix Table 16 shows the average arsenopyrite and pyrite flotation rate, the confidence interval and the percentage of error (confidence interval) represented as the percentage of the average.

Appendix Table 16 - Confidence interval at 95% level of confidence for arsenopyrite and pyrite flotation rate

Component	Average k_i	95% Confidence Interval	% of the variation of confidence interval compared to the average
Arsenopyrite	0.97	0.14	14
Pyrite	0.98	0.13	13

According to Appendix Table 16, the average flotation rates and confidence intervals of arsenopyrite and pyrite were similar.

Flotation Reproducibility in the CCRD

The flotation reproducibility in the full CCRD design was assessed via 10 repeats of the centre point. The repeats were performed as part of the main body of the full CCRD design in blocked order, which minimises the effect of length of experiments. Due to operational problems during the tests, one of the 10 tests was rejected. The objective of the repeats was to estimate the experimental error. The flotation operation conditions in the repeat tests were 35 g of pyrite, 16 g of arsenopyrite, 20 ppm of Dowfroth 250, 300 g/t of PAX, 27.5% w /w solids. The repeatability of the test was evaluated in 3 stages: cumulative mass recovery of solids and water, cumulative component recovery based on assays and grade recovery.

Appendix Table 17 - Confidence Interval at 95% level of confidence for Solids Cumulative Mass Recovery (%)

Concentrate (min)	Average Total Recovery Solids	95% Confidence Interval Solids Recovery	% of Confidence Interval compared to the average
0.5	2.58	0.07	2.87
1	4.14	0.14	3.49
2	5.33	0.22	4.03
6	7.34	0.22	3.05
10	8.39	0.27	3.25

Appendix Table 17 shows the average solids recovery, the confidence interval and the relative error (confidence interval represented as the percentage of the average). After 10 minutes of collection of concentrate, the error associated with the total mass recovered to the concentrate is 3.25%. Appendix Figure 5 shows the graphic representation of the confidence intervals. The confidence interval trends were selected for displaying the error instead of error bars because, in batch flotation tests, the error associated to each timed concentrate is different.

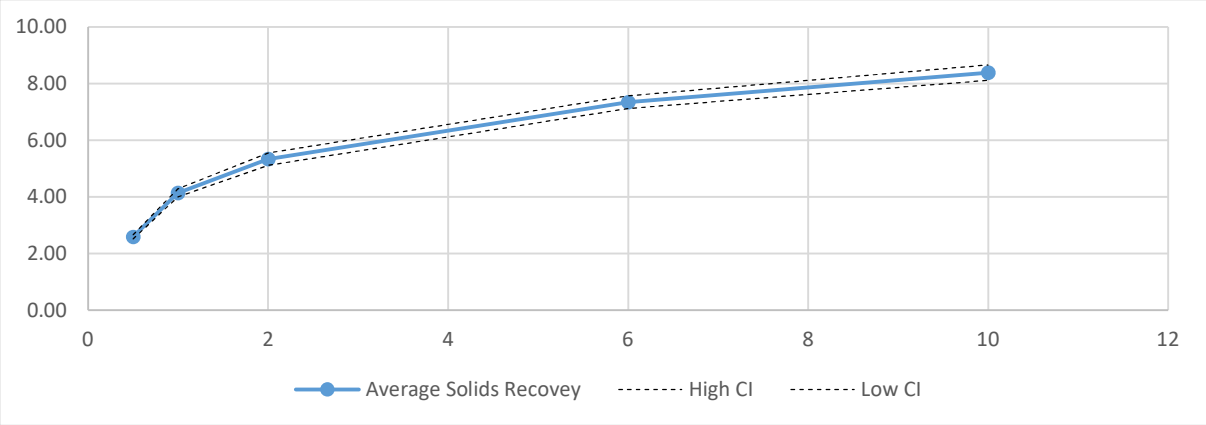

Appendix Figure 5 - Confidence Internal at 95% solids for the solids recovery

Appendix Table 18 shows the average solids recovery, the confidence interval and the percentage of error (confidence interval) represented as the percentage of the average. After 10 minutes of concentrate collection, the error associated with the total mass of water recovered to the concentrate is 6%. Appendix Figure 6 shows the graphic representation of the confidence intervals.

Appendix Table 18 - Confidence Interval at 95% level of confidence for Water Cumulative Mass Recovery (%)

Concentrate (min)	Average Total Water Recovery (%)	95% Confidence Interval Water Recovery (%)	% of Confidence Interval compared to the average
0.5	2.47	0.20	7.92
1	5.60	0.37	6.68
2	10.31	0.71	6.93
6	24.52	1.36	5.54
10	34.13	2.01	5.88

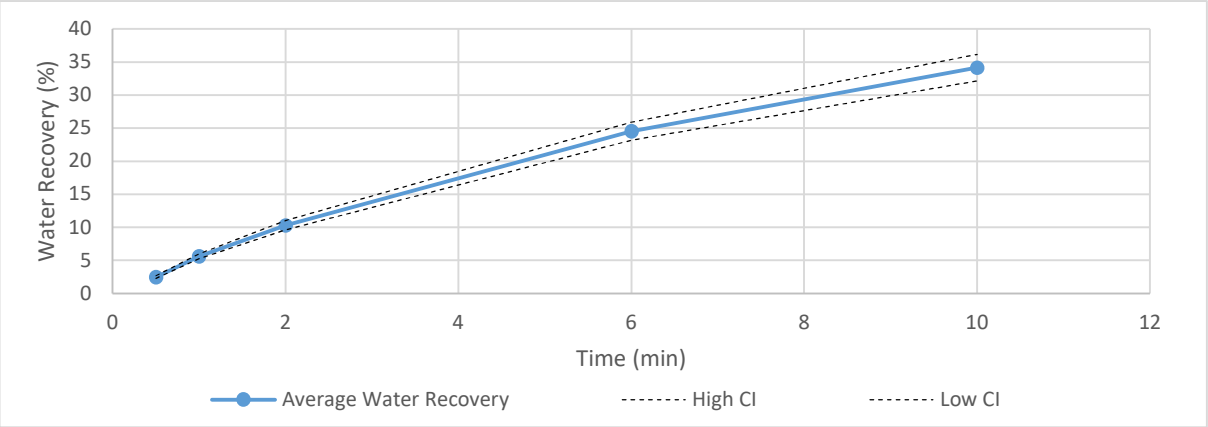

Appendix Figure 6 - Confidence Interval at 95% level of confidence for Water Cumulative Mass Recovery (%)

The error values for recovery of arsenopyrite varied from 0.5 to 18% as showed in Appendix Table 19. Their values are in the normal error range according to Sandoval-Zambrado and Montes-Atenas (2012). Appendix Figure 7 shows the graphic representation of the confidence intervals.

Appendix Table 19 - Confidence Interval at 95% level of confidence for Arsenopyrite Cumulative % Recovery

Concentrate (min)	Average Total Recovery Arsenopyrite	95% Confidence Interval Arsenopyrite Recovery	% of the variation of Confidence Interval compared to the average
0.5	55.55	1.32	2.37
1	81.01	1.15	1.42
2	92.39	0.61	0.66
6	97.44	0.27	0.28
10	98.15	0.25	0.26
Flotation Rate Constant (k)	1.67	0.06	3.51

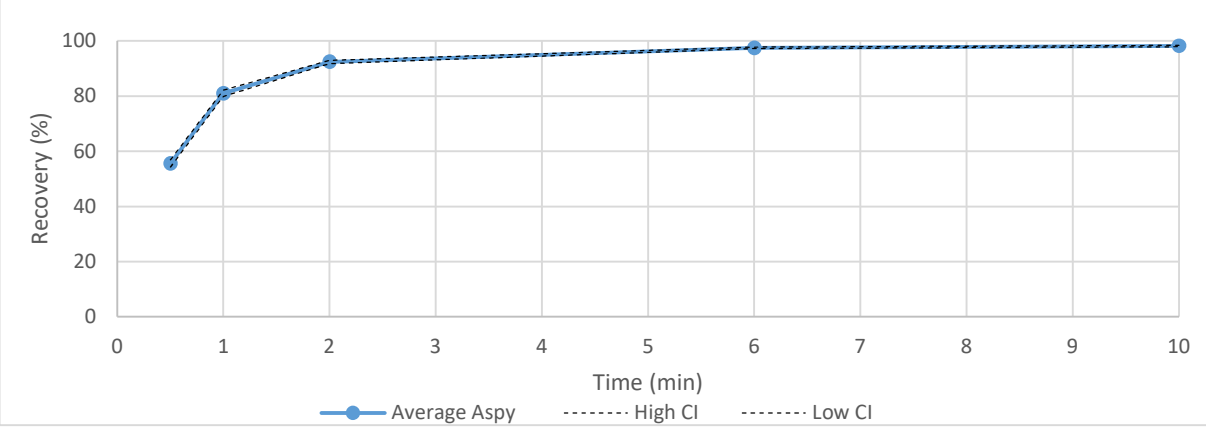

Appendix Figure 7 - Confidence Interval at 95% level of confidence for Arsenopyrite Cumulative % Recovery

The error values for recovery of pyrite varied from 0.3 to 20%, as per Appendix Table 20. Appendix Figure 8 shows the graphic representation of the confidence intervals.

Appendix Table 20 - Confidence Interval at 95% level of confidence for Pyrite Cumulative % Recovery

Concentrate (min)	Average Total Recovery Pyrite	95% Confidence Interval Pyrite Recovery	% of the variation of Confidence Interval compared to the average
0.5	59.16	2.85	4.82
1	84.66	1.16	1.37
2	94.87	0.46	0.48
6	98.46	0.16	0.16
10	98.89	0.16	0.16
Flotation Rate Constant (k)	1.83	0.09	4.88

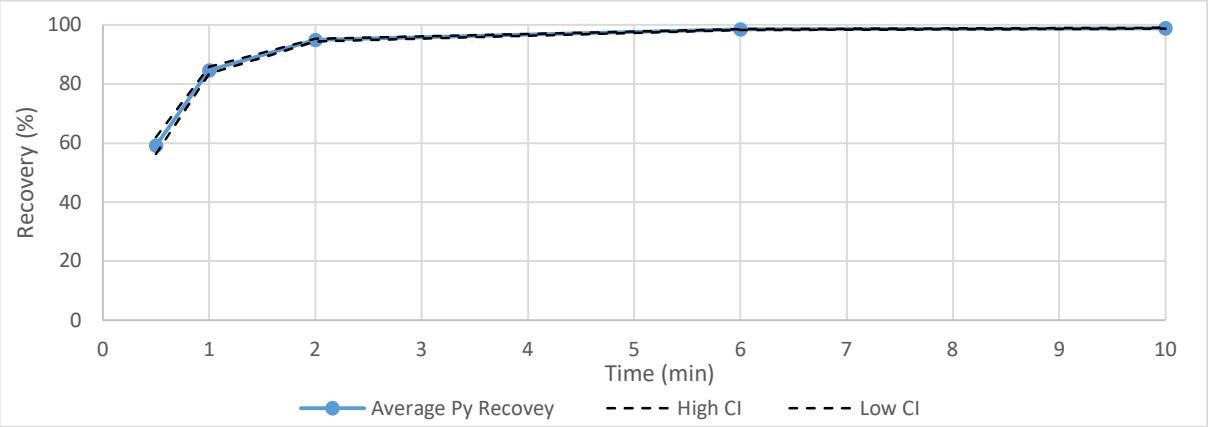

Appendix Figure 8 - Confidence Interval at 95% level of confidence for Pyrite Cumulative % Recovery

In addition to the recovery repeatability, the repeatability of the concentrate grade was calculated. There was no reference in the literature for concentrate grade repeatability. According to Savassi (1998), the normal error associated with assays is 5%. Appendix Table 21 and Appendix Figure 9 show the confidence interval at 95% level of confidence for the arsenopyrite and pyrite cumulative grade in the concentrate. Appendix Table 22 and Appendix Figure 10 show the graphic representation of the confidence interval at 95% level of confidence for the arsenopyrite and pyrite cumulative grade in the concentrate.

Appendix Table 21 - Confidence Interval at 95% level of confidence for Arsenopyrite Cumulative Grade in the Concentrate

Concentrate (min)	Average Grade Arsenopyrite	95% Confidence Interval Arsenopyrite Grade	% of the variation of Confidence Interval compared to the average (relative)
0.5	22.61	0.43	1.90
1	20.72	0.65	3.12
2	18.39	0.64	3.46
6	14.02	0.38	2.73
10	12.38	0.36	2.90

The repeatability of the grade of arsenopyrite after 10 minutes is 7%, which is higher than the range indicated by Savassi (1998). It means that the predictions of recovery and grade of arsenopyrite by the regression model are not very accurate.

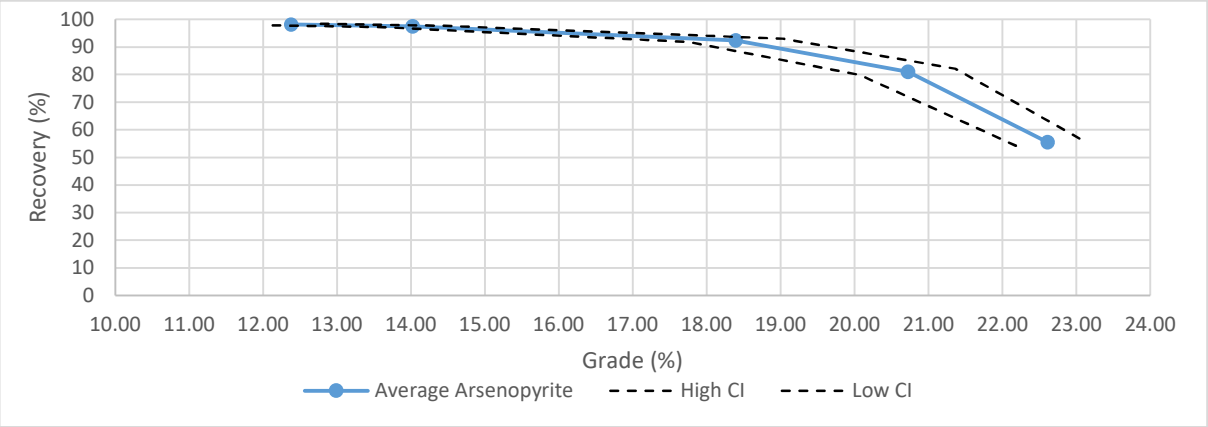

Appendix Figure 9 - Confidence Interval at 95% level of confidence for Arsenopyrite Cumulative Grade in the Concentrate

The repeatability of the grade of pyrite after 10 minutes is 5.6%, which is approximately the same as rage as indicated by Savassi (1998).

Appendix Table 22 - Confidence Interval at 95% level of confidence for Pyrite Cumulative Grade in the Concentrate

Concentrate (min)	Average Pyrite Grade	95% Confidence Interval Pyrite Grade	% of the variation of Confidence Interval compared to the average
0.5	56.78	1.32	2.32
1	49.53	1.64	3.32
2	43.14	1.58	3.66
6	32.47	1.02	3.14
10	28.61	0.98	3.42

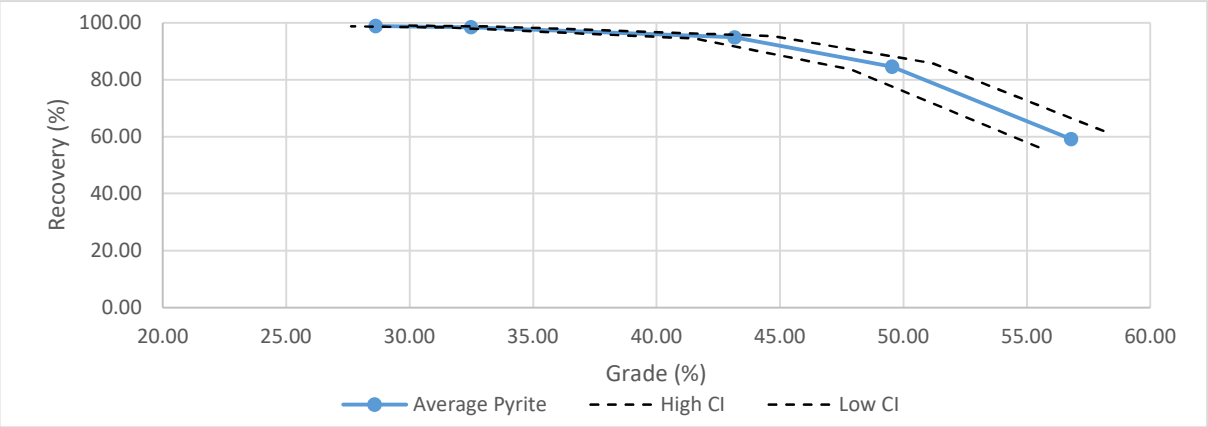

Appendix Figure 10 - Confidence Interval at 95% level of confidence for Pyrite Cumulative Grade in the Concentrate

Appendix 4

Rheograms

CCRD Flotation Feed Rheograms

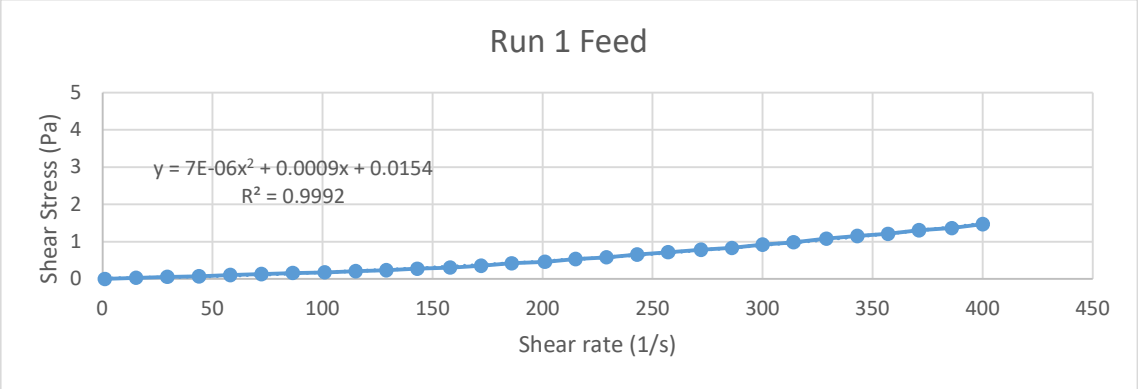

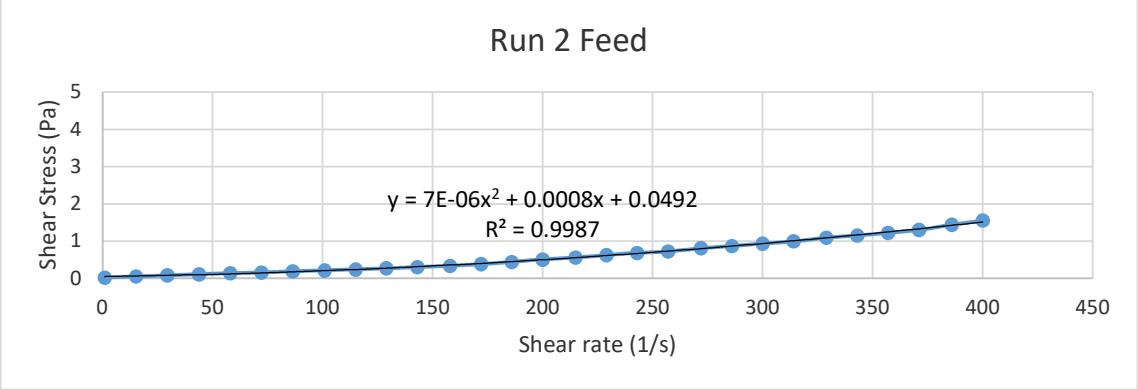

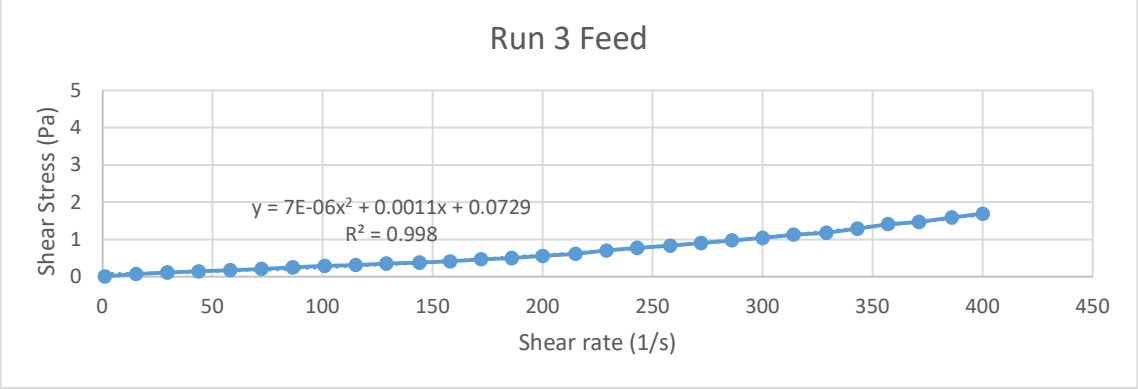

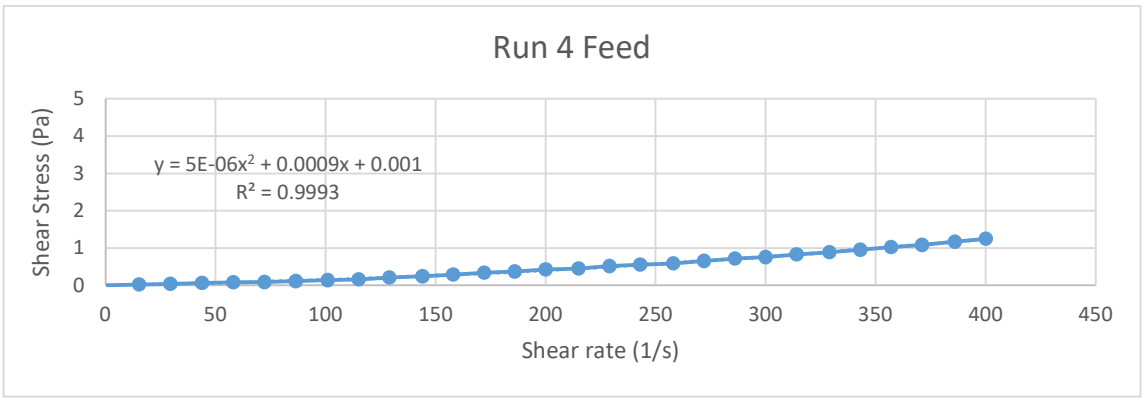
Run 4 Feed
Shear Stress (Pa)
y = 5E-06x² + 0.0009x + 0.001
R² = 0.9993
Shear rate (1/s)

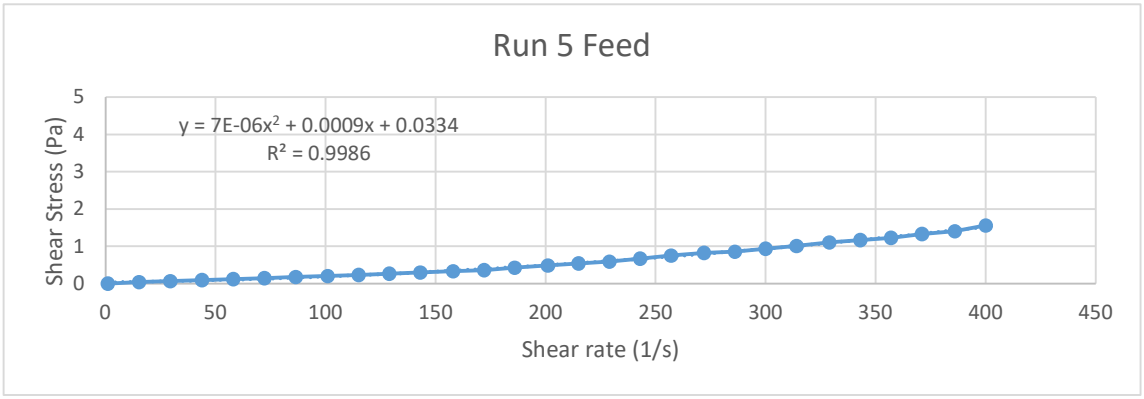
Run 5 Feed
Shear Stress (Pa)
y = 7E-06x² + 0.0009x + 0.0334
R² = 0.9986
Shear rate (1/s)

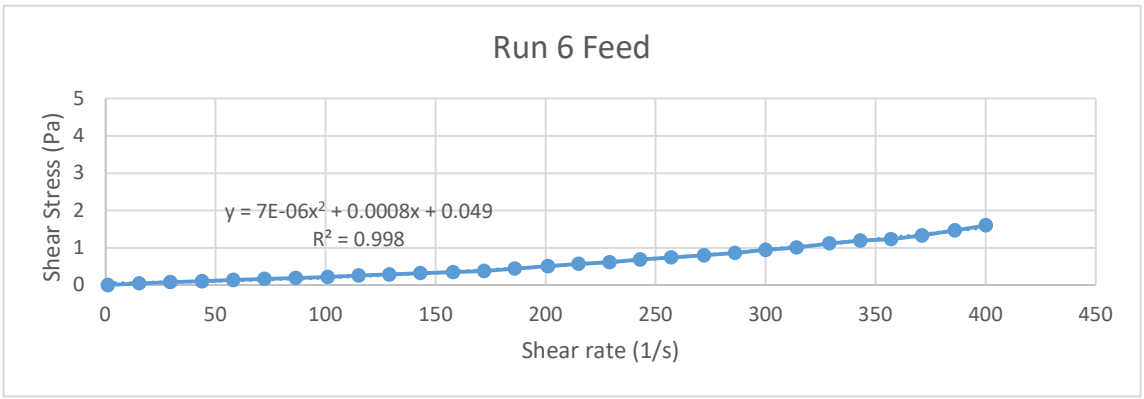
Run 6 Feed
Shear Stress (Pa)
y = 7E-06x² + 0.0008x + 0.049
R² = 0.998
Shear rate (1/s)

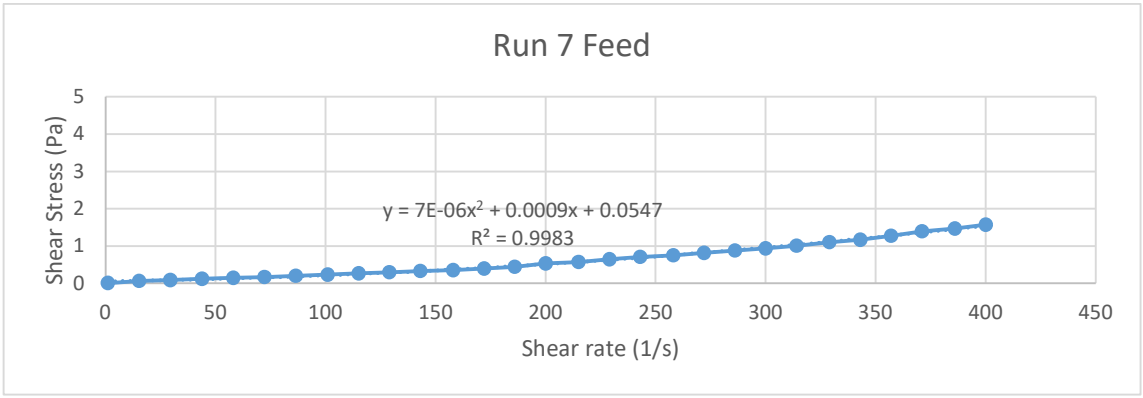
Run 7 Feed
Shear Stress (Pa)
y = 7E-06x² + 0.0009x + 0.0547
R² = 0.9983
Shear rate (1/s)

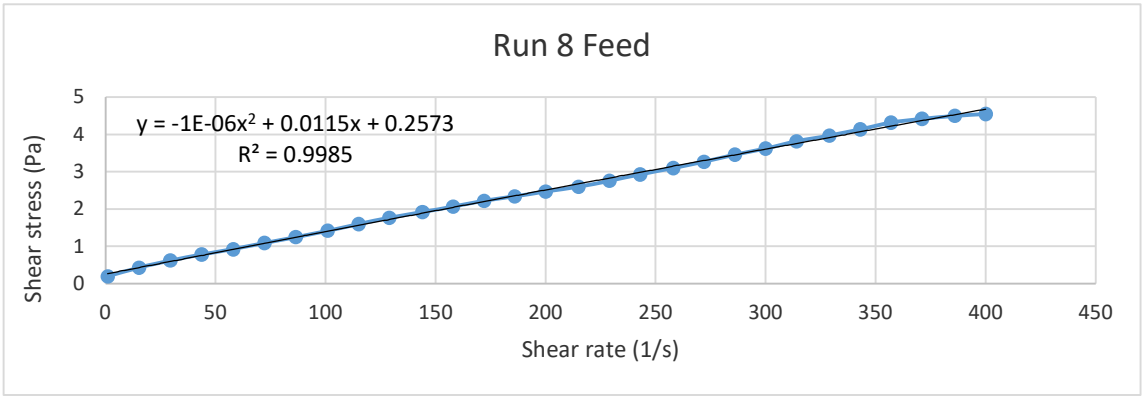
Run 8 Feed
Shear stress (Pa)
y = -1E-06x² + 0.0115x + 0.2573
R² = 0.9985
Shear rate (1/s)

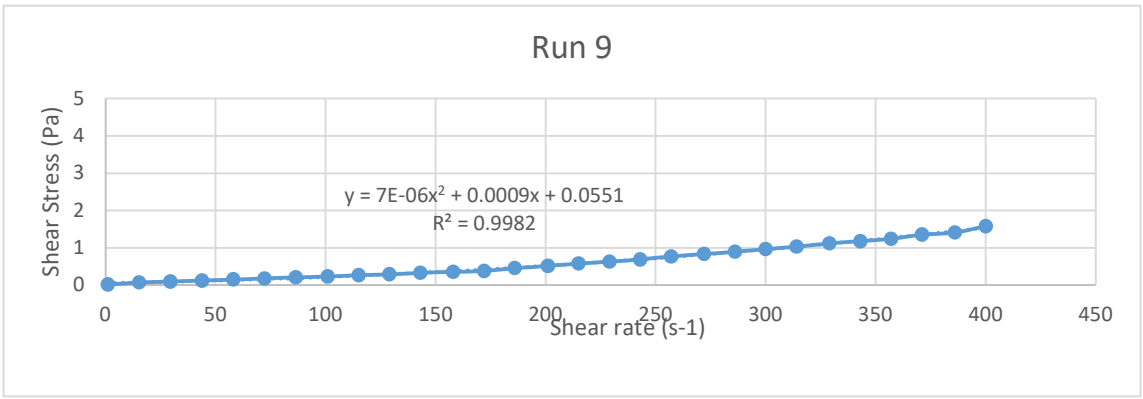
Run 9
Shear Stress (Pa)
y = 7E-06x² + 0.0009x + 0.0551
R² = 0.9982
Shear rate (s-1)

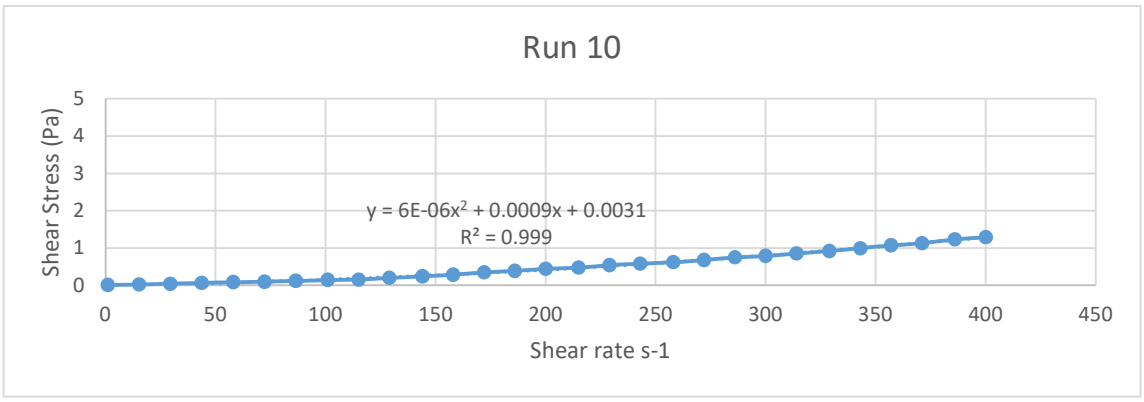
Run 10
Shear Stress (Pa)
y = 6E-06x² + 0.0009x + 0.0031
R² = 0.999
Shear rate s-1

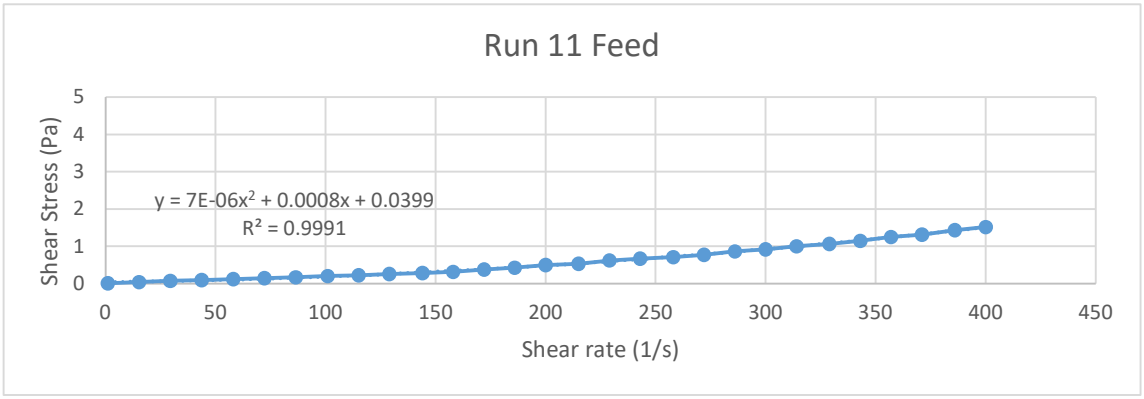
Run 11 Feed
Shear Stress (Pa)
y = 7E-06x² + 0.0008x + 0.0399
R² = 0.9991
Shear rate (1/s)

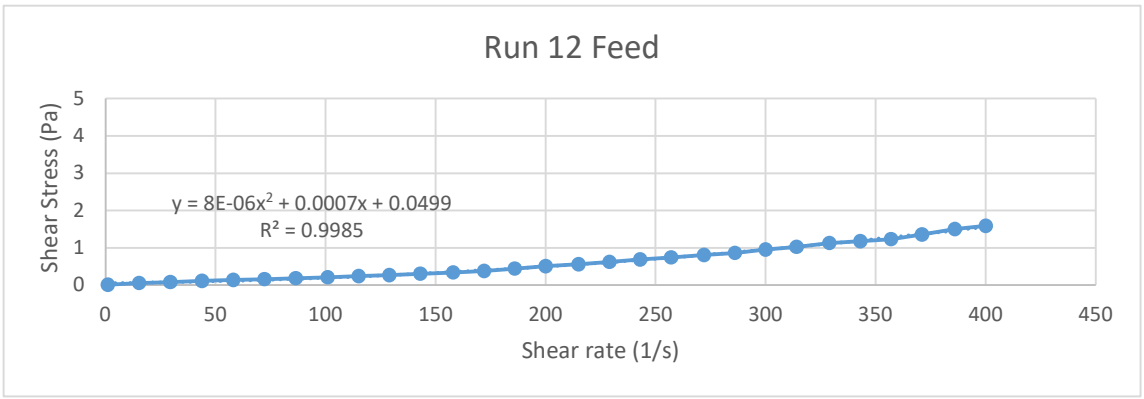
Run 12 Feed
Shear Stress (Pa)
y = 8E-06x² + 0.0007x + 0.0499
R² = 0.9985
Shear rate (1/s)

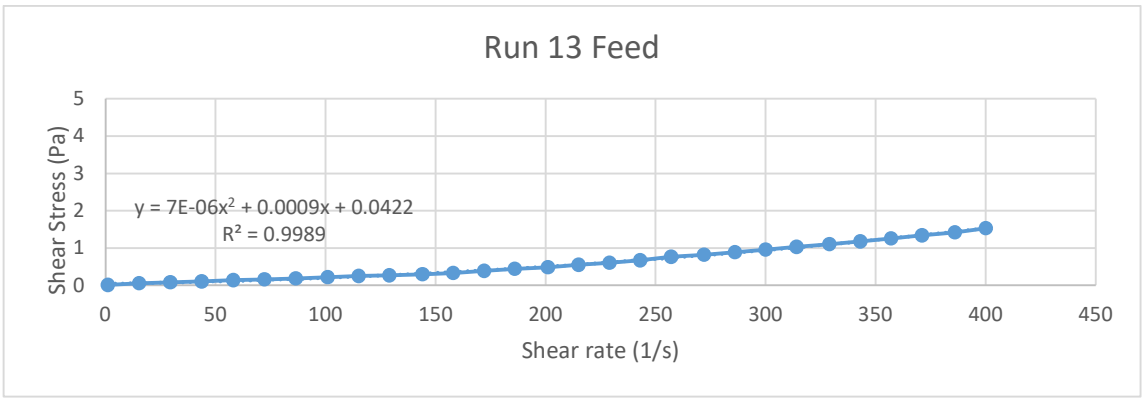
Run 13 Feed
Shear Stress (Pa)
y = 7E-06x² + 0.0009x + 0.0422
R² = 0.9989
Shear rate (1/s)
0
1
2
3
4
5
0
50
100
150
200
250
300
350
400
450

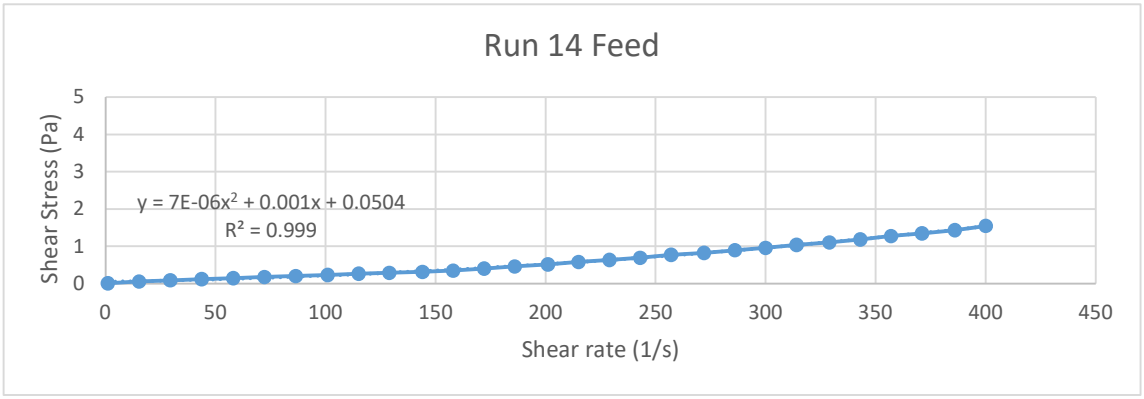
Run 14 Feed
Shear Stress (Pa)
y = 7E-06x² + 0.001x + 0.0504
R² = 0.999
Shear rate (1/s)
0
1
2
3
4
5
0
50
100
150
200
250
300
350
400
450

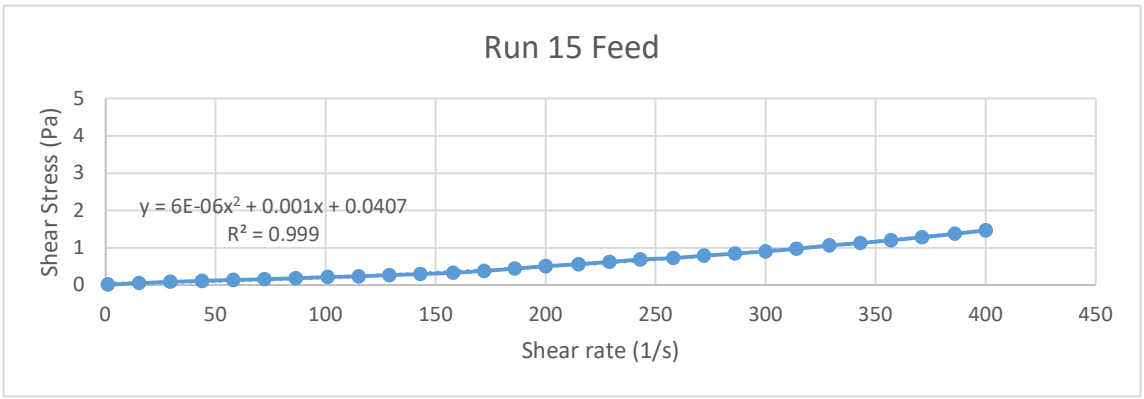
Run 15 Feed
Shear Stress (Pa)
y = 6E-06x² + 0.001x + 0.0407
R² = 0.999
Shear rate (1/s)
0
1
2
3
4
5
0
50
100
150
200
250
300
350
400
450

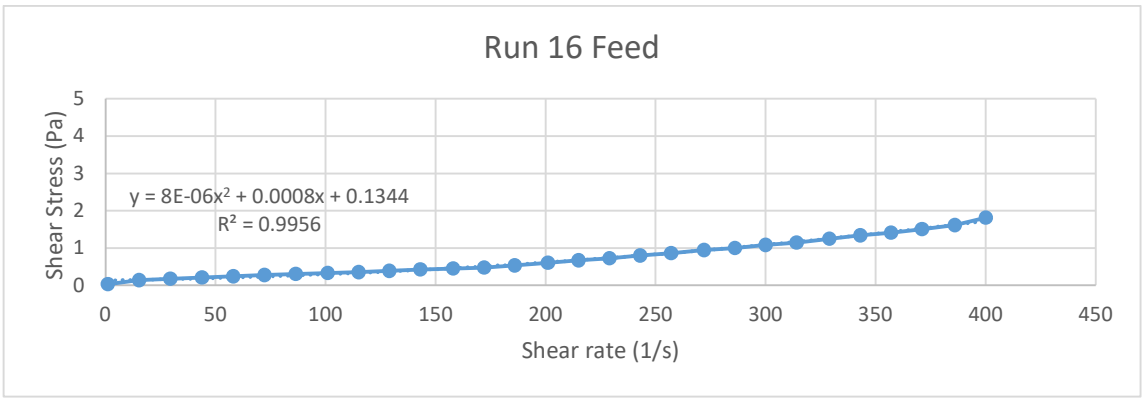
Run 16 Feed
Shear Stress (Pa)
y = 8E-06x² + 0.0008x + 0.1344
R² = 0.9956
Shear rate (1/s)
0
1
2
3
4
5
0
50
100
150
200
250
300
350
400
450

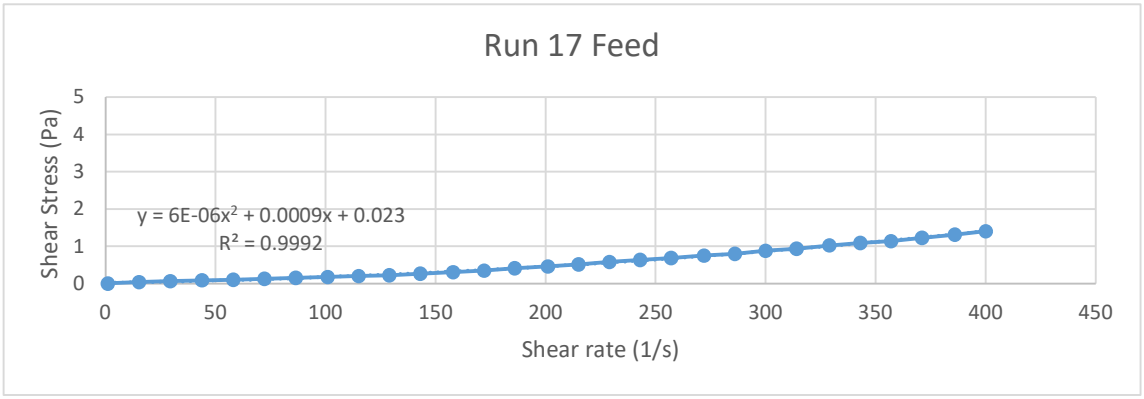
Run 17 Feed
Shear Stress (Pa)
y = 6E-06x² + 0.0009x + 0.023
R² = 0.9992
Shear rate (1/s)
0
1
2
3
4
5
0
50
100
150
200
250
300
350
400
450

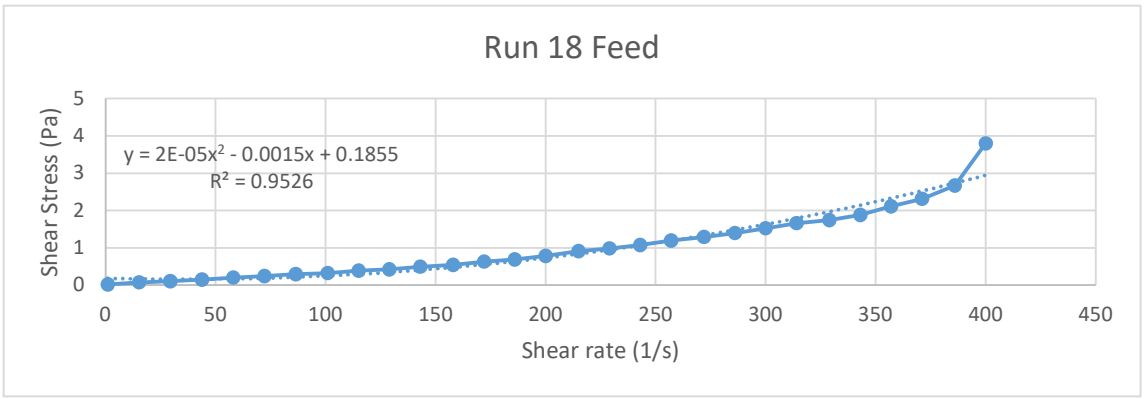
Run 18 Feed
Shear Stress (Pa)
y = 2E-05x² - 0.0015x + 0.1855
R² = 0.9526
Shear rate (1/s)
0
1
2
3
4
5
0
50
100
150
200
250
300
350
400
450

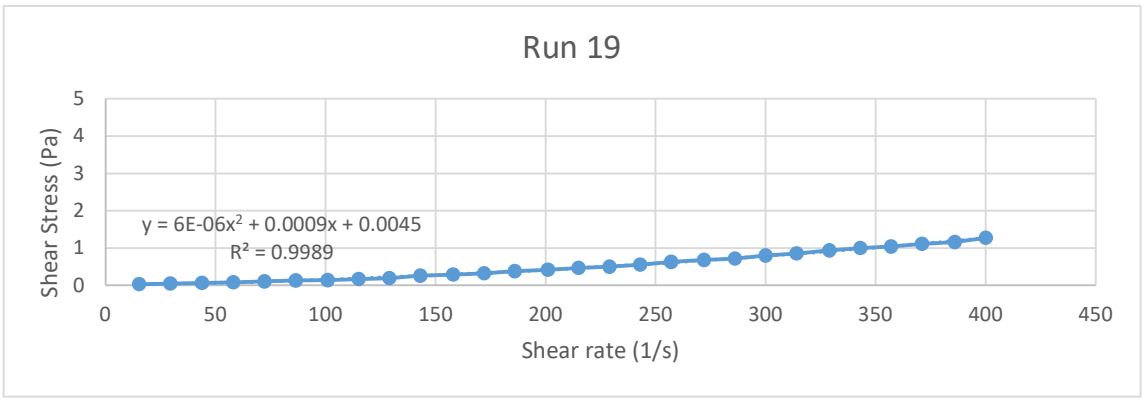
Run 19
Shear Stress (Pa)
y = 6E-06x² + 0.0009x + 0.0045
R² = 0.9989
Shear rate (1/s)

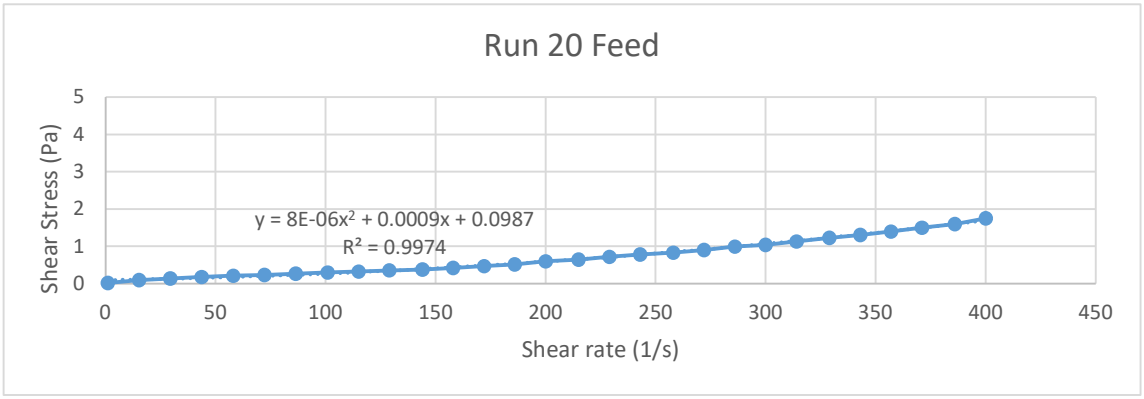
Run 20 Feed
Shear Stress (Pa)
y = 8E-06x² + 0.0009x + 0.0987
R² = 0.9974
Shear rate (1/s)

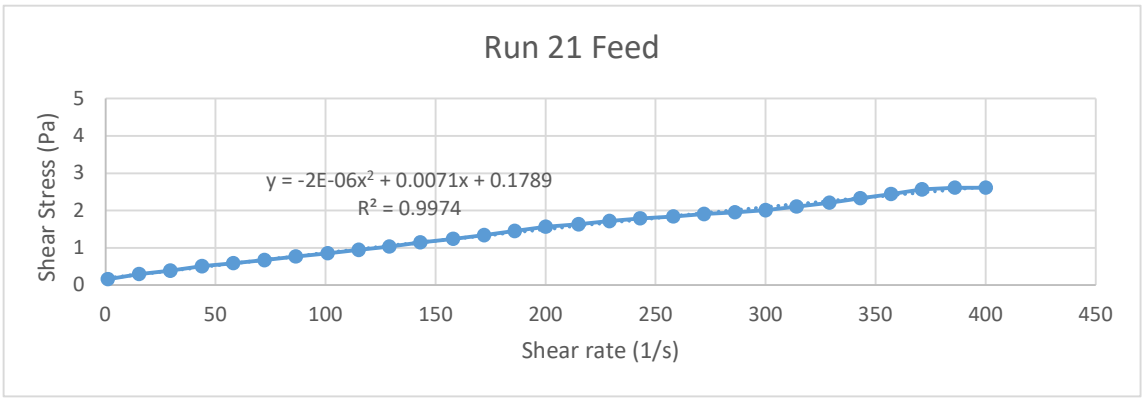
Run 21 Feed
Shear Stress (Pa)
y = -2E-06x² + 0.0071x + 0.1789
R² = 0.9974
Shear rate (1/s)

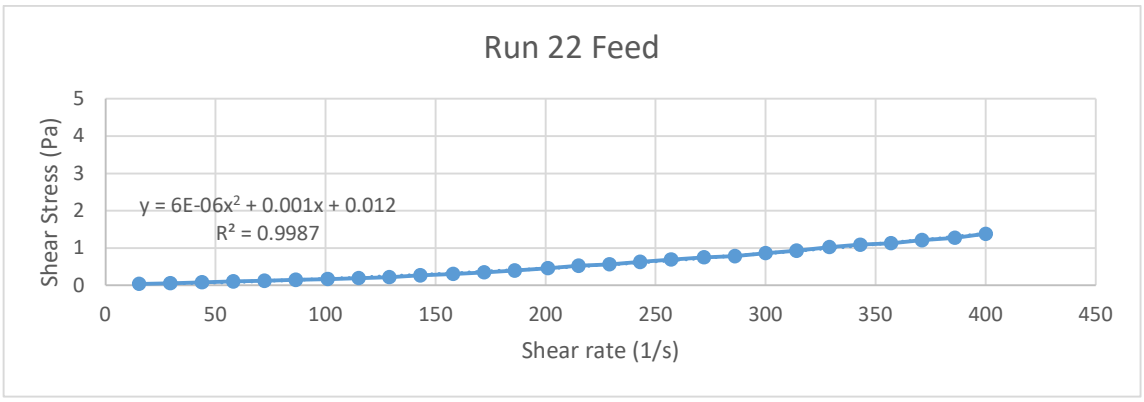
Run 22 Feed
Shear Stress (Pa)
y = 6E-06x² + 0.001x + 0.012
R² = 0.9987
Shear rate (1/s)

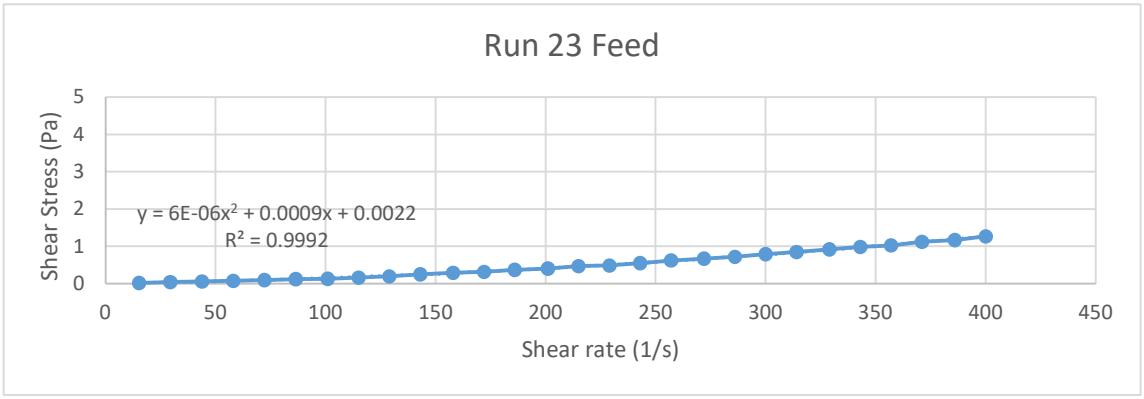
Run 23 Feed
Shear Stress (Pa)
y = 6E-06x² + 0.0009x + 0.0022
R² = 0.9992
Shear rate (1/s)

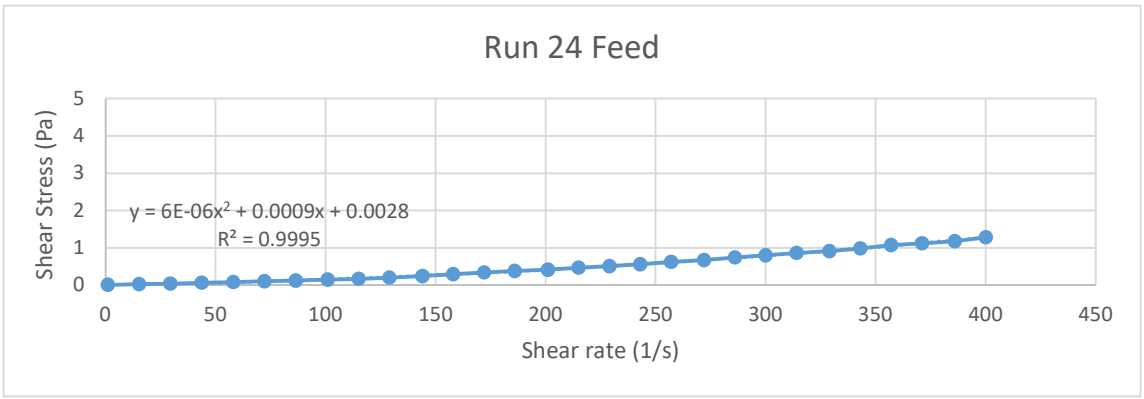
Run 24 Feed
Shear Stress (Pa)
y = 6E-06x² + 0.0009x + 0.0028
R² = 0.9995
Shear rate (1/s)

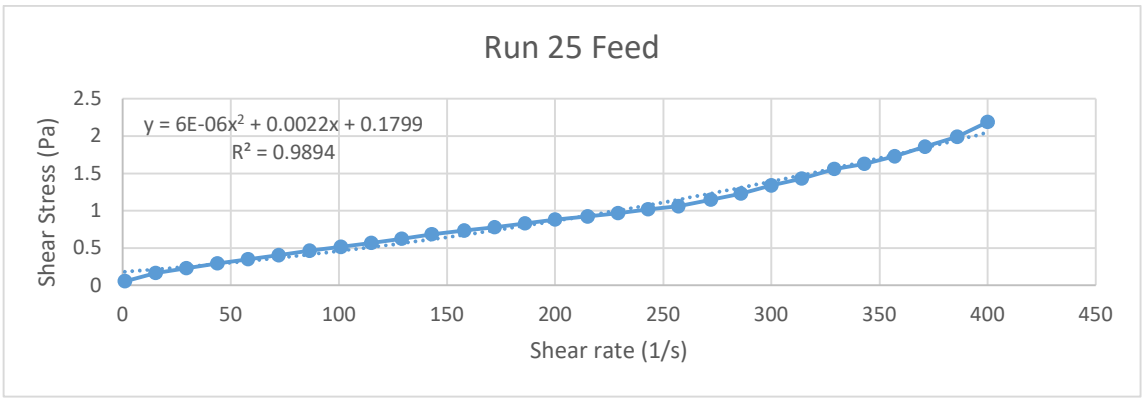
Run 25 Feed
y = 6E-06x² + 0.0022x + 0.1799
R² = 0.9894
Shear Stress (Pa)
Shear rate (1/s)
0
0.5
1
1.5
2
2.5
0
50
100
150
200
250
300
350
400
450

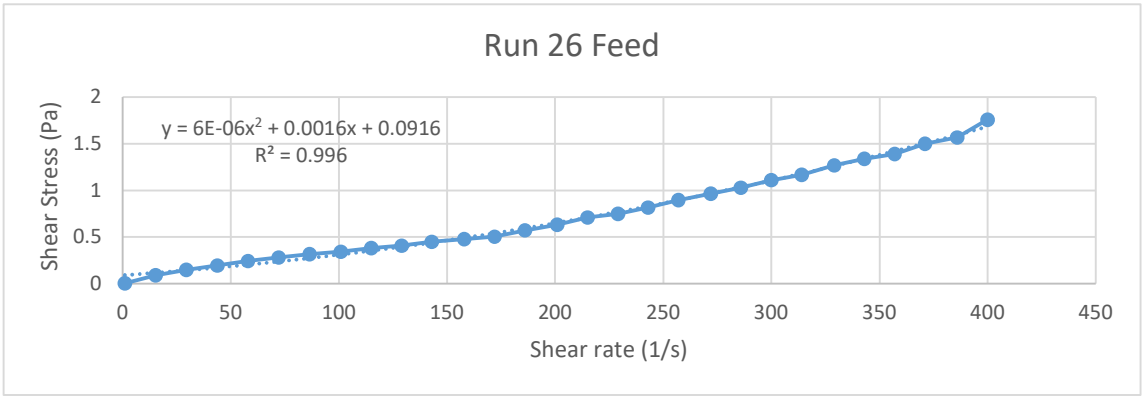
Run 26 Feed
y = 6E-06x² + 0.0016x + 0.0916
R² = 0.996
Shear Stress (Pa)
Shear rate (1/s)
0
0.5
1
1.5
2
0
50
100
150
200
250
300
350
400
450

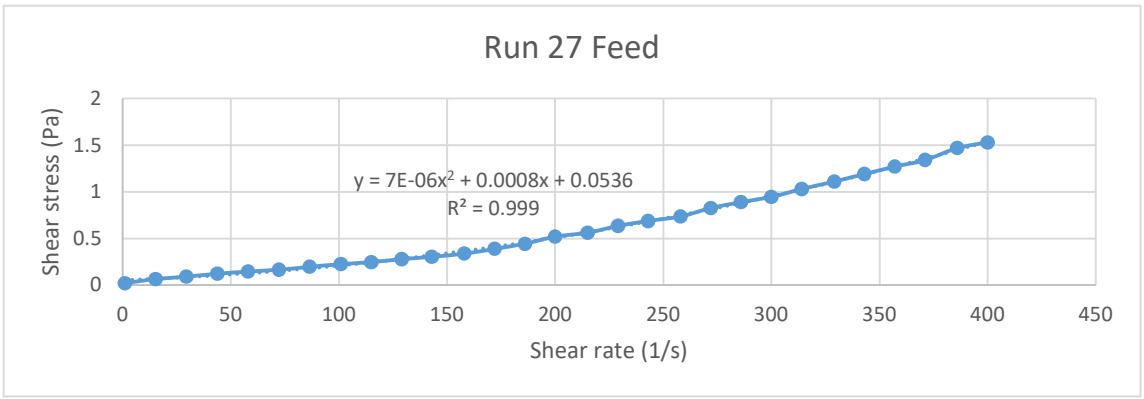
Run 27 Feed
y = 7E-06x² + 0.0008x + 0.0536
R² = 0.999
Shear stress (Pa)
Shear rate (1/s)
0
0.5
1
1.5
2
0
50
100
150
200
250
300
350
400
450

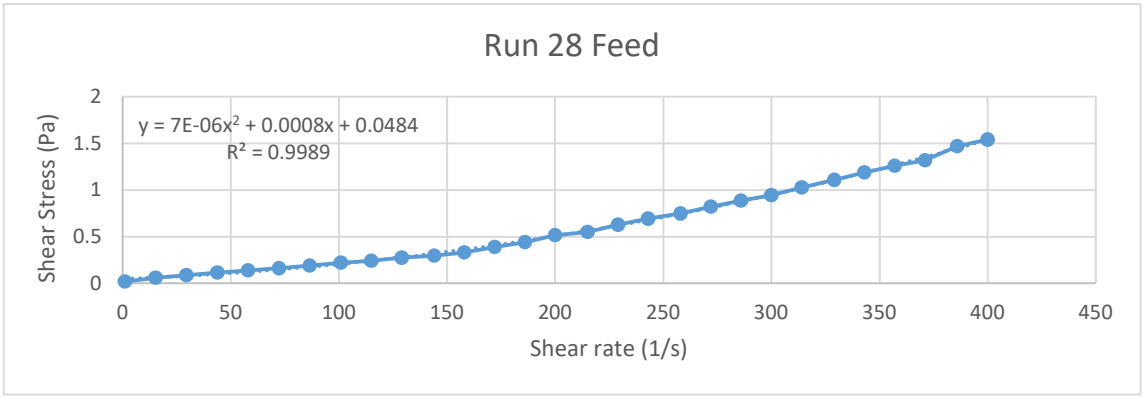
Run 28 Feed
y = 7E-06x² + 0.0008x + 0.0484
R² = 0.9989
Shear Stress (Pa)
Shear rate (1/s)
0
0.5
1
1.5
2
0
50
100
150
200
250
300
350
400
450

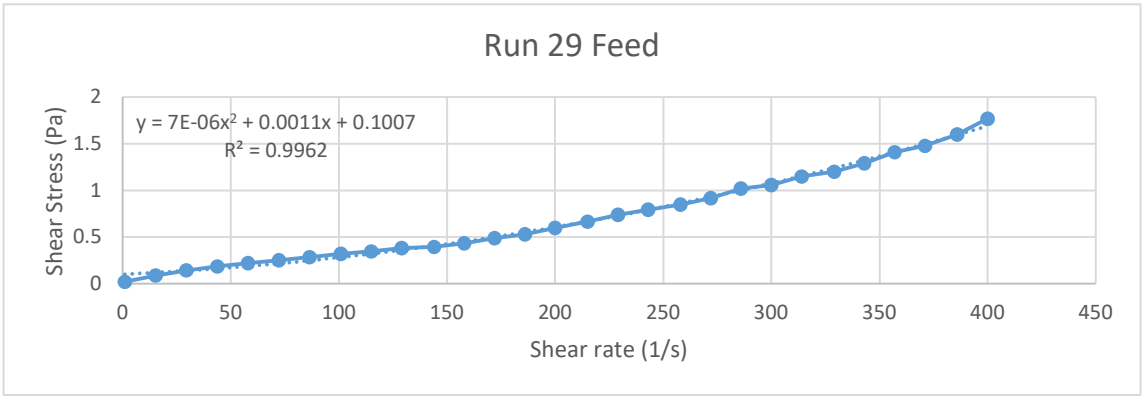
Run 29 Feed
y = 7E-06x² + 0.0011x + 0.1007
R² = 0.9962
Shear Stress (Pa)
Shear rate (1/s)
0
0.5
1
1.5
2
0
50
100
150
200
250
300
350
400
450

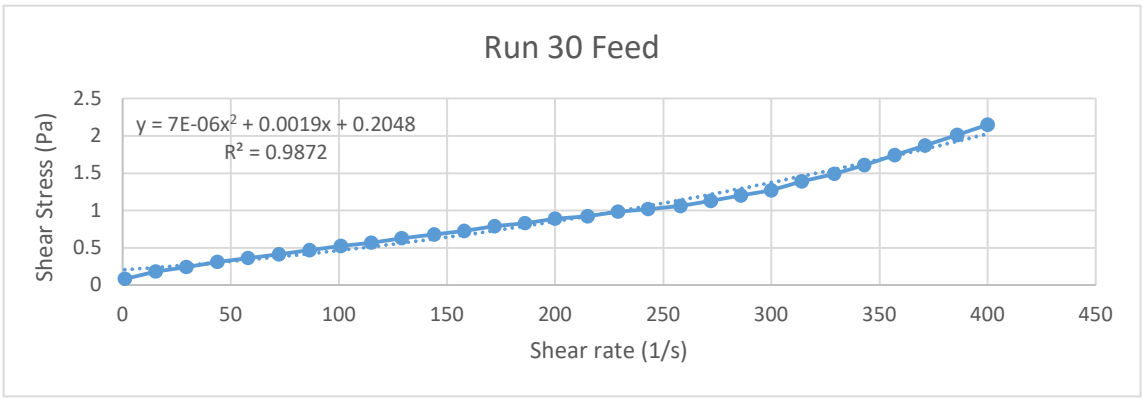
Run 30 Feed
y = 7E-06x² + 0.0019x + 0.2048
R² = 0.9872
Shear Stress (Pa)
Shear rate (1/s)
0
0.5
1
1.5
2
2.5
0
50
100
150
200
250
300
350
400
450

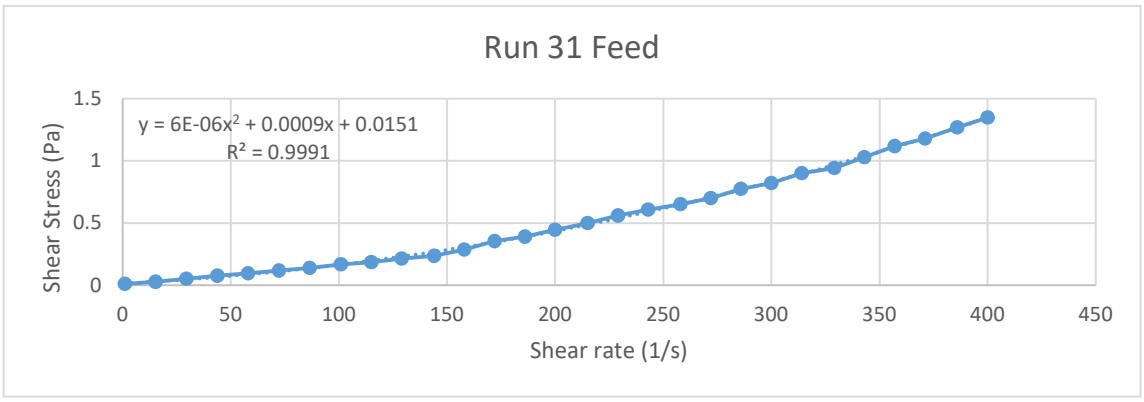
Run 31 Feed
y = 6E-06x² + 0.0009x + 0.0151
R² = 0.9991
Shear Stress (Pa)
Shear rate (1/s)
0
0.5
1
1.5
0
50
100
150
200
250
300
350
400
450

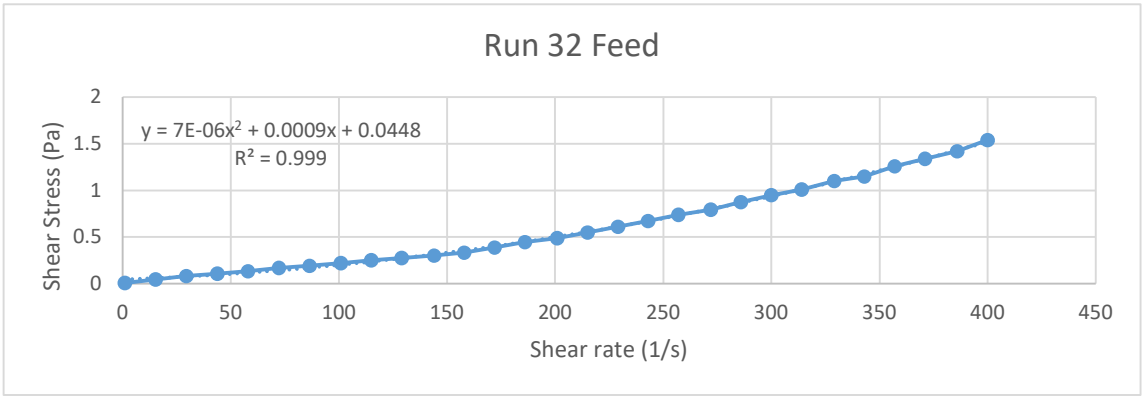
Run 32 Feed
y = 7E-06x² + 0.0009x + 0.0448
R² = 0.999
Shear Stress (Pa)
Shear rate (1/s)
0
0.5
1
1.5
2
0
50
100
150
200
250
300
350
400
450

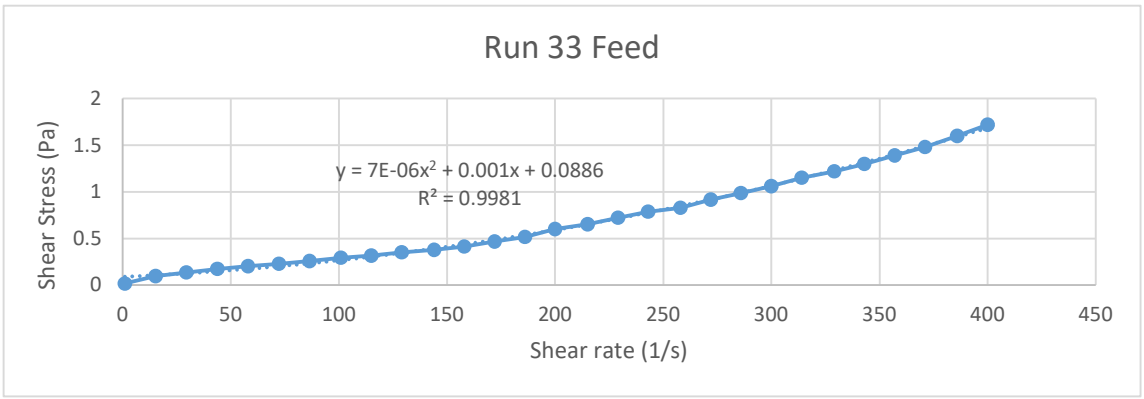
Run 33 Feed
y = 7E-06x² + 0.001x + 0.0886
R² = 0.9981
Shear Stress (Pa)
Shear rate (1/s)
0
0.5
1
1.5
2
0
50
100
150
200
250
300
350
400
450

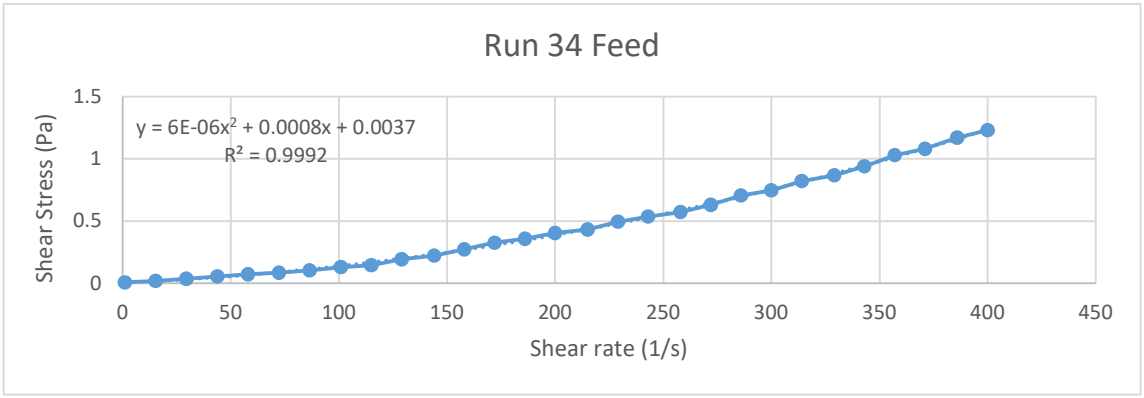
Run 34 Feed
y = 6E-06x² + 0.0008x + 0.0037
R² = 0.9992
Shear Stress (Pa)
Shear rate (1/s)
0
0.5
1
1.5
0
50
100
150
200
250
300
350
400
450

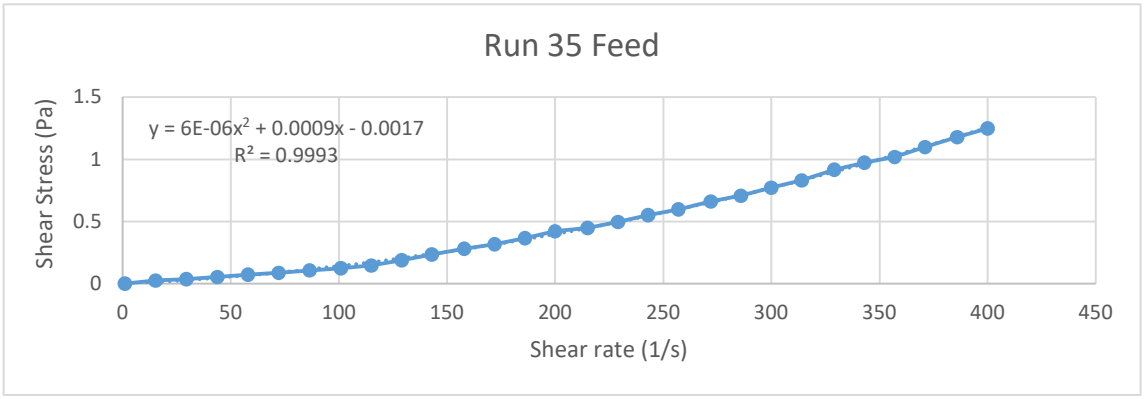
Run 35 Feed
y = 6E-06x² + 0.0009x - 0.0017
R² = 0.9993
Shear Stress (Pa)
Shear rate (1/s)
0
0.5
1
1.5
0
50
100
150
200
250
300
350
400
450

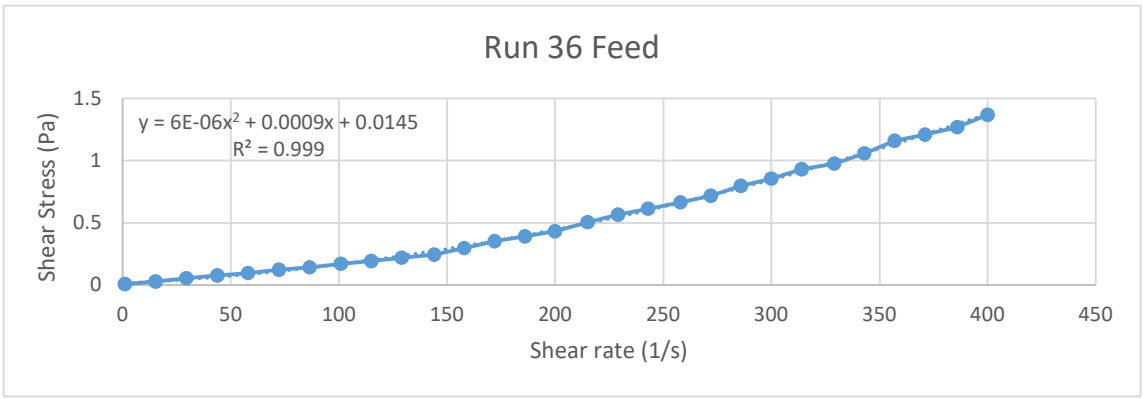
Run 36 Feed
y = 6E-06x² + 0.0009x + 0.0145
R² = 0.999
Shear Stress (Pa)
Shear rate (1/s)
0
0.5
1
1.5
0
50
100
150
200
250
300
350
400
450

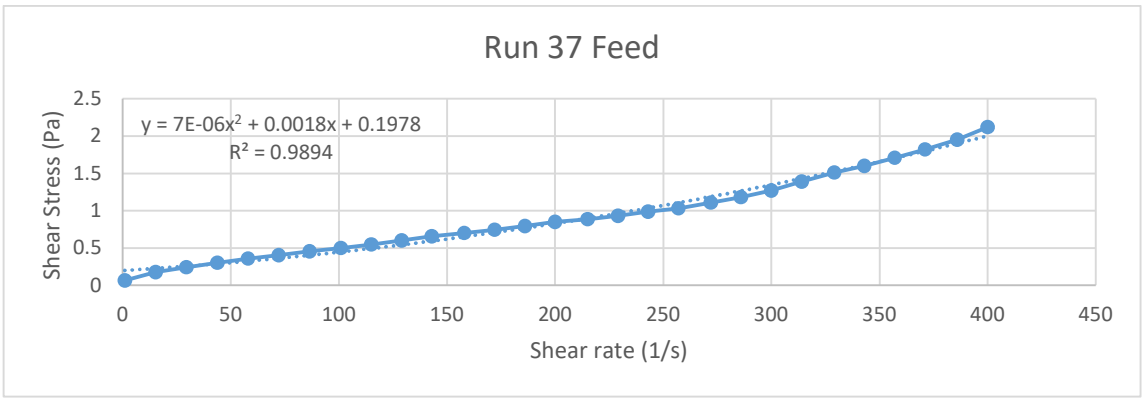
Run 37 Feed
y = 7E-06x² + 0.0018x + 0.1978
R² = 0.9894
Shear Stress (Pa)
Shear rate (1/s)
0
0.5
1
1.5
2
2.5
0
50
100
150
200
250
300
350
400
450

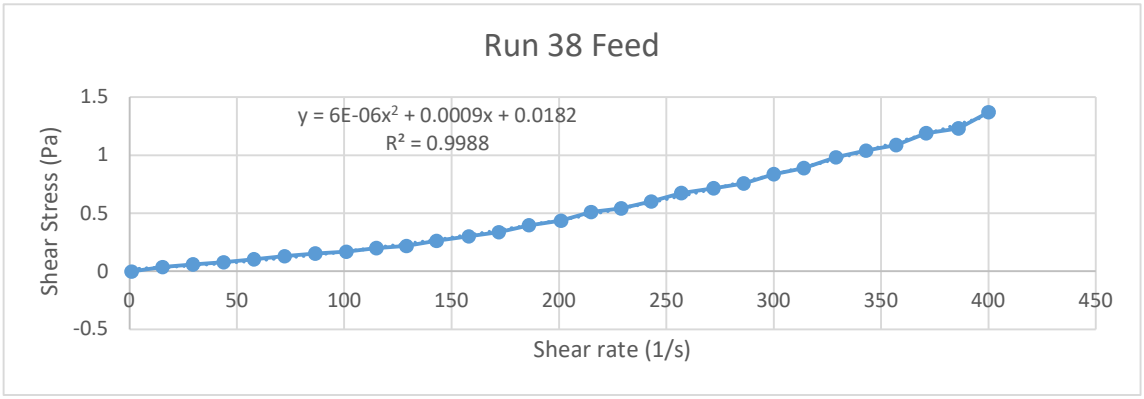
Run 38 Feed
y = 6E-06x² + 0.0009x + 0.0182
R² = 0.9988
Shear Stress (Pa)
Shear rate (1/s)
-0.5
0
0.5
1
1.5
0
50
100
150
200
250
300
350
400
450

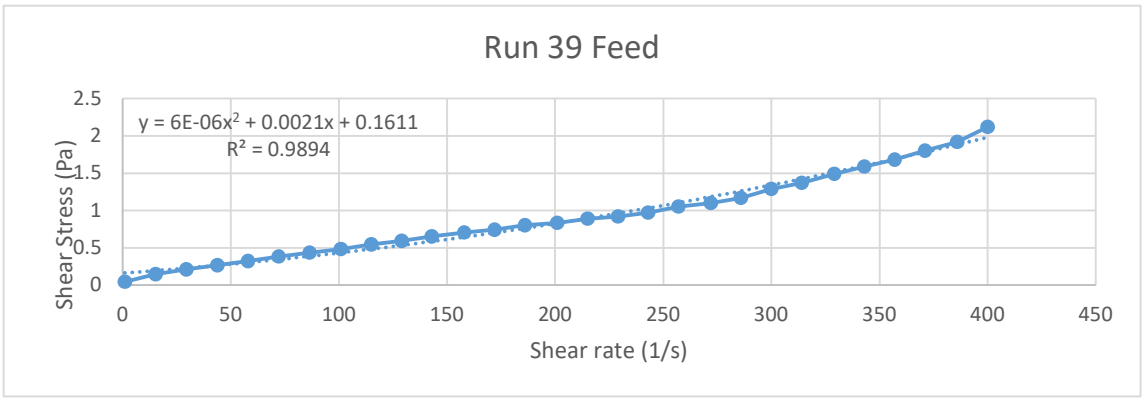
Run 39 Feed
y = 6E-06x² + 0.0021x + 0.1611
R² = 0.9894
Shear Stress (Pa)
Shear rate (1/s)
0
0.5
1
1.5
2
2.5
0
50
100
150
200
250
300
350
400
450

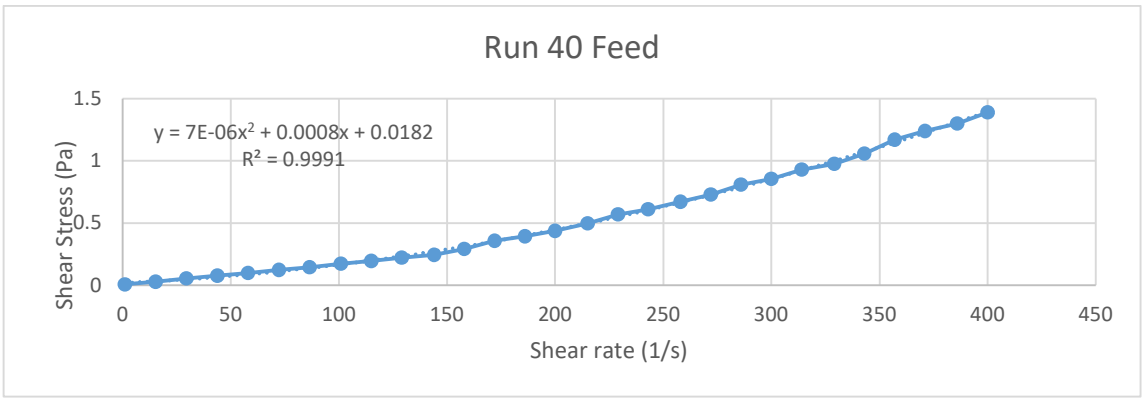
Run 40 Feed
y = 7E-06x² + 0.0008x + 0.0182
R² = 0.9991
Shear Stress (Pa)
Shear rate (1/s)
0
0.5
1
1.5
0
50
100
150
200
250
300
350
400
450

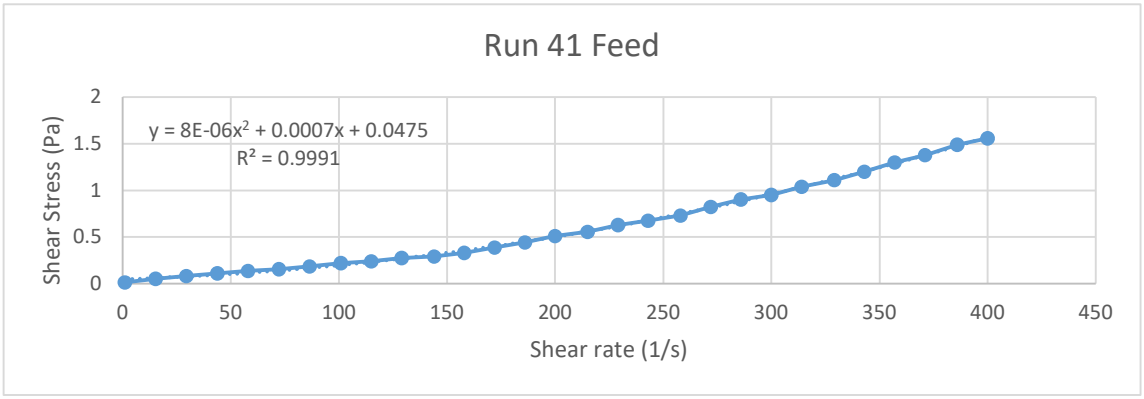
Run 41 Feed
y = 8E-06x² + 0.0007x + 0.0475
R² = 0.9991
Shear Stress (Pa)
Shear rate (1/s)
0
0.5
1
1.5
2
0
50
100
150
200
250
300
350
400
450

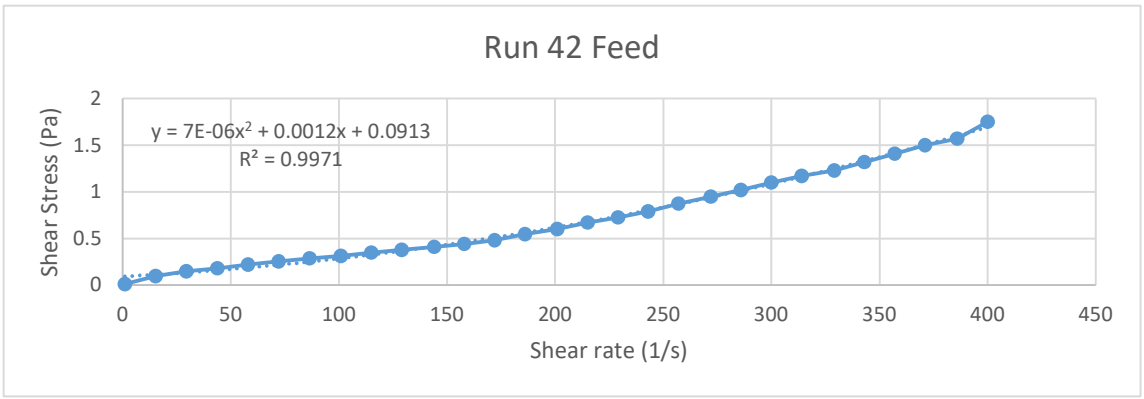
Run 42 Feed
y = 7E-06x² + 0.0012x + 0.0913
R² = 0.9971
Shear Stress (Pa)
Shear rate (1/s)
0
0.5
1
1.5
2
0
50
100
150
200
250
300
350
400
450

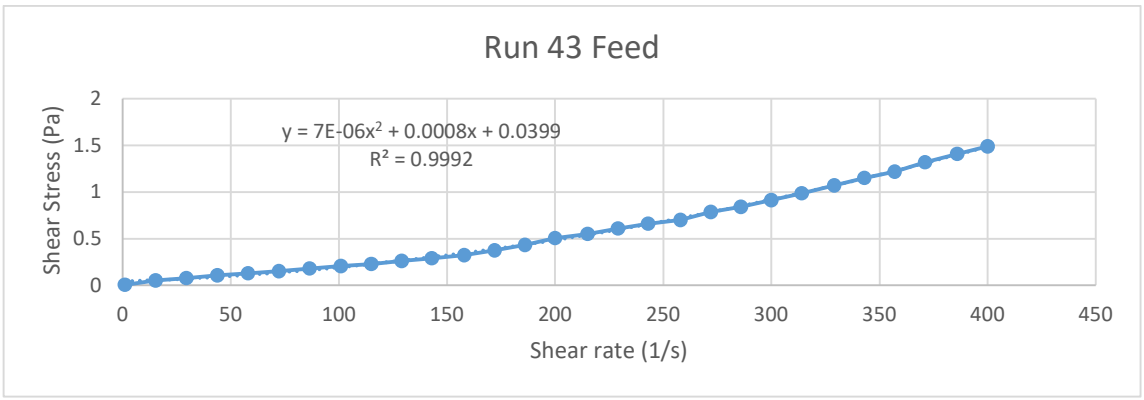
Run 43 Feed
y = 7E-06x² + 0.0008x + 0.0399
R² = 0.9992
Shear Stress (Pa)
Shear rate (1/s)
0
0.5
1
1.5
2
0
50
100
150
200
250
300
350
400
450

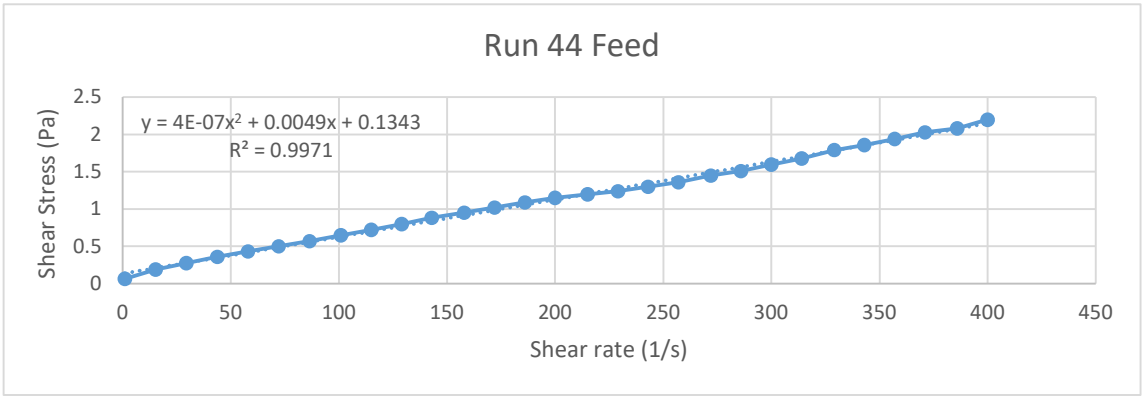
Run 44 Feed
y = 4E-07x² + 0.0049x + 0.1343
R² = 0.9971
Shear Stress (Pa)
Shear rate (1/s)
0
0.5
1
1.5
2
2.5
0
50
100
150
200
250
300
350
400
450

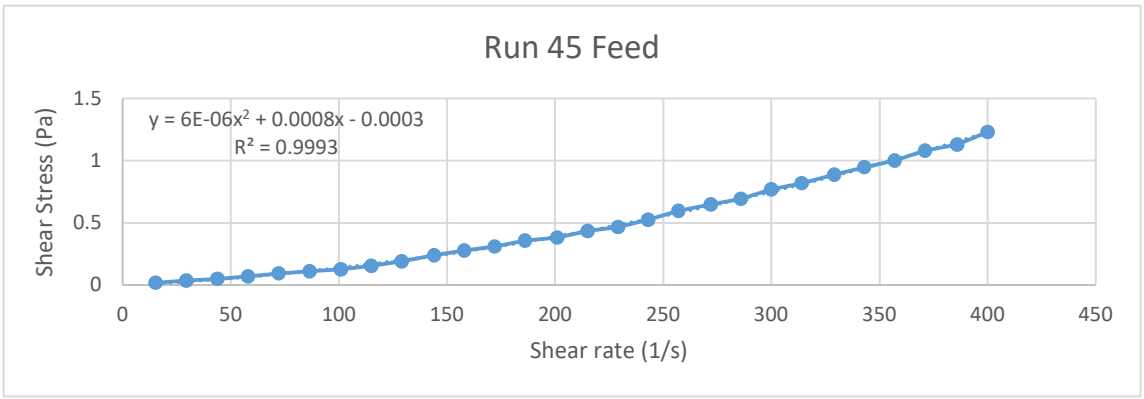
Run 45 Feed
y = 6E-06x² + 0.0008x - 0.0003
R² = 0.9993
Shear Stress (Pa)
Shear rate (1/s)
0
0.5
1
1.5
0
50
100
150
200
250
300
350
400
450

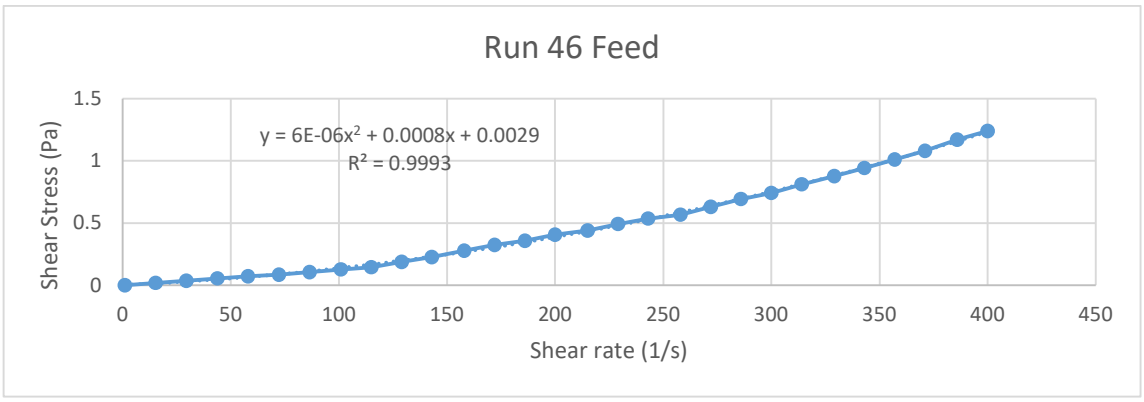
Run 46 Feed
y = 6E-06x² + 0.0008x + 0.0029
R² = 0.9993
Shear Stress (Pa)
Shear rate (1/s)
0
0.5
1
1.5
0
50
100
150
200
250
300
350
400
450

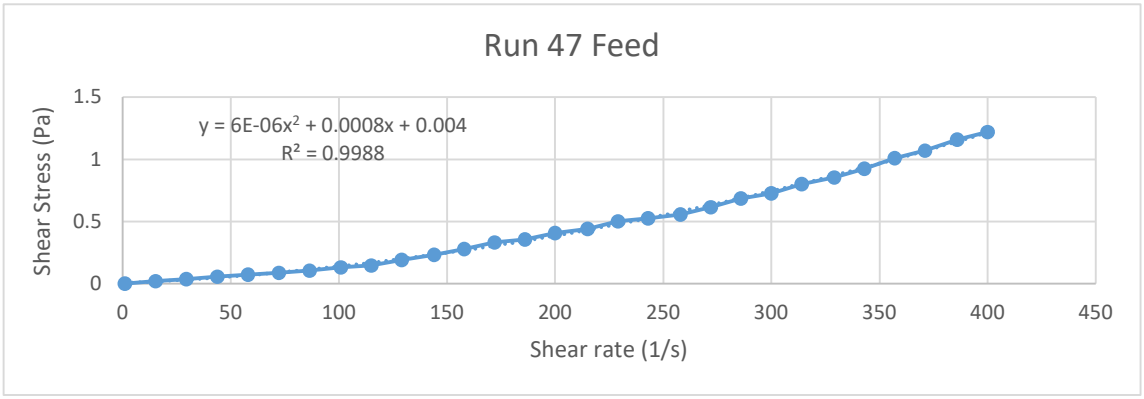
Run 47 Feed
y = 6E-06x² + 0.0008x + 0.004
R² = 0.9988
Shear Stress (Pa)
Shear rate (1/s)
0
0.5
1
1.5
0
50
100
150
200
250
300
350
400
450

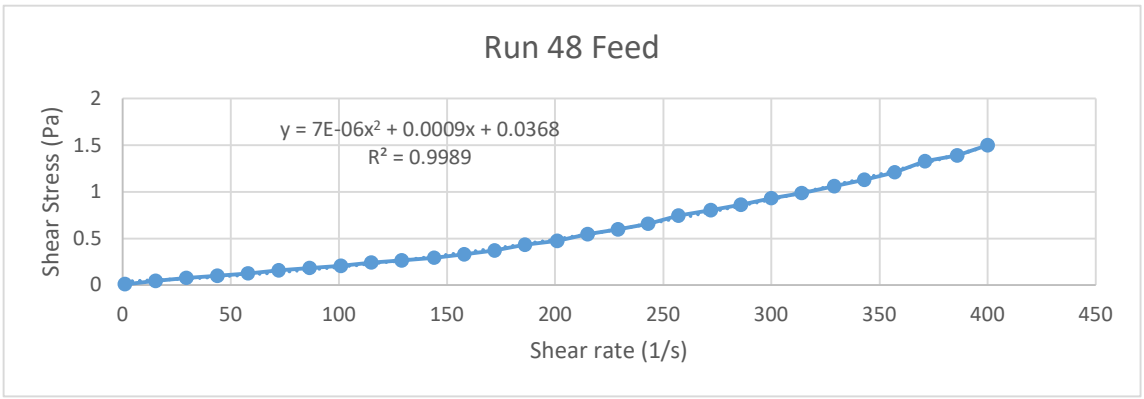
Run 48 Feed
y = 7E-06x² + 0.0009x + 0.0368
R² = 0.9989
Shear Stress (Pa)
Shear rate (1/s)
0
0.5
1
1.5
2
0
50
100
150
200
250
300
350
400
450

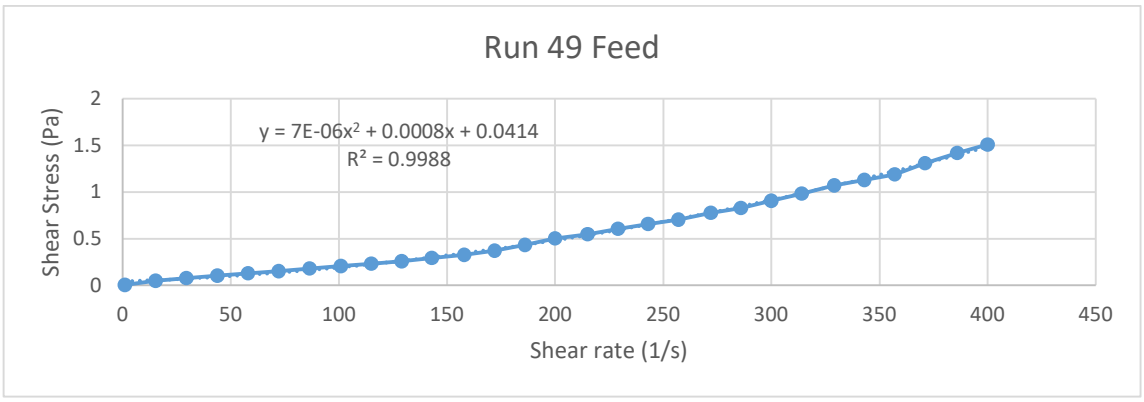
Run 49 Feed
y = 7E-06x² + 0.0008x + 0.0414
R² = 0.9988
Shear Stress (Pa)
Shear rate (1/s)
0
0.5
1
1.5
2
0
50
100
150
200
250
300
350
400
450

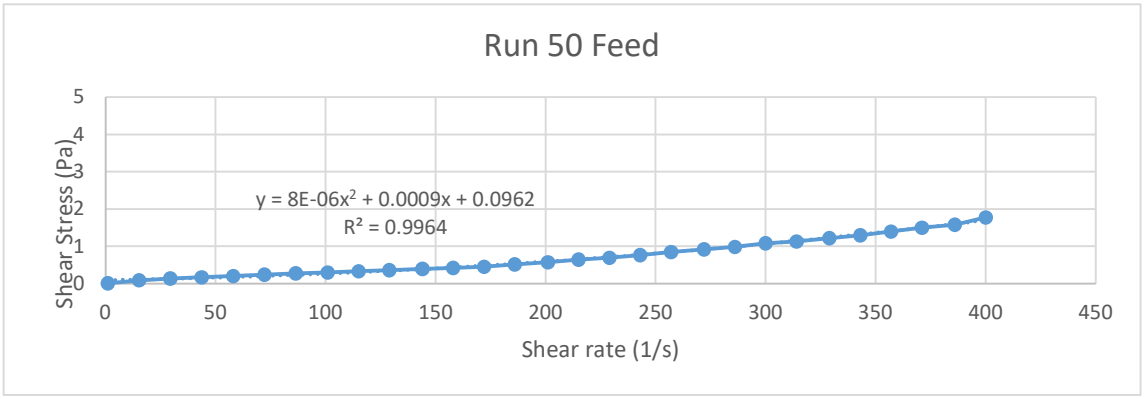
Run 50 Feed
y = 8E-06x² + 0.0009x + 0.0962
R² = 0.9964
Shear Stress (Pa)
Shear rate (1/s)
0
1
2
3
4
5
0
50
100
150
200
250
300
350
400
450

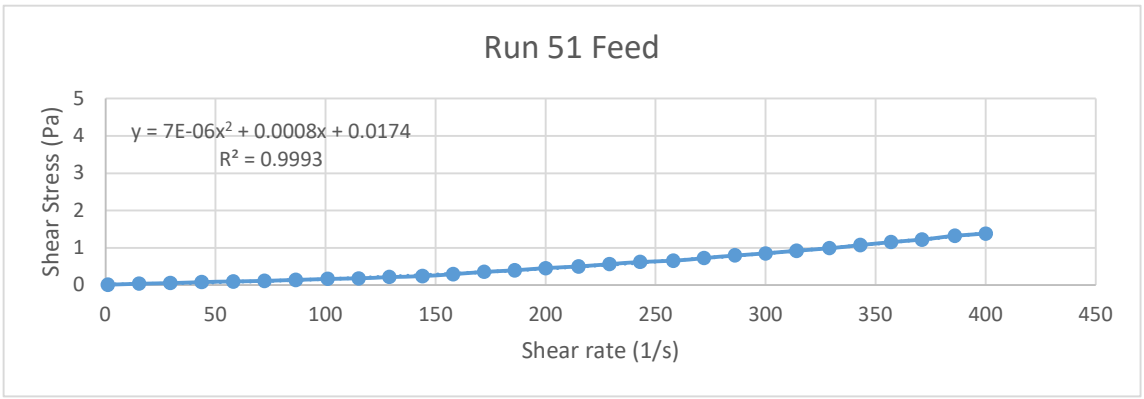
Run 51 Feed
y = 7E-06x² + 0.0008x + 0.0174
R² = 0.9993
Shear Stress (Pa)
Shear rate (1/s)
0
1
2
3
4
5
0
50
100
150
200
250
300
350
400
450

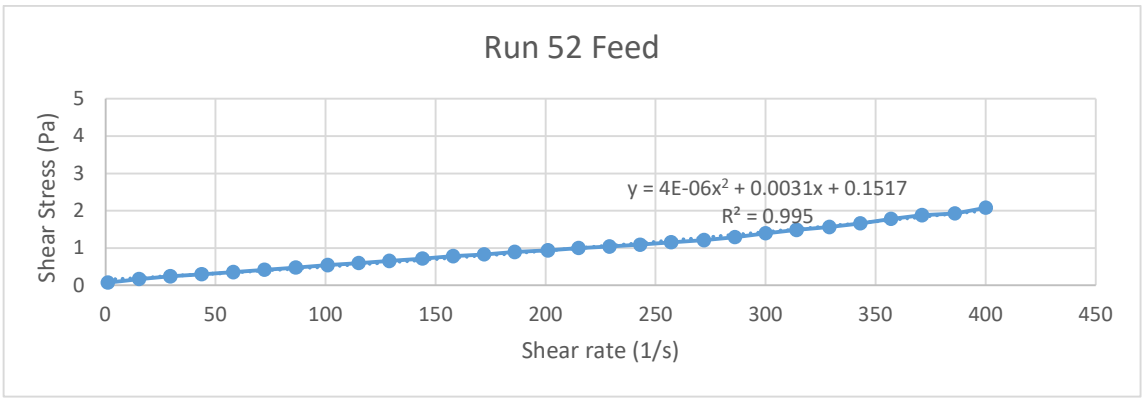
Run 52 Feed
Shear Stress (Pa)
Shear rate (1/s)
y = 4E-06x² + 0.0031x + 0.1517
R² = 0.995
0
1
2
3
4
5
0
50
100
150
200
250
300
350
400
450

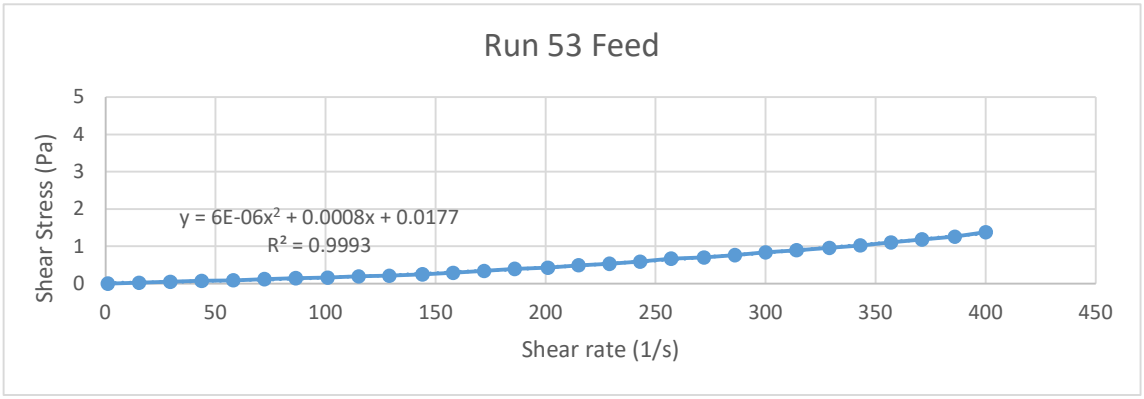
Run 53 Feed
Shear Stress (Pa)
Shear rate (1/s)
y = 6E-06x² + 0.0008x + 0.0177
R² = 0.9993
0
1
2
3
4
5
0
50
100
150
200
250
300
350
400
450

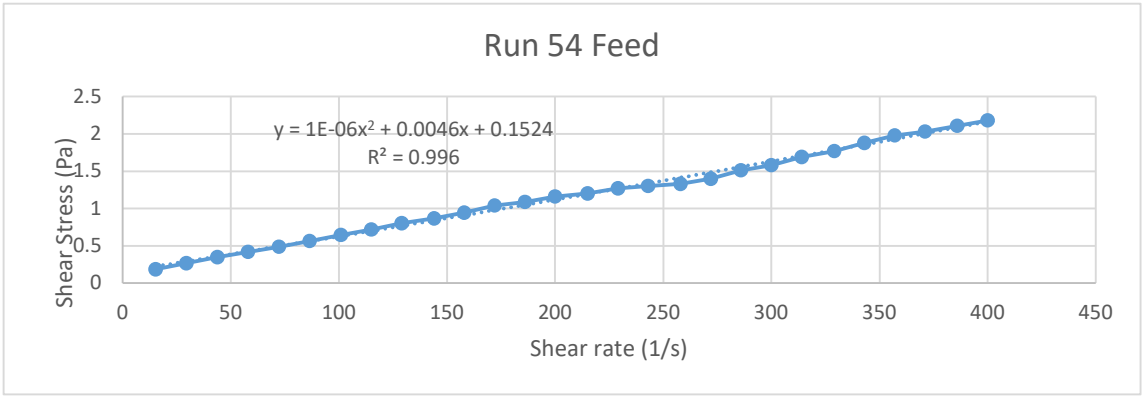
Run 54 Feed
Shear Stress (Pa)
Shear rate (1/s)
y = 1E-06x² + 0.0046x + 0.1524
R² = 0.996
0
0.5
1
1.5
2
2.5
0
50
100
150
200
250
300
350
400
450